Distribution Agreement

In presenting this thesis or dissertation as a partial fulfillment of the requirements for an advanced degree from Emory University, I hereby grant to Emory University and its agents the non-exclusive license to archive, make accessible, and display my thesis or dissertation in whole or in part in all forms of media, now or hereafter known, including display on the world wide web. I understand that I may select some access restrictions as part of the online submission of this thesis or dissertation. I retain all ownership rights to the copyright of the thesis or dissertation. I also retain the right to use in future works (such as articles or books) all or part of this thesis or dissertation.

Signature:

_____ _____

Mariko S Peterson Date

Malaria disease severity and resilience: *Plasmodium knowlesi* infection of *Macaca mulatta* and *Macaca fascicularis*

By

Mariko S. Peterson
Doctor of Philosophy

Graduate Division of Biological and Biomedical Sciences
Population Biology, Ecology, and Evolution

_____
Mary R. Galinski
Advisor

_____
Jacobus de Roode
Committee Chair

_____
John W. Barnwell
Committee Member

_____
Levi Morran
Committee Member

_____
Rustom Antia
Committee Member

_____
Joshy Jacob
Committee Member

Accepted:

_____
Lisa A. Tedesco, Ph.D.
Dean of the James T. Laney School of Graduate Studies

_____
Date

Malaria disease severity and resilience: *Plasmodium knowlesi* infection of *Macaca mulatta* and *Macaca fascicularis*

By

Mariko S. Peterson
B.S., Microbiology, Iowa State University
B.S., Genetics, Iowa State University
M.S., Biochemistry, Iowa State University

Advisor: Mary R. Galinski, PhD

An abstract of a dissertation submitted to the Faculty of the
James T. Laney School of Graduate Studies of Emory University
in partial fulfillment of the requirements for the degree of
Doctor of Philosophy in Population Biology, Ecology, and Evolution
2020

Abstract

Malaria disease severity and resilience: *Plasmodium knowlesi* infection of *Macaca mulatta* and *Macaca fascicularis*

By Mariko S. Peterson

Plasmodium knowlesi is an emergent zoonotic malaria parasite that has become the most common cause of malaria in Malaysia. Patients infected with *P. knowlesi* present across the clinical spectrum, and the accepted paradigm is that the natural monkey host in Southeast Asia, *Macaca fascicularis* (long-tailed macaques) does not exhibit severe disease, while the experimental host, *Macaca mulatta* (rhesus macaques, of Indian origin) experiences rapidly rising parasitemia and death if not treated. These striking differences provide a unique opportunity to examine determinants of disease severity, with direct application to understanding human *P. knowlesi* pathophysiology. Here we utilize *M. fascicularis* and *M. mulatta* and take a comparative approach to understand *P. knowlesi* disease severity and its resolution. A mixed cohort of these two species was infected with *P. knowlesi* Malayan strain sporozoites and studied longitudinally. Temperature was captured continuously via surgically implanted telemetry devices. As expected, *M. fascicularis* experienced much lower and controlled parasitemias compared to *M. mulatta* which required treatment. Recrudescent parasitemic peaks in *M. fascicularis* did not result in temperatures in the febrile range, suggesting that recrudescent parasitemias may not be clinically important. Yet, *M. fascicularis* did experience severe anemia, with hemoglobin nadirs as low as 4.8 g/dL and kidney injury. Chronicity and resolution of clinical conditions were achieved naturally in *M. fascicularis*, and only after subcurative treatment in *M. mulatta*. Twenty-two tissues were analyzed for the presence of parasites, their adhesion to the vascular endothelium, and pathology. Evidence for infected erythrocyte adhesion was observed in the gut tissues of *M. mulatta*, including by electron microscopy, while parasite adhesion was not clearly evident in *M. fascicularis*. Bone marrow, splenic and temperature responses occurred earlier in *M. fascicularis* infections, suggesting a role for immune response timing in disease resilience to this parasite. These findings contribute to better defining determinants of malarial disease in macaque hosts, understanding *P. knowlesi* pathophysiology, and improving diagnosis and treatment strategies in clinical settings.

Malaria disease severity and resilience: *Plasmodium knowlesi* infection of *Macaca mulatta* and *Macaca fascicularis*

By

Mariko S. Peterson
B.S., Microbiology, Iowa State University
B.S., Genetics, Iowa State University
M.S., Biochemistry, Iowa State University

Advisor: Mary R. Galinski, PhD

A dissertation submitted to the Faculty of the
James T. Laney School of Graduate Studies of Emory University
in partial fulfillment of the requirements for the degree of
Doctor of Philosophy in Population Biology, Ecology, and Evolution
2020

Acknowledegements

My interest in infectious disease began when I was in grade school in northern Arizona in 1993 when the Sin Nombre hauntavirus emerged in the Four Corners region of the American Southwest. As I grew up, my interests expanded to include not only the pathogens themselves, but also the ecology, clinical impact, and other factors surrounding their biology and societal impact. In order to maximize my ability to integrate all of these facets of infectious disease in my future career, I decided to pursue an MD/PhD dual degree in population biology, ecology and evolution. In true form, my dissertation project reflected this interdisciplinary approach, combining elements of basic biology, field work, in-vitro and in-vivo model systems, and clinical, histological, and wetbench experiments, all in the context of multi-institutional and multi-national collaborative efforts to explore disease severity and resilience determinants based on host species upon infection with a malaria parasite.

It is no surprise given the complexity and number of moving parts and the directions my dissertation took that I had a strong team of mentors supporting and advising me every step of the way. I especially want to thank my dissertation adviser, Dr. Mary R. Galinski for her time and effort in leading the malaria consortium that provided a nurturing and rich environment in which to do my work. Dr. Galinski has been a ceaseless advocate for me scientifically and professionally, not only supporting the pursuit of my dissertation questions, but also by enabling me to participate a rich set of unique experiences that I do not believe would have been possible without her advocacy, including training at CDC, international travel, including to the ground-zero field site in Sarawak, Malaysia, and to conferences in Switzerland and Brazil, and of course having the opportunity to work on multplie research questions with the benefit of nonhuman primate models, among many other things. I would also like to thank Dr. John W. Barnwell, who not only trained

me while he was at CDC, but also spent countless hours sharing his extensive knowledge and love for malariology with me discussing next steps, designing experiments, and debating data over coffee at his and Dr. Galinski's kitchen table. Dr. Barnwell freely gave his time, and also shared materials including parasites and cell lines to enable me to complete the work described in this dissertation. I am deeply and forever indebted to both Dr. Galinski and Dr. Barnwell, and my life is all the richer for having had the honor of being their student.

I have also been extraordinarily fortunate to have a supportive committee, including Dr. Jacobus De Roode, my committee chair, Dr. Levi Morran, Dr. Rustom Antia, Dr. Joshy Jacob, and Dr. John Barnwell. They challenged me to keep the big questions in mind, even as I focused on smaller details, helped me to refine my analyses (especially statistically) and directions, and kept their doors open to me for when I had a puzzling question or exciting results. Their ceaseless advocacy and investment in me, and their addition of their own expertise to help me grow scientifically humbles me.

As mentioned above, I benefitted from being plugged into a multi-institutional collaborative effort in Dr. Galinski's lab. I benefitted from discussions and presentations given monthly at our consortium meetings. I thank all members, past and present, of the MaHPIC and HAMMER teams (supported by NIH/NIAID and DARPA contract awards, respectively), but would especially like to thank Dr. Jessica C. Kissinger and Dr. Jeremy D. DeBarry at the University of Georgia for their work on data access and their attention to detail to ensure our data were the best quality and the most consistently reported. Data management is often overlooked, but is so important and I am grateful to them and their team for doing the outstanding job that made this analysis possible. I would also like to thank Dr. Juan B. Guitierrez, his former student, Dr. Jessica Brady, and their team at the University of Georgia, who through their expertise made

the telemetry data analysis possible. I thank Stacey A. Lapp, Dr. Rabin Tirouvanziam, Dr. Dave Anderson, and from Georgia Tech, Dr. Eberhard O. Voit and Dr. Luis L. Fonseca for important discussions and their scientific mentorship. I am extremely grateful to Dr. Sanjeev Gumber who was extremely involved in mentoring me in pathology and worked side-by-side with me on all of the histopathological analysis. I would like to thank Dr. Alberto Moreno, a fellow clinician for his invaluable contributions to the clinical questions, guidance, and interpretations of these data, and Dr. Jennifer S. Wood who oversaw the veterinary care of our animals and provided invaluable advise and input throughout the course of their infections.

I am especially indebted and grateful for the mentorship that I received from members of the Galinski Lab, my friends and colleagues, Dr. Regina Joice Cordy and Dr. Chester (Chet) J Joyner. They were there to share my triumphs and disappointments, to talk about life and science, to refine my questions and writing, to suggest new directions and analyses, and to help me grow personally, scientifically, and professionally. This work would not have been possible without them.

These data could not have been collected without a strong team of technical support, both within our team and at Yerkes. For that I especially thank Monica Cabrera Mora who lead daily and twice daily efforts to collect the parasitemiological and clinical data that enabled me to perform the analysis to the granularity presented here. I also thank the Yerkes necropsy team for their time and attention to detail with our very detailed and extensive necropsy protocols, Mr. Evan Desausau for his expertise in light microscopy slide and electron microscopy grid preparation, and Dr. Deepa Kodandera for lending her expertise in immunohistochemistry.

I had the benefit of being a member of the MSTP at Emory who provided who have unboundless support and advocacy throughout my career thus far. I am grateful to all of the

directors and staff past and present, but especially indebted to Mary Horton, Dr. Anita Corbett, Dr. Cathy Quiñones-Maeso, Dr. Joanna Bonsall, Dr. Andy Neish, Dr. Bob Gross, and Dr. Paul Garcia for their support as I navigate my training.

I have also been blessed with an incredible group of friends who have grown to be like family to me in both my PBEE and MSTP cohorts (and beyond) and have supported me emotionally, scientifically, and everything in between, even when I have been grumpy. I especially thank Nick, Toni, and Lily Butts, Dr. Nate Jacobs and Dr. Mary Bushman from PBEE, Drs. (or soon-to-be Drs.) Saumya Gurbani, Daniel Whittingslow, Myles McCrary, David Trac, Matt Stern, Arielle Valdex-Sinon, and Steve Yarmoska from my MSTP cohort, and Drs. Lisa Tang, Sidd Kosajaru, Sarah Gurbani, Rewa Choudhary, Ankita Tippur, and Mr. Naman Kanakiya from my medical school cohort – you have all related to me on a deeper level, been there for me in the frustrating times, lifting me up with an ice cream and a smile, and have generally made life more bright.

Though my family lives across the country, I'd like to thank them (Michael, Kathy, and my sister Sarah) for all the love and support they've given me through the years, for everything they taught me about hard work and perserverence, and for being available for late night calls to share exciting and not-so-exciting details. I'd also like to thank my bachan, Keiko Glasscoe for everything she did to inspire me to pursue and prioritize my education, and my aunts, Erika and Maggi Glasscoe who supported her vision and me as I continued along this path. I've also been blessed with supportive in-laws, and I would especially like to thank my mother-in-law, Robin Hammill Oberbroeckling for her support.

Lastly, and importantly, I'd like to thank my husband, Aaron Topliss. AJ relocated across the country to be with me when I chose to go to Emory nearly seven years ago, and though times

have not always been easy, he has stayed by my side through the ups and downs, international travel, late nights culturing parasites, early mornings necropsying, and everything in between. His love, support, and endless supply of hugs, smiles, and food bribes have given me life and strength to continue when the going gets tough, and I look forward to sharing the journey ahead with him.

Table of Contents

Chapter 1: Introduction

Malaria is a febrile illness caused by the obligate infection and lysis of erythrocytes by members of the eukaryotic intracellular parasite genus, *Plasmodium* [1]. Attributed to the rise of the sickle cell mutation, and described classically in ancient Greek, Roman, Egyptian and Chinese medical texts, malaria is an ancient disease that represents a serious modern health challenge worldwide, causing 435,000 deaths in 2017, the majority of whom are children [2–4]. Despite global strategies and efforts to eradicate the parasite, malaria continues to thwart elimination efforts, and the decline in cases occurring since 2010 has slowed, and potentially reversed: 2017 saw 219 million cases, compared with 217 million cases in 2016 [2]. Historically, four species of *Plasmodium* have caused malaria in humans: *P. falciparum*, the most feared, *P. vivax*, the most geographically widespread, *P. ovale*, and *P. malariae* [5]. However, recently *P. knowlesi*, a parasite of pig-tailed macaques (*Macaca nemestrina*) and kra monkeys (*M. fascicularis*), has emerged as a major cause of human malaria in Malaysian Borneo as a zoonosis, and threatens to upend malaria elimination efforts in the country [6–8].

Plasmodium knowlesi has the capacity to cause severe disease in humans, however the factors surrounding virulence and the determinants for the trajectory of infection are poorly understood. That *P. knowlesi* is a parasite of macaque species that are established models for biomedical research provides a unique advantage to studying a zoonotic pathogen in natural and unnatural hosts, with the findings providing direct relevancy to human health.

1.1 Back to basics: biology of *Plasmodium knowlesi*

Plasmodium knowlesi is similar to other *Plasmodium* species that infect humans, and has the same general life cycle [1,9,10]. It is vectored by the bite of female Anopheline mosquitoes.

Upon probing and biting, the mosquito releases sporozoites which escape the skin and migrate to the liver. In the liver, the sporozoites invade hepatocytes, where they differentiate and replicate many fold, eventually rupturing the liver cell and spilling erythrocyte-invasive merozoites into the blood stream. In some species (*Plasmodium vivax* and *Plasmodium ovale*), parasites may produce a dormant form of parasitized hepatocytes known as a hypnozoites, which can be reactivated many months or years after the initial infection, resulting in a relapse [1]. *Plasmodium knowlesi* does not form hypnozoites; recurrence of disease, known as a recrudescence, results from an expansion of circulating blood form populations [9,10].

After invasion of a red blood cell (RBC) by a merozoite, the parasite grows larger feeding on hemoglobin, forming a trophozoite, which matures, finally dividing its nucleus to form a schizont. The reactive heme molecule is detoxified to form hemozoin, or malaria pigment, a crystal that accumulates as the parasite matures and that discolors host tissues [9,10]. The cytoplasm of the schizont eventually segments around each nucleus to form merozoites and the RBC is ruptured to release on average ten merozoites (in *P. knowlesi*) to begin another round of asexual replication [10,11]. This rupture of RBCs is the cause of the malarial paroxysm, characterized by a cold stage with intense chills, shivering and rigors, followed by a hot stage with high fever, flushing, headache, nausea, delirium, and vomiting, and finally, a sweating stage [12]. In monkeys, the paroxysm is less clinically evident because the animals are prey animals and often mask their symptoms unless critically ill, however, common signs include anorexia, lethargy, vomiting, and diarrhea [13]. The frequency of the paroxysm is defined by the period of the parasite life cycle, which ranges from 48-72 hours in the classic four human *Plasmodium* parasite species, and is 24 hours in *Plasmodium knowlesi* [12]. Additionally, the synchronicity at which maturation and lysis occurs determines how neatly the paroxysm can be detected, and even the time of day it is expected

to occur: in asynchronous infections, or in infections that result from the release of multiple broods from the liver, the patient may experience continuous fever and malaise, or paroxysms that occur multiple times in the expected maturation period. In synchronous infections, patients may experience neatly defined paroxysms that occur at a similar time in the maturation period.

The parasite is transmitted by formation of sexual forms known as gametocytes which are derived from immature (ring) form blood-stage parasites by differentiation signals that are not well-defined [14]. When the mosquito takes a blood meal, all of the asexual forms are destroyed, leaving the sexual forms to undergo sexual reproduction, making the mosquito rather than the vertebrate host the definitive host. The temperature change from 37 C to roughly 25 C in the mosquito midgut triggers a process known as exflagellation in the male gametocyte, whereby slender microgametocyte forms are released to fertilize the female gametocyte [5]. Fertilization results in formation of the ookinete, which traverses the midgut epithelium to form a cyst-like structure on the serosal side of the midgut known as an oocyst, wherein sporozoites are formed. Sporozoites then rupture the oocyst and migrate to the salivary glands to be injected into a host the next time the mosquito takes a blood meal [1,9].

1.2: A tale of two hosts: disease resilience and severity

Plasmodium knowlesi is a natural cause of malaria in kra monkeys (*Macaca fascicularis*) and pig-tailed macaques (*M. nemestrina*) [8,15–18]. Kra monkeys thrive across a wide host range that extends from Borneo and the Indonesian and Philippine archipelagos through the Indochina and Malay peninsulas to the northern border of Thailand [8,19]. The parasite was first isolated from a kra monkey that was imported to India in the 1930s from Singapore [20]. It was injected into the model-of-choice there, the rhesus macaque (*M. mulatta*) of Indian origin, where it caused

fulminant disease: catastrophically rising parasitemias, that resulted in 80% parasitemia, and death. Infection of kra monkeys did not result in severe disease, as far as the investigators could tell, as the monkeys quickly controlled parasitemia and developed chronic infections that did not result in death [20]. Subsequent studies involving kra monkeys, though few in number, seemed to confirm the paradigm that based on the metrics of survivability, control of parasitemia, and initiation of chronicity, they did not develop severe disease [21–23]. However, it is important to note, that other metrics of disease severity such as anemia were not widely assessed. The exceptions included a study that reported accidental nosocomial infection of kra monkeys in a drug trial, that demonstrated anemia and high reticulocyte counts, and a small histopathology study that demonstrated low parasite burden in the spleen and liver, moderate anemia, and hypoglycemia [23,24]. Likewise, the nearly universal development of severe disease, hyperparasitemia, and death (without anti-malarial treatment) was established as a feature of *P. knowlesi* infection of rhesus macaques [9,10,25–28].

It is notable that with the exception of a small area of intergradation in northern Thailand, the host ranges of kra monkeys and rhesus monkeys do not overlap: the host range of rhesus monkeys extending from the mid and northern areas of the Indian subcontinent north and eastward throughout southern China [19]. To date, *P. knowlesi* has not been identified in the Indian subcontinent. The extreme virulence of *P. knowlesi* infection in rhesus macaques has been proposed as a factor in macaque species distribution in Southeast Asia, with rhesus macaques being excluded from the Malay and Indochina peninsulas by *P. knowlesi* infection, and the macaques endemic to the regions being excluded from more northern territories by competition with rhesus macaques [29]. Interestingly, the single study documenting resistance to severe disease by rhesus macaques described the monkeys as having longer tails than those of Indian origin, suggesting that

the macaques were misidentified or crossed with kra monkeys (famous for their long tails, and also called long-tailed macaques) [30].

1.3: Making the jump: *P. knowlesi* in humans: history, ecology, and clinical importance

The documented story of *P. knowlesi* infection in humans began in the 20th century with experimental infections of humans [20]. Once it was established that *P. knowlesi* could cause a patent infection in humans, the pathogen was used as a treatment for tertiary syphilis (neurosyphilis) [31]. Known as malaria therapy, patients with tertiary syphilis were infected with blood-stage *P. vivax*, *P. falciparum* or *P. knowlesi* parasites, in many cases resulting in resolution or improvement of the syphilis, presumably through the induction of fever [31–33]. The patient would then be cured of the experimentally induced malaria, with quinine [33]. Malaria therapy ended with the development of penicillin, a much safer and effective syphilis treatment that halted the development of the infection to tertiary syphilis [34].

Until 1965, natural infection of humans by *P. knowlesi* had not been described. That changed when a United States Army surveyor who was camping in Peninsular Malaysia in 1960 contracted malaria and sought medical attention when he returned home [35]. After a diagnostic odyssey to identify the cause of his illness, and then the parasite, it was found that he had contracted *P. knowlesi* when a rhesus macaque that was inoculated with parasites originating from him died from severe malaria [35]. The prospect of the emergence of zoonotic malaria sparked an extensive survey into the prevalence of *P. knowlesi* in the jungles of peninsular Malaysia, which offered the first clues of the ecology of the disease as a zoonosis: over 1110 people from surrounding villages were surveyed and not a single one was positive for *P. knowlesi* (as determined by the clinical outcome in rhesus monkeys that were inoculated with their blood) [18]. Kra monkeys in the area

were demonstrated to carry the parasite, and while no sporozoites that were recovered from trapped mosquitoes produced a patent infection when inoculated into rhesus monkeys, the species identified using human- and macaque-baited traps were forest mosquitoes that did not frequent villages. The conclusion was that *P. knowlesi* could be prevented by avoiding journeys into the forest, where the vector and reservoir were prevalent [18].

From there, cases of *P. knowlesi* seemed to fade back into the mists of the jungle until 2004 when a large rash of cases in Sarawak, Malaysian Borneo presented with naturally acquired *P. knowlesi* infections [6]. As in the 1960 case, people had been originally misdiagnosed as either having been infected with *P. falciparum* or *P. malariae,* however, the clinical manifestations of the cases in question did not fit for those diagnosed with *P. malariae*. *Plasmodium malariae* is typically associated with mild disease; patients in Sarawak were suffering from severe malaria. Driven by this mismatch, patient samples were tested for a variety of *Plasmodium* species using nested PCR techniques, and *P. knowlesi* was identified as the causative agent [6]. Subsequently, cases were identified throughout the region, including in Thailand, the Philippines, Vietnam, Cambodia, Singapore, southern China, Indonesia, and in travelers to the region [36–44].

The rise of *P. knowlesi* in Borneo seems to have occurred as malaria control in Malaysia greatly reduced the number of locally acquired *P. vivax* and *P. falciparum*, suggesting that competition with parasites more suited to humans may have prevented many cases in the past [45]. Additionally, a rise in logging and more transportation into the interior also provide more opportunities for exposure in Sarawak [6,8,46]. Genomics studies suggest that *P. knowlesi* has been able to infect humans for millennia, however, exposure to the parasite and its vector were limited, as many earlier human settlements were restricted to coastal areas, which were easier to settle than was the dense jungle interior [7]. Retrospective studies of archived blood smears also

ruled out a role for misdiagnosis and reduced surveillance prior to the recognition of *P. knowlesi* as a zoonosis [47]. As the 1970 survey suggested, transmission of *P. knowlesi* in Sarawak is highly correlated with jungle trekking, especially in the evenings, and when macaque troops are sighted near camp, including logging, hunting, and hiking activities [46]. The vector implicated in *P. knowlesi* transmission in Sarawak is *An. latens*, a forest-dwelling mosquito that feeds in the evenings [48].

Shortly after the identification of *P. knowlesi* transmission in Sarawak, another focus of intense transmission was found in Sabah, the Bornean state north east of Sarawak [47]. Transmission in Sabah broke the paradigm that monkey malaria could be prevented by avoiding jungle trekking. In contrast to Sarawak, which is covered in primary rainforest, Sabah has been heavily developed for the cultivation of palm oil. With disturbance and the transition from primary to secondary forest and agriculture, came a change in vector [49]. *Anopheles balabacensis*, a mosquito more tolerant of disturbance and peri-domesticity than *An. latens*, is the primary vector of *P. knowlesi* in Sabah [50]. The existence of peri-domestic macaque troops, in combination with *An. balabacensis*, has resulted in clustering of human cases in villages without the need for forays into the jungle [47,51,52]. The proximity of vector and reservoir to villages has made it difficult to determine if human-to-human transmission is occurring, as continuous spillover cannot be ruled out. Additionally, the ability for *An. balabacensis* to serve as a competent vector for *P. knowlesi*, and its tolerance for development, suggests that *P. knowlesi* will remain an important cause of malaria in the region even as jungle areas are developed for agricultural and other uses.

Anopheles latens and *An. balabacensis* feed before people are often in bed and can be protected by a bed net, and many logging and other workers sleep in hammocks, complicating the prospect of using insecticide treated bed nets as a prevention strategy for *P. knowlesi* malaria in

jungle areas; however modeling studies have predicted a benefit to their use [50,53]. Additionally, in Sabah, the presence of a constant reservoir in peri-domestic macaque troops that have established themselves closer to human settlements in response to environmental changes, complicates malaria eradication efforts and threatens to upend malaria elimination in the region.

In addition to presenting a new challenge to malaria control, *P. knowlesi* represents a public health threat. As eluded to above, this parasite can and does cause severe malaria. It has been found to cause severe disease more often than *P. falciparum* and *P. vivax* [54]. Symptomatic disease occurs at lower parasitemias than in *P. falciparum* [54], however cerebral malaria is uncommon. Severe disease is often associated with hyperparasitemia and thrombocytopenia. An intriguing hallmark for severe disease is the presentation of patients with gastrointestinal symptoms [8,54]. At present, it is unknown if gastrointestinal involvement is associated with severe disease because it is intrinsic to the disease process, or because it provides a distraction to the diagnosing physician and therefore represents a delay in treatment. Though clinical indicators of severe and uncomplicated disease have been extensively described, the underlying pathophysiology of the disease and mechanisms that determine disease severity are not well understood in humans [46,54,55]. Only a single autopsy case has been recorded in the literature, due to cultural restrictions on the practice [56]. The natural host, kra monkeys, representing malaria disease on the mild end of the spectrum, and the experimental host, rhesus monkeys, representing malaria disease on the severe end of the spectrum, provide a critical model system to attempt to elucidate the determinants of disease severity that can be applied directly to better understand clinical disease.

1.4: A sticky situation: a role for sequestration in disease severity

Specific host-parasite interactions and disease determinants are not well characterized in the progression to severe disease in humans, or the dichotomy in presentation and outcome in rhesus and kra monkeys. One explanation may be the propensity of the parasite to interact with the endothelium in individual hosts through sequestration. Sequestration is specifically defined as the removal of circulating maturing parasites from peripheral circulation through the cytoadhesive interaction of mature parasitized RBCs with the host endothelium mediated by protein-protein interactions. It is most classically characterized in *P. falciparum*, where the binding partners are *P. falciparum* erythrocyte membrane protein 1 (PfEMP1) and a suite of endothelial proteins associated with endothelial activation [57–60]. The sequestration phenotype manifests histopathologically as tight packing of mature infected RBCs in the capillaries and small venules of tissues, and in some cases, clear studding of larger vessels with parasitized RBCs. Sequestration is associated with disease severity – especially in sites such as the brain and placenta [61–63]. Sequestration in *P. knowlesi* has been eluded to throughout the literature, including histopathological evidence for parasite tissue accumulation in rhesus monkeys that resembles that of *P. falciparum* and parasite replication kinetic patterns [11,25,28,64,65]. However, most of the published rhesus histopathology data involved rhesus infections with high parasitemia, which makes specific scoring of parasitized vessels difficult to distinguish a specific sequestration phenotype from one that is simply full of parasites due to high circulating parasitemias [25–28,64].

Sequestration hinges on there being a specific protein-protein interaction between the endothelium and the parasite, and a candidate to mediate this interaction on the parasite side in *P. knowlesi* is the large (~200 kD) surface-expressed schizont-infected cell agglutination (SICA) protein, encoded by *SICAvar* gene family [66–70]. SICA proteins are responsible for mediating

antigenic variation in response to the production of parasite-specific antibodies produced by the host, which results in waves of recrudescent parasitemia peaks, punctuated by times of low or subpatent parasitemia [71–73]. A function for SICA proteins, aside from antigenic variation, is unknown. While antigenic variation serves as a mechanism to evade the immune response and therefore augment persistence and chronic infection (which may in turn increase transmission by increasing the length of infection and therefore the opportunities to transmit), the parasite could elude immune detection more easily by not altering the host cell surface at all, especially in an RBC that lacks MHC I expression. It begs the question, therefore, what the essential biological purpose of the protein must be, that the parasite would invest such a large energy cost in expressing it, and protecting it by varying it. In *P. falciparum*, the variant antigen PfEMP1 mediates cytoadhesion, which is postulated to prevent the mature, more rigid infected RBCs from circulating through the spleen and being removed in the splenic sinusoids [60,74,75]. SICA proteins are similar to PfEMP1 in many regards: both are encoded by a multi-member gene family (*SICAvar* in the case of SICA proteins, and *var* in the case of PfEMP1), are similar structurally, linked to virulence, involve multiple binding domains, mediate antigenic variation, and are surface-expressed; therefore it follows that a potential function for SICA proteins is cytoadhesion [66–68,72,73,76–81].

Sequestration, should it be occurring in *P. knowlesi*, does not happen to the same extent as does *P. falciparum*, however, it may still be important to pathophysiology. For instance, *P. vivax*, like *P. knowlesi* demonstrates kinetics that suggest the existence of a population of sequestering parasitized RBCs: fewer than expected maturing infected RBCs are noted in circulation [82]. Though shown to lack large variant antigens, *P. vivax* has been demonstrated to bind endothelial proteins and cells through interactions with its VIR proteins (which are smaller surface-expressed

variant antigens, encoded by the *vir* gene family unrelated to *SICAvar* and *var* genes) [82–84]. While it is unclear if this is one possible mechanism of several, or the primary mechanism of *P. vivax* tissue accumulation, it has been revealed that tissue accumulation of *P. vivax* parasites has biological consequences for the host (Chapter 2, and [85]).

Sequestration could explain the role for gastrointestinal symptom presentation in severe disease. *Plasmodium falciparum* has been demonstrated to sequester extensively in the gastrointestinal tract, which in turn has been associated with clinical signs and symptoms such as epigastric pain, nausea, vomiting, and diarrhea, and histopathological evidence such as gastritis and duodenitis [62,63,86,87]. Parasite accumulation could elicit an immune response and inflammation in the gastrointestinal tract, thereby causing a direct mechanism for the symptoms observed in patients. The link of SICA proteins and sequestration to virulence could also explain the different host disease outcomes that are observed in kra and rhesus monkeys.

1.5 The early bird and moderation: a role for host response in disease severity

Invasion studies of RBCs from various primate species quantifying replication rate and merozoite attachment have not explained the rapidly rising parasitemias of *P. knowlesi* in rhesus monkeys [88]. However, invasion gene duplication and expanded RBC age preference has been demonstrated to occur in response to selection of *in vitro* culture of *P. knowlesi* parasites to human RBCs, and may represent an adaptation relevant to the spillover and development of severe malaria in humans [89,90]. Another factor that could explain the differences in presentation in humans and in rhesus and kra monkeys is the timing of the host response, and how the host modulates that response. That *P. knowlesi* asexual blood stage parasites mature in 24 hours is critical, as it is unique amongst primate-infecting *Plasmodium* parasites to do so; the other species require about

48 hours, or 72 hours in the case of *P. malariae* [91]. *Plasmodium knowlesi*, therefore takes half to one third the amount of time to replicate at least ten-fold. As such, the host ability to sense and respond to the parasite may be critical to controlling replication quickly before the parasite reaches densities that cannot be contained. Systemic endothelial activation has been linked to disease severity in humans, offering up an additional factor to consider: the host must respond in a timely fashion, but do so appropriately [92]. Clinical parameters have not been described in detail for *P. knowlesi* infections of kra monkeys. Understanding how the natural host controls infection may shed light on understanding what seems to go so terribly awry in rhesus macaques, and taken together with rhesus data, may reveal important details relevant to which *P. knowlesi* patients are at risk for developing severe malaria.

1.6 Concluding remarks

Plasmodium knowlesi is a unique and emergent zoonotic parasite that represents a public health threat. The parasite has been documented to cause a spectrum of disease, including severe manifestations and death in humans, and is lethal in the experimental host, rhesus macaques. Despite the proclivity for severe disease in humans and rhesus macaques, the natural host, kra monkeys, do not experience hyperparasitemia or death. Many aspects concerning why these hosts experience such a disparity in disease presentation, progression, and outcome are unknown, but may include a role for sequestration or host response.

This dissertation seeks to begin to answer central questions concerning the life history of *P. knowlesi* infection in hosts susceptible and resistant to the development of severe disease. For the first time, clinical parameters in kra monkeys will be described in an effort to identify points in the infection that may be important to parasite control. Parallel infections in rhesus monkeys

were also performed and designed to understand disease processes that occur before hyperparasitemia, and in such a way that the parasitemias can be compared to those occurring in severe cases of human *P. knowlesi* cases. Additionally, the role of parasite accumulation with malaria caused by parasites traditionally not thought to sequester, including *P. vivax* and *P. knowlesi,* will be explored and mapped, with special emphasis on the gut to begin to assess its role in the development of severe malaria in humans.

Chapter 2: *Plasmodium vivax* parasite load is associated with histopathology in *Saimiri boliviensis* with findings comparable to *P. vivax* pathogenesis in humans[1]

2.1 INTRODUCTION

Plasmodium vivax is the most widespread malaria parasite and causes an estimated 15.8 million clinical cases annually [93]. Although *P. vivax* can cause serious and fatal disease [94], the mechanisms that underpin these complications remain poorly defined [95,96].

Several studies have explored the association between the *P. vivax* parasite tissue load and disease severity. Clinical studies have correlated plasma parasite biomass markers to systemic inflammatory markers [97] and intravascular accumulation of immune cells or parasites to lung injury [98]. Autopsy analyses have demonstrated the presence of parasites in histopathological sections [94], and in vitro adhesion of *P. vivax* infected red blood cells (iRBCs) to lung endothelial cells suggests that a cytoadhesion mechanism may be functioning in the lungs [82–84]. However, none of these studies have directly examined how histopathology relates to tissue parasite load.

Pathology studies with human cases can be limited by confounding factors such as coinfections, chronic diseases, and lack of information on exposure status or duration of infection. Nonhuman primate models can be utilized to overcome these limitations and expand knowledge on *P. vivax* pathogenesis, through the direct study of *P. vivax* in New World monkeys [99,100].

---

[1] This chapter has been previously published:
Mariko S. Peterson, Chester J. Joyner, Regina J. Cordy, Jorge L. Salinas, Deepa Machiah, Stacey A. Lapp, Esmeralda V.S. Meyer, Sanjeev Gumber, Mary R. Galinski. (2019). "*Plasmodium vivax* Parasite Load is Associated With Histopathology in *Saimiri boliviensis* With Findings Comparable to *P vivax* Pathogenesis in Humans." *Open Forum of Infectious Diseases.* 6(3): ofz021.

Results from this chapter were presented as a poster at the 6th International Conference on *Plasmodium vivax* Research in Manaus, Brazil. June 11-14, 2017, abstract number 63215.

Here, we demonstrate that histopathology is directly associated with parasite prevalence and hemozoin deposition in specific tissues. We scored the histopathology observed in organ tissue sections from a cohort of *Saimiri boliviensis* that were experimentally infected with *P. vivax* (Brazil VII strain) [101] and quantified the parasite load in each tissue type to assess the relationship of parasite load and the severity of histopathology. Pathology was mainly observed in the lungs, liver, and kidneys and determined to be generalizable to findings from malaria autopsy cases [94,102].

2.2 METHODS

Tissue acquisitions from *Saimiri boliviensis* infected with *P. vivax*

Tissues were collected at necropsy from seven *S. boliviensis* that were infected with *P. vivax* Brazil VII strain iRBCs [101] for multi-omic studies, as described in detail elsewhere [103,104]. Healthy, malaria-naïve squirrel monkeys (*S. boliviensis,* six male, one female*)* were acquired from the Michale E. Keeling Center for Comparative Medicine and Research at the University of Texas-MD Anderson Cancer Center and transferred to the Yerkes National Primate Research Center (YNPRC), an AAALAC International-accredited facility. Male monkeys were preferably selected to eliminate confounding variables such as anemia stemming from menstruation. Six monkeys were splenectomized prior to infection to ensure highest parasitemias, and one was left intact. Appropriate enrichment activities were provided and prior to being infected, the animals received positive reinforcement training to perform leg-prick procedures to attain capillary blood samples for making smears. Veterinary and behavior experts monitored the animals daily for signs of disease and distress. All experimental plans were approved by Emory University's Institutional Animal Care and Use Committee (IACUC).

To initiate infections, about $1x10^7$ cryopreserved iRBCs were thawed and injected intravenously into one *S. boliviensis*. The remaining monkeys were serially inoculated by transferring 0.5 mL of parasitized blood from infected monkeys when their parasitemia was approximately 1%. Parasitemias were monitored daily by quantifying the number of iRBCs out of 1000 total RBCs or by the Earle and Perez method [105] in Giemsa-stained thin and thick films, respectively. As parasitemias peaked and at necropsy, peripheral blood was collected, and aliquots were cryopreserved for future use [103,104]. Each animal was euthanized according to IACUC approved guidelines. Infected tissue samples were collected from selected organs as noted in the results. Normal tissue sections were obtained for comparison from the YNPRC archival bank of NHP specimens.

Histopathology, pathology scoring, and parasite quantification

Tissue samples were fixed in 10% neutral buffered formalin, paraffin embedded, sectioned at 4 μm, and stained with hematoxylin and eosin (H&E) [106]. Where indicated, sections were also stained with Masson's trichrome or Perl's stain [106]. Sections were blinded for pathological and parasitological analysis. The organs were scored in 11 categories: inflammation, edema, necrosis, hemorrhage, hyperplasia, fibrosis, vasculitis, hypoplasia, degeneration, hemosiderosis, and others. Within each of these categories, the scores were determined on a range from 0 to 4, with 0 representing normal tissue, 1 minimal damage, 2 mild damage, 3 moderate damage, and 4 severe damage. Scores were then summed to obtain a total pathology score for each organ for every monkey. Parasites were quantified by counting the total number of parasites observed (mature trophozoites and schizonts) in 60 consecutive, 1000X light microscopic fields. In total, 319 sections were quantified for parasite load and examined histologically. These included

multiple sections for every organ to ensure representative coverage of the pathology and parasite load of each organ.

Immunohistochemistry

Immunohistochemical (IHC) staining of lung, liver, and kidney sections was performed using a biotin-free polymer system. The sections were deparaffinized in xylene, rehydrated in graded series of ethanol, and rinsed with distilled water. Antigen retrieval was performed by immersing sections in DIVA Decloaker (Biocare Medical) at 125°C for 30 seconds in a steam pressure decloaking chamber (Biocare Medical) followed by blocking for 10 minutes with SNIPER Reagent (Biocare Medical). The sections were incubated with mouse anti-human CD163 (clone 10D6; Abcam), mouse anti-human thyroid transcription factor 1 (TTF-1) (clone 8G7G3/1, Dako), or mouse anti-*Plasmodium* lactate dehydrogenase (LDH) (clone 19, MyBioSource) overnight at 4°C followed by a detection polymer system (MACH 2™; Biocare Medical, or in the case of anti-TTF1 staining, EnVision+ System-HRP Labeled Polymer, Dako). Antibody labelling was visualized by alkaline phosphatase chromogen development (Warp Red Chromogen Kit; Biocare Medical), or for anti-TTF1 staining, immunoperoxidase with 3-3' diaminobenzidine. Nuclei were counter stained using Mayer's hematoxylin (Vector Laboratories).

Statistical analysis

The Fisher's Exact test, multiple linear regression and Spearman correlations were calculated to determine relationships between pathology score and tissue parasite load. The Tukey post-hoc honest significant difference (HSD) comparisons test was used to determine significant

differences between parasite load and histopathology score groups. All statistical analyses were produced using R Studio version 1.1.383, under R version 3.4.3 GUI version 1.70.

2.3 RESULTS

Parasite kinetics of *P. vivax* Brazil VII infection in *S. boliviensis*

Parasitemia was monitored daily after inoculation of the monkeys (Supplemental Figure 6.1) [107] (mean maximum parasitemia was 70,572 parasites/μL with a range of 55,000 – 90,000 parasites/μL). Mean parasitemia at necropsy was 61,572 parasites/μL, and the range was 25,000 – 90,000 parasites/μL. The animals were euthanized after reaching a sustained parasitemia close to 1% and immediately necropsied for pathology analyses. The mean duration of infection was 15.71 days (with a range of 10 – 24 days). Infection parameters are summarized in Supplemental Table 6.1.

Plasmodium vivax Brazil VII infection of *S. boliviensis* causes lung, liver, and kidney tissue damage

Lung, liver, kidney, brain, gastrointestinal tract, gonads, heart, adrenal gland, lymph nodes, bone marrow, and spleen (from the one spleen-intact monkey) were acquired at necropsy for histopathology analyses. Brain, gastrointestinal tract, gonads, heart, adrenal gland, and lymph node sections did not reveal major pathological lesions specific to malaria. However the lungs, liver, and kidneys exhibited significant histopathological damage (Supplemental Table 6.2, Figures 2.1-2.3) similar to that observed in human malaria cases [63,94]. Additionally, H&E-stained sections of the bone marrow revealed hypercellularity in all monkeys. All monkeys had mild to moderate

pulmonary edema. Multifocal areas of alveolar wall thickening and inflammation were observed in the lung tissues consistent with interstitial pneumonia (Figure 2.1A). Type II cell hyperplasia, indicative of lung injury, was demonstrated by increased numbers of cells labeled with anti-thyroid transcription factor 1 (TTF-1) (Figure 2.1B). Interstitial collagen deposition was observed in the lung sections from two monkeys (Figure 2.1C). The tissues from four monkeys exhibited focal hemorrhage. Birefringent pigment consistent with hemozoin, was diffusely observed in CD163+ macrophages and infected erythrocytes [108]. Infiltration of CD163+ cells was also observed in the alveolar wall and the alveoli, and these were increased relative to normal *Saimiri* lung tissue (Figure 2.1D).

Diffuse hepatocellular vacuolar degeneration was observed in all monkeys (Figure 2.2A). The periportal areas were infiltrated by moderate numbers of mononuclear cells (Figure 2.2A). Pigment-laden macrophages and pigmented parasites were diffusely distributed in the sinusoids throughout the liver. The pigment was birefringent under polarized light (Figure 2.2B). In two individuals, the portal areas were occasionally expanded by a small to moderate amount of collagen (Figure 2.2A), also shown highlighted by Masson's Trichrome (Figure 2.2C). In addition, the liver parenchyma had an increased number of pigment-laden CD163+ macrophages with morphology consistent with Kupffer cells compared to normal *Saimiri* liver tissue (Figure 2.2D). Overall, inflammation and fibrosis were localized in the perivascular spaces, including sinusoidal and periportal regions, suggesting liver injury originating from the presence of circulating parasites.

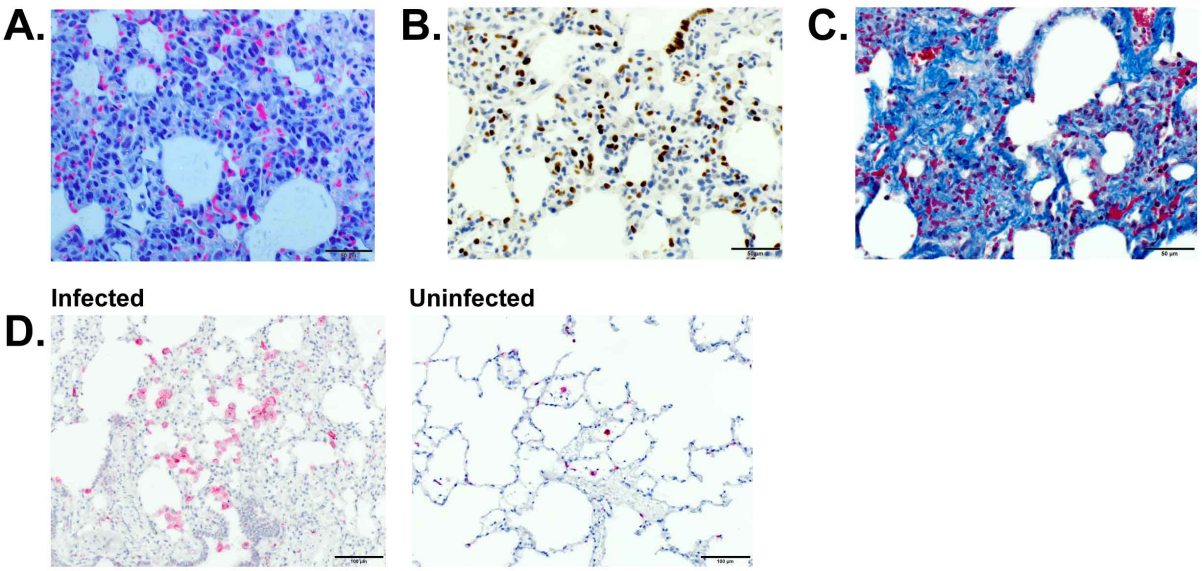

Figure 2.1 Lung tissue sections with representative micrographs showing histopathology. A, Marked type-II pneumocyte hyperplasia alveolar wall thickening and inflammation in a splenectomized monkey, and hemozoin-laden cell infiltration in an H&E-stained section under polarized light. Scale bar = 50 μm. B, Anti-αTTF1 immunohistochemical staining highlights type II pneumocyte hyperplasia in a splenectomized monkey. Type II pneumocytes are indicated by dark brown labeling. Scale bar = 50 μm. C, Extensive interstitial collagen deposition in alveolar wall stained blue with Masson's trichrome in the spleen-intact monkey. Scale bar = 50 μm. D, Numerous immunohistochemically labeled CD163+ cells (fuschin red) infiltrate the alveoli and alveolar walls in the spleen-intact monkey (left) relative to few CD163+ cells in the lungs of an uninfected *S. boliviensis* monkey (right). Scale bar = 100 μm.

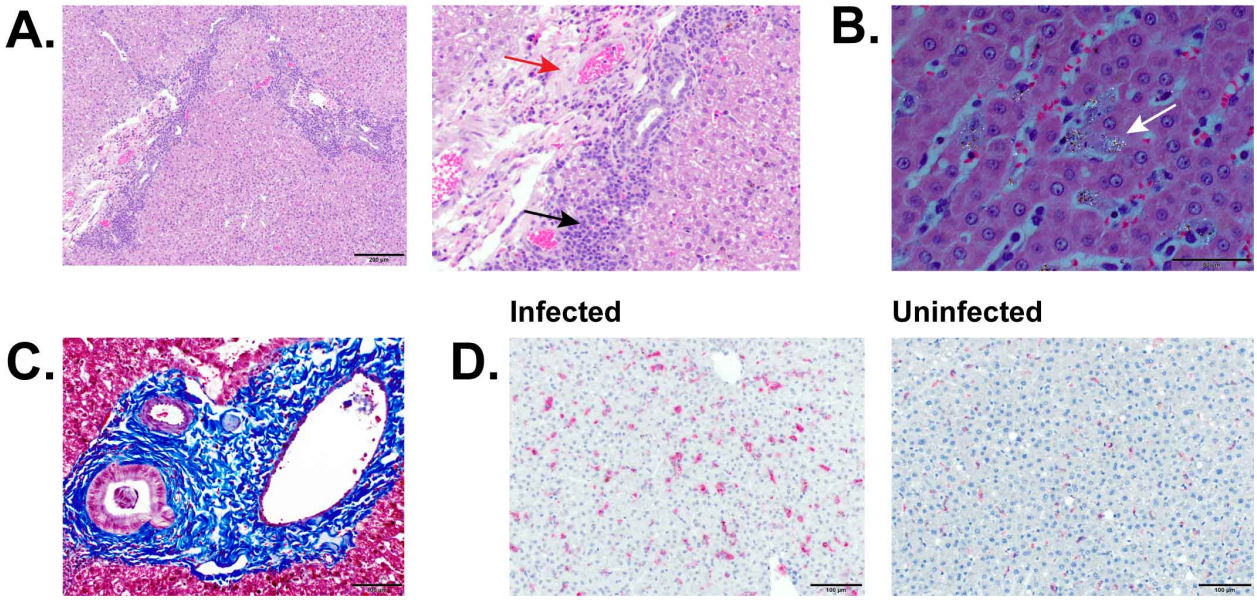

Figure 2.2 Liver tissue sections of splenectomized monkeys with representative micrographs showing histopathology. A, H&E-stained section shows small amounts of collagen deposition and two foci of mononuclear periportal infiltrate (left). Scale bar = 200 µm. A zoomed in image at the same magnification is shown to highlight the collagen deposition (red arrow) and mononuclear infiltrate (black arrow). B, H&E-stained section viewed with polarized light shows hemozoin-laden macrophages highlighted by white birefringence with sinusoidal congestion (white arrow). Scale bar = 50 µm. C, Masson's trichrome stained section with collagen deposition in the periportal region shown by deep blue staining. Scale bar = 100 µm. D, Immunohistochemically stained section showing numerous CD163+ stained cells (fuschin red) and counter stained with hematoxylin in the hepatic parenchyma (left) relative to uninfected *S. boliviensis* liver tissue (right). Scale bar = 100 µm.

The kidneys showed multifocal cortical interstitial mononuclear infiltrates, especially in the periglomerular regions, consistent with nephritis (Figure 2.3A). The tubules were eosinophilic and swollen, with hyaline casts. Each infected monkey had enlarged, hypercellular glomeruli, infiltrated with hemozoin-laden CD163+ macrophages, relative to normal *Saimiri* glomeruli (Figures 2.3B, 2.3D). To differentiate hemosiderin, which can result from erythrocyte lysis, and parasite hemozoin, Perl's stain was employed, which reacts with hemosiderin, coloring it blue. This stain does not react with hemozoin, leaving it black. Interestingly, Perl's stain revealed localization of pigment consistent with hemosiderin in the glomeruli and stained granules in the tubules blue, consistent with hemosiderin secretion (Figure 2.3C).

To compare the extent of histopathological changes, the tissues from each infected *S. boliviensis* were scored, on a scale from 0 to 4, in 11 criteria and these criteria were summed to obtain a total pathology score for each organ. Mean total pathology scores (Figure 2.4A) for the organs of seven monkeys were highest for lung (mean=7.29, standard error = +/-0.81), kidney (7.00, +/-0.65), and liver (mean=6.14, +/-0.63). The gastrointestinal tissues, colon and stomach (mean=2.67, +/-0.67; mean=2.33+/-0.61, respectively) had low scores. The brain was normal (mean=0, +/-0). The mean score across all tissues was 5, +/-0.50, and the median was 4.33. Lymph nodes, gonads, heart, spleen, and bone marrow were not scored because they showed no major histopathological lesions. Statistically significant differences between organ scores were assessed using Tukey's HSD post-hoc pairwise comparison test. The mean pathology scores of kidney, liver, and lung, were significantly higher than brain, stomach, and colon (Supplemental Table 6.3).

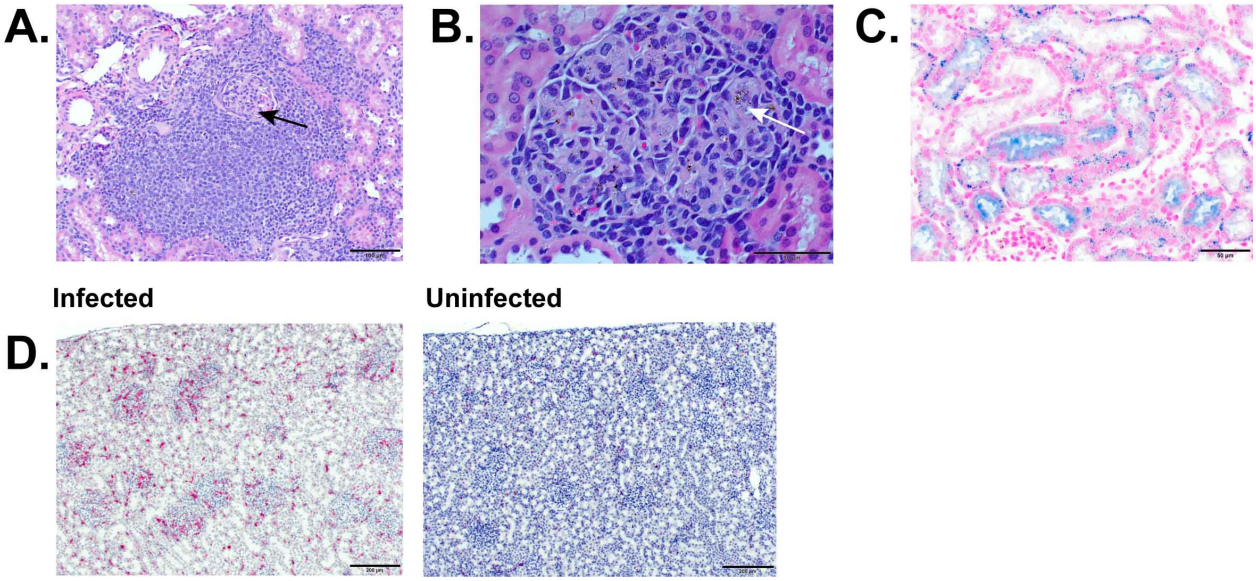

Figure 2.3 Kidney tissue sections of splenectomized monkeys with representative micrographs showing histopathology. A, An H&E-stained section of renal cortex showing massive mononuclear infiltrate surrounding a glomerulus (black arrow). Scale bar = 100 µm. B, H&E section with polarized light showing a hypercellular glomerulus with hemozoin-laden macrophage infiltrate (white arrow). Scale bar = 50 µm. C, Positive Perl's stain in the tubules showing hemosiderin deposits (blue). Counter stain is eosin (pink). Scale bar = 50 µm. D, Marked CD163+ cell infiltration in the glomeruli and renal cortex (fuschin red) and counter stained with hematoxylin in this IHC-stained section, relative to an uninfected *S. boliviensis* kidney section (right). Scale bar = 200 µm.

Tissue damage is associated with parasite prevalence in specific organs

To test if *P. vivax* parasite load correlated with organ pathology, parasite counts were obtained from sections of 10 organs, plus the spleen from the intact animal (Figure 2.4B). In total, parasites were counted in 319 sections. Trophozoites, schizonts, and gametocytes can be readily visualized in H&E-stained histological sections (Figure 2.4C) [62], and select sections were also stained with anti-*Plasmodium* lactate dehydrogenase (pLDH) antibody as a confirmation method (Figure 2.4C) [99,109]. The mean number of parasites across all sections was 17.61 per 1000X high-power field (HPF), with a standard error of 2.24. As expected due to high erythrocyte density in the red pulp (Figure 2.4D), the spleen sections contained the most parasites per HPF (the mean between two sections from the non-splenectomized animal was 206, with a standard error of 25). The liver (mean=71.56 +/-15.11), lungs (mean=52.20, +/- 7.13), bone marrow (mean=39.43, +/- 10.08, Figure 2.4D), and adrenal glands (mean=35.2, +/- 4.97) also carried significant parasite loads. The gastrointestinal organs (mean=0.92, +/- 0.18), brain (mean=1.95, +/- 0.32), heart (mean=4.05, +/- 1.2), and kidneys (mean=7.35, +/- 1.27) exhibited low parasite loads. The gonads and lymph nodes also exhibited a paucity of parasites (mean=0.8, +/- 0.18; mean=2.97, +/- 0.59, respectively).

Parasite counts were analyzed for significant differences using the Tukey's HSD post-hoc pairwise comparisons tests (Supplemental Table 6.4). The spleen tissue section counts were significantly higher as compared with all other organs. The liver and lung parasite counts were not significantly different from one another, nor from the bone marrow and adrenal gland counts. However, they were significantly higher than the parasite counts from kidney, heart, lymph node, brain, gastrointestinal tract, and gonad sections.

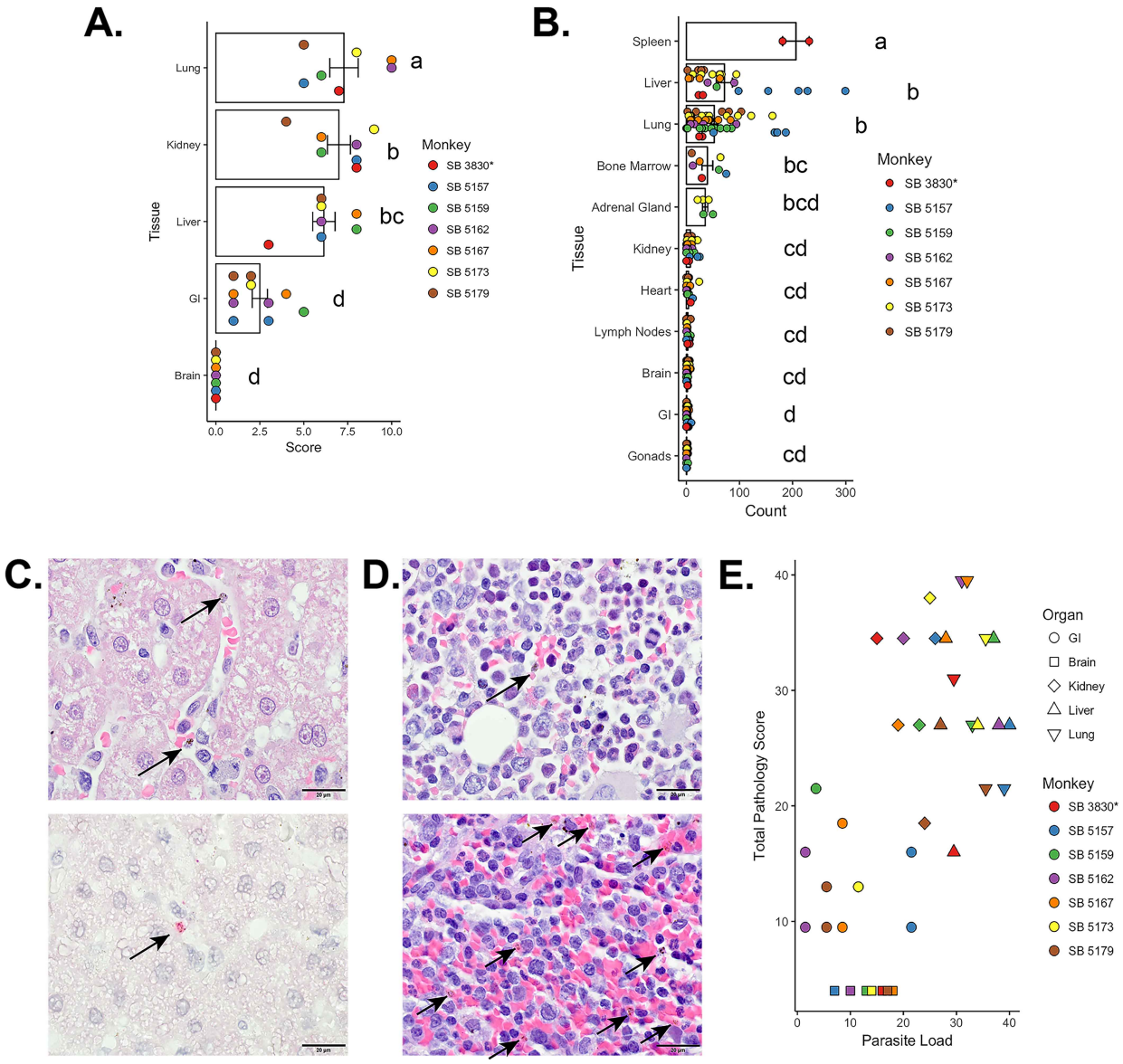
A.
Lung
Kidney
Liver
GI
Brain
a
b
bc
d
d
Tissue
0.0
2.5
5.0
7.5
10.0
Score
Monkey
SB 3830*
SB 5157
SB 5159
SB 5162
SB 5167
SB 5173
SB 5179
B.
Spleen
Liver
Lung
Bone Marrow
Adrenal Gland
Kidney
Heart
Lymph Nodes
Brain
GI
Gonads
a
b
b
bc
bcd
cd
cd
cd
cd
d
cd
Tissue
0
100
200
300
Count
Monkey
SB 3830*
SB 5157
SB 5159
SB 5162
SB 5167
SB 5173
SB 5179
C.
D.
E.
40
30
20
10
Total Pathology Score
0
10
20
30
40
Parasite Load
Organ
GI
Brain
Kidney
Liver
Lung
Monkey
SB 3830*
SB 5157
SB 5159
SB 5162
SB 5167
SB 5173
SB 5179

Figure 2.4 Histopathological and parasitological tissue analysis, in the organs of seven infected *S. boliviensis*. The asterisk indicating spleen-intact animal. A, Histopathological tissue scores: the means, data points, and standard errors are reported, with the height of the bar showing the mean, the dots indicating individual data points, and error bars showing the standard error of the mean. Statistical significance as determined by the Tukey HSD test is indicated by letters above the bars. Each data point represents the whole organ score obtained from examination of H&E stained tissue sections. B, Quantification of parasite load in the organs. 319 sections were examined. Each data point represents the total number of parasites in 60 consecutive oil-immersion (1000X) fields in a single H&E stained section. C (top), Mature parasites are readily identifiable in H&E-stained sections (black arrows). Scale bar = 20 μm. C (bottom), Select sections were stained with anti-parasite LDH antibody (fuschin red) and counterstained with hematoxylin as an alternative means to show and confirm parasite presence (black arrow). Scale bar = 20 μm. D, Representative H &E stained sections of bone marrow from a splenectomized animal (top), and the spleen from the intact animal (bottom) indicating the distribution of parasites (black arrows). E, Histopathological score versus organ parasite load. Scatter plot of the rank of the sum of the parasite counts in 60 consecutive oil-immersion (1000X) fields in all sections of a given organ in a given monkey plotted against the rank of the total pathology score. Only tissues with scores were included.

To test the association between parasite load and histopathological scores, the parasite count data from individual sections were averaged to obtain whole organ counts for each monkey and these were divided into high parasite load (greater than the mean of the organ parasite averages, 23) and low parasite load (less than 23) categories. Only organs for which there were scores available were considered. Organ histopathological scores were divided into high score (greater than the mean score, 5) and low score (less than 5). The resultant 2 x 2 contingency table is presented in Supplemental Table 6.5. Organs with high pathology scores were 22.09 times more likely to have a high parasite load than a low parasite load, with a p-value of 0.00057.

To test the correlation between histopathological score and parasite load, multiple linear regression was performed. The parasite count was weakly, but significantly positively linearly associated with pathology score, with an adjusted $R^2 = 0.105$ and p-value = 0.0235 (Supplemental Table 6.5). However, once organ was added as an effect in the regression model, the trend became strongly linear (R^2=0.7505, $p < 0.00001$), with the organ effect being so strong that the contribution of parasite count to pathology score was no longer significant. Multicollinearity and interaction between count and organ were ruled out. Additional parameters that might affect histopathology including the maximum parasitemia (defined as the maximum parasitemia reached in parasites/μL), days at parasitemia equal to or greater than 50,000 parasites/μL, the proportion of days with parasitemias equal to or greater than 50,000 parasites/μL, the duration of the infection, and the parasitemia at the time of necropsy were also considered and tested using a hierarchical multiple linear regression modeling approach. None of these parameters contributed significantly to the model.

As the regression analysis demonstrates, pathology score and parasite count do not have a linear relationship. To test the association between pathology score and parasite count, Spearman

correlation coefficients were calculated (Supplemental Table 6.6). Here, pathology score showed a significantly and moderately strong positive association with parasite count, with Spearman's ρ = 0.6034, and an adjusted p-value of 0.0002 (ranked values plotted in Figure 2.4E). Maximum parasitemia, days at parasitemia greater than or equal to 50,000 parasites/μL, proportion of days at or greater than 50,000 parasites/μL, duration of infection, and parasitemia at the time of necropsy were also tested, and none of the resultant ρ values were found to be significant. p-values were corrected using Bonferroni's post-hoc correction to account for multiple tests.

2.4 DISCUSSION

This quantitative analysis of tissues from longitudinal infections of *P. vivax* (Brazil VII) in a cohort of naïve *S. boliviensis* has enabled the discovery of specific relationships between parasite load and histopathology. Previous work showed that a reduction of the proportion of circulating schizonts compared to rings and trophozoites in clinical cases is associated with increased adherence of the more mature iRBCs to endothelial cell lines [82], potentially mediated by membrane-associated variant interspersed repeat (VIR) proteins [84]. Additionally, gas exchange studies have pointed to parasite or immune cell accumulation in lung vasculature as a possible mechanism for respiratory distress in patients [98]. Recent retrospective tissue analyses of *P. vivax* (Salvador-I strain) infections of non-naïve *Aotus nancymae* and *S. boliviensis* monkey highlighted enrichment of parasites in the bone marrow, liver and lungs, providing further evidence of the accumulation of *P. vivax* iRBCs in tissues [99].

Important pathological findings from *P. vivax* clinical cases have been replicated here in the *S. boliviensis* model, particularly in the lungs, liver and kidneys. Mononuclear infiltrates were

evident in tissue sections from lungs, periportal areas of the liver, and kidneys. This is consistent with autopsy assessments from human *P. vivax* and *P. falciparum* cases [63,94,102,110] and necropsy analysis from a severe infection of the *P. vivax* model organism, *P. cynomolgi* in a rhesus macaque [111]. More macrophages were observed in the lungs, liver and kidneys, compared to uninfected individuals. Alveolar wall thickening with macrophage infiltration, type II pneumocyte hyperplasia and collagen deposition, and histological evidence of pulmonary edema were all evident in the *S. boliviensis* tissues. Respiratory complications in vivax malaria have been well-documented [102,112–114] and associated with significant mortality in humans [115], and *P. vivax* iRBCs have been visualized in the lungs of autopsy cases [94]. Periportal inflammation, sinusoidal congestion and Kupffer cell hyperplasia have been demonstrated here and with severe *P. falciparum* malaria [116]. Hemozoin-laden CD163+ macrophages were identified in the kidneys (Figure 2.4B) and noted with *P. falciparum*-associated kidney damage [110]. Lastly, a significant number of *P. vivax* iRBCs were observed in the bone marrow. This is consistent with studies noting enrichment of *P. vivax* and *P. falciparum* iRBCs and hemozoin in the bone marrow, especially gametocytes, in support of this tissue being a niche for parasite persistence to ensure transmission [99,117].

The linear regression analysis indicated organ-specific tissue injury was attributed to the presence of parasites. The lungs and liver exhibited high parasite loads and corresponding high pathology scores. The kidneys on the other hand had low parasite counts, but significant damage. We speculate that this represents an example of organ-specific injury arising from systemic or local inflammation due to the presence of parasite byproducts; namely hemozoin. Strikingly, nearly every glomerulus contained hemozoin-pigmented macrophages. Hemozoin is an immunomodulatory insoluble crystalline metabolite of heme detoxification [118], which has been

implicated in kidney damage with *P. berghei* infection [119], chronic inflammation after *P. yoelli* and *P. chabaudi* blood-stage infections [120], and dyserythropoiesis in *P. falciparum* malaria [121]. Additionally, Perl's stain confirmed the presence of hemosiderin in the renal tubules, consistent with RBC destruction. Hemosiderin is a byproduct of erythrocyte lysis, and studies have shown that most RBCs destroyed during malaria are uninfected [122,123]. Hemosiderin deposition as a sentinel to free hemoglobin and heme-mediated tissue injury during malaria has been associated with acute kidney injury [124].

The spleen is a critical organ for malarial immunity [125–127]. Importantly, the pathology scores overall across the tissues from the one spleen-intact animal were comparable to those from the splenectomized animals, suggesting that splenectomies intended to increase parasitemias may not be needed to study pathology. That is, next to the spleen, most parasites from this animal were similarly found in the liver, lung, and bone marrow. Another recent NHP study involving *P. vivax*-infected common squirrel monkeys (*Saimiri sciureus*) and night monkeys (*Aotus lemurinus lemurinus*), which quantified parasites from organ crushes and blood films, suggested that *P. vivax* parasites preferentially distribute to the spleen, and then to secondary sites [100]. Our observations are consistent with this interpretation. This increased distribution to secondary sites in the absence of a spleen may also explain the relatively large parasite load observed in the bone marrow by Obaldia, *et al* [99].

Parasite biomass has been associated with increased disease severity in clinical studies, however, these findings in humans failed to find an association between parasite biomass and soluble endothelial activation markers systemically [97]. The authors proposed a significant parasite reservoir in organs where the microvasculature is not lined with endothelium, such as the bone marrow and spleen [97]. Our observations of significant numbers of parasites in the spleen

of the intact monkey, primarily concentrated in the red pulp, and reduced numbers of parasites in other organs relative to the splenectomized individuals, supports this hypothesis. Parasite or parasite byproduct presence in specific organs, such as the lung, kidney, or liver, may cause local inflammation, tissue damage, and disease manifestations, as we observed, but may not result in systemic endothelial activation.

This study, which directly associates organ parasite load with histopathology using an NHP model of *P. vivax* infection, it is not without limitation. The animals were splenectomized to ensure higher peripheral parasitemias for the collection of infected RBCs. The experimental removal of the spleens could raise questions on the translatability of this model to humans. However, the data from the single spleen intact animal used for comparisons here suggests that histopathology will be similar irrespective of the presence or absence of a spleen. Notably, this conclusion must be interpreted with caution, however, because only a single spleen-intact animal was included here. Nevertheless, our data suggests that spleen-intact animals can be used for future studies with this parasite strain. Finally, complete blood counts and blood chemistries were not available for analysis here due to the retrospective nature of the study. This limitation makes it difficult to correlate the histopathology with systemic changes indicative of disease such as decreases in hemoglobin, increases in liver enzymes, indicators of lung function, or disruption of kidney function. Future prospective studies should include these measurements to determine how the histopathological changes may influence disease presentation.

In summary, this quantitative study has demonstrated the accumulation of *P. vivax* iRBCs in spleen, lung, liver, bone marrow and adrenal gland tissues, and a paucity of iRBCs in highly perfused organs including the gastrointestinal tract, heart, kidney and brain. Histopathology was most notable in the lung, liver, and kidney. Moreover, the accumulation of iRBCs in tissues is

positively associated with tissue damage, with multiple linear regression models suggesting a strong effect for tissue-specific histopathological changes. However, as shown for the kidney, disease processes can be attributed to parasite byproducts. Future research using this animal model could be warranted to study tissue-specific *P. vivax* pathological manifestations, the relationship between parasite biomass, systemic immune activation and pathology, and to test interventions.

Chapter 3: Disease resilience and malaria: host resistance and disease severity in *Macaca mulatta* and *M. fascicularis* to *Plasmodium knowlesi* infection[2]

3.1 INTRODUCTION

Since its relatively recent recognition as an emergent zoonosis, *Plasmodium knowlesi* has risen as the major cause of human cases of malaria in Malaysia, and threatens to upend malaria elimination in the region [6,8,128,47,45]. Human cases have been identified throughout Southeast Asia, including Thailand, Indonesia, the Philippines, Singapore, and Vietnam [36,38,40,42,43,129]. Two species of macaques endemic to the Malayan peninsula and Borneo, *Macaca fascicularis* (the kra monkey), and *Macaca nemestrina* (the pig-tailed macaque) are natural hosts of the parasite and are thought to be major reservoirs for human infection [130,16,15]. The parasite causes a spectrum of disease in humans, ranging from asymptomatic and mild presentations to organ failure and death, however it is thought that it does not cause severe disease in kra monkeys [8,22,54,56,131]. A paucity of studies exist, however, they describe the natural course of infection in kra monkeys with host-limited parasitemias that reach at most 1-3%, and that reach chronicity with little mortality [10,20–23]. *Macaca mulatta*, the rhesus macaque, however, exhibits a catastrophically expanding primary parasitemia peak that reaches upwards of 50% infection of red blood cells, and nearly universal clinical collapse and mortality if no treatment is administered [10,20,28,91,132]. The rhesus macaque is an experimental host, and is not naturally infected with *P. knowlesi*, nor does its host range significantly overlap with that of pig-tailed macaques and kra monkeys [8,10,19]. Understanding the factors that determine host disease

[2] Results from this chapter were presented as a poster at Gordon Research Conference: Malaria. June 30 – July 5, 2019 in Les Diablerets, Switzerland, and also as a poster in the associated Gordon Research Seminar (June 29 – 30, 2019).

severity and resiliency is a major puzzle in infectious disease, and we use this two-host model: the kra monkey, which is resilient to lethal disease, and rhesus macaque, which succumbs to lethal disease nearly universally, for susceptible and severe disease in *P. knowlesi* malaria to address this question. Here we report that although none of the kra monkeys succumbed to infection and few (2/15) developed parasitemias greater than 1%, all of the kra monkeys developed malaria disease, including anemia, thrombocytopenia, fever, and in some monkeys kidney derangement. Additionally, despite the development of severe malaria, all of the kra monkeys spontaneously improved without the use of anti-malarial drugs. Finally, kra monkeys responded earlier to infection than did rhesus monkeys, and when rhesus monkey parasitemias were controlled subcuratively, they eventually were able to control infection on their own.

3.2 METHODS

Experimental Design and Infections

Macaca mulatta (rhesus) and *Macaca fascicularis* (kra) monkeys were selected as hosts susceptible and resilient to fatal disease, respectively, to study the acute and chronic manifestations of *Plasmodium knowlesi* malaria, and ascertain determinants of malaria resiliency. A total of 11 rhesus macaques and 15 kra monkeys, across five cohorts were included in this study. All monkeys were healthy and malaria-naïve. Male monkeys were selected to eliminate exacerbation or confounding of malarial anemia by menstruation. Kra monkeys were obtained from Manheimmer Foundation, Inc. (Homestead, FL, USA) and rhesus macaques were born and raised at Yerkes National Primate Research Center (YNPRC), and assigned to this study. The animals were fed monkey chow biscuits supplemented with fruits and vegetables, and given constant access to water. They were housed socially, with 12-hour light-dark cycles, in housing compliant with the Animal Welfare Act and the Guide for the Care and Use of Laboratory Animals. All animals

received feeding, physical, and manipulanda enrichment. Prior to infection, all monkeys received positive reinforcement training to habituate them to ear-stick blood collection to eliminate the need for anesthesia during these collections. Animals were monitored regularly for behavioral stress by YNPRC behavioral staff. All experiments and procedures were performed at YNPRC, an AAALAC (Assessment and Accreditation of Laboratory Animal Care) International-accredited facility.

Briefly, cohort descriptions are as follows: the first cohort, E30 (n = 2), served as an all-rhesus pilot as a proof of concept for the use of implanted telemetry devices in malaria disease. One animal was sacrificed at Day 10, and the other at Day 19, after being subcuratively treated with artemether and allowed to recrudesce. The second cohort, E07 (n = 7), was an all-kra monkey longitudinal study that involved the planned sacrifice of animals throughout the 45-day time course to study telemetric and tissue involvement, and multi-omic indicators throughout the acute and chronic stages of a malaria infection. No anti-malarials were administered. Next, E06 (n = 4), was an all-rhesus telemetry study to examine acute infection in rhesus monkeys. E33 (kra = 4, rhesus = 2) was a mixed cohort to explore the role that chloroquine subcurative treatment had on multi-omic signals and tissues; telemetry devices were not implanted. E34 was an uninfected mixed cohort (kra = 3, rhesus =3) to obtain control samples and tissues. Finally, E35 (kra = 4, rhesus = 3) was a non-telemetric longitudinal study to replicate chronicity in kra monkeys, and induce chronic infection in rhesus monkeys. Cohorts are summarized in Supplemental Table 6.8.

All animals were infected intravenously with cryopreserved sporozoites originating from *P. knowlesi* clone PK1 (A+) [76]. E07 was first inoculated with fresh sporozoite preparations dissected from infected *Anopheles dirus* mosquitos fed off of a donor rhesus monkey. This inoculation did not yield a patent infection, and the monkeys were confirmed by PCR to have not

been infected. They were subsequently successfully infected with cryopreserved sporozoites. Three cohorts of monkeys were surgically implanted with telemetry devices prior to infection for real-time monitoring of select vital signs (vide infra).

Time point collections were performed under ketamine anesthesia at pre-determined points before and during the infection, as illustrated by idealized infection schematics (Supplemental Fig 6.2-6.6). These included the collection of saliva, rectal and fur swabs, rectal temperature, bone marrow aspirates, capillary blood and venous blood for blood chemistries, proteomic (including targeted proteomics using SomaScan technology), transcriptomic, lipidomic, metabolomic, and immunological studies. Beginning at Day 1 post infection, the animals were monitored for blood parasites by microscopic examination of daily (1 – 3 pm) Giemsa-stained blood smears obtained by ear-stick. When the monkeys became patent, twice-daily parasitemia samples were taken in acute infection (8 am and 1 – 3 pm). During chronic infection, or recrudescent peaks, once daily samples were taken in the afternoon when the parasites do not sequester. Thick, and once parasitemia reached greater than 1%, thin smears were enumerated by the Earle and Perez method [105], or the number of infected red blood cells out of 1000 total red blood cells, respectively. Complete blood counts were performed daily. For those rhesus monkeys planned for chronic infection studies, the animals were subcuratively treated with artemisinin at peak parasitemias to prevent rapidly rising parasitemias and fatality. One cohort of animals was subcuratively treated with chloroquine to study its effects on host systems biology. Animals were monitored regularly for stress by veterinary staff, and antipyretics, analgesics, vitamin B12, and fluid support were administered where appropriate to minimize pain and suffering.

At the termination of each infection, the animals were anesthetized with ketamine, sacrificed by barbiturate overdose, and necropsy performed. Collection of samples of small and

large intestinal contents, saliva, bone marrow, cerebral spinal fluid, venous blood, fecal and fur swabs, capillary blood, and tissue sections from organs was performed at this time. Gross organ abnormalities were photographed.

All experimental, surgical, and necropsy procedures were approved by IACUC and followed accordingly, with veterinary supervision.

Tissue Acquisition and Histopathology

Tissue sections were collected from 20 different organs, including lung, liver, kidney, ventricle, aorta, stomach, duodenum, jejunum, colon, muscle, skin, eye, cerebrum, cerebellum, midbrain, bone marrow (from the femur as well as the costochondral junction), testis, and omentum. In addition, sections were collected from gross lesions (e.g., petechia), and the implantation sites of the telemetry devices. They were preserved in 10% neutral buffered formalin, embedded in paraffin, sectioned at 4 μm, and stained with hematoxylin and eosin (H & E) for histological examination [106]. Masson's trichrome and Perl's stain were also employed where appropriate [106]. Frozen sections (preserved in optimal cutting temperature compound), sections for electron microscopic examination (preserved in 2.5% glutaraldehyde), and samples for tissue transcriptomic analysis (preserved in RNALater) were also collected.

Tissues were examined and assigned a diagnosis (e.g., gastritis), and scored from 1 (low) to 4 (high) based on criteria: inflammation, edema, necrosis, hemorrhage, hyperplasia, fibrosis, vasculitis, and other. Categories were summed and whole organ scores obtained for comparison, as described previously [85].

Telemetry Data Acquisition

At least 30 days prior to infection, six rhesus macaques and seven kra monkeys were surgically implanted with telemetry devices that recorded high-frequency readings of temperature,

electrocardiogram activity, blood pressure, and physical activity, as described elsewhere (Brady, manuscript in preparation). Pre-operation and post-operation baselines were obtained. The devices were activated 10 days prior to inoculation and remained active throughout the duration of the infection, until they were removed at necropsy.

From these high-frequency data sets, simplified and smoothed temperature data that included readings every 30 minutes were produced to assess rises in temperature as a proxy for paroxysm, and clinically correlated with parasitemia data. Febrile parasitemia thresholds were calculated using the first temperature peak above normal as defined by the non-human primate formulary for rectal temperatures, or the first peak above the individual baseline range for telemetry data and compared to the parasitemia reading directly preceding the temperature peak.

Calculation of severity metrics

Several parameters were calculated to further explore disease severity in *P. knowlesi* infection, including cumulative parasitemia, replication rate, and febrile threshold. Cumulative parasitemia was calculated by two metrics: area under the curve using the PKNCA package in R (which assumes a trapezoidal model), and the sum of the daily parasitemias from the day of inoculation to the day of necropsy. Animals were divided into three categories: acute (necropsied days 10-14), early chronic (necropsied days 15-19), and chronic (necropsied days 45-50). Two kra monkeys were excluded because they were necropsied at Day 27, and there were no rhesus animals necropsied at that time to provide a paired comparison. Replication rate was calculated by considering the first day of patency to the day of parasitemia peak (or in the case of rhesus monkeys, the day of treatment or necropsy), natural-log-tranforming this region, and finding the slope of the points on the line. Only the first peak was considered because it had the most robust sample size. Febrile threshold was calculated using down-sampled telemetric temperature data.

The normal temperature range for each animal was defined as the range of temperatures prior to inoculation. The febrile threshold was determined by considering the parasitemia prior to the time when the temperature rose above the individual's threshold.

Statistical Analysis

Statistical analyses and figures were produced in either R Studio version 1.1.383, under R version 3.4.3 GUI version 1.70, or JMP Pro version 13.0.0. Pairwise comparisons were performed using either Welch's T-Test or the Wilcox Sum Rank test. Multiple comparisons were performed using ANOVA analysis, and Tukey HSD Post-Hoc Comparison Test. Multiple comparisons ANOVA was employed where appropriate. Correlation analyses were performed using both Spearman and Pearson correlations. Mixed effects models were also employed where appropriate. Comparisons were considering significant if the p-value was below 0.05. All multiple comparisons were adjusted using the Bonferroni method.

3.3 RESULTS

Parasitemia in *P. knowlesi* infection of a natural host and an experimental host: kinetics and burden.

A classical indicator of severe malaria disease is hyperparasitemia, which varies by host and parasite species. In human *P. knowlesi* infections, disease severity correlates very strongly with parasitemia, with a greater than 28-fold risk of developing severe disease at parasitemias greater than 100,000/μL [54]. The WHO has defined hyperparasitemia in humans as 100,000 parasites per microliter, or, in the presence of jaundice, 20,000 parasite per microliter in *P. knowlesi* infection [133]. Parasitemia is also important in nonhuman primates. Disease severity in macaques has historically been defined by two indicators: parasitemia, and death, with a paucity of studies considering other metrics, such as tissue histopathology and blood chemistries [10,134].

The disease course in kra monkeys, the natural host, has canonically been described as mild, and the host resistant to severe disease because these monkeys have been demonstrated to control parasitemia to a level below 10^5 parasites per microliter without antimalarial intervention, and do not typically succumb to infection [21,23,134]. Rhesus macaques however, nearly universally suffer from catastrophically rapidly expanding parasitemias that are not controlled and that result in death [10,20,28].

As parasitemia is an important indicator of severe disease in humans and in macaques, we sought to examine parasitemia, parasite burden, and kinetics in our two-host system. The semi-daily and daily parasitemia curves for all of the monkeys in our multi-cohort study are presented in Fig. 3.1A (individual curves are given in Supplemental Fig. 6.2-6.6). Parasitemia was patent by day 6.61 on average (+/- 0.70) post-inoculation with sporozoites, with no statistical difference between the species. The majority of kra monkeys experienced peak parasitemias below 1% total red blood cells infected, which corroborates previous studies. The animals began controlling parasitemia by days 10 – 15 post-infection, and developed chronic, low-parasitemia infections universally. Importantly, parasitemia control was attained by the host, without the assistance of anti-malarial interventions.

The rhesus monkeys nearly universally reached parasitemias of at least 1%, after which they were subcuratively treated with either intramuscular artemether, or in the case of one cohort, chloroquine, to avoid dangerous parasitemias and fatalities, or euthanized. As the natural course of infection in rhesus monkeys results in fatality due to uncontrolled expansion of the primary peak before the development of an adaptive immune response and emergence of circulating antibody, and we were interested in side-by-side comparisons of each stage of infection to kra monkeys, we were interested to see if the macaques in our cohort would be able to control parasitemia if artificial

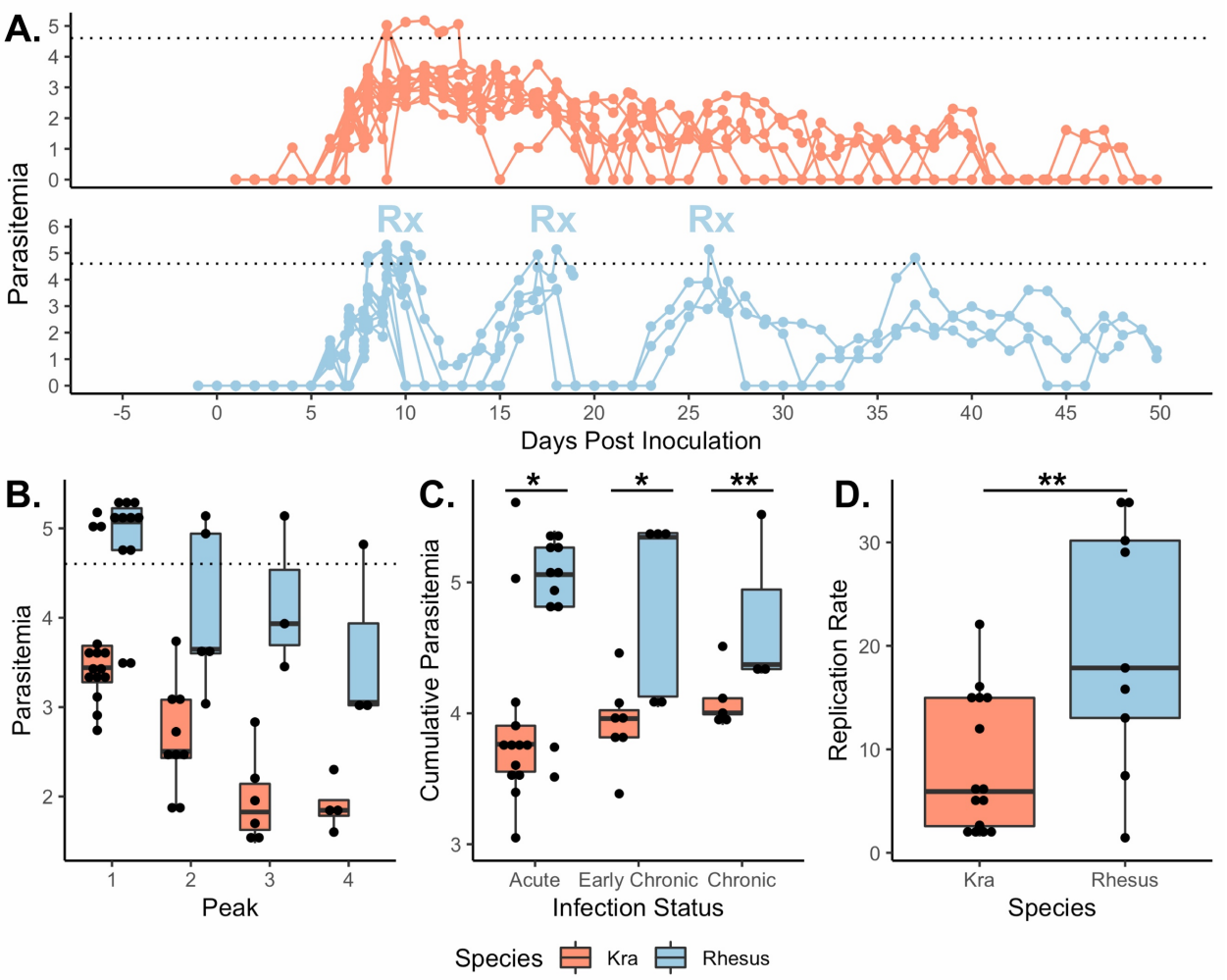

Figure 3.1 Parasitemia in rhesus and kra monkeys. A, Longitudinal plots of daily and semi-daily parasitemia readings in $\log_{10}$-transformed parasites per microliter. B, The dotted line in both plots indicates 1% infected RBCs, and Rx denoting peaks that were subcuratively treated. Mean peak parasitemias decline in both species as chronicity is established. C, Cumulative parasitemia of monkeys throughout the course of infection, in $\log_{10}$-transformed parasites per microliter, calculated as a sum of data points. D, Rhesus monkeys demonstrate a greater parasite burden throughout every stage of infection, despite subcurative treatment (*p-value < 0.05, **p-value < 0.005). Parasite replication rates during the primary peak of infection are significantly higher (**p-value < 0.005) when compared with a Welch's T-test.

control of parasitemia by subcurative antimalarial treatment was applied, as has been demonstrated previously [71,72,77]. A chronic response was successfully induced in these animals: at the third recrudescence, two of the three rhesus monkeys did not require sub-curative anti-malarial treatment to control their parasitemias, and by the fourth recrudescence, none of the animals required treatment (indicated by "Rx" on the parasitemia traces in Fig. 3.1A). Additionally, by the final recrudescence, all three animals' parasitemia kinetics resembled that of kra monkeys with chronic infection: relatively low parasitemia that plateaued. While the kra monkeys were able to develop this response nearly directly after the initial peak, it took rhesus monkeys roughly over one month to do so (Fig 3.1A). Peak parasitemias decline as chronicity is established in both species (Fig. 3.1B). Notably, maximum parasitemia at each recrudescence (or peak) trends downward in rhesus monkeys, relative to their artificially capped earlier peaks.

Next, we were interested in testing if the continual low-level parasitemia present in kra monkeys resulted in a comparable total parasite burden throughout the course of infection to rhesus monkeys, that experienced episodic peaks decreasing in magnitude, punctuated by periods of zero parasitemia. To compare total parasite burden throughout the infection, cumulative parasitemias were calculated by summing the parasitemia taken at each afternoon parasitemia reading (Fig. 3.1C). Afternoon readings were selected for two reasons: first, all monkeys had afternoon timepoints (morning timepoints were not taken for secondary and subsequent peaks in some cohorts, or when the parasitemia was very low); secondly, the parasites were ring trophozoites in the afternoon and were least likely to sequester and artificially deflate the parasitemia. To verify this method, area under the curve (AUC) was also calculated (Supplemental Fig. 6.7). Monkeys were grouped and categorized as Acute, Early Chronic, and Chronic by their necropsy dates, Days 9-14, 15-20, and 45-50 Post Inoculation, respectively. Longitudinal animals that had

measurements within earlier timepoints from when they were necropsied were included. Two kra animals were excluded because no rhesus monkeys were necropsied in a comparable timeframe (Day 27).

Using a repeat measures ANOVA, the role of species in affecting cumulative parasitemia was assessed. Species was found to be a significant contributor to the differences in parasitemia observed. Next, post-hoc comparisons analysis, adjusted using the Bonferroni method for multiple comparisons was conducted, using the psycho package in R. At all three timepoints, rhesus monkeys exhibited a statistically significant higher cumulative parasitemia than did kra monkeys (p-values = 0.028, 0.022, and 0.003, for Acute, Early Chronic, and Chronic, respectively).

We were next interested to see if peak magnitude and the delay in response in earlier peaks was correlated with increased replication rate of the parasite. Replication rate begins to decline as immune systems controls infection. Therefore, we would expect rhesus monkeys to have infections with higher replication rates than those in kra monkeys. To test this, we considered the afternoon time points of the first peak in all of the rhesus and kra monkey infections. Afternoon timepoints were selected for the same reasons as stated above for cumulative parasitemia calculation. Because the error in reading thick smears is higher with lower parasitemias, the time interval between patency and the peak parasitemia were considered (Supplemental Figures 6.8-6.9). The data were natural log-transformed, and the line of best fit and slope calculated. On average, kra monkey infections replicated at a rate of 8.59, which is roughly what would be expected by assuming the number of merozoites per infected cell as the brood size [9]. Rhesus monkeys, however, experienced a replication rate of 20.28, over twice that of kra monkeys (Fig. 3.1D). This was found to be statistically significantly different (p-value = 0.005). Rhesus monkeys therefore are capable of controlling infections, if provided time to respond to the infection (illustrated by declining peak

magnitude in latter peaks, ability to control later peaks without antimalarial intervention, and kinetics curves that plateau), but are more likely to reach parasitemias of at least 1% (before intervention), experience greater cumulative parasitemias, and greater primary peak replication rates.

Kra monkeys develop a temperature response faster than rhesus monkeys

Temperature is an important indicator clinically for the presence of infection, generally, and specifically, is characteristic of acute malaria disease [33–35, 35]. An important question is if symptomology in patients at presentation can be used to extrapolate if the patient is experiencing the primary peak of an acute infection, or a recrudescence. Understanding pathophysiology in chronic infections allows clinicians to understand what proportion of the overall disease burden of a population is due to new transmission events. Temperature dynamics have not been published for either species of monkey when infected with *P. knowlesi*, thus we next sought to explore the timing and kinetics of temperature responses in our monkey infections.

We measured temperature using two techniques. The first was per rectum, which is the accepted method to record temperatures in veterinary medicine, and as such, has accepted temperature ranges, and the second was nearly instantaneous temperature readings taken by telemetry implant (vide infra). Rectal temperatures were taken at each time point, when the monkeys were sedated. Figure 3.2A shows the parasitemia of all of the animals in the study, with a dotted line representing a parasitemia of 1% in the top panel, and the rectal temperatures for the same animals below it. The dashed line represents the febrile threshold according to the Yerkes Nonhuman Primate Formulary.

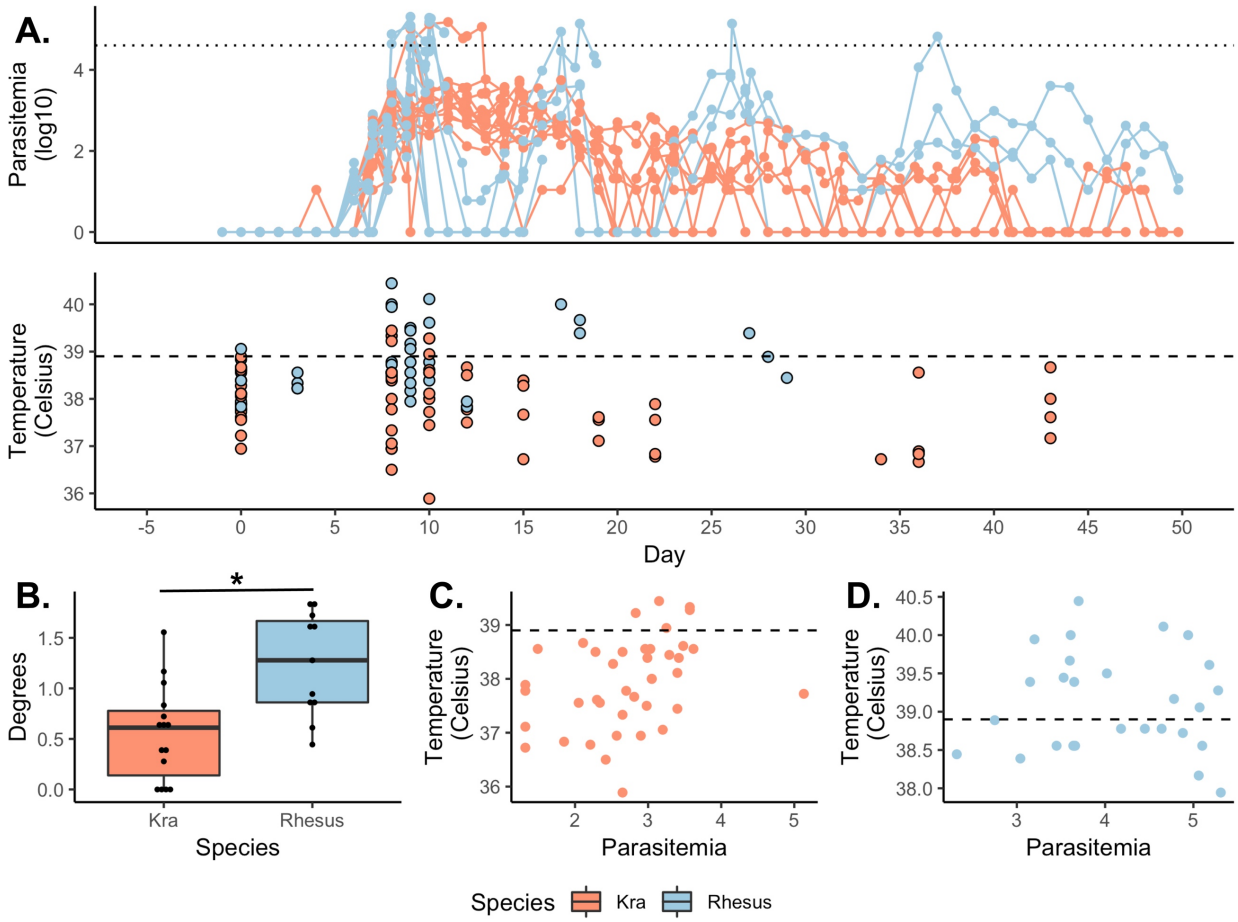

Figure 3.2 Temperature in *P. knowlesi* Infection. A., Rectal temperatures of all of the monkeys taken at scheduled time points, bottom panel, with parasitemia as a reference, top panel. The dotted line denotes a parasitemia of 1% on the top panel, and the dashed line represents the febrile threshold on the bottom panel. B.,The difference in temperature from baseline (day 0 of the infection) and the maximum temperature is lower in kra monkeys than rhesus monkeys (*p-value < 0.05, calculated using a Wilcox rank-sum test). C.,Temperature is moderately correlated with parasitemia in kra monkeys (Spearman's $\rho = 0.438$, p-value < 0.005), D., and not correlated in rhesus monkeys (Spearman's $\rho = -0.014$, p-value $= 0.8379$).

Kra monkeys experienced a smaller change in temperature from their baseline (which was considered to be Day 0 of infection) to their maximum temperature, relative to rhesus monkeys. On average, kra monkeys' temperature rose 0.55° C from their baseline, whereas rhesus monkeys' temperature rose by 1.24° C on average (Fig. 3.2B). This difference was statistically significant (P=0.0023, by Wilcox rank-sum test).

Of note, the highest temperature peaks in rhesus monkeys occurred at the primary peaks, and were associated with parasitemias that were above 1% (data after Day 30 were not collected. because timepoints were not scheduled for that point in the infection). Additionally, temperature trends downward with time. The kra monkeys also experienced temperature peaks above the febrile threshold during their primary peak, but importantly, did not experience febrile temperatures later in infection. To understand the relationship between temperature and parasitemia, we performed Spearman correlation analysis when the animals were patent. Only timepoints in which both temperature and parasitemia data were included, and are plotted in Fig. 3.2C and 3.2D. Temperature was modestly correlated with parasitemia in kra monkeys (Spearman's $\rho = 0.438$, p-value = 0.005), but there was no correlation in rhesus monkeys (Spearman's $\rho = -0.041$, p-value = 0.8379).

One measure of antigenicity of *Plasmodium* parasites that has been used in field studies of malaria patients is the pyrogenic threshold [135,137–139]. The pyrogenic threshold is defined as the parasitemia at which the patient first develops a fever response [138], and can be thought of as the dose of parasites that is required to elicit a fever. The magnitude of the febrile threshold can depend on many things, including the immune, or exposure status of the patient (with subsequent infections and recrudescences exhibiting higher pyrogenic thresholds than primary infections), transmission intensity of the region (with higher transmission correlated with higher pyrogenic

thresholds), ethnicity of the patient, and the species of parasite (with *P. vivax* having lower pyrogenic thresholds than that of *P. falciparum*) [33, 35–37]. A drawback of the pyrogenic threshold is that it is highly variable between individuals, and also the logistical challenges regarding data collection density [36, 37]. Temperature and parasitemia readings are typically taken once or twice daily; this lack of granularity may lead to temperature or parasitemia peaks to be missed.

No direct studies in humans have been conducted on the pyrogenic threshold in *P. knowlesi*, however a study in Malaysia comparing *P. falciparum*, *P. vivax*, and *P. knowlesi* infections in the same community suggest it may be lower than that of *P. falciparum* [54]. Thus, we were interested in exploring pyrogenic threshold in *P. knowlesi* infection, generally, and more specifically any differences that may exist between the host species differences in their temperature responses to the same parasite. We used down-sampled temperature data collected by telemetric implant in experiments E30, E06, and E07 (rhesus n = 6, kra n = 7) to calculate pyrogenic threshold in *P. knowlesi*. Since a published, accepted normal temperature range has not been developed for temperature measured using this method, we first defined individual normal temperature as the range in temperature observed (including the normal circadian rhythm) during the baseline period until the day of inoculation (time and parasitemia plots are represented in Supplemental Figures 6.10-6.23). Time points, which involved ketamine administration (which can change the temperature of the animal) were performed during the baseline and included in the individual normal ranges. Daily ear stick samples occurred by the first day post inoculation, and did not result in a spike in temperature above this normal baseline (which may be expected due to stress). Any deviation out of this normal baseline was considered a temperature response. The parasitemia directly before the temperature response was defined as the pyrogenic threshold for the animal.

The mean parasitemia at which kra monkeys responded by mounting a temperature response was roughly twice as low (n = 7, mean = 160 parasites/μl) as that of rhesus monkeys (n = 6, mean = 364 parasites/μl), however the response was statistically insignificant using a Wilcox rank-sum test (p-value = 0.1641), as represented in Fig. 3.3A.

Given that rhesus monkeys classically succumb during the first parasite peak if no intervention is given due to rapidly expanding parasitemias, and we a greater effective brood size in *P. knowlesi* parasites in rhesus monkeys than in kra monkeys (Fig. 3.1D), we were interested to see if there was a difference in the timing of their temperature response relative to that of kra monkeys. To control for individual differences in time to patency and the limitations of microscopy, we used PCR to confirm for the presence of parasites in the blood molecularly. We then recorded the day that the monkeys' telemetric temperature data rose above their individual baseline and calculated the time to temperature response by subtracting the day of molecular positive from the day temperature rise. Every kra monkey responded in two days from a molecular positive result (n = 7), which was an entire day earlier than rhesus monkeys on average (n=6, mean = 3). This result was significant (p-value = 0.018) by Wilcox rank-sum test (Fig. 3.3B).

Next, we sought to compare select cytokine profiles present in each species at the time of these febrile responses. Innate immunity includes both humoral (complement and cytokine modulators) and cellular components and occurs rapidly in response to general, pathogen-associated molecular patterns (PAMPS). Among the cytokines produced by and affecting innate immunity actors are the pyrogenic interleukin-1 (IL-1) and interleukin-6 (IL-6), tumor necrosis factors (TNF) [140]. We compared the baseline and malaria-positive pro-inflammatory molecules, IL-1, IL-6, and TNF-α with immunomodulating cytokines, IL-10 and INF-γ, whose upregulation is paradoxically associated with severe disease, and the immune dampening, TGF-β, for each

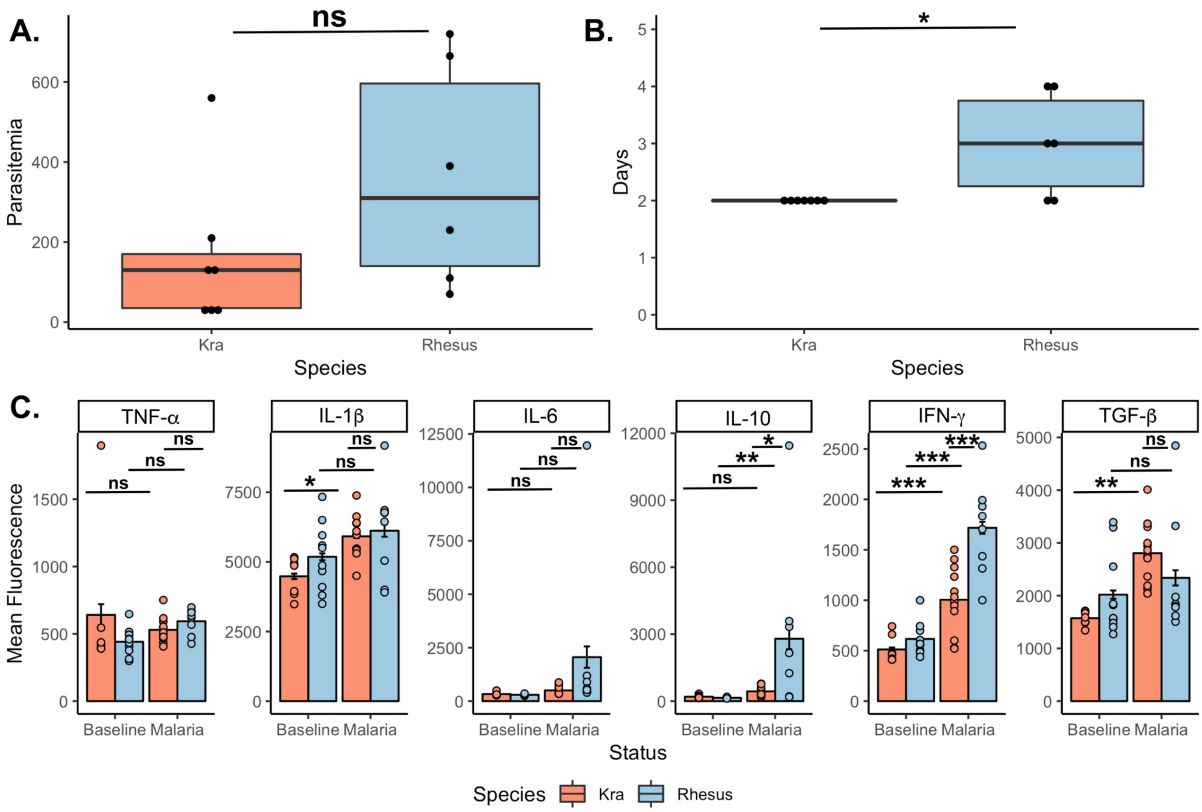

Figure 3.3 Temperature Response and Inflammation in *P. knowlesi* Infection. A., Pyrogenic threshold is lower in kra monkeys than in rhesus monkeys, however the difference is not statistically significant. B., Kra monkeys mount a temperature response an entire day earlier than do rhesus monkeys to parasites (P=0.018, Wilcox rank-sum test). C., SOMAScan targeted proteomics quantification of selected pro-inflammatory and immunomodulatory cytokines, with repeat measure ANOVA between kra baseline and malaria, rhesus baseline and malaria, and kra and rhesus malaria (***P < 0.0005, **P < 0.005, * P < 0.05, ns = not significant.

species [140–148]. SomaScan, a targeted proteomics platform was used to quantify the levels of these cytokines in plasma [149]. Three comparisons, baseline (time points 1 and 2) and malaria (time points 4 and 5), within each species, and kra and rhesus monkeys with malaria were conducted using a repeat measures ANOVA approach and contrast analysis in the psycho package in R, then Bonferroni corrected (Supplemental Figures 6.2-6.6 review when time points were taken).

Though rhesus monkeys appear to have a modest increase in TNF-α when infected with malaria, this increase is not statistically significant, nor are the other pairwise comparisons. Kra monkeys saw a significant rise of IL-1β in malaria infection (P=0.042), however, though rhesus monkeys experienced an increase in IL-1β, relative to baseline, this increase was not statistically significant, nor was the difference in malaria infection between rhesus and kra monkeys. Rhesus monkeys with malaria had higher levels of IL-6 than those without, or than kra monkeys with malaria, however this difference was not significant. Rhesus monkeys with malaria had higher IL-10 levels than at baseline (P = 0.0072), and than kra monkeys with malaria (P = 0.025), and there was no significant difference in kra monkeys between baseline and malaria. Kra monkeys did not show a significant difference in IL-6 levels between baseline and malaria infection. IFN-γ was elevated in both species in malaria infection relative to their baselines (p-value = 0.00092 for kra, and p-value = 8.21×10^{-8} for rhesus), and elevated in rhesus monkeys with malaria relative to kra monkeys with malaria (p-value 0.0001). Last, only the kra monkeys showed a significant increase in TFG- β in malaria infection (P = 0.0021).

Kra monkeys develop and resolve severe anemia.

Severe anemia is a major cause of death among those who succumb to malaria disease, with roughly half of the deaths of children with malaria in Africa attributable to malarial anemia [2]. Though red blood cells are obligately destroyed during the *Plasmodium* replication cycle, and the spleen filters and removes parasitized red blood cells from circulation, the bulk of red blood cells lost is thought to be a result of bystander killing, or removal of healthy red blood cells by the immune system [150]. Classically, kra monkeys are believed to not develop severe malaria disease, as defined by the ability to control parasitemia and produce a chronic infection rather than succumb. We were interested to explore clinical indicators of severe disease that go beyond parasitemia and fatality as severity metrics. We considered hemoglobin concentration as a measure of anemia. We also considered platelet count to assess thrombocytopenia, a condition coincident with malaria and when severe, a harbinger of severe disease and the reticulocyte production index as a means to assess bone marrow response to anemia [54,55,151].

Surprisingly, kra monkeys develop severe anemia. Mild anemia was defined using WHO guidelines as a hemoglobin concentration below 11, moderate anemia as below 10, and severe anemia, below 7 (indicated by dashed lines in Fig3.4B) [2]. The hemoglobin nadir appeared around Day 20, after the peak in parasitemia and establishment of chronic infection (Fig. 3.4B, parasitemia as reference in Fig. 3.4A). Individuals experienced hemoglobin nadirs as low as 4.8 g/dL, that spontaneously improved without antimalarial intervention (Fig. 3.4B). All of the kra monkeys experienced at least some level anemia. Four (just over 25%) of the kra monkeys developed severe anemia (nadirs ranging from 4.8 to 6.5), and an additional two kra monkeys were borderline-severe (hemoglobin nadir of 7), seven (~46.7%) kra monkeys experienced moderate anemia (nadirs ranging from 7.3-8.7), and the final two had mild anemia (nadirs above 10).

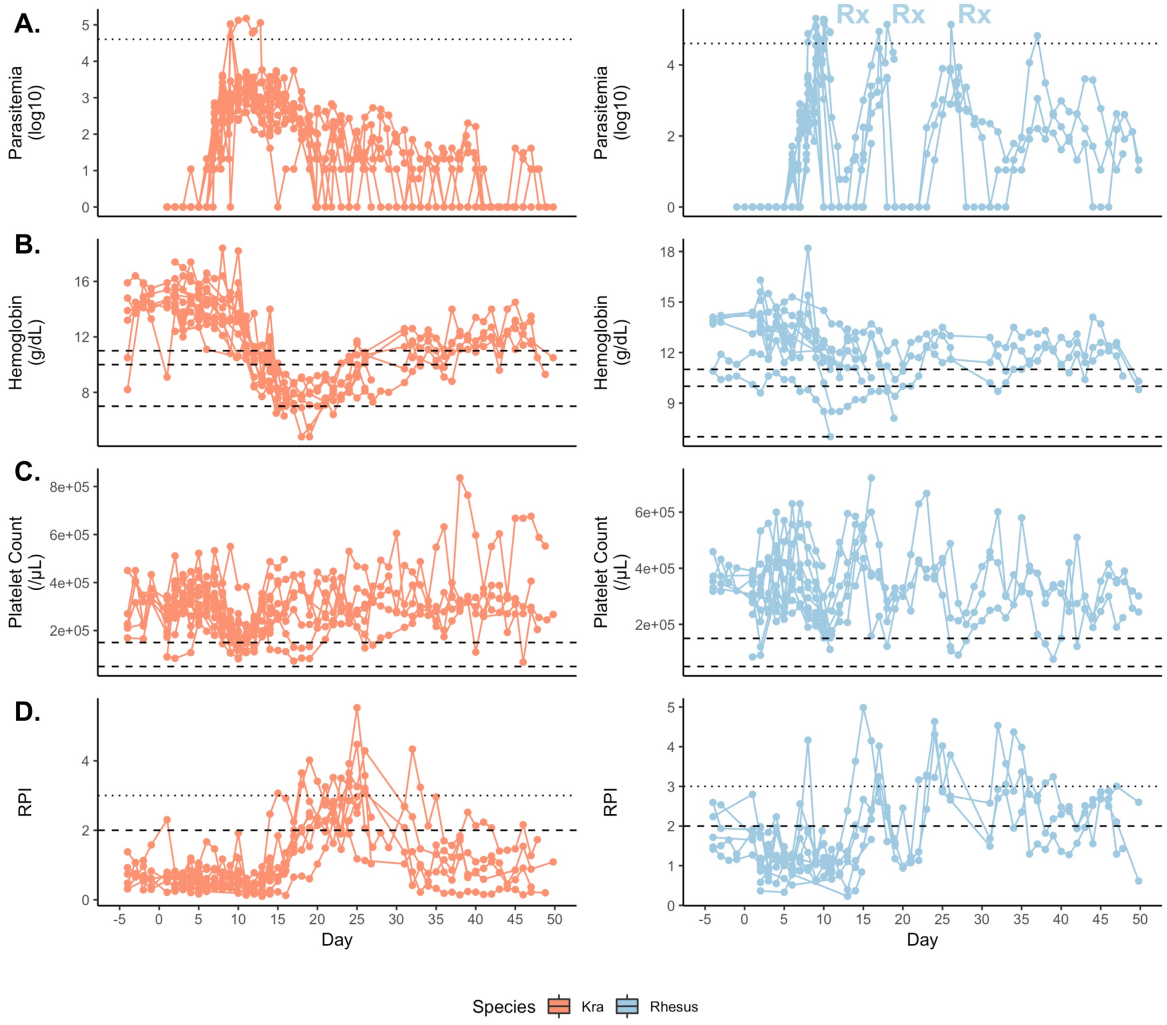

Figure 3.4 Hemoglobin, platelet count, and reticulocyte production index in *P. knowlesi*-infected macaques. A., Longitudinal parasitemia of kra monkeys and rhesus monkeys, with a dotted line indicating a parasitemia of 1%. B.,Hemoglobin concentration in g/dL of kra and rhesus monkeys, with dashed lines highlighting the thresholds for mild (<11 g/dL), moderate (<10 g/dL), and severe (<7 g/dL) anemia. C., Platelet count (platelets per µL of blood), for both species of monkey, with dashed lines for moderate thrombocytopenia (<150,0000 platelets/µL) and severe thrombocytopenia (<50,000 platelets/µL). D.,The reticulocyte production index of kra and rhesus monkeys, with a dotted line marking an RPI > 3, which indicates destruction of red blood cells, and a dashed line marking an RPI > 2, which indicates an appropriate bone marrow response.

Interestingly, rhesus monkeys did not develop severe anemia. One individual had a borderline-severe hemoglobin nadir of 7, however, most were mild to moderate (nadirs of 8.1 to 10.5). Three animals did not develop any anemia, however these were sacrificed early in infection, before the expected nadir. Kinetically, anemia nadirs tended to occur after the primary peak of parasitemia, then improved and remained fairly constant throughout the rest of the infection despite serial large-magnitude parasitemia peaks (in the chronic cohort), as shown in Fig. 3.4B. The average hemoglobin nadir for rhesus monkeys was 10.10 g/dL, which was statistically significant (P=0.00042) from that of kra monkeys, 7.56 g/dL (Fig. 3.5A, top). On average, kra monkeys experienced a hemoglobin drop of over 45% at the nadir, compared to baseline, a result significantly different (P = 0.00037) to the average hemoglobin loss of rhesus macaques, at 26% (Fig. 3.5A, bottom). For monkeys that were patent, hemoglobin was not correlated with parasitemia longitudinally: Spearman's $\rho = 0.125$, $P = 0.142$ for rhesus monkeys, and Spearman's $\rho = 0.116$, $P = 0.066$ for kra monkeys (Fig. 3.5 B). Hemoglobin nadir was not correlated with peak parasitemia in either species (Spearman's $\rho = 0.3$, $P = 0.371$ for rhesus monkeys, and Spearman's $\rho = -0.3005$, $P = 0.276$ for kra monkeys). Individual hemoglobin plots are provided in Supplemental Figures 6.23-6.48, second panel. An important difference between the species is the requisite subcurative treatments rhesus received to avoid fatalities, which will be discussed below.

In addition to anemia, kra monkeys also experienced platelet loss. Mild to moderate thrombocytopenia was defined as described elsewhere, with average platelet/μL below 150,000, and severe thrombocytopenia, associated with retractable malaria illness in the presence of anemia, and when sustained, of 50,000 platelets/μL [55,111,151–153]. Kra monkeys had mild to moderate thrombocytopenia with nadirs as low as 68,000 platelets/μL lasting for 24 – 72 hours (Fig. 3.4C).

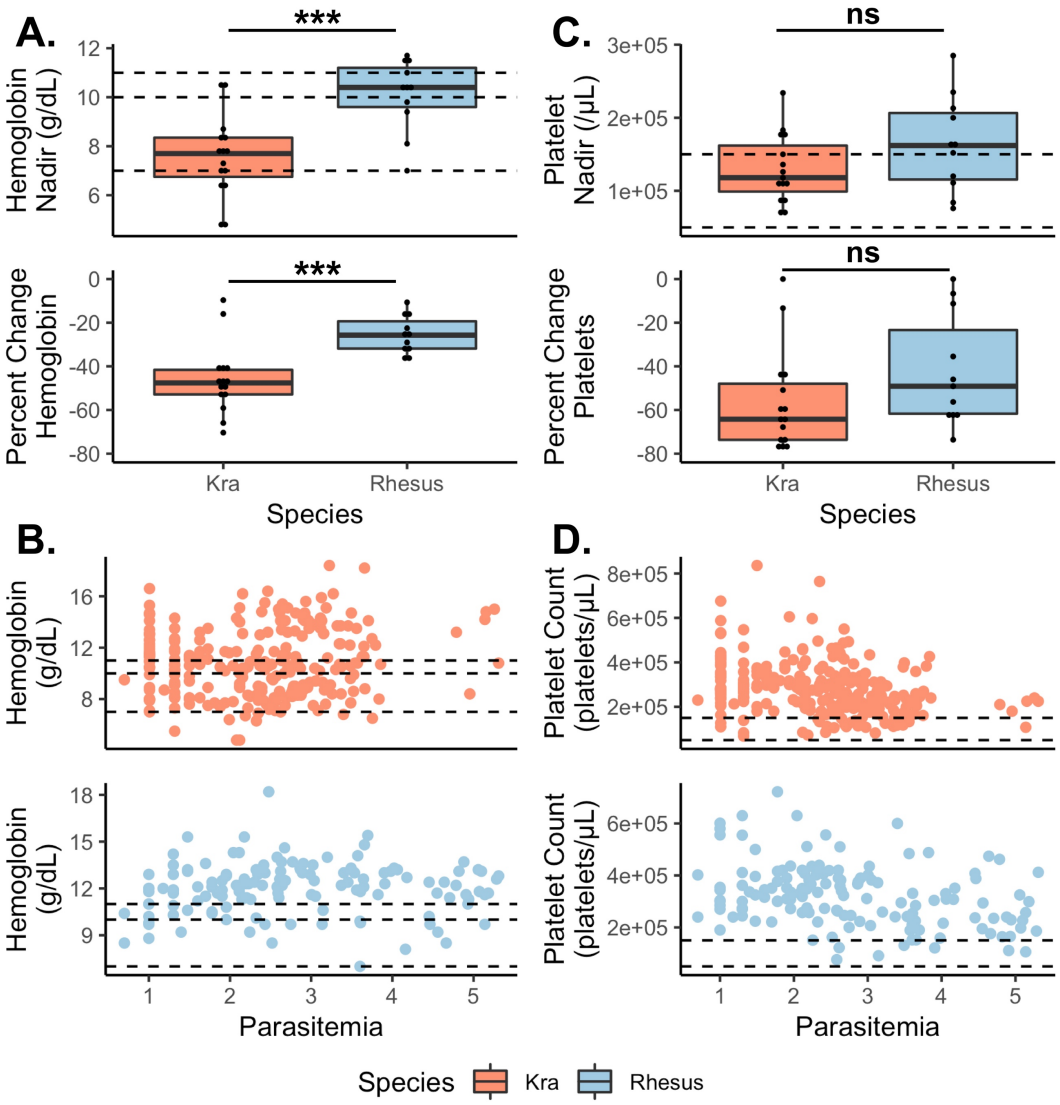

Figure 3.5 Hemoglobin and Platelet Levels in *P. knowlesi*-infected Macaques. A., Kra monkeys experienced both lower absolute hemoglobin nadirs (top), and greater losses in hemoglobin from baseline at nadir than rhesus monkeys, (***P > 0.0005), bottom. B., Hemoglobin concentration was not correlated with parasitemia in either species. C., Although kra monkeys had lower absolute platelet nadirs, and greater losses in platelets than rhesus monkeys, the difference was not significant. D., Platelet concentration was weakly correlated with parasitemia in both species.

Many monkeys experienced a nadir at around Day 10, correlating with the peak of the primary peak of parasitemia, then had periodic drops in platelets throughout the course of infection. Rhesus monkeys also experienced mild to moderate thrombocytopenia and episodic drops in platelets after an initial nadir that corresponded roughly to the primary peak of parasitemia (Fig 3.4 C). However, the degree to which rhesus monkeys lost platelets was less than that of kra monkeys, the lowest nader being 76,000 platelets/μL. On average kra monkeys experienced moderate thrombocytopenia, and had a platelet nadir of about 129,000 platelets/μL, which was less than, but not statistically significantly different (P=0.131) to rhesus monkeys, which had an average platelet nadir of approximately 163,900 platelets/μL (Fig 3.5C, top), a value that does not meet the definition of thrombocytopenia. The average loss in platelets from baseline to nadir, was approximately 56% in kra monkeys, and 42% in rhesus monkeys, a difference that was not statistically significant (P=0.155) as shown in Fig. 3.5C, bottom. As with hemoglobin, individual platelet counts are provided in Supplemental Figures 6.23-6.48, third panel.

Platelet drops seemed to coincide with rises in parasitemia (Fig 3.5D). We tested this observation by calculating Spearman's ρ. Interestingly, in both species, the platelets were weakly inversely correlated with parasitemia ($\rho = -0.335$ and $\rho = -0.332$, with P values of 0.00005 and 7.0×10^{-8}, for rhesus and kra, respectively). Platelet nadir has been inversely correlated to maximum parasitemia in the human *P. knowlesi* literature, so we next sought to determine if this correlation existed in our cohort . This comparison in neither species was significant ($\rho = -0.387$ and $P = 0.239$ for rhesus monkeys, and for kra monkeys, $\rho = 0.264$ and $P = 0.347$).

The normal physiological response to anemia includes activation of the bone marrow to ramp up production of red blood cells to correct the deficit [154]. Anemia can be caused by either a problem in production of red blood cells, or an increase in their destruction [154]. Bone marrow

dysfunction has been documented in malaria caused by other *Plasmodia,* and we sought to explore how the bone marrow responds in our monkey experiments, and to address the potential lack of production of red blood cells as an exacerbation of the anemia we observed [155,156]. We used reticulocyte production index (RPI) as a means to do so. Reticulocyte production index is calculated using the following formula [151,157]:

$$\frac{\%\ Reticulocytes}{Maturation\ Time} \times \frac{Hemoglobin}{Baseline\ Hemoglobin}$$

An RPI less than 2 in the presence of anemia indicates an insufficient bone marrow response, and one greater than three indicates the destruction of red blood cells, which is congruent with parasite- and immune-mediated red blood cell destruction in this context [154]. Appropriate responses in both kra and rhesus monkeys were observed (Fig 3.4D) [154]. Individual reticulocyte and RPI plots can be found in Supplemental Figures 6.23-6.48, fourth and fifth panels, respectively.

Kra monkeys experienced a peak of reticulocyte production that coincided with a response to their anemia nadir (Fig. 3.4B and D). A slight right shift relative to the anemia nadir for the RPI peak can be observed, as the monkeys take time to respond to their anemia. Reticulocyte production index was more strongly correlated with parasitemia (ρ = -0.449, P ~ 0) than with hemoglobin (ρ = -0.383, P =1.0 x 10^{-8}), Fig. 3.6A and B. Rhesus monkeys, on the other hand, did not experience a uniform hemoglobin nadir that resulted in as severe of anemia as did the kra monkeys, thus no single peak is observed in the reticulocyte production index plot, and hemoglobin was not correlated with RPI (ρ = -0.132, P = 0.164), Fig. 3.6D. The resultant plot from graphing parasitemia versus reticulocyte production index in rhesus monkeys is not monotonic (Fig. 3.6C), and the Spearman coefficient test is inappropriate to use in this circumstance. Thus to

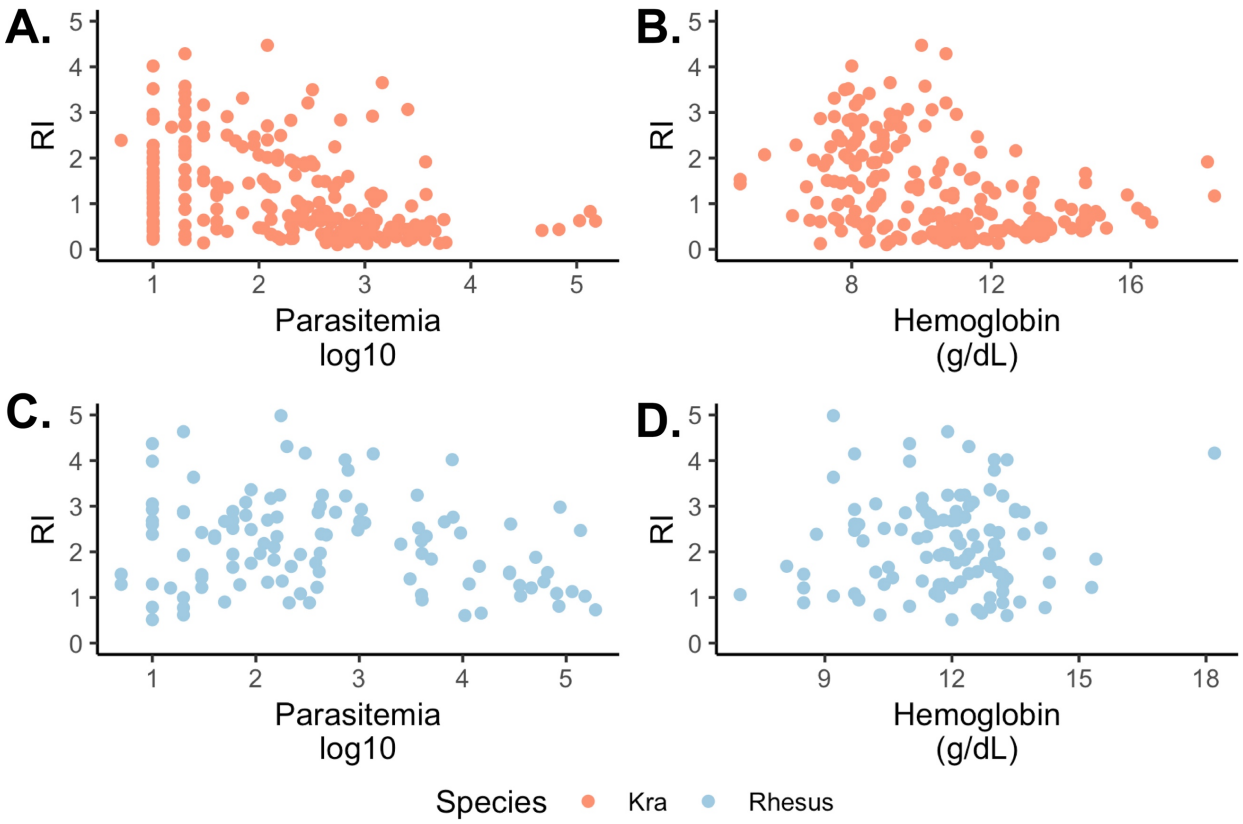

Fig. 3.6 Reticulocyte Production Index as it Relates to Parasitemia and Hemoglobin. A., Reticulocyte production index decreases with both parasitemia (Spearman's r = -0.449, P ~ 0), and hemoglobin (r = -0.383, P =0.00000001), B. in kra monkeys. C., Reticulocyte production index is not monotonic in rhesus monkeys, and demonstrates an inflection point at roughly 10^3 parasites/mL, after which RPI is inversely related to parasitemia (r = 0.492, P = 0.002). D., Reticulocyte production index is not correlated with hemoglobin in rhesus monkeys.

analyze the correlation between parasitemia and RPI, it was necessary to split the data into two sections around the inflection point of the distribution (which was at approximately 10^3 parasites/μL). At parasitemias below 10^3 parasites/μL, the RPI appears to increase, though this relationship was not statistically significant ($\rho = 0.189$, $P = 0.106$). At roughly 10^3 parasites/μL and above, the RPI decreases with increasing parasitemia, a correlation which was statistically significant ($\rho = 0.492$, $P = 0.002$).

Rhesus macaques and kra monkeys show minimal to moderate histopathological changes

The indices of disease manifestations in *P. knowlesi* malaria thus far discussed have been systemic measurements. In addition to the systemic pathology, we were interested in the local consequences of malaria disease in tissues in infected animals. While only a handful of studies have described histopathology in either rhesus monkeys or kra monkeys, there has been no comparative approach between the two host species, or between longitudinal timepoints [23–27,157]. To address this gap in knowledge, and to explore the types and degree of direct damage to tissues, we conducted necropsies on all 26 monkeys in our multicohort study. We collected specimens from 22 different organs, including four from the brain and surrounding tissues (cerebrum, cerebellum, midbrain, and eye), four from the thoracic organs (aorta, thymic region, lung, and left ventricle), eight from the abdominal organs (liver, omentum, colon, stomach, duodenum, mesenteric lymph node (LN), jejunum, and spleen), two from the retroperitoneum (adrenal gland and kidney), and from the testis, bone marrow (from both femur and in some cohorts, the costochondral joint), the skeletal muscle, and the abdominal skin (Fig. 3.7). E33 had an abbreviated collection. Additionally, we collected all 22 tissues from E34, an uninfected control cohort of three kra monkeys, and three rhesus monkeys to serve as examples of normal tissue.

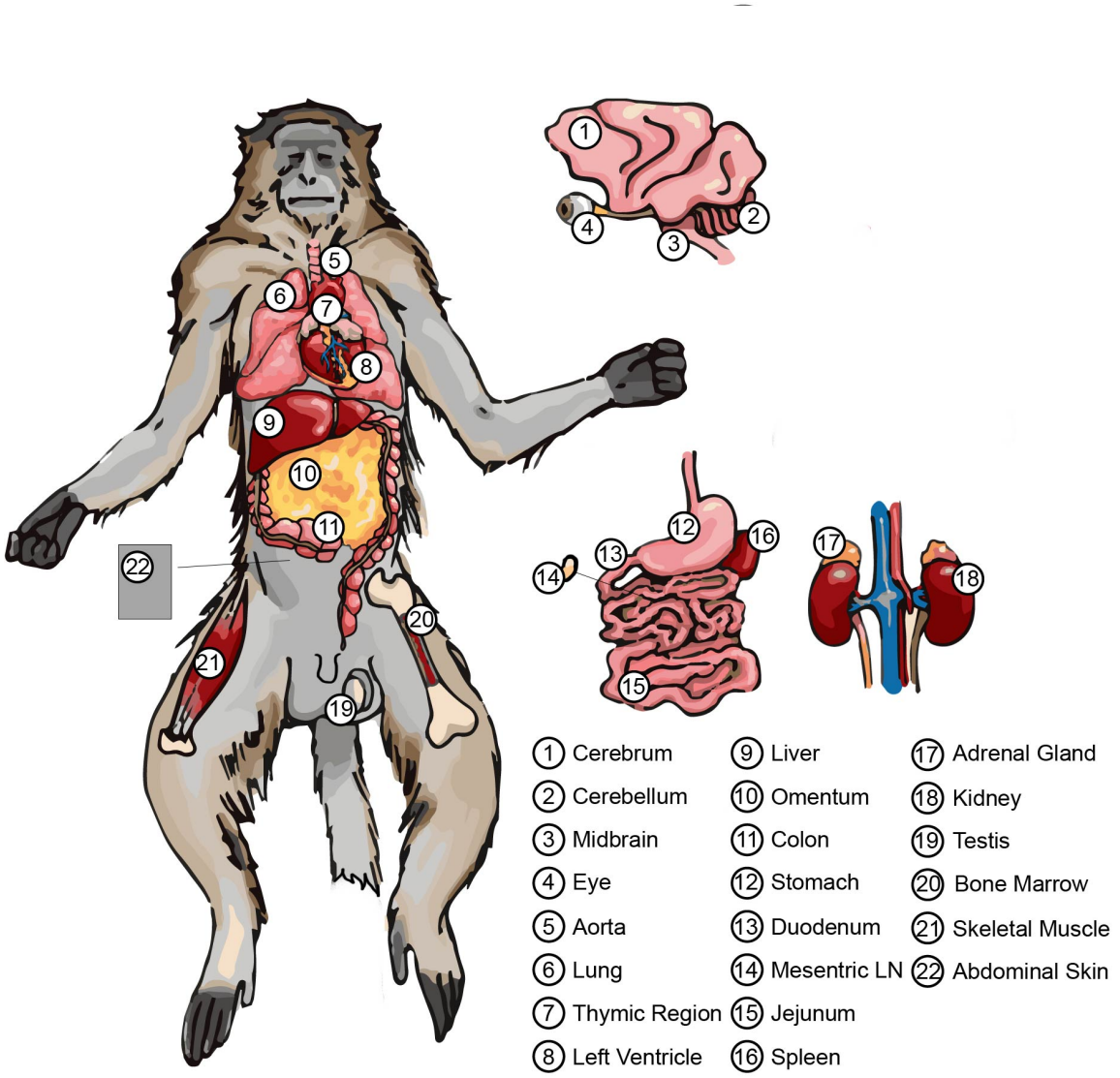

Fig. 3.7 Schematic Illustrating Tissue Collection in *P. knowlesi*-Infected Macaque Necropsies. Specimens were collected from twenty-two tissues in both rhesus (as shown in the figure) and kra monkeys. Tissues are labeled with circles and numbers – these labels are schematic only, and do not indicate the exact location from which each tissue was sampled. Drawing not to scale.

All of the tissue sections were stained with hematoxylin and eosin and examined by Dr. Sanjeev Gumber, a veterinary pathologist. Several tissues underwent histopathological changes in all of the monkeys, including lymph node, spleen, bone marrow, lung, kidney, liver, stomach, duodenum, jejunum, and colon. The organs of the gastrointestinal tract will be discussed in Chapter 4. To compare the extent of damage to these organs in chronic and acute malaria disease, these tissues were semi-quantitatively scored on a scale from 0 to 4 with 0 being normal, 1 only minimal changes, 2 mild changes, 3 moderate changes, and 4 multifocal changes in several categories including inflammation, necrosis, vasculitis, fibrosis, and organ-specific categories such as tubular degeneration [85]. These categories were then summed to obtain the overall damage score for each scored organ. The scores were similar in both acute and chronic stage in both species, with the exception of the stomach (Supplemental Table 6.9). The organs of the lymphoid system, including the lymph node, spleen, and bone marrow were not scored because the changes observed in these tissues reflected expected processes of disease, including germinal center expansion and activation in the lymph node and spleen, and expansion of white and red blood cell precursor populations in the bone marrow.

The spleen is an essential organ in the control and in the pathophysiology of malaria [127]. Malaria patients without spleens are at risk of death and severe disease, and retain parasite debris longer after treatment than are patients with intact spleens [125,126,158–161]. Monkeys without spleens also suffer more severe disease, and the removal of the spleen is used as a technique to acquire higher parasitemias in experimental studies in species otherwise recalcitrant to infection [162]. The spleen is also essential in regulation of parasite virulence, with its presence being critical for the expression of variant antigens in *P. knowlesi* [74,76,163,164]. The role of the spleen in our cohorts is also critical, and the timeline set forth by the clinical data: that the kra monkeys

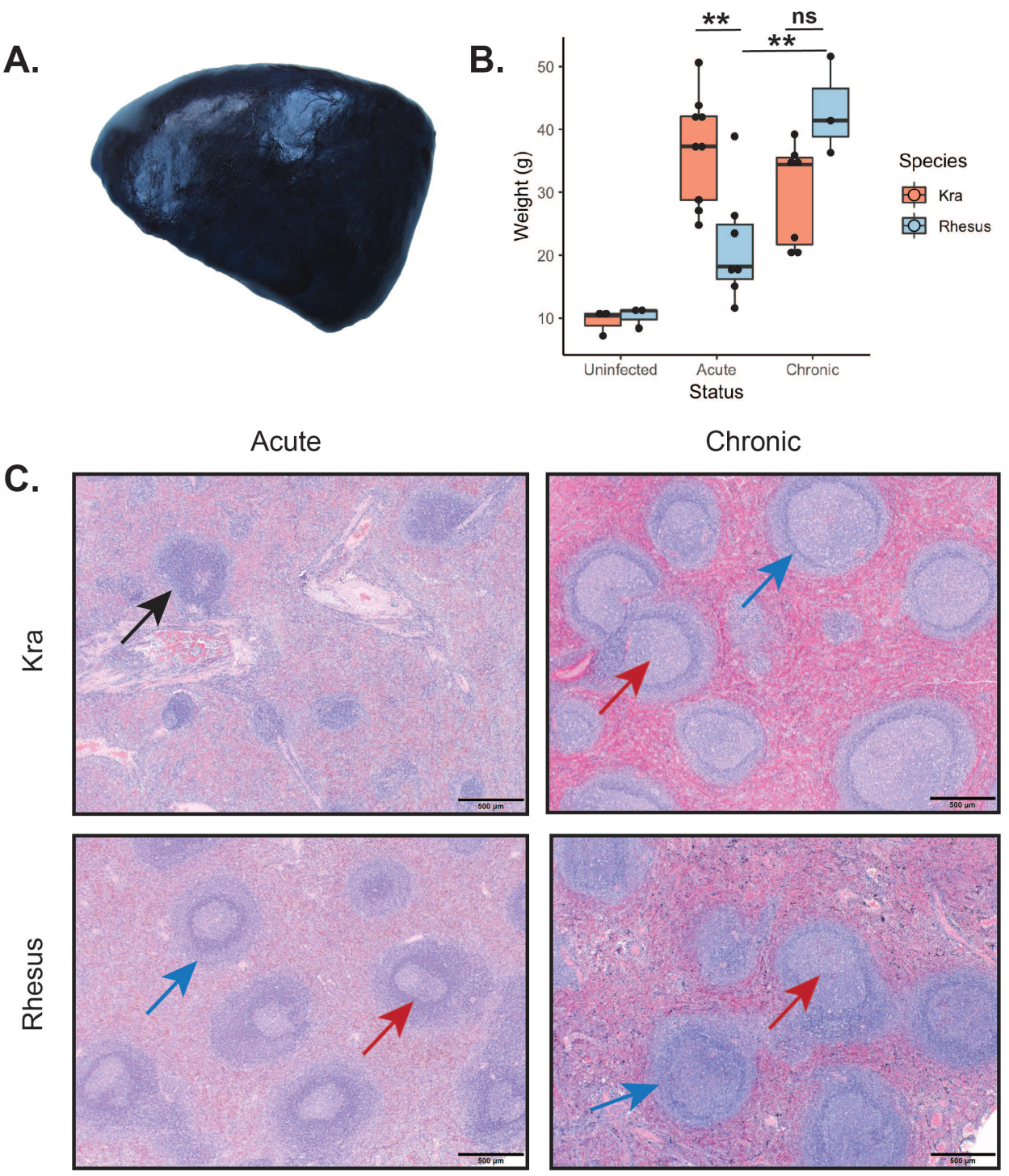
A.
B.
**
ns
**
50
40
30
20
10
Weight (g)
Uninfected
Acute
Chronic
Status
Species
Kra
Rhesus
C.
Acute
Chronic
Kra
Rhesus
500 µm

Figure 3.8 Splenic changes in macaques with *P. knowlesi.* A., Grossly, the spleen in both animal species is appears black due to the deposition of hemozoin. B., Spleen weight longitudinally in P. knowlesi infection. The enlargement is statistically significant (**P < 0.005) relative to kra baseline and rhesus monkeys with malaria. Rhesus monkey spleens, though enlarged in acute infection, are not statistically significantly different from baseline. Rhesus monkeys become statistically insignificant from kra monkeys in chronicity. C., H & E staining of spleen histology. In acute infection, both animals see follicular hyperplasia (follicle marked with black arrow), however rhesus monkeys have increased numbers of germinal centers (red arrow) and thicker mantle zones (blue arrow). By chronicity, the species resemble each other histologically, except for diffuse malaria pigment deposition in the rhesus spleen.

mount an earlier immune response that is of the appropriate scale to control parasitemia without massive inflammation, is illustrated in the gross and histopathology of the spleen. At baseline, the spleens weighed roughly 10 g, and were not statistically significant from one another. Grossly, a normal spleen is smooth, and brown. However, in malaria infection, both species exhibited darkened, nearly black (Fig 3.8 A), enlarged spleens relative to baseline which were bumpy on cut surface, indicating follicular hyperplasia. Kra monkey spleens were significantly more enlarged on average in acute infection than were rhesus monkeys (mean for kra monkeys: 37.1 g, mean for rhesus monkeys: 21.6 g, p-value = 0.007). In chronic infection, rhesus monkey spleens become much more enlarged, with an average spleen weight of 43.1 g (a difference that is statistically significantly different from acute stage, p-value = 0.006), and kra monkeys make a modest (but statistically insignificant) decrease, averaging at 29.8 g. The difference in means at chronicity between the two species is statistically insignificant. Despite being larger, kra monkeys had fewer follicles and activated germinal centers, with thinner mantle regions than rhesus monkeys at the same time point. By the time both monkey species reach chronicity, their spleens are identical histologically, with the exception that rhesus spleens have much more hemozoin deposition in chronicity.

Comparative histology of the bone marrow between the two species longitudinally also offers a snapshot into the disparate presentations of, and the spontaneous improvement of anemia in both species. As discussed previously, RPI was calculated and found to be appropriately elevated in response to anemia in kra monkeys. In early infection, kra monkeys demonstrate a massive expansion of erythroid lineage cellular precursors, as evident by the absence of fat cells in the section. As blood cell precursors replicate, they crowd out adipocytes to form the dense cellularity represented in Fig 3.9. In contrast, rhesus monkeys early in infection do not respond as

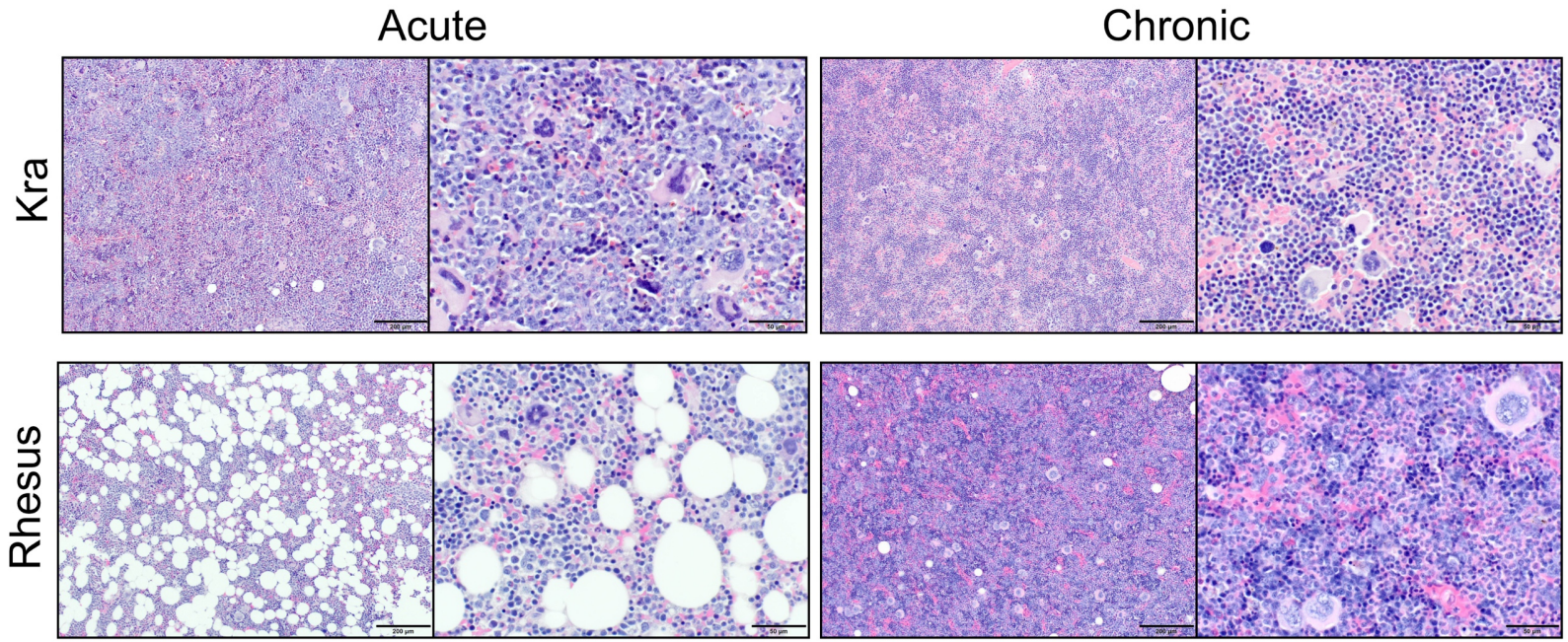

Figure 3.9 The bone marrow responds earlier in kra monkeys. Hematoxylin and eosin stained tissue section of bone marrow showing low-magnification and high-magnification views from kra monkeys (top) and rhesus monkeys (bottom) demonstrates bone marrow hyperplasia in both species, with kra monkeys responding more robustly in acute infection.

dramatically, and have less dense cellularity. As chronicity is achieved, both monkey species have dense celluarlity, and a shift to myeloid precursors from erythroid precursors is seen. Taken with the clinical data, this suggests that the bone marrow is not suppressed in kra monkey hosts with *P. knowlesi* infection, and that while rhesus monkeys respond late, if their parasitemia is controlled, they are eventually able to mount a response that controls malaria disease.

Injury to the lungs has been demonstrated extensively in human malaria patients and in monkey models, especially in vivax and including knowlesi malaria, and includes hemorrhage, interstitial pneumonia, fibrotic changes, edema, and in severe cases, acute respiratory distress syndrome and death [25,56,85,94,98,112,113,115,163]. Lungs in this case were scored based on eight categories: inflammation, edema, necrosis, hemorrhage, hyperplasia, fibrosis or interstitial thickening, vasculitis, and other. Interestingly, no significant species difference was observed in lung pathology overall, and the extent of damage fairly low, compared to findings in other malaria studies. None of the monkeys had inflammation in their lungs in the acute infection. Seven out of eight kra monkeys and seven out of eight rhesus monkeys in acute infection had minimal to mild interstitial thickening or fibrosis (Fig. 3.10A). The same kra and rhesus individuals also had minimal to mild hyperplastic changes in acute infection (Fig. 3.10A). Hemozoin in infected RBCs and in phagocytes was notable (Fig. 3.10B), especially in the rhesus animals, and was distinguished from hemosiderin, a byproduct of hemolysis, by imaging under a polarized light. Hemozoin crystals are birefringent under polarized light, appearing white and “sparkly” in the section, whereas hemosiderin does not [108]. Two rhesus monkeys and no kra monkeys had mild to moderate hemorrhage in acute infection (Fig. 3.10B). Notably, one rhesus demonstrated moderate, multifocal fibrotic changes, as evidenced by palisading fibroblasts and deposition of a light-pink material (3.10C, left). Fibrin deposition was highlighted by employing a trichrome stain

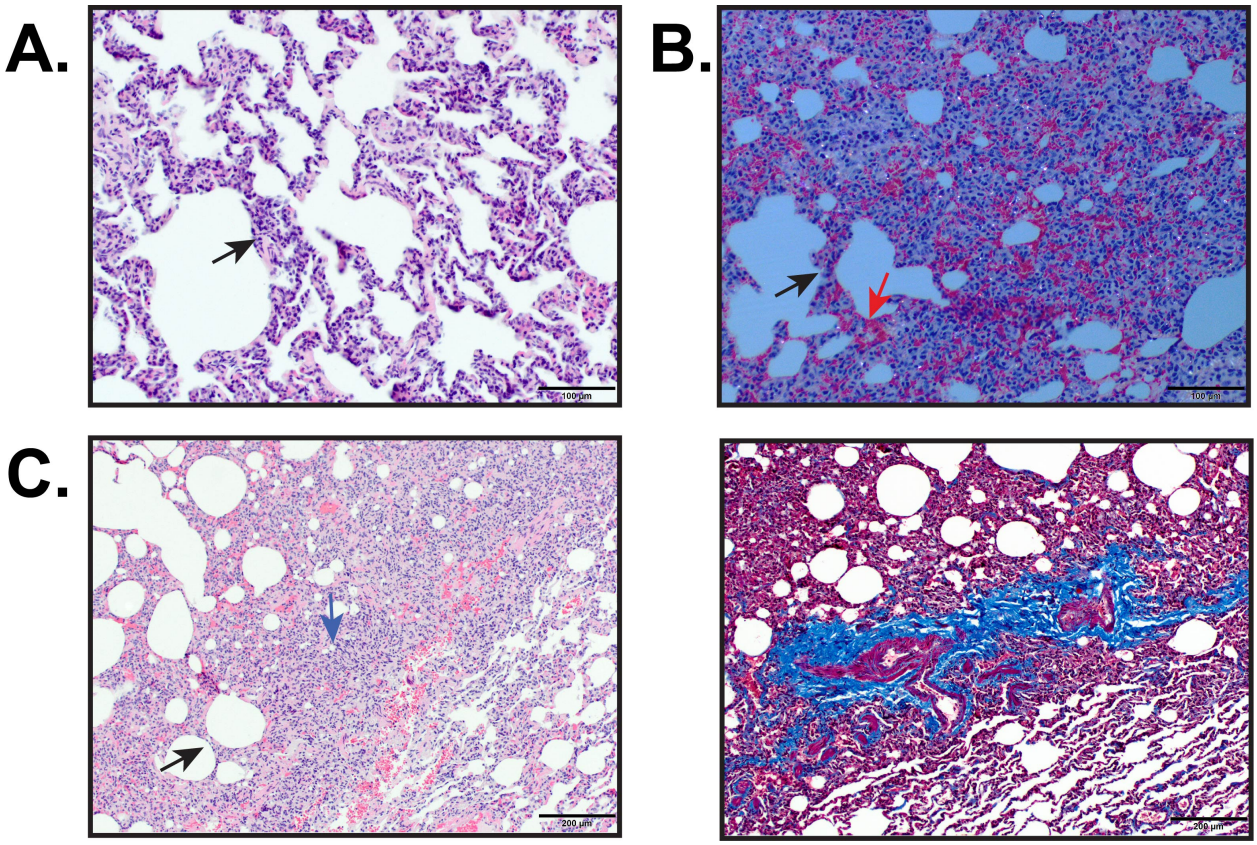

Figure 3.10: Lung Involvement in *P. knowlesi* is Similar to Lung Involvement in Malaria Caused by Other Parasites. A., H and E light microscopy demonstrating thickened alveolar wall with lymphocytic infiltration (black arrow) in a kra monkey with chronic malaria. B., H and E light microscopy under polarized light demonstrating hemozoin (white sparkles), alveolar thickening and infiltration (black arrow) consistent with interstitial pneumonia, and hemorrhage (red arrow), in a rhesus monkey with acute malaria. C., Interstitial thickening and infiltration (black arrow), palisading fibroblasts (blue arrow) and fibrin deposition shown in an H and E stained section (left), and with fibrin highlighted in blue with a trichrome stain (right), in a rhesus monkey with acute malaria after treatment with chloroquine.

which colors fibrin bright blue (Fig. 3.10 C, right). This animal was a member of the cohort subcuratively treated with chloroquine, an antimalarial drug that may be associated with acute lung injury in human vivax malaria patients [165]. In chronic infection, three of four kra monkeys had mild hemorrhage, and all of the rhesus monkeys had minimal or mild hemorrhage. All of the rhesus and kra monkeys had minimal to mild hyperplasia. Both species of monkeys saw an increase in fibrosis and interstitial thickening in chronicity with most individuals with mild to moderate changes. Two kra monkeys also had inflammation in their lungs in chronic infection.

Kidney damage is also very well described in vivax, knowlesi, and falciparum malaria, with acute kidney injury and failure a complication and cause of death in *P. knowlesi* infection [8,25,63,85,111,124,165,165,166]. Several mechanisms have been proposed to explain malarial kidney damage, including inflammation of the glomeruli (associated with the presence of parasites or hemozoin), blockade of microcirculation, immunoglobulin complex deposition, and hypoxic injury secondary to dehydration and/or anemia [167]. Here, we plotted blood creatinine levels, a clinical proxy for kidney function (high levels suggest reduced filtration rates, and therefore reduced kidney function) for all of the monkeys, and include representative micrographs of the histopathological changes observed in each species, longitudinally.

All of the monkeys in both species showed at least some degree of glomerular hypercelluarlity, without glomerulonephritis (Fig 3.11 A). The degree of hypercellularity did not change between acute and chronic cohorts. In acute infection, three of eight rhesus and no kra monkeys showed evidence of inflammation. Two out of three of the chronic rhesus monkeys and one out of five of the kra chronic monkeys had evidence of inflammation. Three monkeys had hemorrhage in the kidneys, one chronic kra monkey, and two acute kra monkeys. In acute infection, one kra monkey and four rhesus monkeys showed evidence of tubular degeneration, and

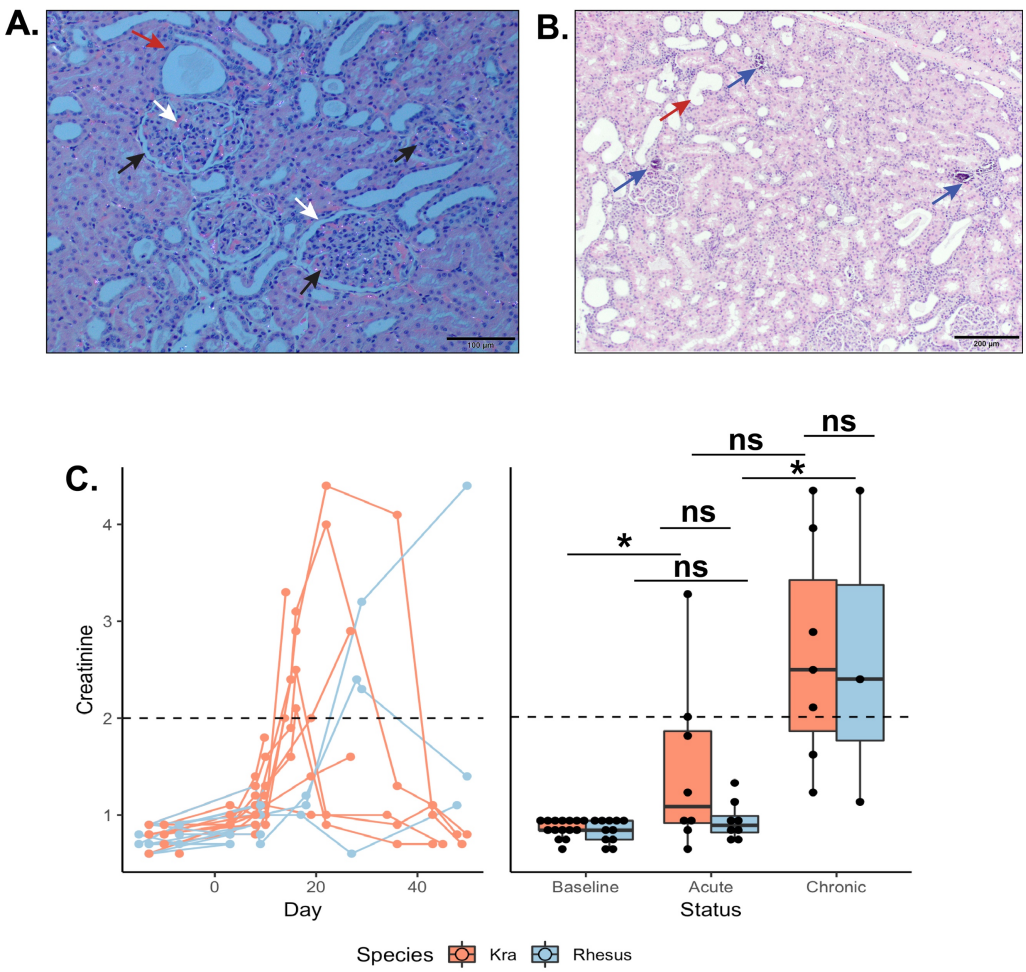

Figure 3.11 Renal Involvement Occurs in Both Macaque Species. H and E of a kidney section demonstrating hypercellular glomeruli (black arrows), tubular degeneration (red arrow with dilated tubular lumen with flattened epithelial cells), and hemozoin (white sparkles, highlighted with white arrows), under polarized light in a rhesus monkey, A. H and E of a kidney section under normal light demonstrating tubular degeneration (red arrow) and crystallization of tubules (blue arrows with dark purple crystals in the tubular lumen). Longitudinal serum creatinine levels, C, and peak serum levels in baseline, acute, and chronic infection, D. Both species experience elevated creatinine in chronic infection. Elevated creatinine is considered greater than 2, and marked with a dashed line.

one animal had calcification or crystalline deposition in the tubules (Fig. 3.11A and B). Two kra monkeys and two rhesus monkeys had tubular degeneration in the chronic infection. High creatinine did not necessarily correlate with evidence of histopathological changes. Longitudinal creatine and peak creatinine levels for acute and chronic infection relative to each monkey at baseline are plotted in Fig 3.11 C. Comparisons were performed using a repeat measures ANOVA, and post-hoc comparisons with Bonferroni correction were conducted in the psycho package in R. Creatinine was significantly elevated relative to baseline in kra monkeys in acute (mean = 2.08, p-value = 0.027) and chronic infection (mean = 2.67, p-value = 6.45×10^{-6}), and elevated above the normal threshold in chronic infection, but was not statistically distinct from rhesus creatinine in acute or chronic infection (means = 1.03, 2.63, respectively). While there was no significant difference between rhesus creatinine levels in acute infection relative to baseline, a significant rise occurred in chronic infection, with the difference being significantly different from acute infection (p-value = 0.045). While H12C59, the kra monkey in acute infection, and RRz15, the rhesus monkey in chronic infection, had both elevated creatinine and tubular degeneration, neither 13C33 nor 13C74 had any evidence of tubular degeneration, or other changes that could explain their high creatinine. Conversely, 13_116 which had a total pathology score comparable to RRz15, including a comparable degree of tubular degeneration, did not have an elevated creatinine concentration.

Last, we examined the liver. Jaundice (yellowing of the skin) and scleral icterus (yellowing of the eyes), caused by elevated bilirubin, are common presentations in malaria, and can be the result of intravascular hemolysis (both from parasite and from splenic removal of uninfected RBCs), and in severe cases, disseminated intravascular coagulation [168]. Liver enzyme derangement may also be present [54,55]. Jaundice, especially, is an indicator for severe disease in *P. knowlesi* malaria in humans, and when present, the hyperparasitemia threshold is lower

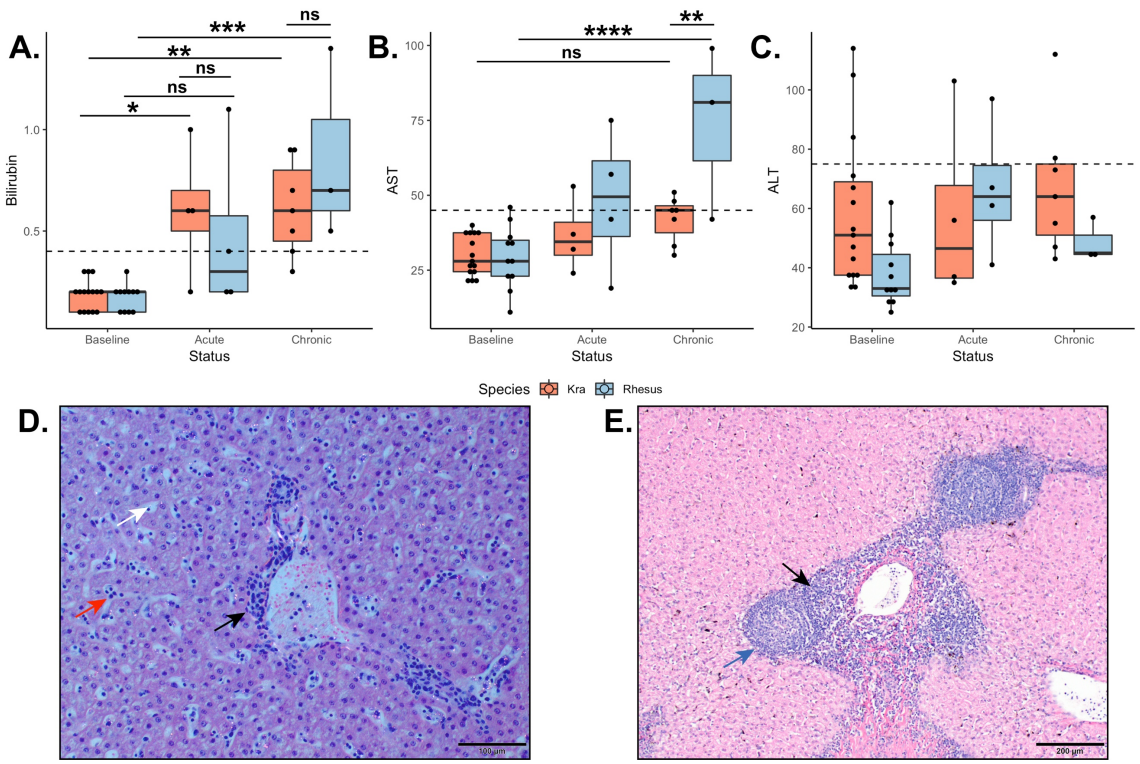

Figure 3.12 Hepatic involvement in P. knowlesi infection. *A.,* Bilirubin levels were elevated in kra monkeys relative to baseline in acute and chronic infection, and in rhesus monkeys in chronic infection, but they were not statistically significantly different from one another. *B.,* AST was statistically significantly elevated in rhesus monkeys only in acute and chronic infection, and was significantly different from kra monkeys in chronic infection. *C.,* ALT disturbances were not statistically significant for either species at any time point. *D.,* H and E stained liver section under polarized light demonstrating minimal to mild peri-portal infiltration (black arrow), sinusoidal congestion with Kupffer cell hyperplasia (red arrow), and hemozoin deposition (white arrow, white sparkles) characterized the typical findings in both rhesus monkeys and kra monkeys in chronic and acute infection. *E.,* One rhesus animal demonstrated moderate periportal infiltrate (black arrow) with lobular infiltrate formations (blue arrow). Dashed lines at 0.4, 45, and 75 indicate the normal threshold for bilirubin, AST, and ALT, respectively. (****P < 0.00005, ***P < 0.0005, **P < 0.005, *P<0.05, ns = not significant).

(20,000 parasites/μL) [54,133,168]. Bilirubinemia, which was defined as a total serum bilirubin above 0.4 was found in kra monkeys in acute infection, and both kra and rhesus monkeys in chronic infection (Fig. 3.12A). Kra monkeys had significantly elevated serum bilirubin levels relative to their baseline in both acute and chronic infection (mean = 0.6, P=0.023; mean=0.614, P =0.0015, respectively), whereas those of rhesus monkeys were only significantly elevated in chronic infection (mean = 0.867, p-value = 0.0002). Kra and rhesus monkeys were not significantly different from one another in either acute or chronic infection. AST elevation was defined as a serum AST above 45 U/l, and was mostly not observed in kra monkeys. However, progressive worsening of AST elevation longitudinally occurred in rhesus monkeys (Fig. 3.12B). Rhesus monkeys were significantly distinct from baseline (mean = 74, p-value = 0.00007), and from kra monkeys (mean = 42) at chronic infection (p-value 0.0097). ALT elevation, defined as serum ALT levels greater than 75 were not observed on average (Fig. 3.12C).

Liver pathology, for example, Kupffer cell hyperplasia, periportal infiltration, cholestasis, and hepatic sinusoid congestion has been documented in vivax, falciparum, and knowlesi malaria [25,63,85]. All of the animals presented with inflammation, especially around the periportal region and congestion in the hepatic sinuses (Fig. 3.12 D). One rhesus monkey in the chronic cohort had marked lobular infiltrates in the periportal region (3.12E). All of the animals exhibited Kupffer cell hyperplasia, with immune cells engorged with malaria pigment. Inflammation around the periportal region is indicative of a blood source for antigen, and is consistent with *Plasmodium* as a blood-borne infection.

Several tissues exhibited no pathology, including adrenal gland, aorta, brain (cerebrum, cerebellum, and midbrain), eye, testis, and thymus. Omentum was normal except for an incidental finding of focal omental fat necrosis in 13_116, which was related to his body habitus, and not his

malaria. The skin was also normal except for an incidental finding of dermatitis with perivasicular hyperplastic lymphohistocytic infiltrate in RRz15, and gross petechial lesions in two kra monkeys and one rhesus monkey. Three kra monkeys exhibited histopathological changes in the heart. Of these three, all of them had inflammation, including one with lymphohistiocytic infiltrate (11C131), two had edema, and one had hemorrhage that was evident grossly.

3.4 DISCUSSION

Understanding the determinants that underlie host susceptibility and tolerance, and parasite virulence is a puzzle central to disease management and prevention. *Plasmodium knowlesi*, as with other malaria parasites, causes disease on a spectrum in humans, and though certain factors such as age, are known to affect presentation in some way, the specific individual mechanisms that would allow precise prediction of patient outcomes are still out of reach [92]. Here we attempt to address the question by utilizing a two-host model that represents resiliency and susceptibility to lethal disease. The literature describes a dramatic dichotomy in terms of presentation and outcome for the resilient host, the kra monkey, and the susceptible host, the rhesus monkey, in which the latter rapidly succumbs to catastrophic parasitemia within days of patent infection, and the former, discussed in the context of the latter, controls parasitemia and does not succumb [10,20–22]. Perhaps due to the stark contrast in the presentation of these hosts, very few studies describe hematological or histological parameters of kra monkey infection with *P. knowlesi* [23,24]. However, it is imperative to consider the host, and the consequences of its response to acute and chronic disease, when defining resilience and susceptibility. We sought to fill this gap by considering a holistic approach to the definition of malaria disease, and thus in addition to outcome and parasitemia, included hematological, omic, histological samples.

As in other studies, we found that kra monkeys controlled parasitemia within a few days of becoming patent, with most animals peaking below 1% parasitemia, and none requiring anti-malarial treatment to reduce parasitemia. Likewise, as in other studies, kra monkeys uniformly formed chronic, very low parasitemia infections. Due to ethical considerations, we did not recapitulate lethal rhesus parasitemia kinetics in our study. All rhesus monkeys were sacrificed at roughly 1-3% parasitemia, or subcuratively treated to prevent rapid parasite expansion and death. Given the manifestations of anemia, and the damage observed in histological sections taken from monkeys with chronic disease (vide infra), and the fact that parasitemia is correlated with disease severity and tissue damage, we were interested to see how the total parasite burden affects these presentations, and how subcurative drug treatment may play a role [25,27,55,56].

We first determined that daily parasitemia was not correlated with hemoglobin in either species, but was weakly correlated with thrombocytopenia, moderately correlated with reticulocyte production index in kra monkeys, and weakly correlated with reticulocyte production index in rhesus monkeys at parasitemias greater than 10^3 parasites/μl. Maximum parasitemia was not correlated with hemoglobin or thrombocytopenia nadir. However, daily parasitemia does not take into account the cumulative burden of parasitemia or its effect on the inflammatory state of the host. Additionally, temporal relationships that result in a delay to response may weaken statistical relationships. Therefore, we used the sum of daily parasitemia readings to estimate the parasite burden on each monkey. We hypothesized that the lower-level of parasitemia that was nearly constantly present in kra monkeys would result in higher parasite burdens than in rhesus monkeys which saw parasite burdens punctuated by periods of subpatency to explain the different presentations. However, rhesus monkeys had higher total parasite burdens than kra monkeys at early, middle, and late points in the infection, despite having periods of no parasitemia.

In our study, parasite load, whether calculated by correlations between daily parasitemia and hematological readings, maximum parasitemia and nadirs, or cumulative parasitemia could not explain the difference in presentation. The role of parasite biomass in causing disease in our study may be obscured due to the low sample size and lack of representation along a range of parasitemias in each case. Additionally, it is likely that parasite burden plays different roles in disease mechanism for each species. If untreated, rhesus monkeys die in the first peak, before the immune system is able to mount a response able to control parasitemia, however kra monkeys, as the natural host have likely evolved the response we observed to survive natural infections with the parasite. Biomass was estimated using the sum of daily parasitemia readings, which does not take into consideration populations of parasites concealed from circulation in deep capillary beds. Upon tissue examination, kra monkeys did not have a large population of parasites that could explain the disparity, however, rhesus monkeys demonstrated a large pool of parasites sequestered in the tissues, especially in the spleen (Chapter 4), which may contribute to differential immune activation and pathology. Next, that subcurative treatment with artemether may have improved clinical outcome in rhesus monkeys cannot be ruled out. The rhesus monkeys that developed moderate anemia had either not been treated with artemether before they were sacrificed, or had received only one dose before improving after subsequent doses. Though a specific mechanism is not known, it is possible that direct anti-inflammatory drug effects, the controlled exposure of antigen, or the antigen bolusing pattern that resulted from serial subcurative treatment all play a role. These results may suggest that deployment of malaria preventative measures such as intermittent preventative treatment may have pathophysiological benefit in addition to an epidemiological one over no intervention in chronic, but asymptomatic or subclinical malaria [169].

Perhaps the most surprising result was that kra monkeys, despite being able to control parasitemia and relatively quickly (within roughly two weeks of inoculation with sporozoites) transition to chronicity, developed severe malaria, as defined by the presence of severe anemia. Strikingly, kra monkeys developed anemia with hemoglobin nadirs as low as 4.8 g/dL and hemoglobin loss of 45% on average, and were able to spontaneously improve, without the administration of anti-malarial medications or blood transfusion. Bystander killing is heavily implicated as a mechanism for red blood cell removal, as this magnitude of hemoglobin loss cannot be explained by direct parasite destruction alone, as discussed above, and studies of the bone marrow response, including the calculation of the reticulocyte production index and direct examination of the bone marrow demonstrate an adequate production response to red blood cell loss. This result underlines the importance of considering multiple factors when considering disease presentation, but also suggests an adaptive role for the development of anemia in malaria. Several studies have demonstrated that the administration of iron to anemic malaria patients may increase risk of development of severe malaria [170,171]. Additionally, in vitro studies have shown impaired replication of *P. falciparum* parasites in red blood cells isolated from anemic patients that improves when the parasites are given with RBCs from patients that received iron supplementation [172,173]. This result, taken in context with malarial anemia as a whole suggests that anemia is a double-edged sword that is effective in controlling parasitemia and death from acute malaria, but if unchecked, or if present in the background of exacerbating factors such as nutritional deficiency and co-infection may kill the host outright.

Another striking finding was the contrast in the temperature responses. Infection with *P. knowlesi* resulted in a temperature response at extremely low parasitemias in both species at 10^2 parasites/μL, with kra monkeys responding at roughly half the parasitemia as rhesus monkeys.

Because we used telemetry data to determine when the temperature increased rather than daily temperature taken with a thermometer as in field studies, which can artificially inflate the pyrogenic threshold if the time of temperature change is missed, we cannot directly compare the magntitude of the pyrogenic threshold to that of *P. falciparum* or *P. vivax*. However, for *P. knowlesi* itself, we conclude that pyrogenic is extremely low in naïve hosts. In addition to having a lower pyrogenic threshold than rhesus monkeys, kra monkeys responded an entire day sooner to blood stage parasites. This finding is critical because the *P. knowlesi* erythrocytic cycle is 24 hours long. The temporal response which may result from more sensitive immune sensing, may be key in early control of parasitemia. Last, using telemetry data, we found that kra monkeys did not become febrile in the chronic stage, and that rhesus monkeys, using rectal temperature data, showed decreasing temperature peaks that corresponded to decreasing parasitemia peaks, and that fever occurred with parasitemias greater than or equal to 1%. This may be useful in the field for assessing the clinical and presentation picture of patients with *P. knowlesi*. If fever is associated with acute infection, then serial presentations of the same patient may suggest re-infection, and therefore a higher transmission burden, than if fever were also a consequence of recrudescence. That is not to say that chronic *P. knowlesi* infection is symptom-free, but malaria should not be ruled out in the absence of fever.

Historical studies of *P. knowlesi* in rhesus macaques were able to induce a chronic infection through subcurative treatment of the parasitemia, and these experiments became the basis for understanding and describing antigenic variation in malaria and *P. knowlesi*, specifically [72]. Given our finding that kra monkeys respond quickly to control parasitemia, we were interested in exploring the hematological and pathological parameters associated with the induction of chronic disease in rhesus monkeys. Parasitemias at the primary and recrudescent peaks were artificially

capped with artemether treatment, however, they displayed a downward trajectory with time, as did rectal temperature. By the third peak, two of three rhesus monkeys no longer required arthemether treatment, and by the fourth, all of the animals controlled parasitemia on their own, and their kinetic curves plateaued to resemble that of a chronic infection. Mild anemia was observed, but its lack of severity may be a consequence of anti-malaria treatment (vide supra). Additionally, a shift in response can be seen in the bone marrow of these monkeys, with chronic rhesus and kra monkeys being indistinguishable in cellularity and precursor makeup.

An additional clue in the differences of the species' malaria response lies in the cytokines present at the primary peak and at baseline. We measured cytokine levels using SomaScan, a targeted proteomics approach. Kra monkeys had an increase in IL-1β, but no significant difference was found in the pro-inflammatory molecules, IL-6 and TNF-α, however the presence of a febrile phenotype suggests that the modest differences observed, though not statistically significant, are biologically relevant. All monkeys had an increase in IFN-γ, a cytokine associated with moderation of inflammation and parasite control at moderate amounts, however, rhesus had an increase in IFN-γ and IL-10, cytokines that when upregulated inappropriately, are associated with hyperparasitemia and more severe disease states [141,144]. TGF-β was upregulated only in kra monkeys, which may represent an appropriate moderation of the immune response to allow parasitemia control and also avoidance of severe disease.

We also examined the tissues to correlate systemic measures with the local consequences of parasite burden and inflammation. Interestingly, most tissues showed no pathological changes, a finding particularly relevant in the brain, which at high parasitemias has been shown to display pathological changes that are coincident with a cerebral malaria-like syndrome in monkeys and humans [27,56]. Most changes were restricted to the lungs, liver, gastrointestinal tract, kidneys,

spleen, and bone marrow, and in the case of the lungs, liver, gastrointestinal tract, and kidneys, most of the damage was minimal to moderate, and the findings were within the repertoire of findings that have been described in malaria, including interstitial thickening and alveolar wall infiltration consistent with interstitial pneumonia, fibrotic changes, and hemorrhage in the lungs, periportal infiltration, sinusoidal congestion, and Kupffer cell hyperplasia in the liver, glomerular and interstitial infiltration and tubular degeneration and calcification in the kidneys, splenomegaly with darkening in the spleen, and hyperplasia in the bone marrow [23,25,63,85].

Where possible, we attempted to correlate pathology findings with clinical parameters, which provides an important clinical correlation to direct organ damage and pathophysiology. We did not collect arterial blood gases or perform imaging studies on the lungs of our monkeys, so we were unable to include functional analysis with our histopathological examination of lung tissues. However, we were able to examine reticulocyte production index and bone marrow response, creatinine and kidney damage, and bilirubin, ALT, and AST to liver changes.

Direct comparison of pathology with laboratory values is essential especially in the kidney in our system. Clinically, kidney damage can present with hematuria, proteinuria, nocturia, and oliguria (or no urine output at all) [174]. The glomerular filtration rate is the gold standard for assessing kidney function [174]. The normal ranges for glomerular filtration rate (GFR) for humans were initially defined by measuring the clearance of inulin in the urine relative to how much was administered, and currently mathematical formulas that take into account the creatinine in the blood (a byproduct of muscle turnover that is typically cleared by the kidney), age, race, and gender are used as a simple clinical tool for assessing GFR in place of an inulin clearance test [174]. However, inulin clearance studies have not been done in rhesus and kra monkeys, and therefore no accepted formulas exist to calculate GFR from creatinine. Additionally, urine output

can be difficult to measure in monkeys without sedation and catheterization. As such, blood creatinine levels are used as a proxy to assess kidney injury, with a blood creatinine higher than 2 suggesting kidney injury. Because dehydration can artificially inflate the blood creatinine by essentially concentrating the blood, it is important to consider the entire clinical picture and the available histology when assessing for kidney injury. We found that there was not a perfect correlation with creatinine levels alone with the extent of tubular and other changes in the kidney. Additionally, creatinine levels began to improve in some monkeys after the supportive administration of intravenous saline. Taken with our pathology findings, it is likely that in some cases, the increased creatinines were a reflection of dehydration, and that dehydration and other factors had not progressed to the point of damaging the kidney histologically.

A disease severity metric in *P. knowlesi* infection is the presence of jaundice [54,133]. As such we were interested in assessing if bilirubinemia was present, and if so, if it and elevated ALT and AST levels corresponded with liver injury. Liver injury was mostly restricted to the presence of immune cells in the periportal regions and hepatic sinuses, with one unusual case of a lobar infiltrate forming in the chronic infection of a rhesus monkey. Though bilirubinemia was present, it was not dramatically elevated on average. Likewise, few monkeys had sustained or dramatic liver enzyme levels. This correlated clinically with the extent of the histology findings.

In conclusion, we present the first comprehensive, comparative, longitudinal study of the *P. knowlesi*-infected kra and rhesus monkeys of its kind. Contrary to canon, kra monkeys develop, and spontaneously improve from severe disease, as defined by the presence of severe anemia, despite controlling parasitemia. Given this information, and highly sensitive telemetry data results, we propose that a rapid and sensitive response which is well-controlled is key for controlling the first parasite peak and subsequent disease. Disease, which is sometimes severe, is among the

normal spectrum of disease for these animals. Two reports in the literature describe severe disease in what is described as kra monkeys. The first, the macaques were of Malayan origin, and described as having shorter tails than would be expected, suggesting hybridization with rhesus macaques (a phenomenon known to occur in an intergradation region between the two animals' home ranges) [19,30]. These potentially hybrid macaques all succumbed to infection with *P. knowlesi*. The second occurred in an accidental iatrogenic mass cross-infection of a cohort of kra monkeys undergoing a drug study, in which some of the monkeys experienced quite low hemoglobin nadirs [24]. When rhesus monkey parasitemias are controlled, they are able to produce a chronic infection which kinetically and histologically resembles that of kra monkeys. Punctuated subcurative treatment of rhesus monkeys to produce a chronic infection may also be at least partially responsible for a less severe clinical picture, and may provide insight into intermittent treatment of patients in the field.

Chapter 4: Investigating *Plasmodium knowlesi* infected red blood cell cytoadhesion and sequestration in macaque[3]

4.1 INTRODUCTION

Plasmodium knowlesi is a simian malaria parasite, that has been used extensively to model *Plasmodium* biology, especially the processes of antigenic variation and invasion of red blood cells (RBCs) [91,162,175]. In the absence of treatment, *P. knowlesi* causes severe, lethal disease in the experimental host, rhesus macaques (*Macaca mulatta*), while natural host species (e.g., *M. fascicularis*) do not succumb, and are able to develop chronic infection [20–22,25,28,134]. Recently, as *P. knowlesi* has been established as a causative agent for severe malaria in Malaysia, interest in understanding the pathophysiology of *P. knowlesi* infection and determinants of disease severity has taken on direct clinical importance [6,8,54].

Sequestration, a phenomenon whereby mature infected red blood cells (iRBCs) bind to the microvascular endothelium and are removed from circulation, is canonically described in *Plasmodium falciparum*, and is associated with severe disease outcomes such as placental and cerebral malaria [78]. Sequestration in this species is mediated by protein-protein interactions between endothelial proteins expressed in response to inflammation (such as ICAM1, VCAM1, and CD36), and large (~300 kD), variant antigen PfEMP1s on the surface of mature iRBCs, and

[3] Results from this chapter were presented as a poster at two Gordon Research Conferences:

Gordon Research Conference: Biology of Host-Pathogen Interactions. June 10 – 15, 2018 in Newport RI, USA.

Gordon Research Conference: Malaria. June 30 – July 5, 2019 in Les Diablerets, Switzerland, and also as a poster in the associated Gordon Research Seminar (June 29 – 30, 2019).

is thought to be a mechanism whereby the more rigid mature iRBCs might avoid destruction in the spleen [57,59,74,176].

Classically, the other *Plasmodium* species that cause malaria in humans are thought not to sequester, however experimental and clinical evidence point to the contrary in *P. knowlesi* infections. Classical literature describing *P. knowlesi*-rhesus macaque infections indicates a large number of mature parasitized RBCs in the microvasculature of several tissues, including those of the gastrointestinal tract [25–27,64,177]. More recently, severity in human *P. knowlesi* infections in Malaysia has been strongly associated with the presentation of gastrointestinal involvement [8,55]. Additionally, *P. knowlesi* expresses a large (~200 kD), surface-expressed variant antigen, known as the schizont-infected cell agglutination (SICA) protein, encoded by the ~137-member *SICAvar* gene family [67–70,178]. The exact function of this protein is unknown, however, in addition to mediating antigenic variation, it is associated with virulence and may mediate protein-protein interactions with the endothelium in a manner analogous to that of *P. falciparum* [71–73,76,179]. While autopsy studies in *P. knowlesi* are scarce due to cultural considerations, accumulation of mature iRBCs in the microvasculature of the gastrointestinal tract in *P. falciparum* is well-documented and associated with gastritis, duodenitis, and gastrointestinal symptoms [62,63,87,180]. Since sequestration in certain organs is associated with severe outcomes, and interaction with endothelial proteins is dependent on host species, it is also possible that the degree of sequestration, and where, could explain differences in pathophysiology between macaque host susceptibility to severe disease. We hypothesize that, similar to *P. falciparum*, *P. knowlesi* not only accumulates but cytoadheres and sequesters in certain tissues, but that this interaction is mediated by SICA proteins, and that the inflammation concomitant with parasite accumulation may result in organ histopathology and symptomology, as in *P. falciparum* infection.

4.2 METHODS

Experimental Design and Infections

Tissue and data from the *P. knowlesi*-infected monkey cohorts described in Chapter 3 were used for this study, with the exception of experiment (E33) (cohorts summarized in Appendix Table 6.8). Animals from E33 were excluded because the full suite of tissues that had been collected for the other cohorts was not collected for this one. All of these monkeys were infected with sporozoites produced from *P. knowlesi* clone Pk1(A+), a line that expresses protein from the large, surface-expressed, variant antigen gene family, schizont-infected cell agglutination var (*SICAvar*) [178]. Parasites from this line are abbreviated as SICA[+]. Housing conditions and inoculation information are described in detail in Chapter 3. In addition, two adult male rhesus monkeys were included for the experiments described in this chapter. As with the rhesus monkeys described in Chapter 3, these monkeys were born and reared at the Yerkes National Primate Research Center (YNPRC). Both monkeys were surgically splenectomized, and later infected with *P. knowlesi* clone Pk1(A-)1-, a parasite line that is phenotypically negative for expression of the *SICAvar* family [76]. Parasites from this line are abbreviated as SICA[-]. The monkeys were inoculated with iRBCs via intravenous injection into the saphenous vein, and monitored twice daily by microscopy analysis of thick and thin smears from capillary blood samples collected by ear stick. When the monkeys reached over 5% total iRBCs, they were euthanized, and a maximum bleed was performed to collect parasites. Tissues were collected from the same organs as the previous cohorts: lung, liver, kidney, adrenal gland, ventricle, aorta, stomach, mesenteric lymph node, thymus, duodenum, jejunum, colon, skeletal muscle, skin, eye, cerebrum, cerebellum, midbrain, bone marrow from femur and costochondral junction, testis, and omentum. Gross lesions

were documented with photography, and examples of lesions were collected for histopathological analysis.

All experimental, surgical, and necropsy procedures were approved by IACUC and followed accordingly, with veterinary supervision.

Tissue analysis and parasite enumeration

Tissue sections collected at necropsy were preserved in 10% neutral buffered formalin, embedded in paraffin, sectioned at 4 μm, and stained with hematoxylin and eosin (H & E) for histological examination [106]. Frozen sections (preserved in optimal cutting temperature compound), sections for electron microscopic examination (preserved in 2.5% glutaraldehyde), and samples for tissue transcriptomic analysis (preserved in RNAlater™) were also collected.

Selected sections of stomach, duodenum, jejunum, and colon were immunohistochemically stained for markers of endothelial activation, including ICAM1 (rabbit anti-human ICAM1 IgG1 monoclonal antibody, clone EPR4776, Abcam), and MAdCAM1 (mouse anti-human MAdCAM1 IgG1 monoclonal antibody, clone 314G8, Thermo Fisher), as described elsewhere (Chapter 2).

Electron microscopy grids were prepared by primary fixation in 2.5% glutaraldehyde, followed by washing, secondary fixation in 1% osmium tetroxide, dehydration in graded ethanol solutions and staining with uranyl acetate, treatment with 100% propylene oxide, infiltration of resin, and resin embedding. Semi-thin tissue sections were stained with toluidine blue and examined by light microscopy prior to grid preparation to aid in the proper orientation of samples.

Mature parasites (trophozoites and schizonts) can be readily identified in H & E-stained tissue sections. Tissue parasite densities were determined by counting the number of mature parasites in ten high-power (1000x) microscope fields (HPF) under oil immersion, except for brain and eye tissues, which were quantified in 50 capillaries [181]. Standardized tissue densities to

show relative changes between acute and chronic states, and differences between the two species were determined by dividing each parasite tissue density by the sum of all of the parasite tissue densities in each group (acute rhesus, chronic rhesus, acute kra, chronic kra). The resultant proportions were combined in a vector and binned to create a color scale. The color scale for a parasite distribution heat map was created using the bin_data command in the mltools package in R, with a bin value of seven, and a quantile bin type. The colors in the heat map were assigned by species, and are from the Reds and Blues Brewer Color Palettes from the RColorBrewer package in R, and were imported into Adobe Illustrator as .ase files.

Binding Studies

The cytoadhesion properties of SICA[+] and SICA[-] parasites were tested against *P. falciparum* FVO (gift from Dr. Barnwell), a strain extensively demonstrated to strongly bind CD36 [57], as well as uninfected rhesus blood, and in the case of MAdCAM1 binding, HuT78 cells (ATCC), a human T-lymphocyte line from a patient with Sézary Syndrome that expresses the integrin, $\alpha4\beta7$, which binds MAdCAM1 [182]. Parasites collected at peak parasitemia from two monkeys (RTe16 and RUf16) from E06 at peak parasitemia were inoculated into naïve rhesus monkeys to expand the population. This *in vivo* expansion technique was necessary because strains of parasites involved in our experiments do not readily re-invade RBCs *in-vitro*, and iRBCs directly from the original monkeys was limited because it was earmarked for omics studies. Aliquots of these expanded SICA[+] parasites and the SICA[-] parasites obtained from infecting the two splenectomized rhesus monkeys were used for binding experiments, as described previously (*vide infra*). Parasitized RBCs, uninfected RBCs, and T lymphocytes were added to several cell lines including C32 amelanotic melanoma cells (gift from Dr. Barnwell), ICAM1-, CD36-, and mock-transfected CHO cells (gifts from Dr. Barnwell), to immortalized human

endothelial cell lines, HIMEC.1, HAPEC.S1, HPLNEC.B3 (provided by collaborator Prof. C. Kieda, Centre de Biophysique Moleculaire, CNRS, Orleans, France), and to primary endothelial cells isolated from the microvasculature of human colon (HIMEC cells, Creative Bioarray) to test binding [183–185]. Culture conditions for these primary and immortalized cell lines were different, and were performed according to ATCC or manufacturer protocols unless otherwise specified. Briefly, C32 amelanotic melanoma cells grown in Eagles Minimal Essential Medium (EMEM, ATCC) supplemented with 10% FBS. The transfected CHO cell lines were cultured in Kaighn's Modification of Ham's F-12 Medium (F-12K, ATCC) supplemented with 10% FBS. The immortalized endothelial cell lines were cultured in OptiMem I with Glutamax (Gibco 51985) supplemented with 2% FBS, 0.4% gentamicin (stock concentration of 10 mg/mL), and 0.2% amphotericin B (stock concentration of 250 μg/mL) [185]. The HIMEC cells were cultured in flasks pre-treated with 0.1% gelatin to facilitate cell adhesion, in specialized media. All human cells were cultured in vented flasks at 37° C in 5% atmospheric CO_2 in the presence of a water bath to provide humidification. Adherent cells lines were scraped using plastic cell scrapers to passage, and endothelial and primary cells were removed from flasks using trypsin-EDTA. When the adherent cell cultures were at least 80% confluent, they were seeded onto 15 mm tissue-culture treated coverslips (Thermanox, Thermo-Fisher product number 174969) in a 24-well plate, and grown until approximately 30% confluency. Where indicated, endothelial cells were activated by treatment with LPS or TNF-α. All parasites were thawed using standard techniques the day prior to the assay and allowed to mature until the late trophozoite to four-nucleated schizont stage in RPMI supplemented with bicarbonate and 10% AB+ human serum, without antibiotics. Parasites were cultured by gassing them with blood gas mixture (5% CO_2, 5% O_2, 90% N_2), and incubation

in 37° C. HuT78 cells are a suspension culture and were cultured at cell densities no more than 10^5 cells/mL in Iscove's Modified Dulbecco's Medium (IMDM, ATCC) supplemented with 20% FBS.

Protein and cellular binding assays were performed as described previously [57,186–188]. Briefly, *ex vivo* matured *P. falciparum* and SICA[+] and SICA[-] *P. knowlesi* parasites or HuT78 cells were washed and resuspended in binding buffer (incomplete RPMI without bicarbonate for parasites, D-PBS with Mg, Ca, and Mn for HuT78 cells), and layered on coverslips in washed wells with adherent cells at 1% hematocrit. Plates were gently rocked at 37° C for 1 hour, then the coverslips were removed and washed by gently dipping in PBS until blood no longer ran off the coverslip grossly. Coverslips were then fixed in 0.5% glutaraldehyde, placed on a glass slide, allowed to dry overnight, then stained with 10% Gurr stain for enumeration.

For purified protein binding assays, purified CD36 (R&D Systems), ICAM1 (R&D Systems), MAdCAM1 (R&D Systems), and full-length MAdCAM1 (Origene) were resuspended at a concentration of 100 μg/mL or dialyzed at a concentration of 50 μg/mL into either PBS or PBS with Mg and Ca. A circle was drawn on the bottom of a 60 mm polystyrene bacteriological Petri dish (Falcon, product number 351007) for ease of quantification, and 20 – 40 μL of protein was pipetted inside. The plates were placed in a humidified chamber and protein was allowed to bind either overnight at 4° C, or for four hours at 37° C. After binding, excess liquid was pipetted off, the plates washed twice with excess PBS or PBS with Ca and Mg, and then blocked with 1% bovine serum albumin (BSA) in phosphate buffered saline (PBS) in PBS or PBS with Ca and Mg for one hour at 37° C in a humidified chamber. After blocking, the blocking agent was removed, the plates were washed twice, and *ex-vivo* matured parasites at 1% hematocrit or 10^6 HuT78 cells were added, then rocked for 1 hour in a humidified chamber at 37° C. After binding, plates were gently washed, fixed with 0.5% glutaraldehyde, allowed to dry overnight, stained with 10% Gurr,

then visualized and quantified against background. Expanded and detailed methods are illustrated in Appendix Section 6.3.

RNAseq and Targeted Proteomics Analysis

Blood aliquots taken at the pre-defined time points designed for each experiment (Chapter 3) were analyzed using RNAseq in collaboration with the Yerkes Genomics Core. Briefly, blood samples from Time points 1 or 2 (baseline) and 4 or 5 (peak or necropsy) were collected in Paxgene tubes, extracted, and globin-depleted. Libraries were prepared and the samples were sequenced to a depth of 25-30 million reads per sample before being normalized by DESeq. The pheatmap package in R was used to create heatmaps.

Targeted proteomics were obtained using SOMAScan, as described in Chapter 3.

Statistical Analysis

Statistical analyses and figures were produced in either R Studio version 1.1.383, under R version 3.4.3 GUI version 1.70. Pairwise comparisons were performed using either Welch's T-Test or the Wilcox Sum Rank test. Multiple comparisons were performed using ANOVA analysis, the Dunnett Post-Hoc Test, and Tukey HSD Post-Hoc Comparison Test. For correlation analysis, either the Pearson's or Spearman correlation tests were used. Comparisons were considering significant if the p-value was below 0.05. All multiple comparisons were adjusted using the Bonferroni method.

4.3 RESULTS

Parasite accumulation in tissues varies in host species and infection status

Sequestration results in an accumulation of parasite-iRBCs in the post-capillary venules of tissues through protein-protein interactions that can be tissue-specific, depending on the host endothelial protein involved [78,80,189]. Therefore, we first sought to determine if parasite

accumulation favored certain tissues over others. To accomplish this, the total number of mature parasitized RBCs, defined as those RBCs infected with trophozoites or schizonts, were enumerated in ten HPFs in sections of up to 22 different tissues (described in the Methods). This provided a parasite density that could serve as a proxy for parasite burden across tissue and host species. Additionally, monkeys were divided into acute and chronic groups to address the longitudinal nature of the cohorts: monkeys sacrificed at prior to Day 20 post infection were assigned to the acute group, those sacrificed later were assigned to the chronic group. Log-transformed tissue parasite counts in acute and chronic infection are presented in Fig. 4.1, and means, sample size, and standard deviations are provided as Supplementary Data (Appendix Table 6.10).

Parasites were not distributed uniformly in rhesus macaques with acute infections (χ^2 = 725.27, p-value < 2.2 x 10^{-16}), suggesting preference for the accumulation in some organs over others. The spleen represented a major reservoir for parasite accumulation in rhesus macaques with acute infections (mean = 172 parasites per section +/- 141). The parasites were found predominantly in the red pulp, and were intact, contrary to what would be expected, as the spleen plays a large role in parasite removal (Fig. 4.2A) [127]. The adrenal gland, eye, lung, kidney (Fig. 4.3A-D), stomach, and duodenum (*vide infra*) also contained large parasite burdens, defined as an average of 28 parasites in 10 HPFs (Appendix Table 6.10). Sequestration in the brain is of particular interest because of its involvement in the development to cerebral malaria in *P. falciparum*. Parasite accumulation in the brain tissues (cerebrum, cerebellum, and midbrain) of *P. knowlesi*-infected rhesus macaques, was markedly lower than that of higher-burden organs – averaging between roughly 20 to 26 parasites in 10 HPFs (mean = 26 +/- 18; mean = 22, +/-14; mean = 20 +/- 12, for midbrain, cerebrum, and cerebellum, respectively). In addition to the tissues of the brain, the liver, colon, aorta, the mesenteric lymph node, and jejunum had moderate numbers

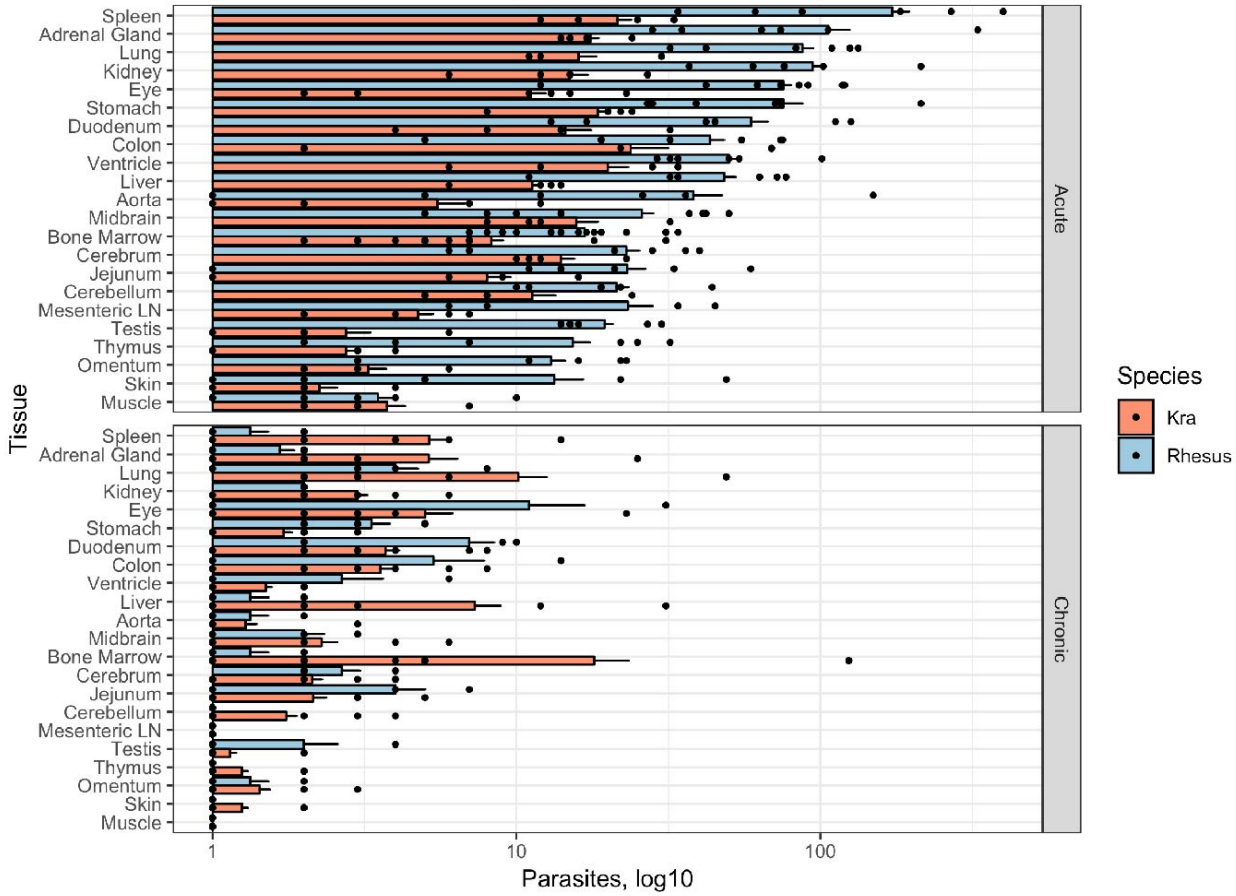

Figure 4.1 Parasite tissue burdens in *P. knowlesi* infection. Log_{10}-transformed parasite densities in acute (top) and chronic (bottom) infection are presented for rhesus and kra monkeys. Bars represent the mean of each tissue. Black dots represent the parasite density (parasites/10 HPFs) in a single tissue section. Error bars represent the standard error of the mean.

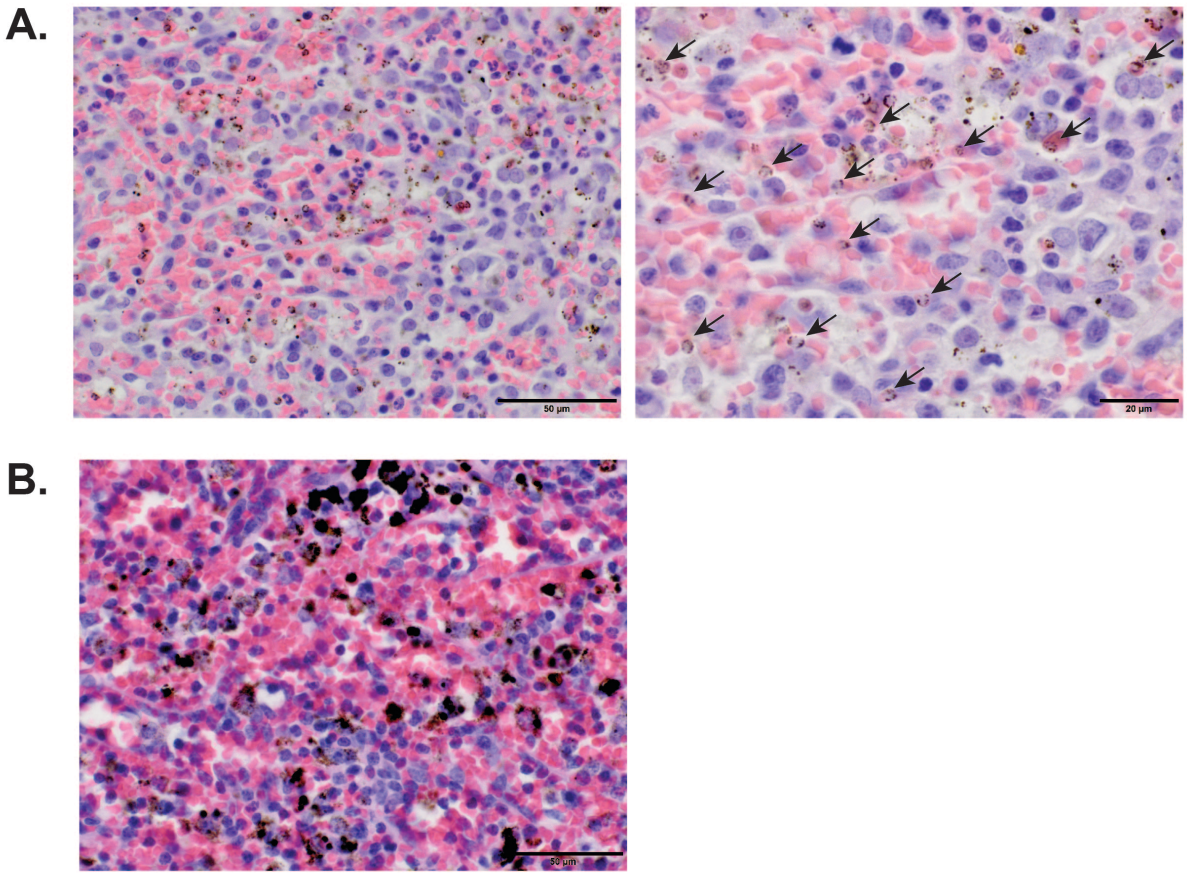

Figure 4.2 Parasite accumulation in the rhesus spleen in acute and chronic infection. A., The red pulp of a rhesus spleen in acute infection is a major place of parasite accumulation, and is shown at 600X (left) and 1000X (right) magnification with examples of intact parasites indicated by black arrows. B., The red pulp of a rhesus spleen in chronic infection has very few intact parasites, and many heavily pigmented macrophages (600X).

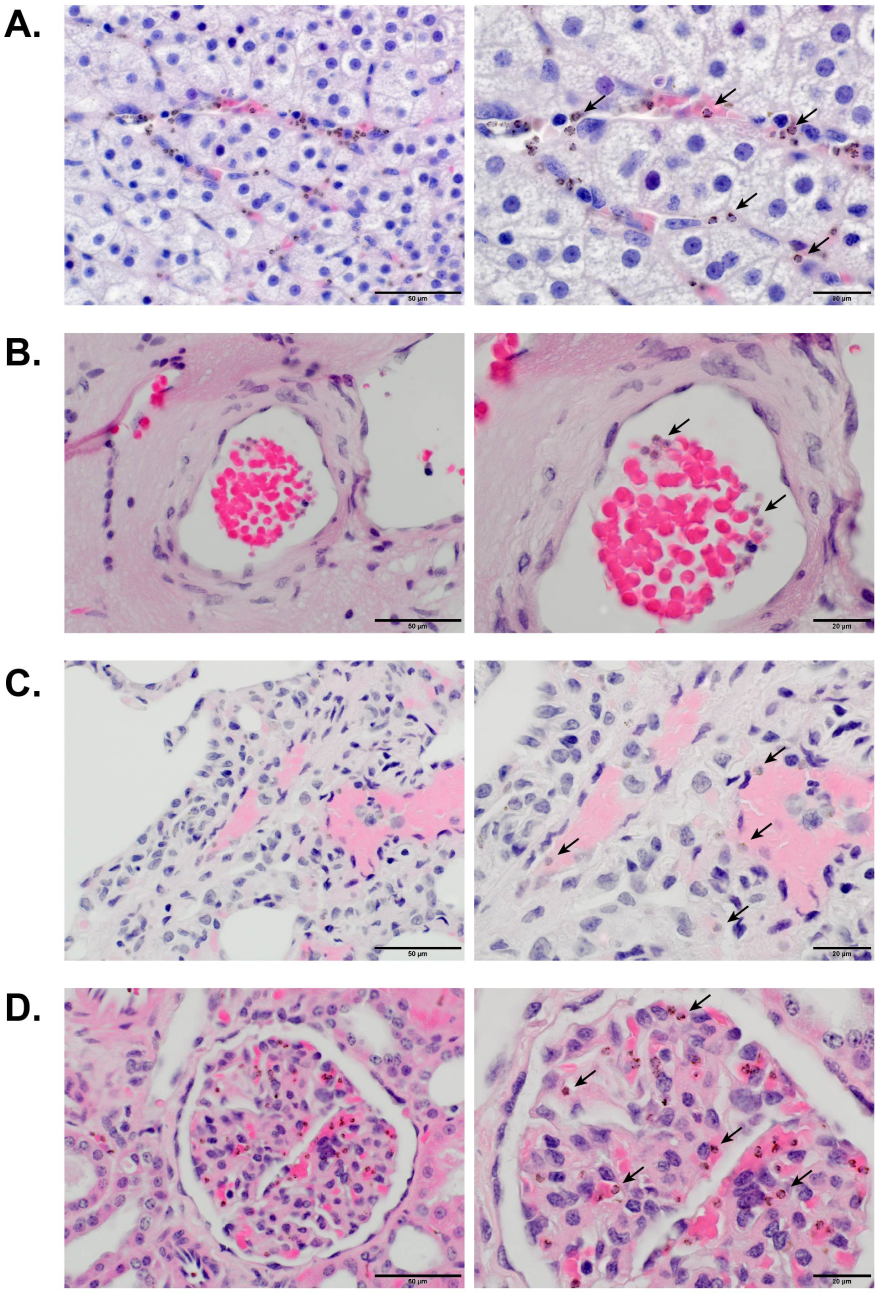

Figure 4.3 Parasite accumulation in the rhesus tissues in acute infection. Representative micrographs of tissues with high parasite burdens are given, with the left column at 600X, the right column the same section at 1000X, and examples of parasites indicated by black arrows in the 1000X micrograph: A., The adrenal gland. B., The eye. C., The lung., D., The glomerulus of the kidney.

of parasites, averaging from 48 for the liver, to 21 in the cerebellum. The skin and skeletal muscle, two tissues that have been demonstrated to be important sites for *P. falciparum* sequestration [62,190], were among the lowest burden of parasites (mean = 12 +/- 19; mean = 3 +/-3, respectively). The bone marrow, thymus, and omentum also had relatively low parasite accumulation (Fig. 4.1 and Appendix Table 6.10).

Acute *P. knowlesi* infections in *M. fascicularis* had lower parasite burdens relative to those of rhesus monkeys, across all tissues on average, which was widely consistent with the lower, on average, circulating parasitemias that were observed in these animals. As in rhesus monkeys, parasite accumulation was not uniformly distributed ($\chi^2 = 82.62$, p-value = 2.93×10^{-9}), however the distribution of parasites was not as heavily biased toward one or a few of tissues as in rhesus macaques (Fig. 4.1). Additionally, though the spleen was a major place of parasite accumulation (mean 21 +/-9), it was comparable to the colon (mean = 23 +/-32). The ventricle, stomach, adrenal gland, and lung, midbrain, and kidney also represented higher parasite loads in kra monkeys, all averaging equal to or greater than 15 parasites in 10 HPFs (Supplemental Table 6.10). The duodenum, cerebrum, liver, cerebellum, and eye all contained a relatively moderate parasite density (averaging from 15 for duodenum to 11 for the eye). As in rhesus monkeys, the skin (mean = 1 +/-1), and muscle (mean = 3 +/-2) tissues were not a major site for parasite accumulation. Additionally, the bone marrow, jejunum, aorta, mesenteric lymph nodes, omentum, thymus and testes all contained fewer than 10 parasites per 10 HPFs (Fig 4.1 and Appendix Table 6.10).

Though the spleen seems to be a critical location for parasite accumulation during acute infection in rhesus monkeys, intact parasites are widely not present in this organ during chronic infection (mean = 0, +/-1). In their place, debris and hemozoin were observed (Fig. 4.2 B). The

adrenal gland, omentum, liver, bone marrow, aorta, and thymus also had very low parasite densities. The skin, muscle, and mesenteric lymph node all contained no parasites. In rhesus monkeys, there are very few parasites in the tissues by the time of chronic infection, which is reflective of the lower circulating parasitemia. However, parasites could still be found in the eye (mean = 10 +/-17), the duodenum (mean = 6, +/-4), and the colon (mean = 4, +/-8). The lung, jejunum, stomach, ventricle, cerebrum, testes, midbrain, and kidney had average parasite densities between less than or equal to four, and greater than or equal to two.

Despite very low parasitemias with chronicity (<100 parasites per microliter), kra monkeys also retained parasites in their tissues. The most striking compartment for parasite accumulation was the bone marrow, which had an average of 18 parasites in 10 HPFs (Fig 4.4). The lung, liver, spleen, adrenal gland, and eye had moderate numbers of parasites, though it is notable that the spleen had many fewer parasites in the chronic infections relative to the acute infections (Fig. 4.1). Along with the kidney, midbrain, cerebrum, cerebellum, ventricle, omentum, aorta, thymus, skin, testes, muscle, and mesenteric lymph node, the tissues of the gastrointestinal tract, including duodenum, colon, jejunum, and stomach contained few parasites, during the chronic stage, despite their role as a parasite reservoir during the acute infection.

To illustrate the relative differences in parasite organ density between the two macaque species in acute and chronic infection, a heat map was created (Fig. 4.5) based on relative parasite tissue densities (Appendix Table 6.11). With the acute infections, the colon, spleen, and ventricles of the heart (together representing roughly 27% of the tissue compartment parasite density together), followed by stomach, adrenal glands, and lungs (7.6%, 7.2%, and 6.5%, respectively) were important sites of parasite accumulation in kra monkeys. During the chronic infection, the parasite reservoir shifted to the lungs, liver, eye, and bone marrow, with these four tissues

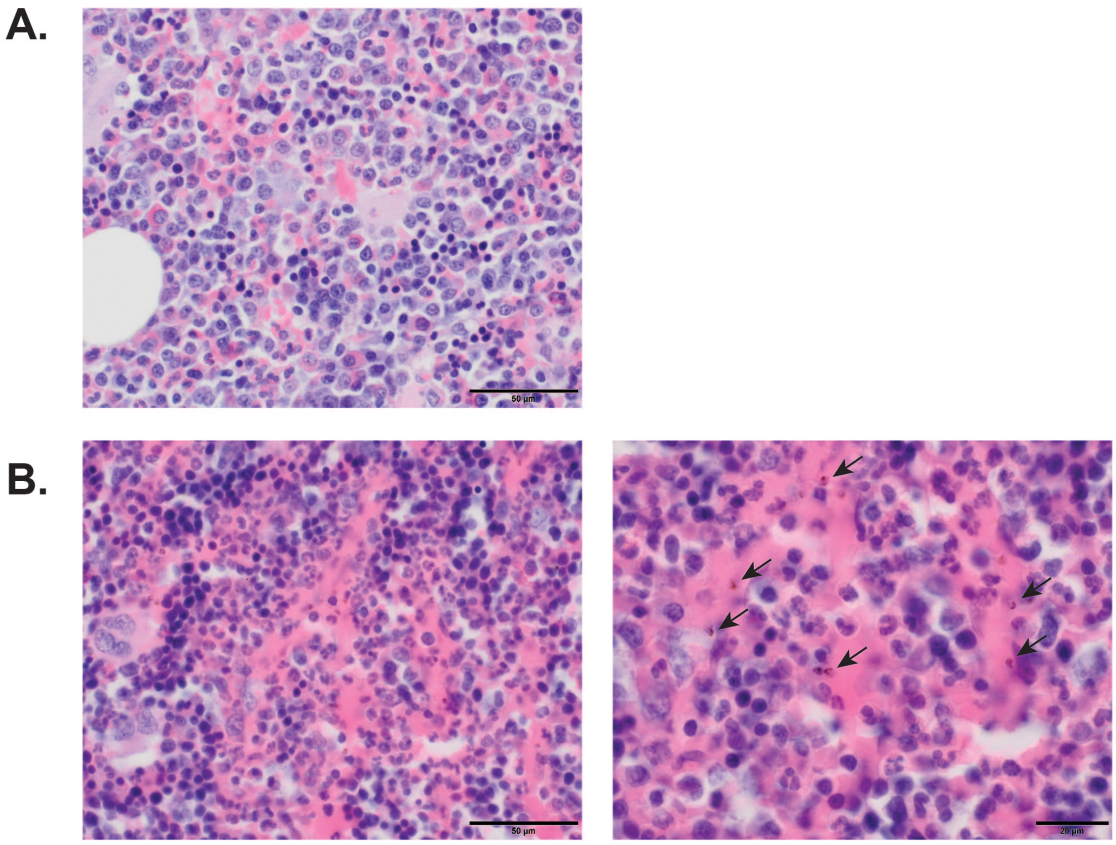

Figure 4.4 Parasite accumulation in kra bone marrow in acute and chronic infection. A., The bone marrow in kra monkeys is not a significant niche for parasite accumulation in acute infection (600X). B., In chronic infection however, many parasites can be found, and a representative section is shown at 600X (left) and 1000X (right) magnification with examples of intact parasites indicated by black arrows.

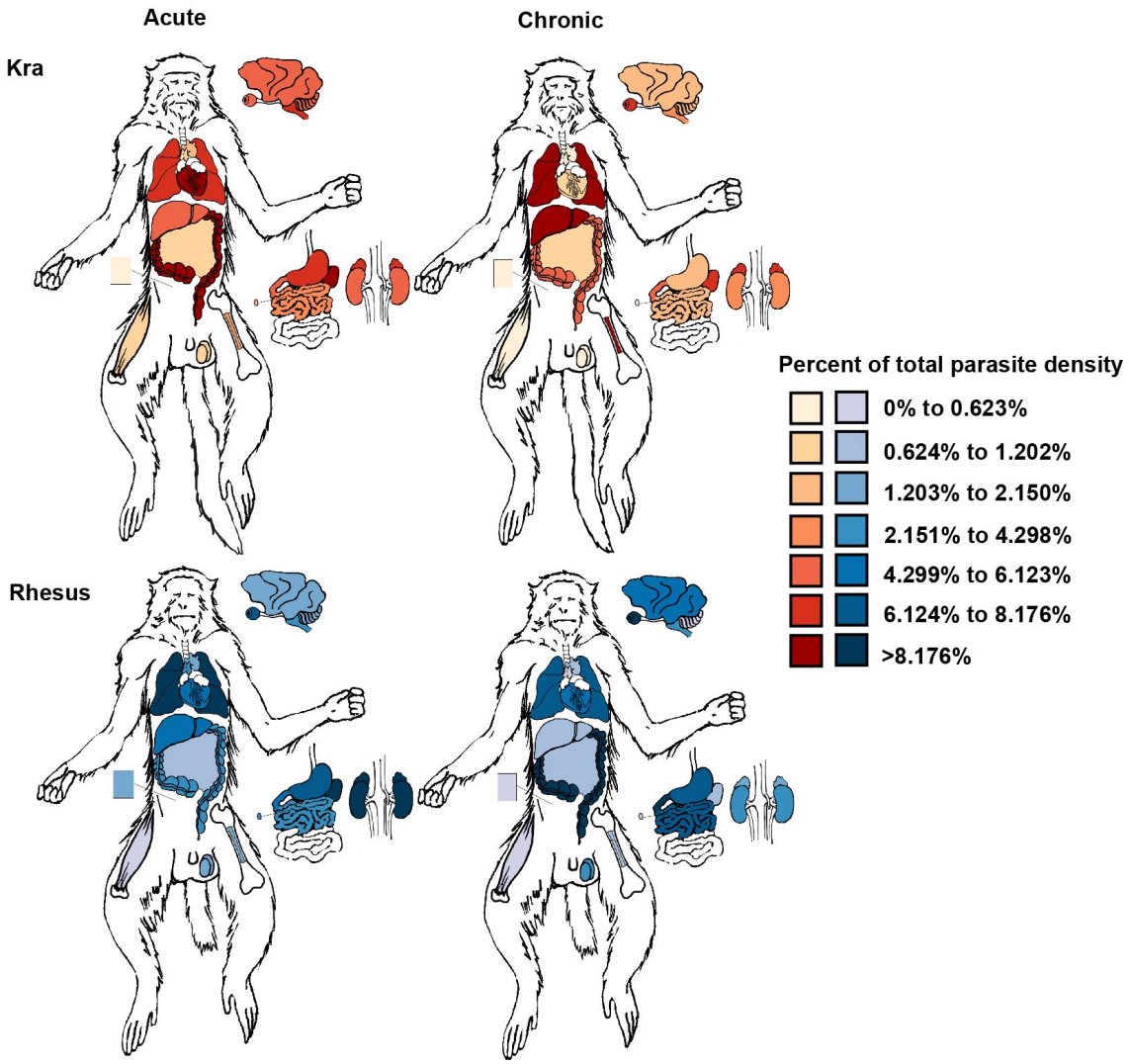

Figure 4.5 Relative parasite tissue densities in kra and rhesus monkeys in acute and chronic infection. A heatmap representing the relative parasite densities in each tissue indicates that the proportion of parasites is different between species and in acute and chronic infection within species.

accounting for over 60% of the tissue compartment parasite density. Though the number of parasites is greatly reduced between the acute infections and chronic infections (an average of 21 parasites in 10 HPFs versus 4 parasites per 10 HPFs), the splenic proportion of parasite density changed little between the acute (8.9%) and chronic (7.1%) infections. In rhesus monkeys, with acute infection, the spleen, adrenal glands, kidneys, lung, eye, stomach, duodenum, and ventricle play an important role in acute infection, represented 16.7%, 10.2%, 9.1%, 8.4%, 7.3%, 7.3%, 5.6%, and 4.8% of the total tissue compartment parasite density enumerated, respectively. During chronicity, the burden shifted to heavier accumulation in the eye and gastrointestinal tract (26.8%, for the eye, and 16.1%, 11.6%, 8.0%, 6.2% for the duodenum, colon, jejunum, and stomach, respectively). Notably, the parasites were not evident in the adrenal glands, kidneys and the spleen during chronic infection.

Degree of histopathology is weakly correlated with parasite tissue density

Semi-quantitative histopathology scores were presented in Chapter 3 for tissues that were observed to exhibit histopathological changes. To test if the damage the host sustained during infection is related to the presence of parasites, parasite tissue burdens (*vide supra*) were correlated with histopathology score. The spleen, bone marrow, and lymph node data were not included, because the histological changes in these tissues were considered to be in the normal range of these organs' function in the context of infection.

First, to determine if the proportions of tissues with and without high parasite load were different from those with and without pathology, a Fisher-Exact Test was performed on the data from acute infections. The data for parasite accumulation and histopathology scores were assigned

to a 2 x 2 contingency table (Table 4.1 and 4.2) with high parasite burden defined as any tissue with an average parasite density greater than the median of overall parasite density (28 parasites

Table 4.1: Fisher Exact Test Contingency Table

	High Parasite Burden (%)	Low Parasite Burden (%)
Positive Score	6 (60%)	1 (11%)
Negative Score	4 (40%)	8 (89%)

Table 4.1: Fisher exact test for tissue score and parasite burden in rhesus acute infection. The Fisher Exact Test Contingency table and results are summarized. $\alpha = 0.05$; $P = 0.057$; Odds ratio: 10. 37.

in 10 HPFs for rhesus macaques, and 7 parasites in 10 HPFs for kra monkeys). The median rather than the mean was selected due to the skewed nature of the data. Pathology data were assigned as those with a positive histopathology score (score greater than 0), and those without histopathological changes (score = 0). For rhesus monkeys, the odds ratio for a tissue with pathology to have a high parasite burden was 10.37, however the p-value was 0.057. However, for kra mokeys, the odds ratio is infinity, with a p-value of 0.0174.

Table 4.2: Fisher Exact Test Contingency Table

	High Parasite Burden (%)	Low Parasite Burden (%)
Positive Score	7 (58%)	0 (0%)
Negative Score	5 (42%)	7 (100%)

Table 4.2: Fisher exact test for tissue score and parasite burden in kra acute infection. The Fisher Exact Test Contingency table and results are summarized. $\alpha = 0.05$; $P = 0.017$; Odds ratio: infinity

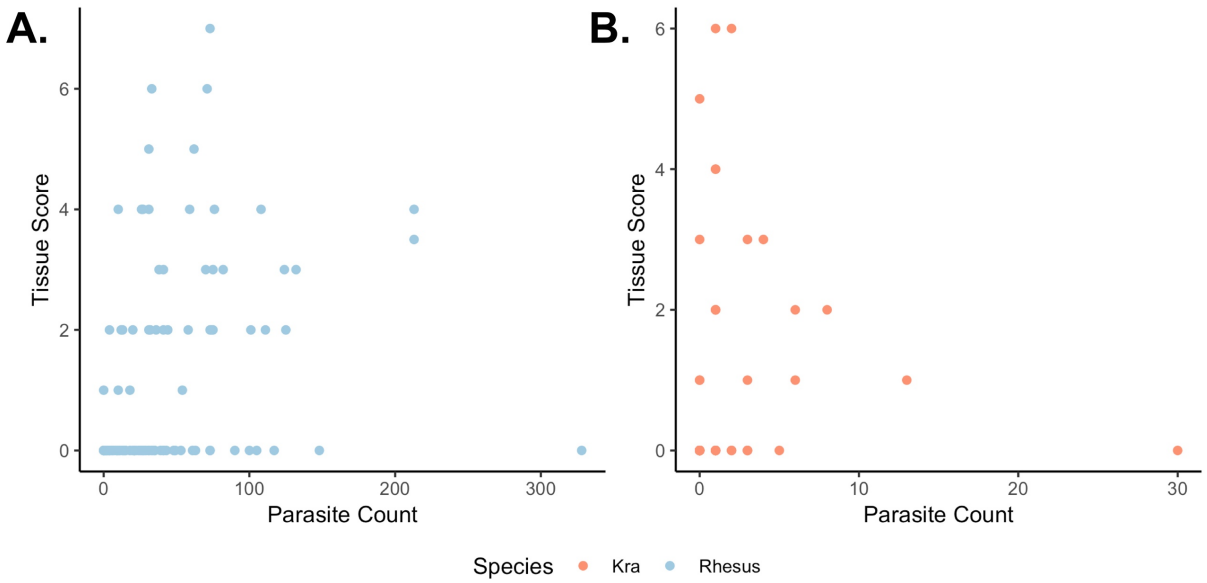

Figure 4.6 Tissue score vs. parasite count. Total histopathology score plotted against the number of parasites in 10 HPFs (1000X) in acute infection of A., rhesus monkeys, and B., kra monkeys. Spleen, bone marrow, and lymph node were excluded because the changes observed in these tissues were normal responses within organ function.

Next, to determine if score and parasite tissue density are correlated, they were plotted against each other in a scatter plot and both Pearson and Spearman coefficients were calculated (Fig. 4.6 A and B). For rhesus monkeys in acute infection, the Pearson coefficient was 0.309, with a p-value of 0.0008, and Spearman's $\rho = 0.434$, with a p-value of 1.59×10^{-6}, demonstrating a weakly linear positive correlation between score and parasite tissue density. In acute kra monkey infections, the Pearson coefficient was 0.206, with a p-value of 0.0739, suggesting no linear relationship. Spearman's ρ was 0.272 with a p-value of 0.017 which indicates a weakly positive correlation between score and tissue density.

Parasite tissue burden may not be the only thing that is correlated with histopathological damage. The circulating parasitemia, which has been associated with severity of presentation in patients, can be an indicator of inflammatory response and other factors that might result in tissue damage. Along similar lines, the cumulative parasitemia over time may also be correlated with the degree of tissue damage, and may especially be important in chronic infections, where the host has been exposed to inflammatory stimuli for a longer period of time. Therefore, a hierarchical multiple linear regression analysis was performed to determine which factors affected these scores the most (Table 4.3). A model considering only parasite tissue burden did not result in a linear relationship (adjusted $R^2 = 0.048$, p-value = 1.548×10^{-5}), however, when combined with tissue, the relationship was strongly linear (adjusted $R^2 = 0.7504$, p-value = 2.2×10^{-16}). The contribution to the model parasite tissue burden remained significant after the addition of tissue (p-value = 0.0086). A model including an interaction term between tissue parasite burden and score did not improve the fit of the model ($R^2 = 0.7531$, p-value = 2.2×10^{-16}), and the interaction term was not a significant contributor. Multicollinearity was assessed using the "olsrr" package in R by generating variance inflation factors (VIFs), and by examining the eigen values of the variance

Table 4.3: Linear Regression

	Model 1					Model 2				
	Estimate	Std. Error	t value	p-value	Significance	Estimate	Std. Error	t value	p-value	Significance
Intercept	0.727	0.087	8.360	$1.43x10^{-15}$	***	-0.128	0.180	-0.712	0.477	NS
Count	0.010	0.002	4.382	$1.55x10^{-5}$	***	-0.003	0.001	2.643	0.009	**
Tissue										
Aorta						0.085	0.247	0.344	0.731	NS
Cerebellum						0.097	0.247	0.392	0.695	NS
Cerebrum						0.093	0.247	0.378	0.706	NS
Colon						1.378	0.246	5.604	$4.35x10^{-8}$	***
Duodenum						1.772	0.249	7.122	$6.44x10^{-12}$	***
Eye						0.039	0.245	0.160	0.873	NS
Jejunum						1.360	0.247	5.496	$7.67x10^{-8}$	***
Kidney						2.333	0.245	9.529	0.000	***
Liver						4.448	0.249	17.86	0.000	***
Lung						3.563	0.248	14.36	0.000	***
Midbrain						0.094	0.247	0.379	0.705	NS

Midbrain	0.094	0.247	0.379	0.705	NS
Muscle	0.123	0.249	0.495	0.621	NS
Omentum	0.113	0.248	0.455	0.650	NS
Skin	0.114	0.248	0.458	0.648	NS
Stomach	2.43	0.245	9.914	0.000	***
Testis	0.106	0.248	0.429	0.668	NS
Thymus	0.111	0.248	0.448	0.654	NS
Ventricle	0.533	0.246	2.170	0.031	*
	N = 358; df = 356; Adjusted R^2 = 0.048; F-statistic = 19.2; p-value = 1.54 x 10^{-5}		N = 40; df = 338; Adjusted R^2 = 0.751; F-statistic = 54.48; p-value = 2.2x10^{-16}		

Table 4.3 Linear Hierarchical Linear Regression Analysis. MLR was performed to test the relationship between score, count, and organ. For organ, adrenal gland was selected as the reference tissue. Parameter is significant at $\alpha = 0.05$; *P < 0.05, **P<0.005, ***P<0.0005.; NS= not significant.

that result from linear combinations of each variable and their condition indices. No multicollinearity was noted (indicated by a VIF > 10, or a condition index > 30 with a correspondingly high eigen value, defined as > 0.5). Species, status (acute vs. chronic), parasitemia at necropsy, and cumulative parasitemia were not significant.

SICA protein-expressing RBCs infected with mature parasites clearly sequester in rhesus monkeys

Several mechanisms may explain a given parasite species' propensity to accumulate in tissues, including but not limited to altered physical or rheological properties of the iRBCs (increases or decreases in stiffness as may occur in mature *P. falciparum* and *P. knowlesi,* or *P. vivax*, respectively), and/or specific protein-protein interactions with the endothelium [80,84,191–193]. When observed kinetically, parasites that sequester typically display a z-pattern longitudinally if smears are taken to observe multiple stages in the life cycle, with fewer-than-expected or an absence of mature forms peripherally [11]. In the cohorts of *P. knowlesi*-infected macaques, parasitemia kinetics from capillary samples manifested a saw-tooth pattern (Supplemental Fig. 6.2-6.6), and though circulating mature forms were observed, they were fewer than predicted (Supplemental Fig. 6.49), suggesting the possibility of incomplete levels of sequestration, if it was occurring.

During the quantification of all 22 tissues collected from the *P. knowlesi*-infected macaques, vessels were examined for any evidence that would suggest cytoadhesion and sequestration was occurring as a mechanism for parasite accumulation. Sequestration occurring in the tissues of autopsied *P. falciparum*-infected patients and new world nonhuman primates presents with a very characteristic phenotype in which smaller vessels are crowded with tightly-packed mature iRBCs, and larger vessel endothelia are lined with mature iRBCs [61–63]. In th

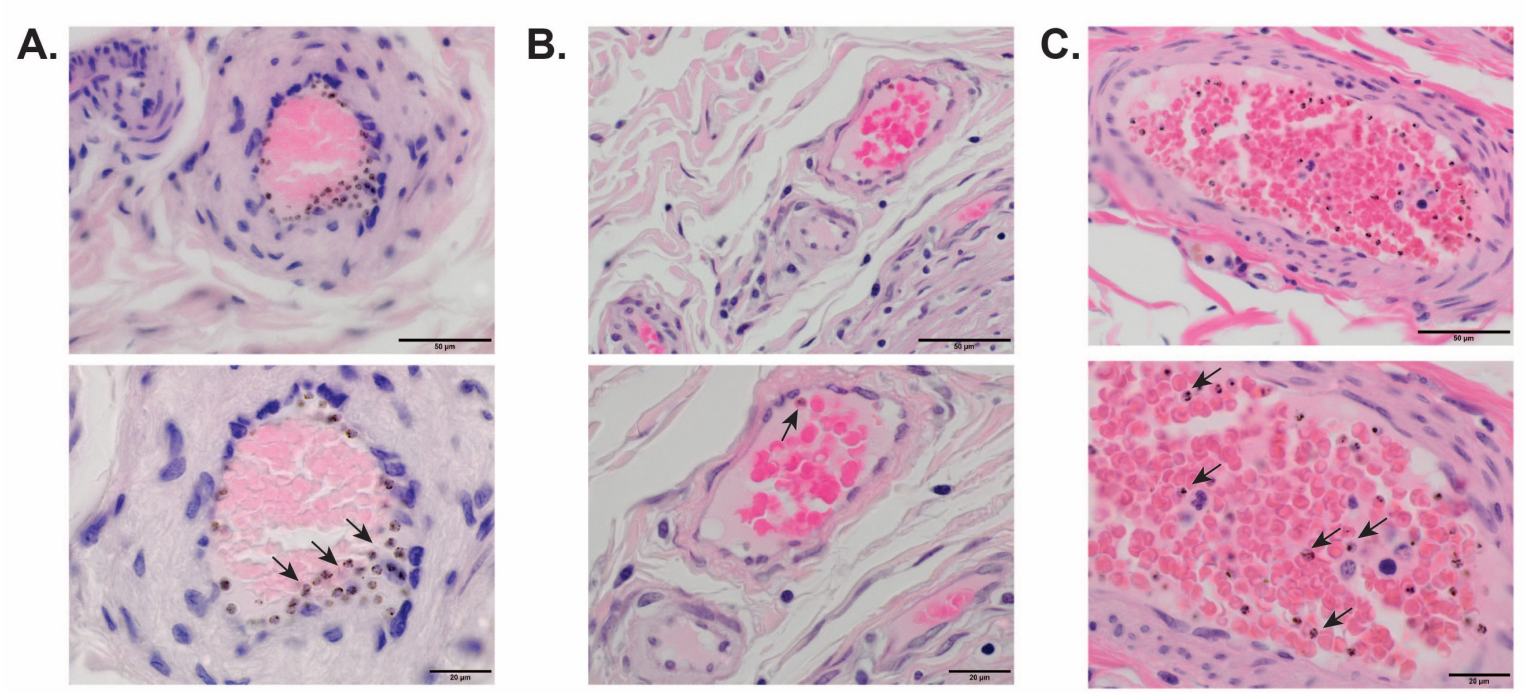

Figure 4.7 Light microscopy: SICA protein expression and sequestration in the stomach. Micrographs demonstrating the margination phenotype as it relates to SICA protein expression were taken showing vessels in the submucosa, with 600X images on top, and 1000X images on the bottom and black arrows demonstrating parasites in the higher power image. Sections stained with H & E. A., Mature, pigmented iRBCs stud the endothelium of this submucosal vessel in a rhesus macaque infected with SICA[+] parasites, with clear preference for the margins of the vessel over the lumen. B., A clear margination phenotype was not as obvious in kra monkeys infected with SICA[+] parasites. C., Despite high parasitemia, mature SICA[-] parasites in an infected splenectomized rhesus monkey do not show a preference for the endothelium.

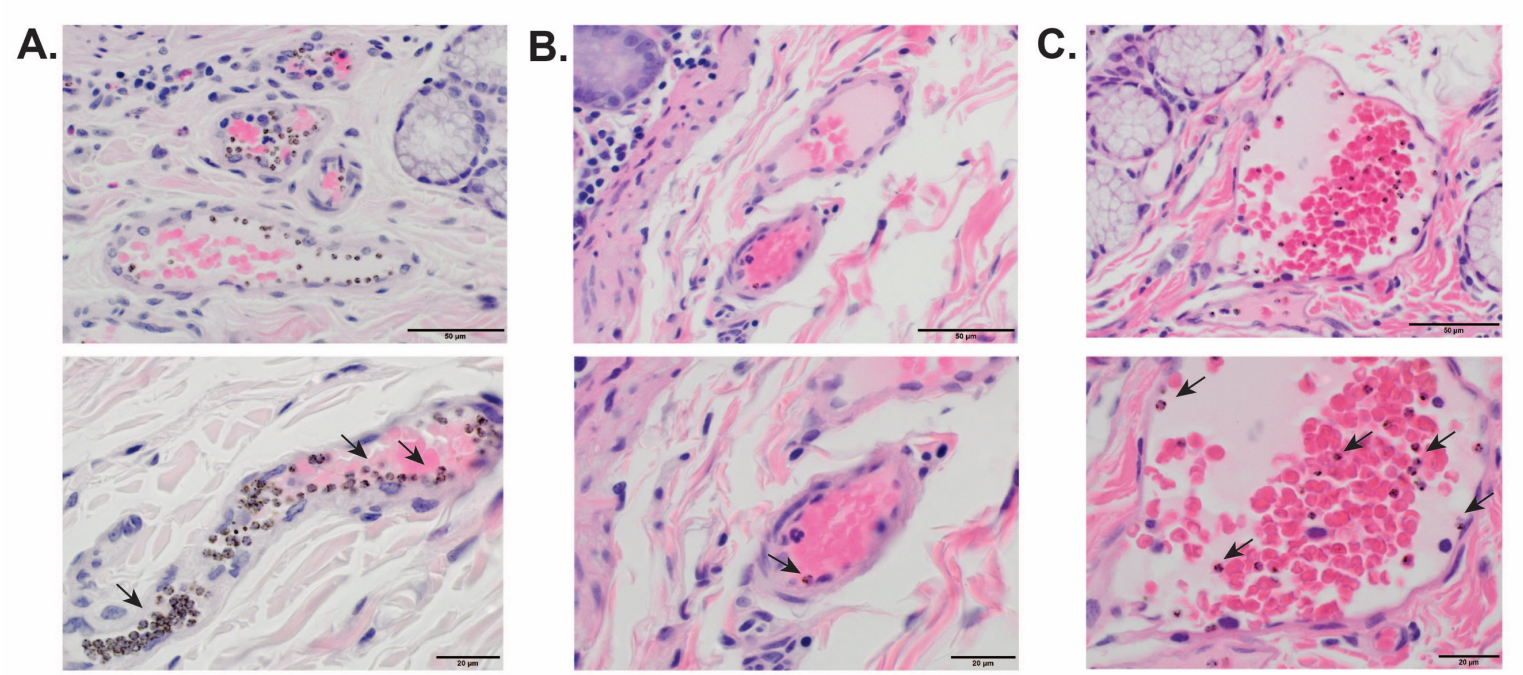

Figure 4.8 Light microscopy: SICA protein expression and sequestration in the duodenum. Micrographs of vessels in the submucosa of the duodenum, with 600X images on top, and 1000X images on the bottom and black arrows demonstrating parasites in the higher power image. Sections stained with H & E. A., Top: Mature, pigmented iRBCs stud the endothelium of submucosal venules in a rhesus macaque infected with SICA[+] parasites, with clear preference for the margins of the vessel over the lumen (600X). Bottom: endothelial studding and dense packing of parasites in a venule in a rhesus monkey with SICA[+] parasites (1000X). B., A clear margination phenotype was not as obvious in kra monkeys infected with SICA[+] parasites. C., As in the stomach, mature SICA[-] parasites in an infected splenectomized rhesus monkey do not show a preference for the endothelium.

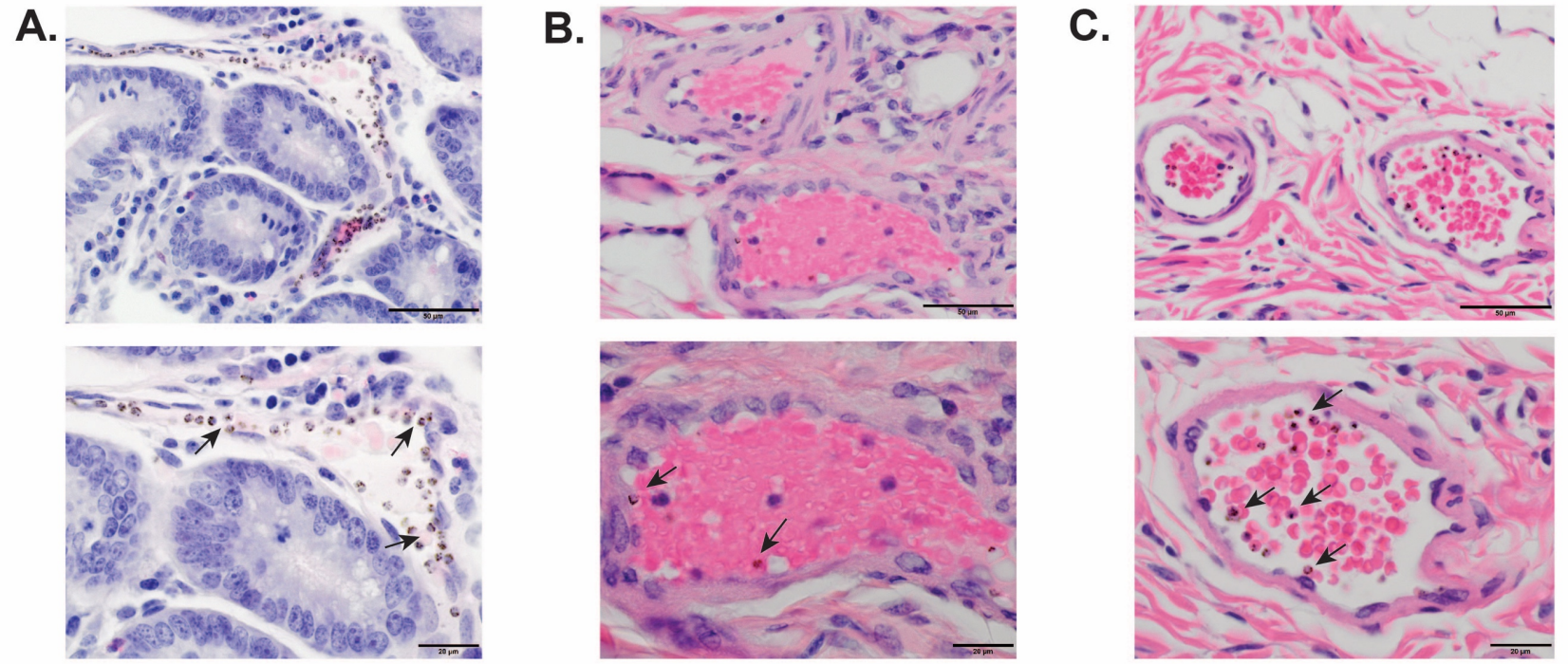

Figure 4.9 Light microscopy: SICA protein expression and sequestration in the jejunum. Micrographs of vessels in the submucosa of the jejunum, with 600X images on top, and 1000X images on the bottom and black arrows demonstrating parasites in the higher power image. Sections stained with H & E. A., Clear studding of larger vessels in the mucosa of a rhesus infected with SICA[+] parasites, with congestion in capillaries. B., A clear margination phenotype was not as obvious in kra monkeys infected with SICA[+] parasites. C., Mature SICA[-] parasites in an infected splenectomized rhesus monkey do not show a preference for the endothelium, despite endothelial cell morphology consistent with activation.

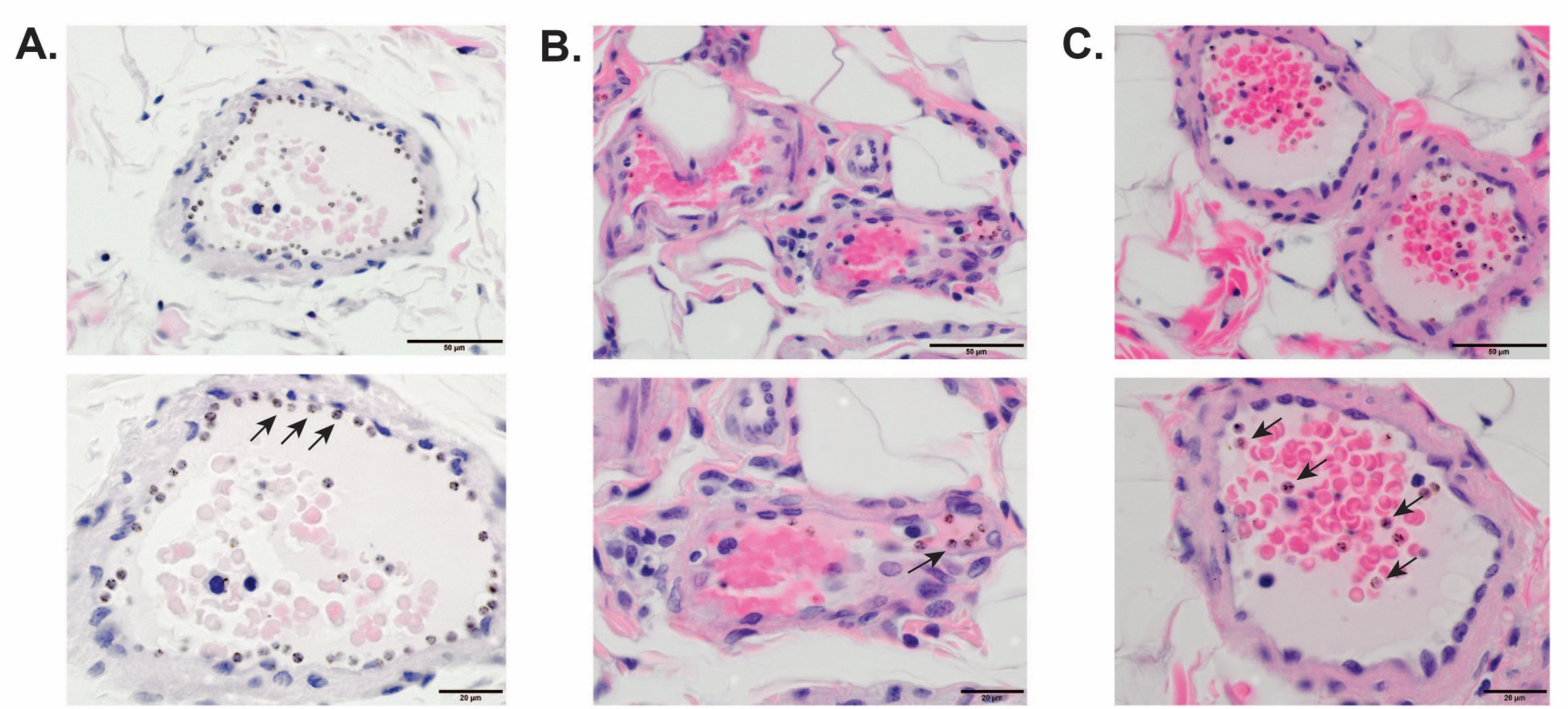

Figure 4.10 Light microscopy: SICA protein expression and sequestration in the colon. Micrographs of vessels in the submucosa of the colon, with 600X images on top, and 1000X images on the bottom and black arrows demonstrating parasites in the higher power image. Sections stained with H & E. A., Nearly complete preference for the endothelium over the lumen in a large vessel in the submucosal vessel of a rhesus infected with SICA[+] parasites. B., Some margination observed in a small vessel in a kra monkey infected with SICA[+] parasites. C., Mature SICA[-] parasites in an infected splenectomized rhesus monkey do not show a preference for the endothelium.

rhesus gastrointestinal tract, clear evidence of an interaction between endothelium and iRBCs was noted in the stomach (Fig. 4.7 A), with smaller capillaries and post-capillary venules packed with mature iRBCs (as indicated by the hemozoin pattern). Most notably, a clear preference for the margins over the lumen of larger venules was noted, whereby mature iRBCs clearly studded the endothelium of vessels (Fig. 4.7 A). Vessel endothelia were activated, as was evidenced by the plump appearance of endothelial cells, and the expression of immune-cell homing receptors such as ICAM1 (*vide infra*). Similar phenotypes were also observed in the duodenum (Fig. 4.8A), the jejunum (Fig. 4.9A), and the colon (Fig. 4.10A). This phenotype seemed to be restricted to the vessels of the mucosa and submucosa, and occurred only in the gastrointestinal tract (though the size of blood vessels and the location of the section taken in other tissues may have precluded the observation of the phenotype in other organs). Additionally, the phenotype was observed to occur in five out of six rhesus monkeys with acute infections. In the kra monkeys, however, a clear margination phenotype was not observed in most of the monkeys (Figures 4.7 – 4.10, panel B). Only one out of seven of the kra monkeys from E07 exhibited this phenotype. When considered in a 2 x 2 contingency table (Table 4.4), the odds ratio for parasites in a rhesus monkey to marginate in the rhesus monkey tissue was 19.74 over those in a kra monkey, with a p-value of 0.029 by Fisher-Exact Test.

Table 4.4: Fisher Exact Test Contingency Table

	Sequestration (%)	No Sequestration (%)
Rhesus	5 (83%)	1 (14%)
Kra	1 (17%)	6 (86%)

Table 4.2: Fisher exact test for sequestration and species. The Fisher Exact Test Contingency table and results are summarized. $\alpha = 0.05$; $P = 0.029$; Odds ratio: 19.74

The next question in the puzzle involved the identity of parasite and host factors that could mediate this interaction(s). On the parasite side, SICA proteins are a primary candidate, based on their relationship to the adhesive, surface-expressed PfEMP1 proteins that mediate sequestration of *P. falciparum* iRBCs [81]. To test the hypothesis that SICAproteins may mediate the margination phenotype, two splenectomized monkeys were infected with phenotypically SICA[-] parasites. This line of parasites was derived from passage of *P. knowlesi* parasites through splenectomized macaques which resulted in the reversible lack of expression of SICA protein at the surface of the RBCs (phenotypic negative) [163]. Splenectomy is requisite to maintain this negative phenotype [74]. The same suite of tissues was collected as for the SICA[+] cohorts and examined. Despite activation of the endothelium, no margination was observed in any of the tissues, including those of the gastrointestinal tract (Figures 4.7 – 4.10 Panel C).

The degree of margination in each tissue comparing rhesus, kra, and splenectomized rhesus monkeys was quantified using several different metrics by light microscopy. Twenty parasitized vessels were quantified, or 350 total vessels, whichever was observed first. Parasites that appeared to abut the endothelium were scored as marginated, those that were clearly in the lumen of the vessel were considered non-marginated, and the number of marginated to total parasites (marginated and non-marginated) were counted (Fig. 4.11). Statistical analysis was completed using the Dunnett post-hoc test to compare the kra and splenectomized rhesus monkeys to the intact rhesus monkeys. In the stomach, the intact rhesus monkeys had a greater proportion of marginated parasites (77.1%, +/- 6.6%) than did kra monkeys (54.1%, +/- 11.7%) or splenectomized rhesus monkeys (36.8%, +/- 7.6%), a difference that was statistically significant (p-value = 0.002 for the kra-intact rhesus comparison, and p-value = 0.00045 for the splenectomized rhesus-intact rhesus comparison). The proportion of marginated parasites in the

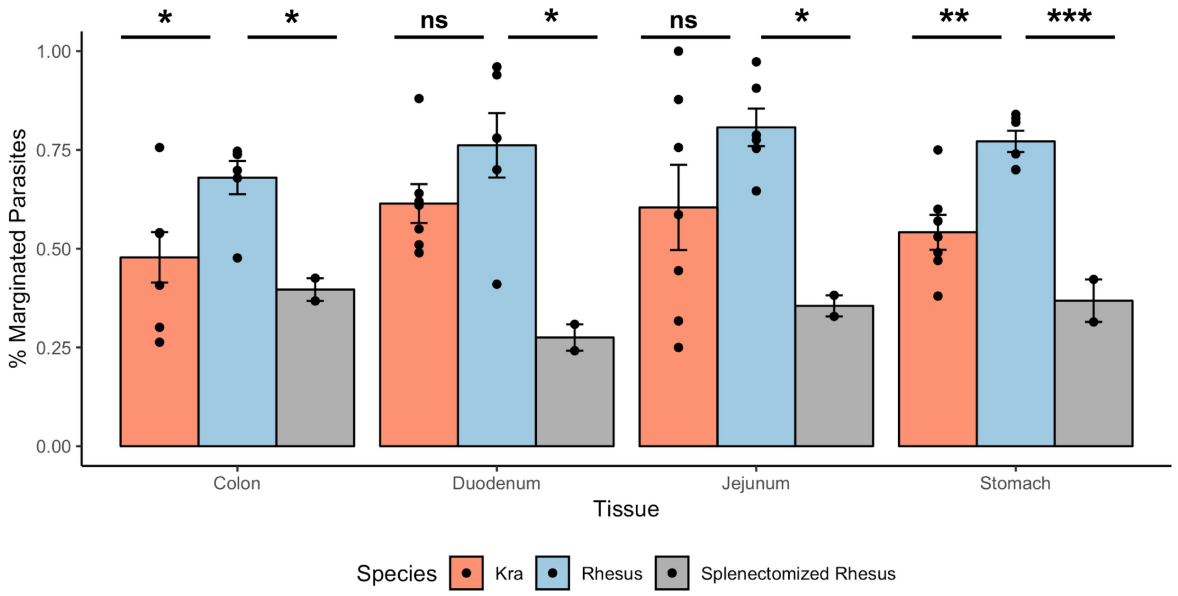

Figure 4.11. Quantification of SICA[+] and SICA[-] parasite margination in the gastrointestinal tissues. Parasites were considered marginated if they appeared to be touching the endothelium by light microscopy. Statistical relationships were tested via Dunnett's test with rhesus monkeys infected with SICA[+] parasites as the reference group. $\alpha = 0.05$; *P < 0.05, **P < 0.005, ***P < 0.0005.

duodenum was 76.1% (+/- 20.0%) which was greater than, but not statistically significant (p-value = 0.213) from that in kra (61.4%, +/-13.0%), and greater than, and statistically significant (p-value = 0.005) from that in splenectomized rhesus (27.5% +/- 4.7%). As in the duodenum, the difference in the proportion of marginated parasites between rhesus and kra monkeys was not stastistically significant (80.7%, +/-11.6%, and 60.4% +/- 28.5%, respectively; p-value = 0.206), and the difference between intact rhesus and splenectomized rhesus was statistically significant (35.5% +/- 3.8% for splenectomized rhesus; p-value = 0.046). Finally, in the colon, the proportion of marginated parasites were statistically significant in both the kra (47.8% , +/-16.9%; p-value = 0.040) and in the splenectomized rhesus (39.7%, +/-4.06%; p-value 0.049) when compared to in the intact rhesus (68.0% +/-10.3).

For the spleen-intact animals, several vessel metrics were quantified as measures of prevalence and representativeness of the phenotype, including the number of vessels with at least one marginated parasite divided by the number of vessels with at least one parasite, marginated or not (Supplemental Fig. 6.50), the prevalence of parasitized vessels, expressed as 20 divided by the total number of vessels observed in the process of finding 20 parasitized vessels (Supplemental Fig 6.51), and the number of vessels with at least one marginated parasite over the total number of vessels observed, with or without parasites, Supplemental Fig 6.52. The peripheral parasitemias for the splenectomized animals were much higher, and as such, every vessel encountered contained at least one parasite. Thus, the only metric considered for them were the percent of vessels that contained marginated parasites divided by the total number of vessels counted (Supplemental Fig. 6. 52).

Next, duodenal tissues from the intact rhesus, kra, and splenectomized rhesus monkeys were examined via transmission electron microscopy (TEM) for physical contact between

parasitized RBCs and the endothelium (Fig. 4.12). Several instances of contact between parasitized RBCs and the endothelium of rhesus monkeys were observed (Fig. 4.12A), with fewer apparent instances of contact occurring in kra monkeys (Fig. 4.12 B). Despite the inspection of multiple grids, no instances of contact between SICA[-] iRBCs and the endothelium of splenectomized animals were observed (Fig. 4.12 C). These data, evaluated together with tissue accumulation, the association with a large surface-expressed variant antigen on mature iRBCs, and the peripheral parasitemia kinetics, strongly suggests the margination phenotype observed by light microscopy (*vide supra*) is the result of cytoadhesion and sequestration of the iRBCs.

Finally, the differential level of frank sequestration that was observed in the kra and rhesus monkeys was hypothesized to be due to either downregulation of the *SICAvar* family in kra monkeys, or potentially, the expression of a different *SICAvar* gene repertoire. RNAseq data generated from the whole blood acquired during the necropsy of these animals was analyzed, but no obvious clustering was observed of *SICAvar* transcripts with the sequestration phenotype was observed (Fig. 4.13).

<u>Consideration of putative iRBC receptors, including Mucosal vascular Addressin Cell Adhesion Molecule 1 (MAdCAM1), which is expressed in the gastrointestinal tract</u>

That differing levels of sequestration were observed in kra and rhesus monkeys infected with the sporozoites derived from the same strain of parasites, and that their blood-stage *SICAvar* transcript expression profiles did not clearly cluster with the phenotype led us to believe that host inflammatory status may be playing a role. Additionally, exploring differential expression, and the tissue expression patterns of endothelial proteins can also help provide a list for presumptive host protein binding partners for the parasite proteins mediating sequestration. Circulating matrix

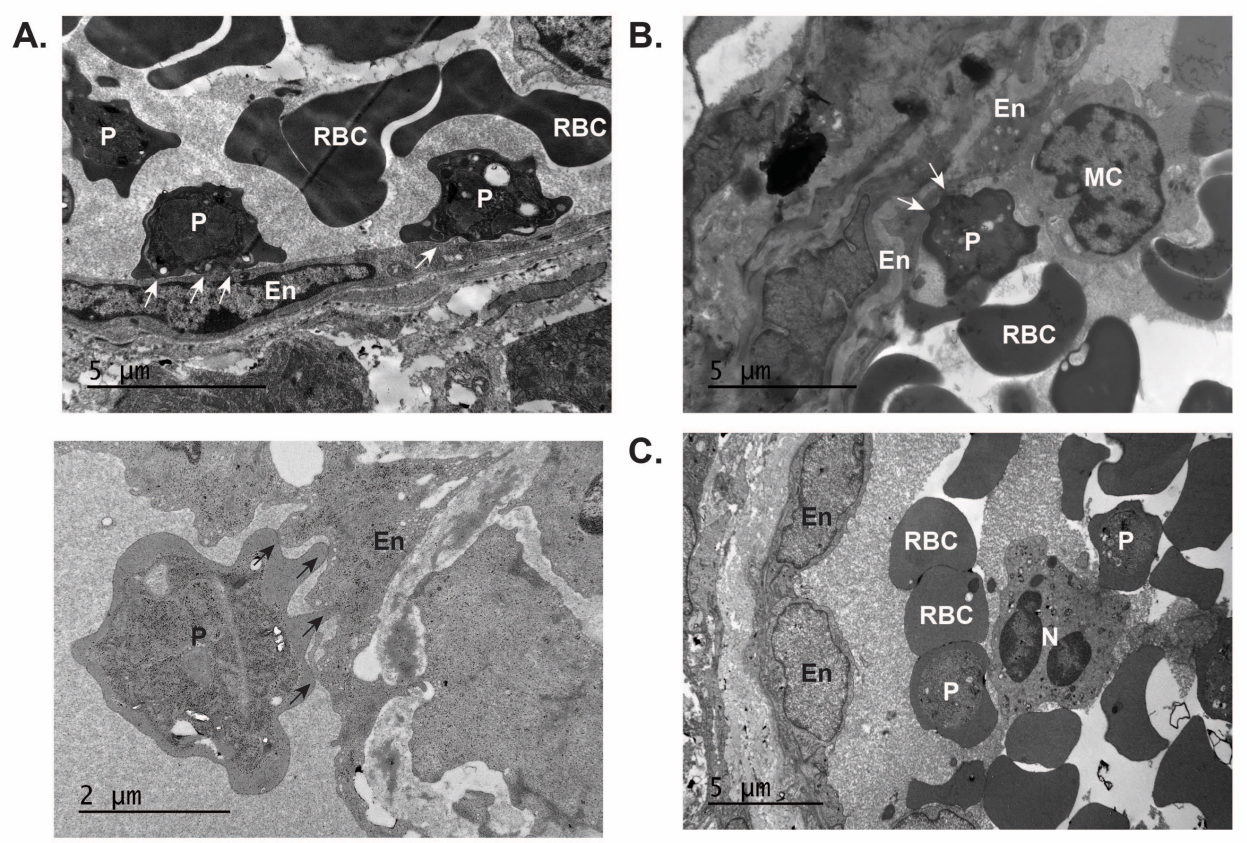

Figure 4.12 Electron microscopy: SICA protein expression and sequestration in the gut. Micrographs of vessels in the submucosa of the colon or duodenum demonstrating direct contact with the endothelium by SICA[+] parasites. Examples of IRBCs (P) erythrocytes (RBC), endothelium (En), monocytes (MC), and neutrophils (N) are labeled. Direct contact is indicated by arrows. A., Top: two iRBCs interact with the endothelium in a duodenal vessel in a rhesus monkey infected with SICA[+] parasites. Bottom: An iRBC seems to form projections that interact with the endothelium of a colonic vessel in a SICA[+]-intected rhesus monkey. B., An iRBC and a monocyte adhere to the endothelium in a SICA[+]-infected kra monkey C., No parasites interact with the endothelium in a SICA[-]-infected splenectomized rhesus monkey.

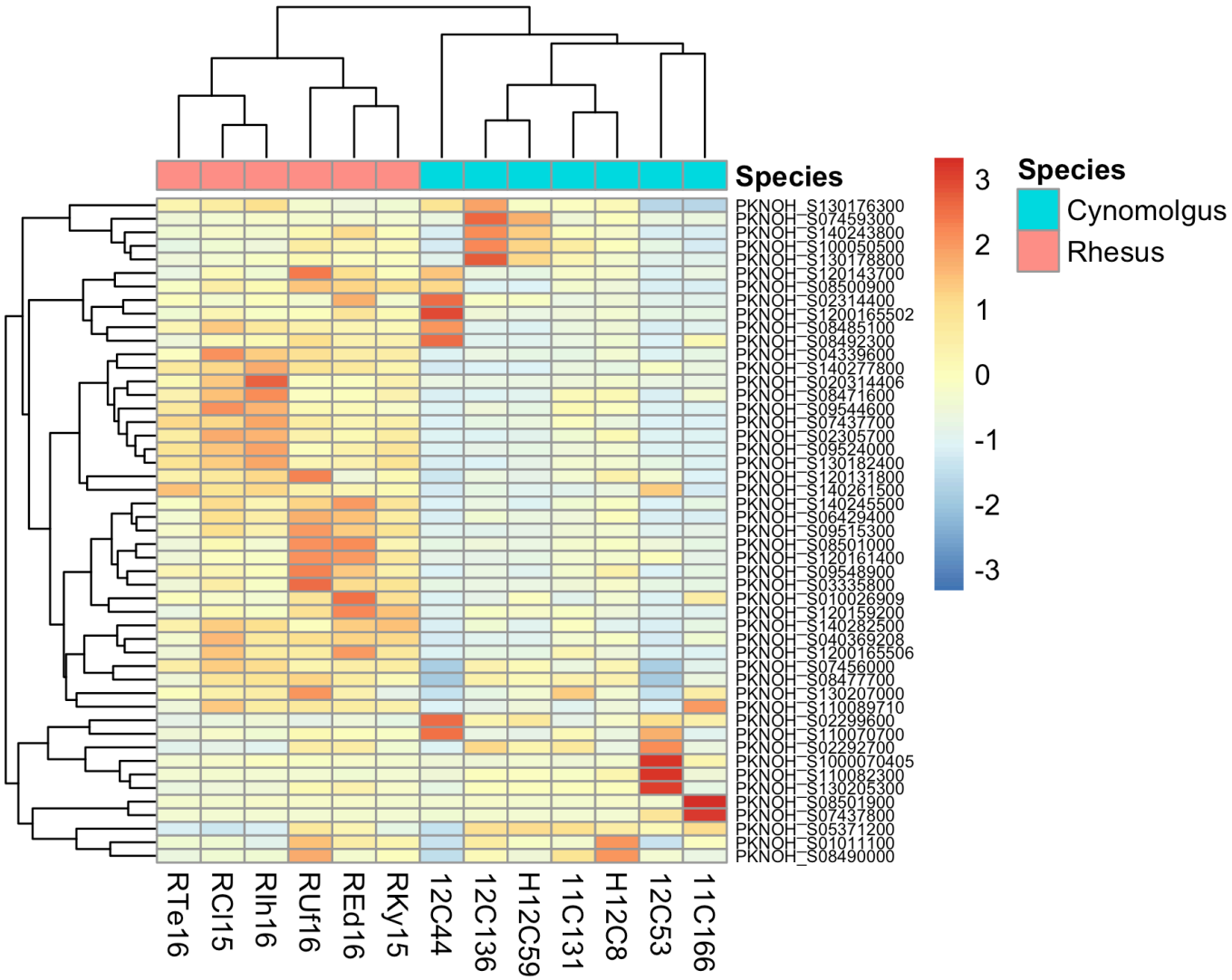

Figure 4.13 SICAvar expression at necropsy SICA[+]-infected monkeys. Heatmap of screened SICAvar transcripts showing clustering by species.

metalloproteases cleave endothelial receptors expressed on the cell surface, releasing them into the plasma as soluble forms that can be measured. Cleaved, soluble indicators of endothelial activation and mediators of sequestration, commonly implicated with *P. falciparum* infection were measured by SOMAScan and compared qualitatively. Included in the analysis were the metalloprotease, ADAMS13, angiopoietin-2, soluble forms of CD36, ICAM1, E-selectin, PECAM, VCAM1, and von Willenbrand's Factor (vWF) [97,194].

ADAMS13, angiopoietin-2, E-selectin, and vWF exhibited no change between baseline and *P. knowlesi* infection in either the kra monkeys or rhesus monkeys (Fig. 4.14). CD36 and PECAM increased in kra monkeys, but not rhesus monkeys. VCAM1 increased in both rhesus and kra monkeys. ICAM1 decreased during *P. knowlesi* infection in the kra monkeys, but not in the rhesus monkeys. This combined with its role as a mediator of *P. falciparum* sequestration distinguished ICAM1 as a potential mediator for *P. knowlesi* cytoadhesion and sequestration. ICAM1 is in fact a well-defined mediator for cytoadhesion and sequestration in cerebral malaria cases caused by *P. falciparum* [58,195].

Soluble levels depend on the extent of cleavage, thus expression levels of ICAM1 as a proxy for endothelial activation were probed using anti-ICAM1 antibodies in immunohistochemistry (IHC) assays. Strong ICAM1 expression was observed in the intact rhesus, kra, and splenectomized rhesus monkeys in selected sections of stomach (Fig. 4.15 A-C), duodenum (Fig. 4.16 A-C) and colon (Fig. 4.17 A-C), demonstrating robust endothelial activation in all samples, but decreasing the likelihood that ICAM1 itself is a mediator of sequestration.

Mucosal vascular Addressin Cell Adhesion Molecule 1 (MAdCAM1) is expressed on the surface of endothelial cells of the vessels in the gastric mucosa, and is known to interact with lymphocytes expressing the $\alpha 4\beta 7$ integrin, mediating tissue-specific homing [182,188,196,197].

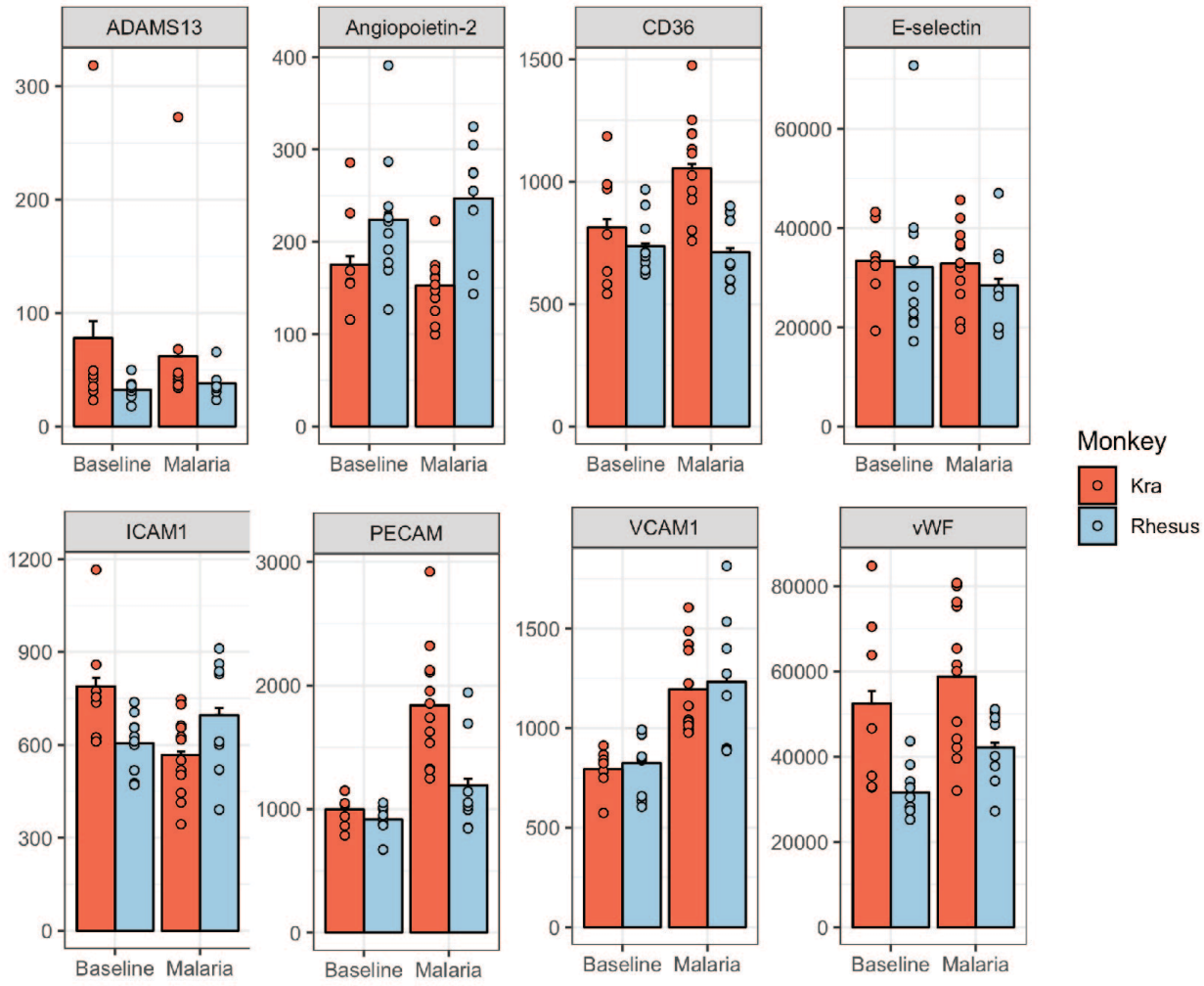

Figure 4.14 Soluble markers of endothelial activation. Common markers of endothelial activation were selected based on their importance to malaria disease and qualitatively assessed to screen for candidates to test for in-vivo expression (via IHC) and parasite binding assays.

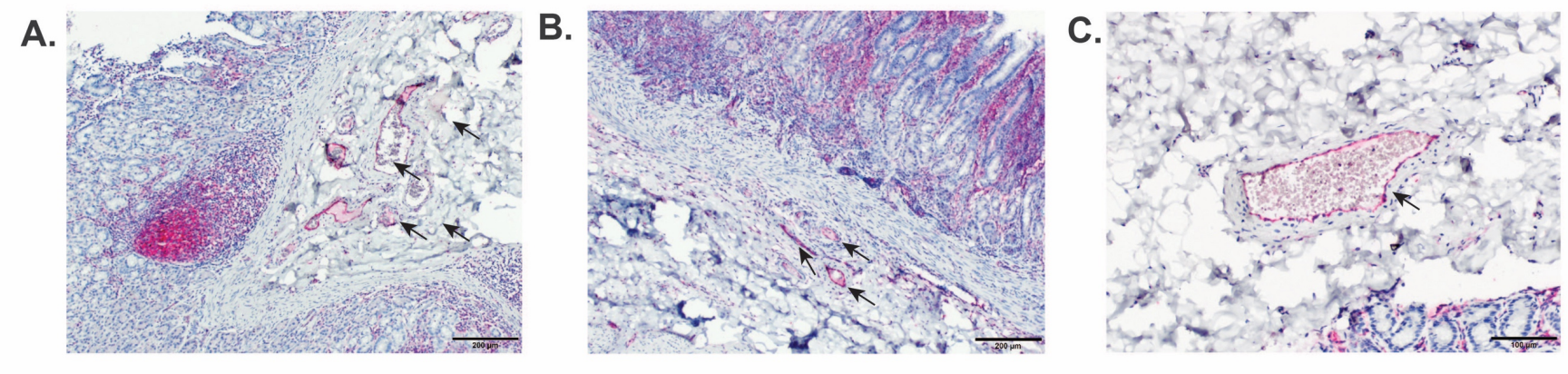

Figure 4.15 ICAM1 Expression in the Stomach. Micrographs of vessels in the mucosa and submucosa of the stomach of IHC staining of ICAM1, fuschin red, with hematoxylin counter-stain. ICAM1-positive vessels are indicated with arrows. A., Rhesus infected with SICA[+] parasites. B., Kra monkey infected with SICA[+] parasites. C., SICA[-]-infected splenectomized rhesus monkey.

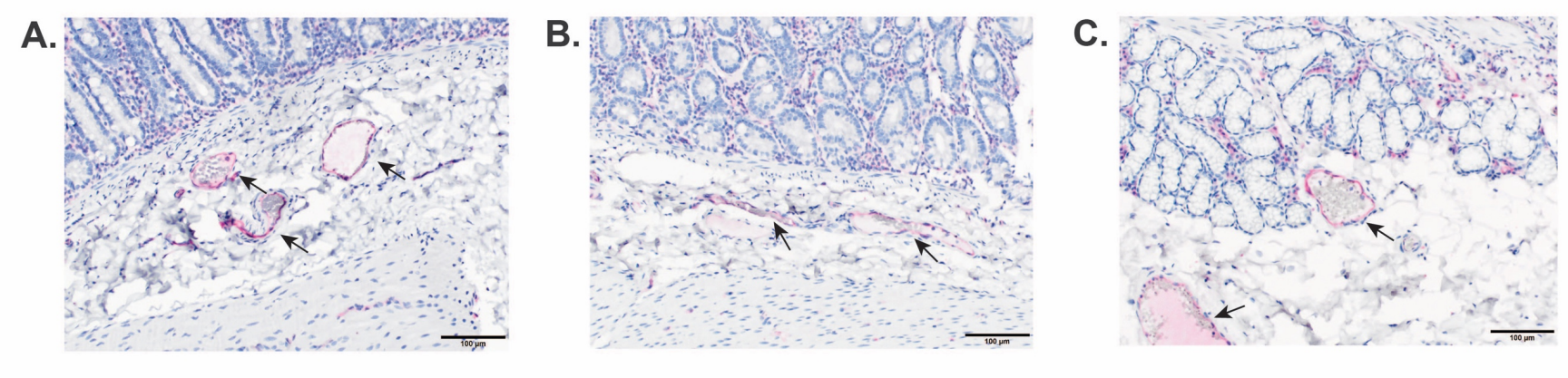

Figure 4.16 ICAM1 Expression in the Duodenum. Micrographs of vessels in the mucosa and submucosa of the duodenum of IHC staining of ICAM1, fuschin red, with hematoxylin counter-stain. ICAM1-positive vessels are indicated with arrows. A., Rhesus infected with SICA[+] parasites. B., Kra monkey infected with SICA[+] parasites. C., SICA[-]-infected splenectomized rhesus monkey.

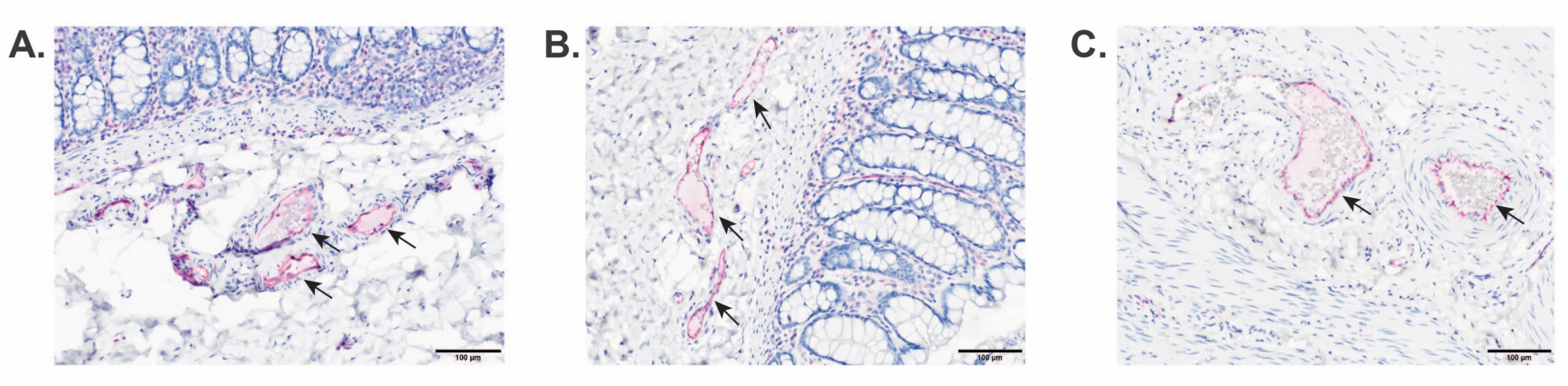

Figure 4.17 ICAM1 Expression in the Colon. Micrographs of vessels in the mucosa and submucosa of the colon of IHC staining of ICAM1, fuschin red, with hematoxylin counter-stain. ICAM1-positive vessels are indicated with arrows. A., Rhesus infected with SICA[+] parasites. B., Kra monkey infected with SICA[+] parasites. C., SICA[-]-infected splenectomized rhesus monkey.

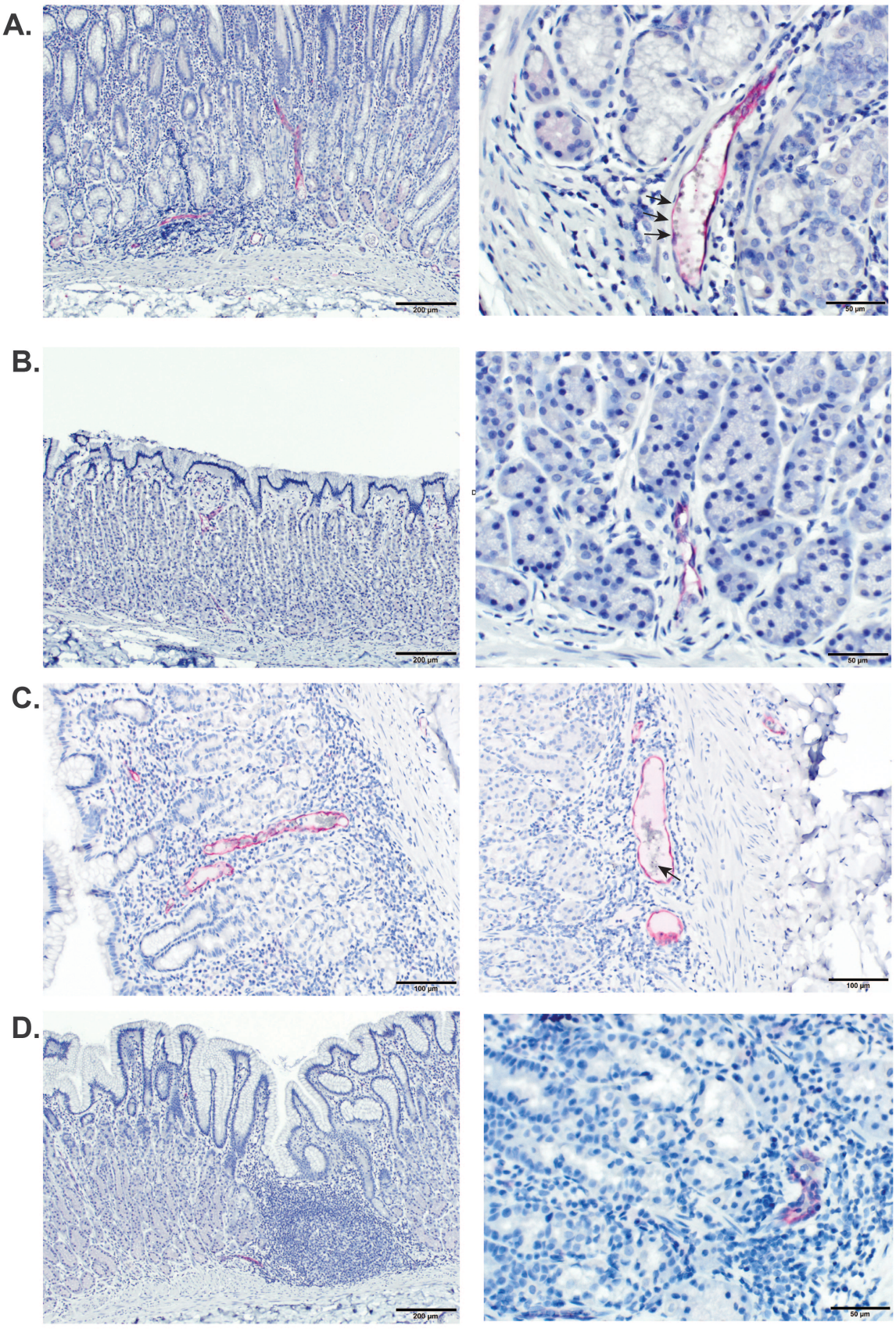
A.
200 µm
50 µm
B.
200 µm
50 µm
C.
100 µm
100 µm
D.
200 µm
50 µm

Figure 4.18 MAdCAM1 Expression in the Stomach. Micrographs of vessels in the mucosa and submucosa of the colon of IHC staining of MAdCAM1, fuschin red, with hematoxylin counter-stain. Marginating parasites are indicated with arrows A., Left, low power magnification of the gastric mucosa of a rhesus monkey infected with SICA[+] parasites demonstrating several vessels with bright expression of MAdCAM1. Right, higher power magnification of a vessel expressing MAdCAM1 with marginating parasites. B., Left, lower power magnification of the gastric mucosa of a kra monkey infected with SICA [+] parasites showing constituitive, baseline expression of MAdCAM1. Right, Higher magnification view of a MAdCAM1-positive vessel in an infected kra monkey. C., Left and right, examples of vessels strongly positive for MAdCAM1 in a splenectomized monkey with SICA[-] parasites. D., Left, low magnification view of the mucosa and submucosa of an uninfected rhesus monkey showing baseline expression of MAdCAM1. Right, higher magnification view of mucosa in an uninfected kra monkey showing an example of constitutive expression of MAdCAM1.

Expression was mostly restricted to the submucosa and mucosa, especially near the mucosal associated lymphoid tissue [196]. The geographic restriction of this receptor (gastric organs, and mucosa and submucosa of these organs) makes MAdCAM1 an attractive presumptive receptor, but binding to *Plasmodium* parasites has not been demonstrated [87]. Anti-MAdCAM1immunohistochemical staining was performed on select stomach (Fig. 4.18 A-D), duodenum (Fig. 4.19 A-C), and colon (Fig. 4.20 A-C) sections from intact rhesus, kra, splenectomized rhesus, and in the case of the stomach, control animals. Notably, MAdCAM1 expression appeared to be elevated in both intact and splenectomized rhesus macaques relative to the kra monkeys or control monkeys in all three tissues, and MAdCAM1 expression was most robust in vessels with parasites, compared to those without parasites. However, based on semi-quantitative scoring, these findings did not prove to be statistically significant.

P. knowlesi-infected RBCs do not bind CD36, ICAM, or MAdCAM1

To directly demonstrate binding in addition to correlation of expression with sequestration, a battery of binding studies was performed. SICA [+] *P. knowlesi* iRBCs, SICA [-] *P. knowlesi* iRBCs, uninfected rhesus iRBCs, and *P. falciparum* FVO iRBCs, a strain demonstrated to bind CD36 were tested [57]. First, these test groups were added to C32 amelanotic melanoma cells, a cell line known to express CD36 [183]. *P. falciparum* FVO binding to C32 amelanotic melanoma cells was recapitulated in a repeatable fashion. However, uninfected rhesus RBCs were found to bind C32 amelanotic melanoma cells regardless of the anticoagulant used for collection (Fig. 4.21 A-C), addition of trypsin (4.22 A-C), or the hematocrit used (Fig. 4.23). BSA (Fig. 4.24), FBS (Fig. 4.25), and naïve monkey serum (Fig. 4.26) were titrated into the experiment to no effect. Neither composition of the binding buffer (Figs. 4.21, 4.23, 4.24), nor if the cells were fresh or cryopreserved had any effect on binding (Figs. 4.25, 4.26). This property seemed to be specific to

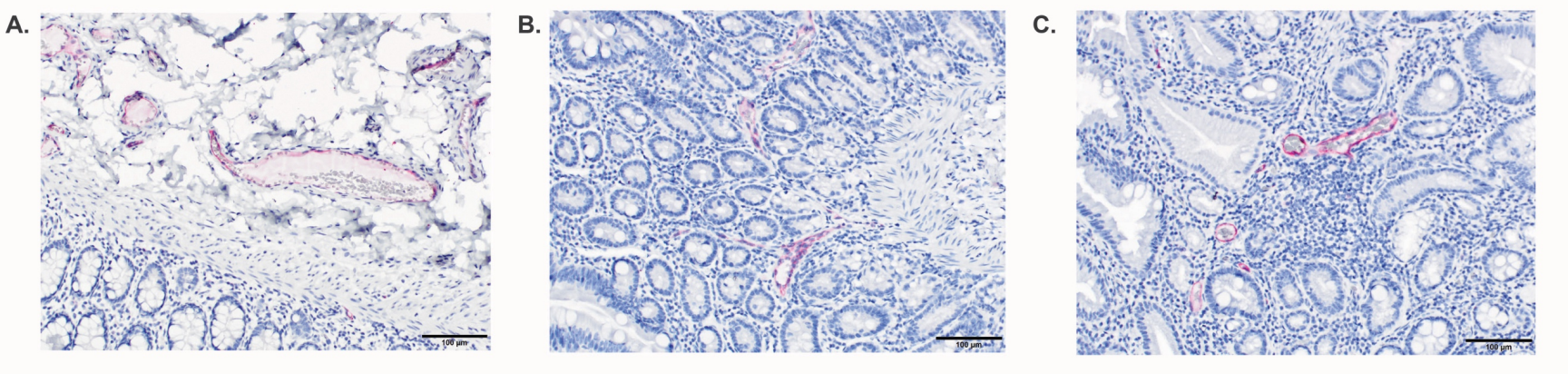

Figure 4.19 MAdCAM1 Expression in the Duodenum. Micrographs of vessels in the mucosa and submucosa of the colon of IHC staining of MAdCAM1, fuschin red, with hematoxylin counter-stain. A., Rhesus infected with SICA[+] parasites. B., Kra monkey infected with SICA[+] parasites. C., SICA[-]-infected splenectomized rhesus monkey.

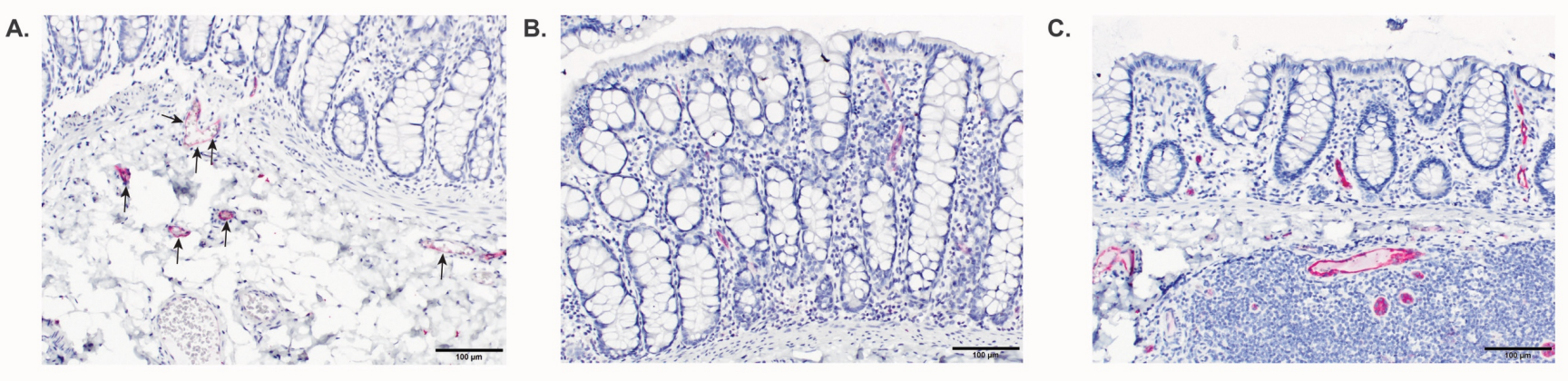

Figure 4.20 MadCAM1 Expression in the Colon. Micrographs of vessels in the mucosa and submucosa of the colon of IHC staining of ICAM1, fuschin red, with hematoxylin counter-stain. MAdCAM1-positive vessels with marginated parasites are indicated with arrows. A., Rhesus infected with SICA[+] parasites. B., Kra monkey infected with SICA[+] parasites. C., SICA[-]-infected splenectomized rhesus monkey.

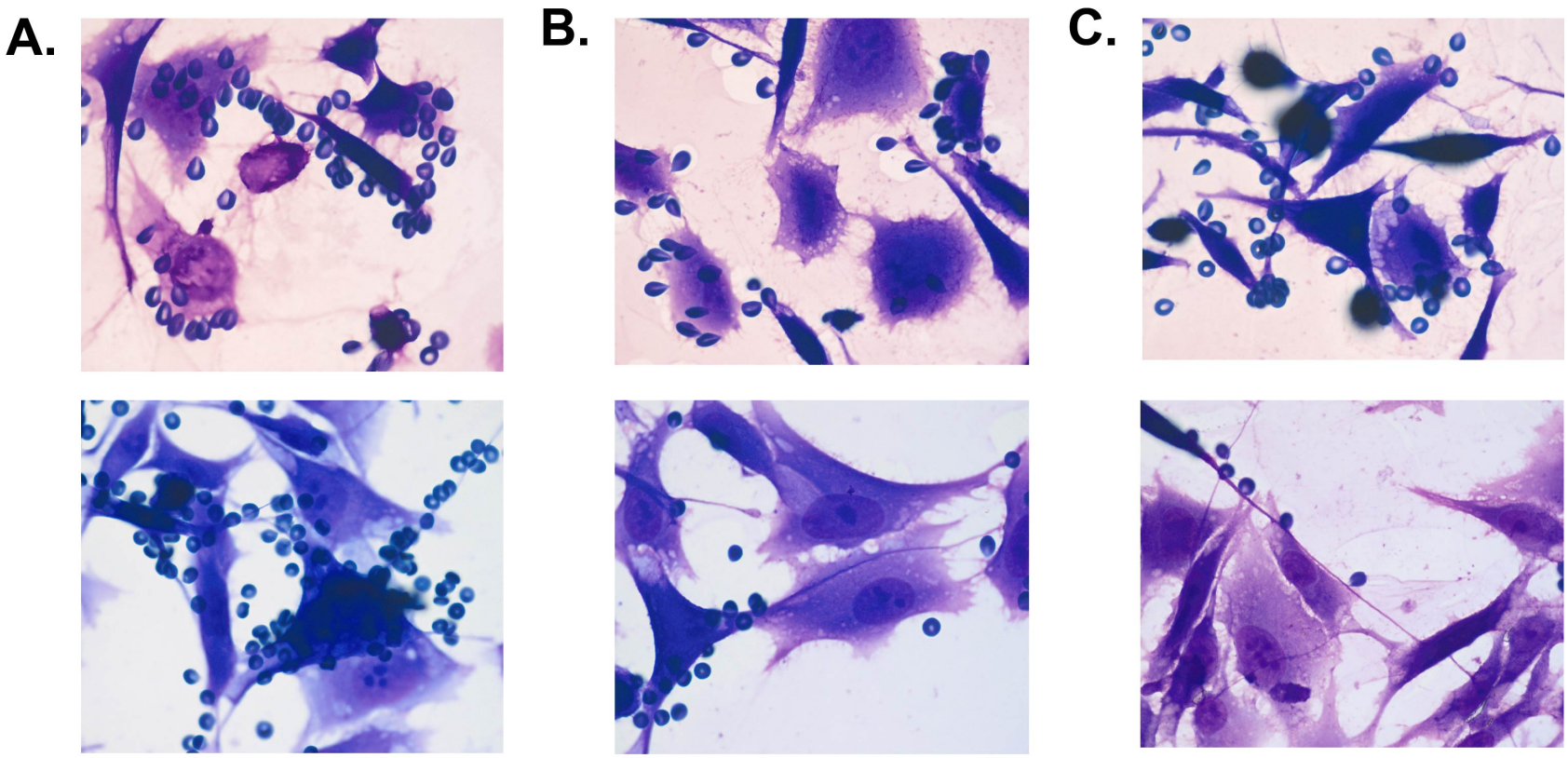

Figure 4.21 The Effect of Anticoagulant and Binding Buffer on Binding of Rhesus RBCs to C32 Amelanotic Melanoma Cells. Micrographs of representative fields of C32 amelanotic melanoma cells with unparasitized rhesus RBCs; stained with Giemsa. The top row represents experiments performed in Hanks Balanced Salt Solution, the bottom in RPMI. A., Blood collected in CPDA. B., Blood collected in EDTA. C., Blood collected in heparin.

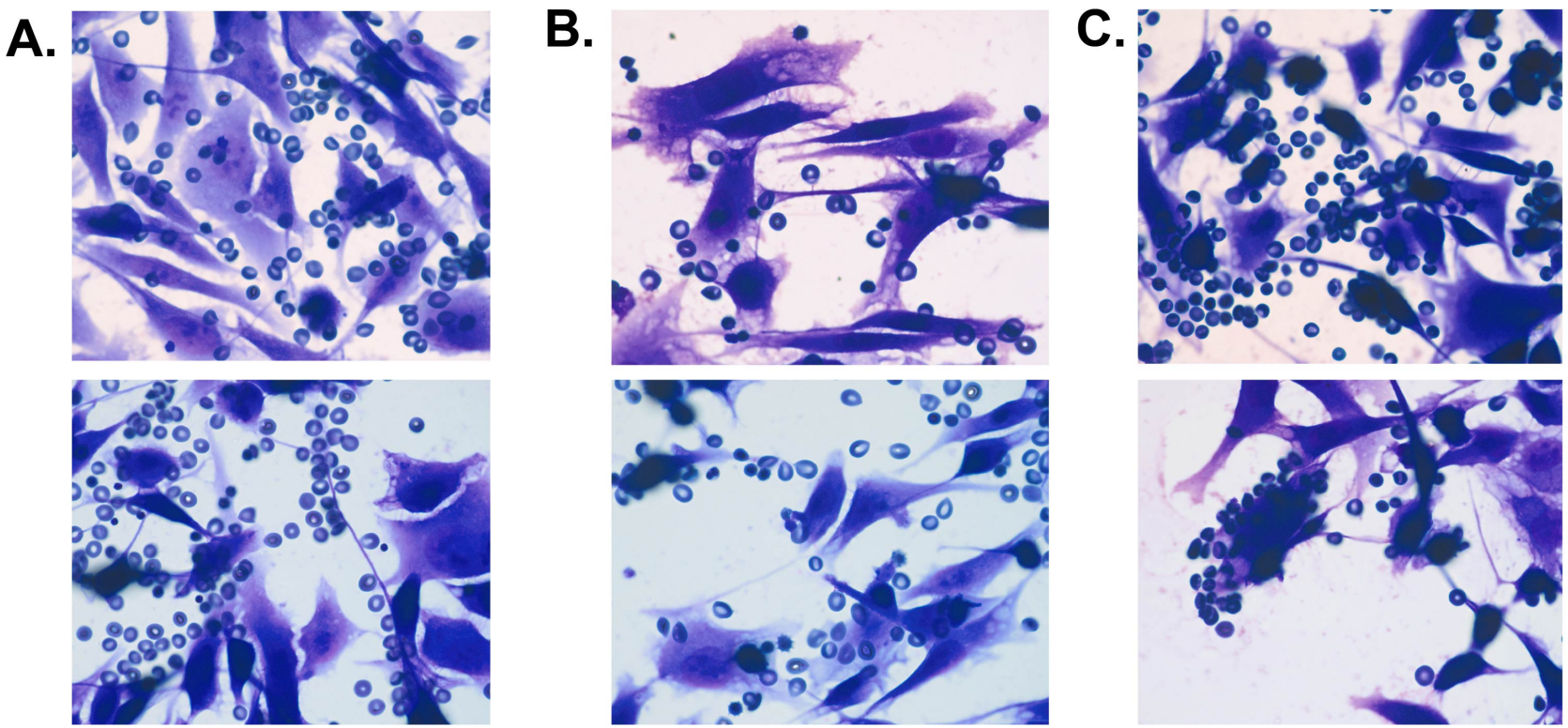

Figure 4.22 The Effect of Trypsin on Binding of Rhesus RBCs to C32 Amelanotic Melanoma Cells. Micrographs of representative fields of C32 amelanotic melanoma cells with either parasitized or unparasitized rhesus RBCs; stained with Giemsa. The top row represents untreated experiments, and the bottom row trypsin-treated experiments. A., Blood from rhesus infected with SICA[+] parasites. B., Blood from rhesus monkey infected with SICA[+] parasites. C., Uninfected rhesus blood.

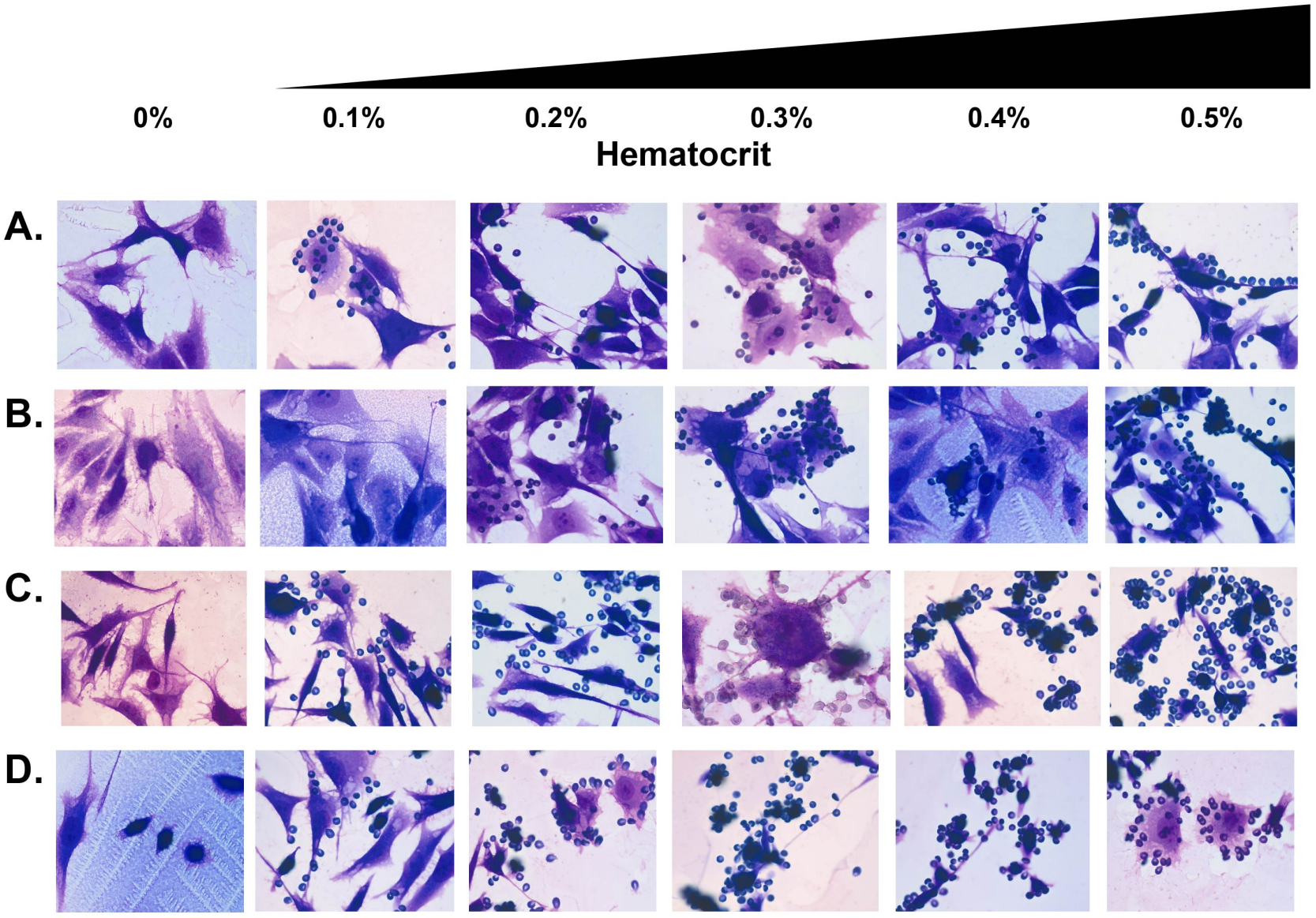
0%
0.1%
0.2%
0.3%
0.4%
0.5%
Hematocrit
A.
B.
C.
D.

Figure 4.23 The Effect of Hematocrit on Binding of Rhesus RBCs to C32 Amelanotic Melanoma Cells. Micrographs of representative fields of C32 amelanotic melanoma cells with unparasitized rhesus RBCs; stained with Giemsa. Uninfected blood was titrated into the experiment (wedge schematic). A., Experiment performed in RPMI, 0% BSA. B., Experiment performed in RPMI, 5% BSA. C., Experiment performed in Hank's Balanced Salt Solution, 0% BSA. D., Experiment performed in Hank's Balanced Salt Solution, 5% BSA.

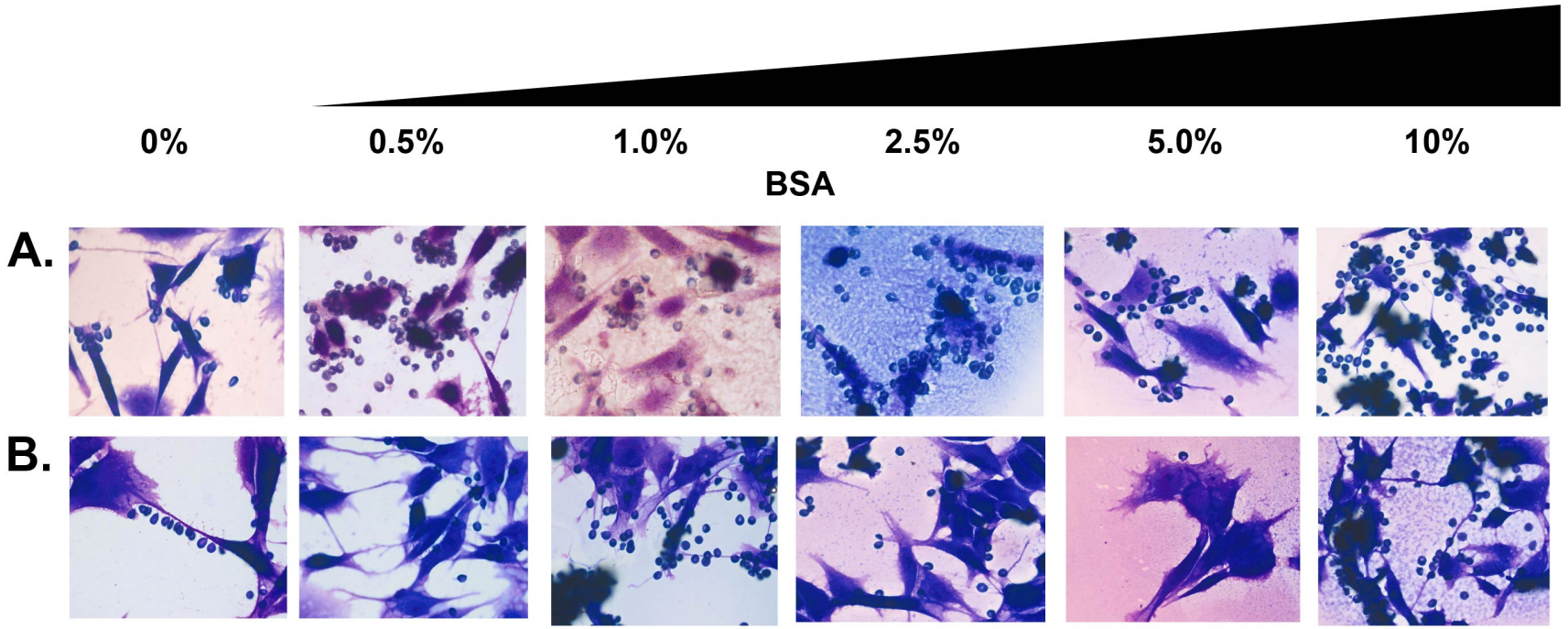

Figure 4.24 The Effect of BSA on Binding of Rhesus RBCs to C32 Amelanotic Melanoma Cells. Micrographs of representative fields of C32 amelanotic melanoma cells with unparasitized rhesus RBCs stained with Giemsa. BSA was titrated into the experiment (wedge schematic). A., Experiment performed in Hank's Balanced Salt Solution. B., Experiment performed in RPMI.

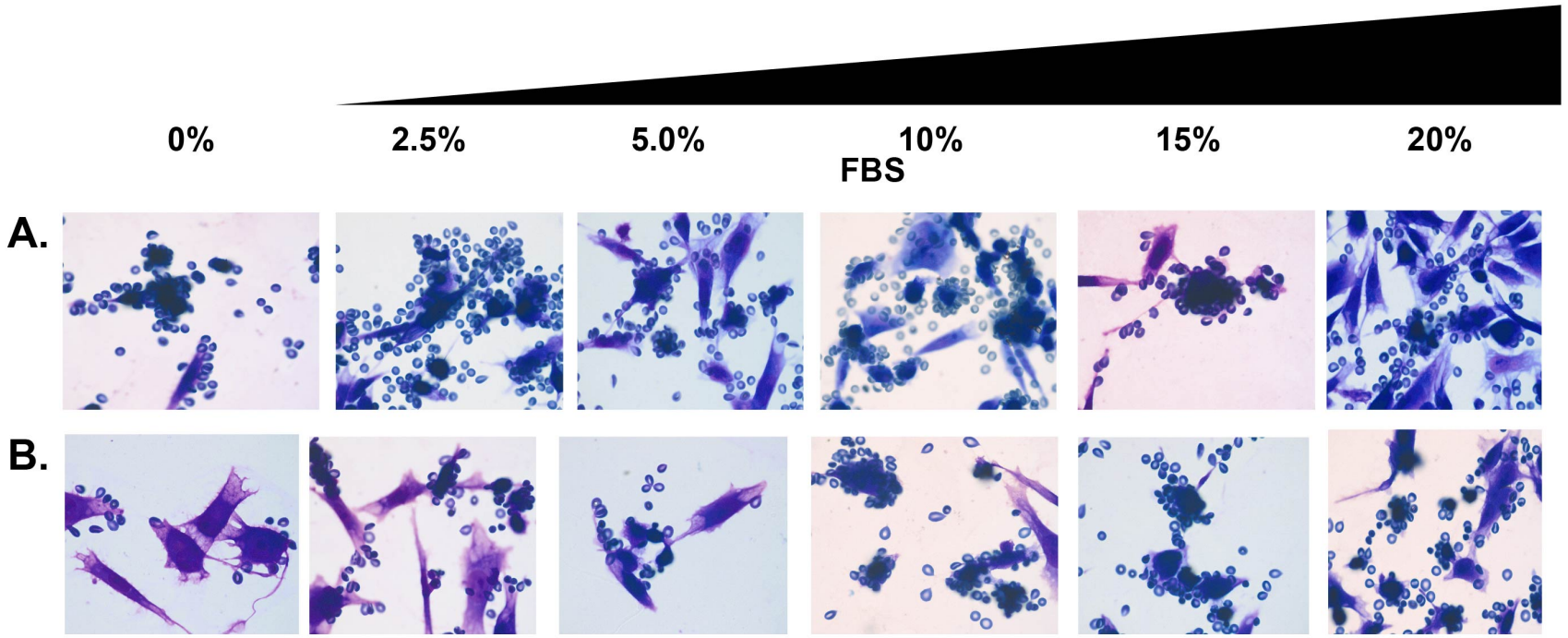

Figure 4.25 The Effect of FBS on Binding of Rhesus RBCs to C32 Amelanotic Melanoma Cells. Micrographs of representative fields of C32 amelanotic melanoma cells with unparasitized rhesus RBCs stained with Giemsa. FBS was titrated into the experiment (wedge schematic). A., Experiment performed using fresh rhesus blood. B., Experiment performed using cryopreserved blood from the same monkey as in A.

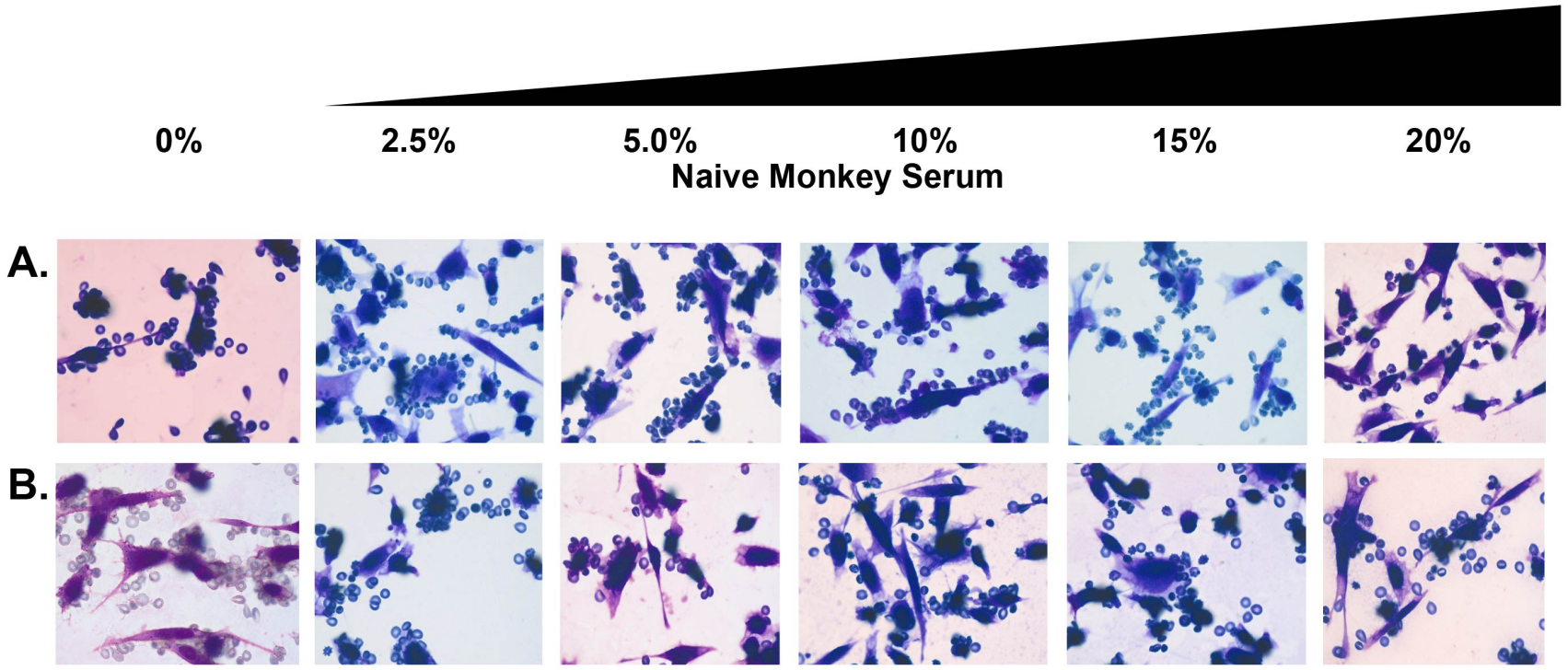

Figure 4.26 The Effect of Naïve Monkey Serum on Binding of Rhesus RBCs to C32 Amelanotic Melanoma Cells. Micrographs of representative fields of C32 amelanotic melanoma cells with unparasitized rhesus RBCs stained with Giemsa. Naïve monkey serum was titrated into the experiment (wedge schematic). A., Experiment performed using fresh rhesus blood. B., Experiment performed using cryopreserved blood from the same monkey as in A.

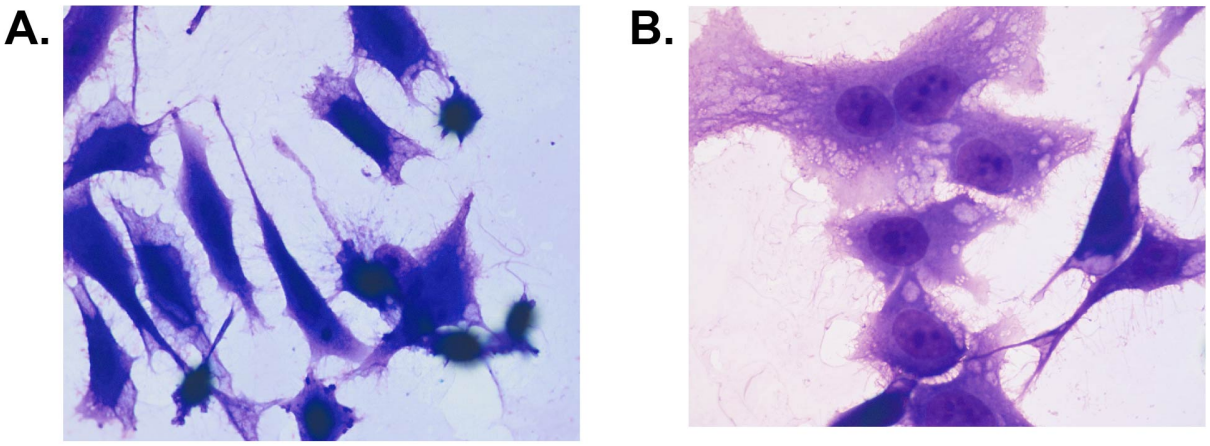

Figure 4.27 Human RBC Binding to C32 Amelanotic Melanoma Cells. Micrographs of representative fields of C32 amelanotic melanoma cells with unparasitized human RBCs stained with Giemsa. A., Experiment performed in RPMI. B., Experiment performed in Hank's Balanced Salt Solution.

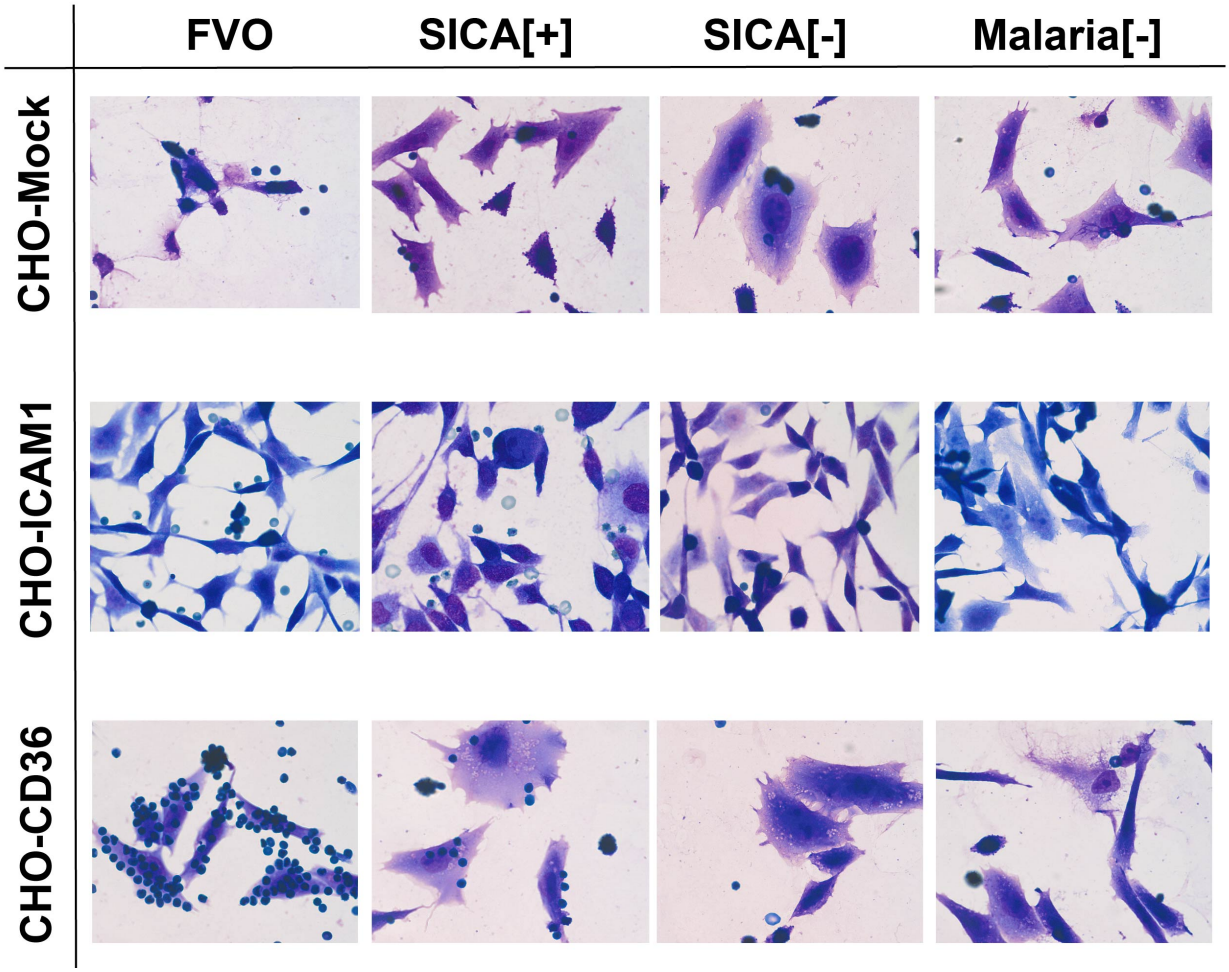

Figure 4.28 Plasmodium-infected RBC Binding to Transfected CHO Cells. Micrographs of representative fields from three experimental replicates testing *P. falciparum* FVO (FVO), SICA[+] *P. knowlesi* (SICA[+]), SICA[-] *P. knowlesi* (SICA[-]), and uninfected rhesus RBCs (Malaria[-]) to Mock-, ICAM1-, and CD36-transfected CHO cells.

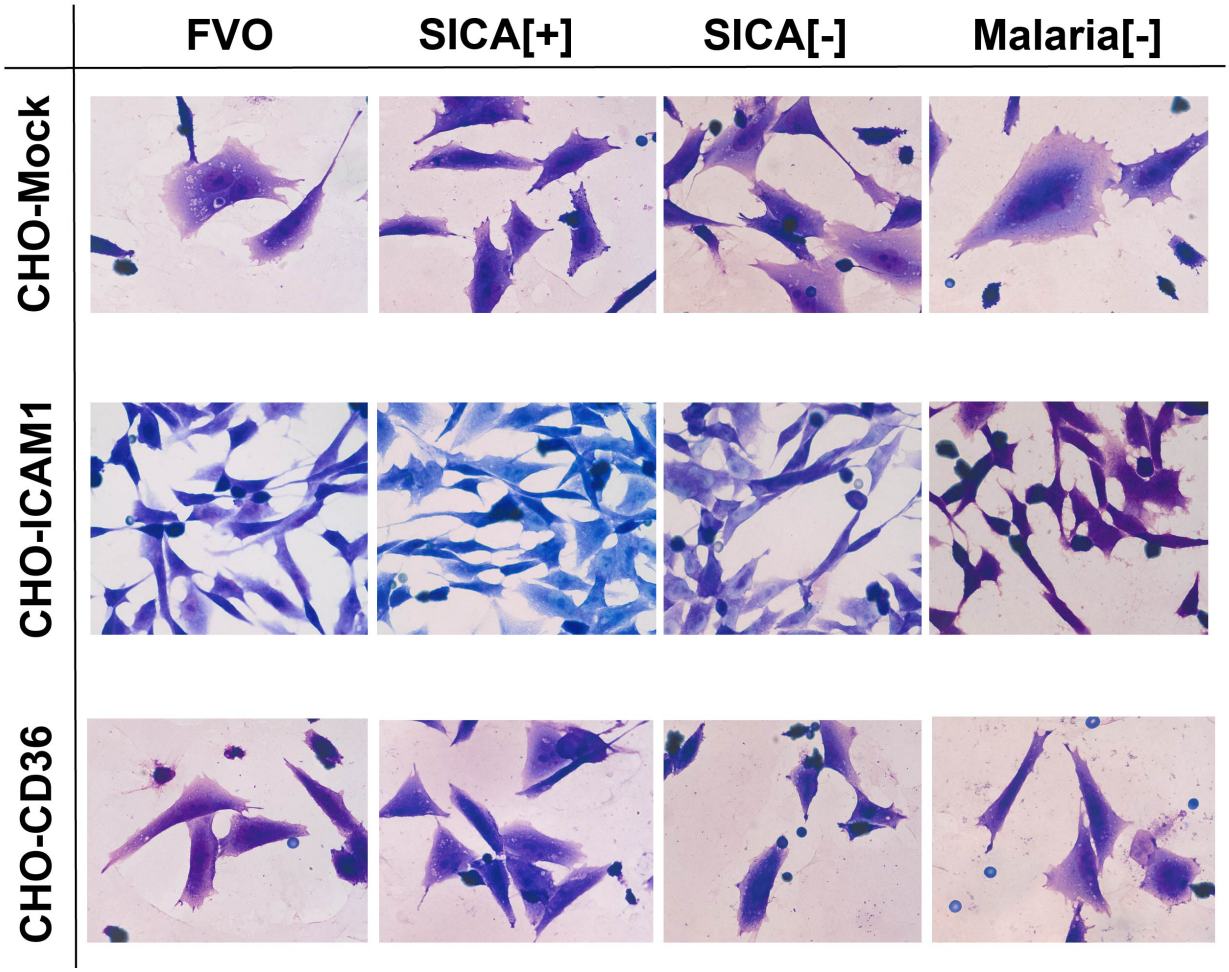

Figure 4.29 Trypsinized Plasmodium-infected RBC Binding to Transfected CHO Cells. Micrographs of representative fields from three experimental replicates testing trypsin-treated *P. falciparum* FVO (FVO), SICA[+] *P. knowlesi* (SICA[+]), SICA[-] *P. knowlesi* (SICA[-]), and uninfected rhesus RBCs (Malaria[-]) to Mock-, ICAM1-, and CD36-transfected CHO cells.

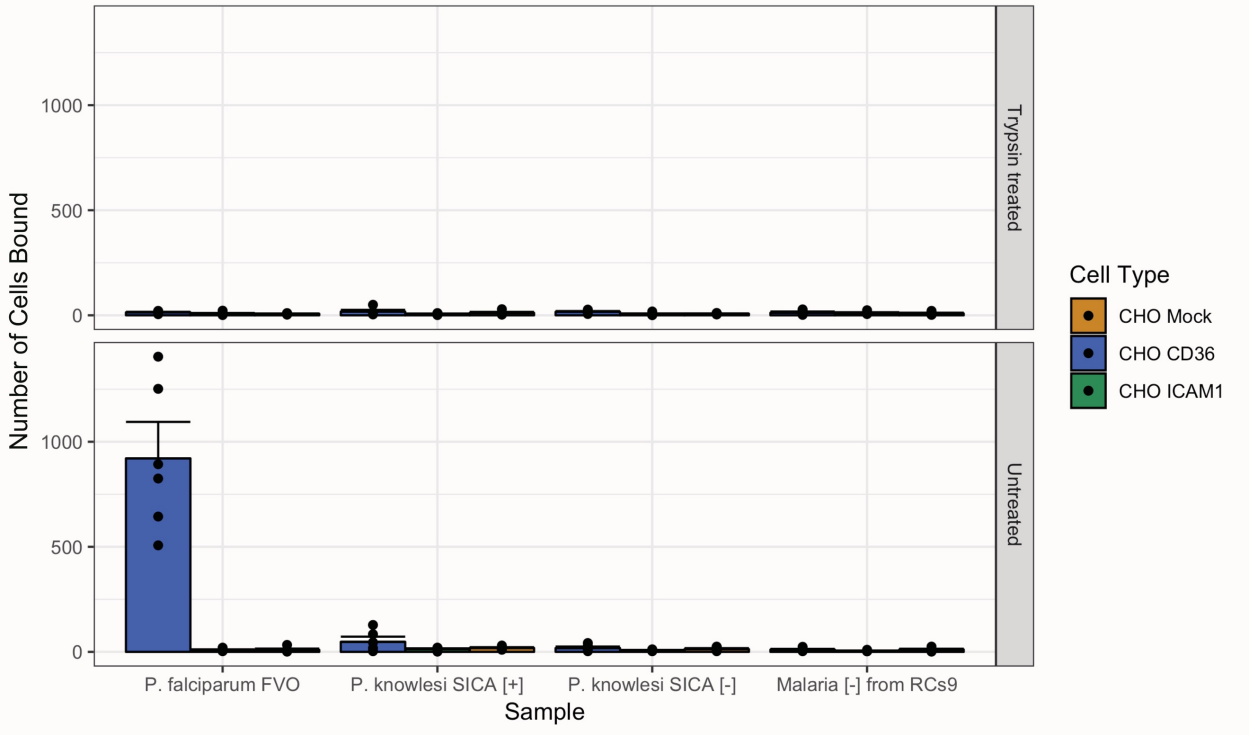

Figure 4.30 Quantification of Untreated and Trypsinized Plasmodium-infected RBC Binding to Transfected CHO Cells. The number of treated (top) or untreated (bottom) RBCs or iRBCs bound to 100 CHO cells were enumerated. RCs9 is a malaria-negative monkey that was used as the donor for the SICA[+] *P. knowlesi* parasites.

rhesus RBCs because uninfected *Aotus* RBCs present in the *P. falciparum* culture did not bind to C32 amelanotic melanoma cells. Likewise, uninfected human RBCs did not bind C32 amelanotic melanoma cells (Fig. 4.27). Due to this heavy amount of background adhesion of uninfected RBCs, *P. knowlesi* iRBC binding to CD36 could not be assessed using C32 amelanotic melanoma cells.

Next, Chinese hamster ovary (CHO) cells were screened for background binding of uninfected rhesus cells. None occurred, therefore trypsin-treated and untreated SICA [+] *P. knowlesi* RBCs, SICA [-] *P. knowlesi* RBCs, uninfected rhesus RBCs, and *P. falciparum* FVO RBCs were added to wells containing a mock-transfected CHO cell line, CD36-transfected CHO line, or an ICAM1-transfected CHO cell line [184]. Clear and robust binding of *P. falciparum* FVO iRBCs that was able to be abolished by trypsin treatment was observed as expected on CD36-CHO cells (Fig. 4.28 and 4.29). However, only very slight binding, which was reduced by trypsin treatment, was observed between CD36-CHO cells and SICA[+] *P. knowlesi* iRBCs (Fig. 4.28 and 4.29). SICA[-] *P. knowlesi* iRBCs and uninfected RBCs did not interact with any CHO cell line (Fig. 4.28). CHO cell experiment quantification is given in Fig. 4.30.

Finally, MAdCAM1 was assessed as a potential binding partner for *P. knowlesi*. First, purified truncated and full-length proteins were tested as described above. HuT78 cells, immortalized $\alpha 4\beta 7$ lymphocytes that bind to MAdCAM1, were used as a positive control [188]. No *Plasmodium* binding was observed to any purified protein product. Next, HIMEC.1, HAPEC.S1, and HPLNEC.B3 cells are immortalized endothelial cells isolated from human small intestine, appendix, and mesenteric lymph nodes, respectively [185]. HIMEC.1 and HAPEC.S1 have been demonstrated to express MAdCAM1, whereas HPLNEC.B3 does not and can serve as a negative control. No *Plasmodium* binding was observed on any MAdCAM1 cell line.

4.4 DISCUSSION

The sequestration of parasites in certain tissues, e.g., the brain and placenta, has been implicated in the development of severe and fatal disease in *P. falciparum* malaria, and several studies have documented parasite tissue distribution in *P. knowlesi*-infected rhesus macaques with very high parasitemias [25–28,62,64,190,198,199]. However, there is a paucity of studies studying the consequences of accumulation or sequestration of *P. knowlesi* parasites in the tissues at lower parasitemias, which are more often observed in human patients [55]. Likewise, no side-by-side analysis of a natural and resilient host (such as *M. fascicularis*) has been performed against rhesus monkeys. Such information is useful not only to advance basic understanding of the life history of *P. knowlesi*, and its interactions with its monkey hosts, but also to understand clinical presentations and pathophysiology caused by a parasite that has emerged as a zoonotic species and currently the most common cause of malaria in Malaysia [128]. This study is the first of its kind to quantify parasite density in both *M. mulatta* and *M. fascicularis* acute and chronic infections in a wide suite of tissues, assess their relationship to tissue damage, and test the binding profile of *P. knowlesi* iRBCs originating from an infection demonstrated to exhibit a clear cytoadhesive sequestration phenotype.

Parasite distribution was not uniform throughout the suite of tissues, suggesting there may be a preference or tropism by *P. knowlesi* for some tissues over others. This tropism may be mediated by physical means or by direct interactions between the surfaces of parasitized RBCs and the repertoire of proteins expressed on tissue endothelia. Parasite tissue densities in *P. knowlesi* acute infection mirrored those in *P. falciparum* or *P. vivax* infections, with spleen, adrenal gland, lung, liver, kidney, eye, ventricle, and gastrointestinal tract being key places for parasite accumulation, and in the case of the gut, sequestration was apparent with iRBCs observed close to

the endothelium and marginating vessels [62,63,85,99,177]. Though parasite burden was significant in the rhesus liver (greater than the overall tissue burden, which was 28 parasites per 10 HPFs), it fell on the lower end for tissues considered to have a high parasite burden (mean 47 parasites per 10 HPFs). A striking feature in the liver was Kupffer cell hyperplasia, and the presence of many heavily pigmented macrophages in the sinusoids. In mouse malaria models, the liver is implicated as an important player in parasite clearance, which is especially obvious in the context of splenectomy [200,201]. Taken together with the parasite density, it is possible the liver plays an important role in parasite clearance in monkeys infected with this parasite species. Interestingly, very few parasites were enumerated in the skin and skeletal muscle, places that are associated with parasite sequestration, especially in *P. falciparum* infection [62,190].

Many intact parasites were found in the spleens of acutely infected animals, especially in those of *M. mulatta*. The spleen plays a central role in malaria immunity and virulence. Consistent with the hypothesis that cytoadhesion and sequestration in various tissues occurs to avoid splenic circulation and of mature forms of the parasite, it would be expected to observe few healthy parasites along with a predominance of of debris and hemozoin-laden phagocytes in the spleen. However, in contrast, many healthy mature parasitized RBCs were observed in the red pulp of both rhesus and kra spleens, and the spleen represented a major proportion of the total parasite density calculated for all of the tissues. Healthy, intact parasites have also been observed in the spleen of a *P. vivax* infected *Saimiri boliviensis* monkey (Chapter 2). While parasite accumulation in the tissues has been described for both *P. vivax* and *P. knowlesi* infections, sequestration, if it is occurring, does not occur to the same extent as in *P. falciparum*, resulting in the circulation of mature forms in both species. *Plasmodium vivax*, trophozoites and schizonts are thought to be more flexible than such maturing *P. falciparum* iRBCs, providing a potential mechanism for

escape from the splenic sinusoids [202]. A similar escape mechanism for *P. knowlesi* is unknown. Splenomegaly in malaria is caused by massive expansion of the red pulp; it is possible that parasite invasion of RBCs and replication may occur in the splenic sinusoids, providing an advantage to the parasite to accumulate in the spleen.

The longitudinal nature of this study allowed for the comparison of parasite reservoirs in both acute and chronic infections, which was described using a heat map. Interestingly, parasites disappear from the spleens of chronically infected rhesus macaques, and are present in other organs, especially those of the gastrointestinal tract, and in kra monkeys, the bone marrow. While they are present in lower densities in kra monkeys, the proportion that the spleen compartment accounts for remains roughly similar between the acute and chronic infections. This could represent a changing of the expressed variant antigen repertoire (i.e., different *SICAvar* expression), different tissue compartments playing important roles in parasite persistence in chronicity, or a snapshot in the parasite clearance process that occurs as the host moves from chronic infection to sterility.

To assess the relationship between parasite accumulation and tissue score, a variety of metrics, including Fisher-exact test, Pearson and Spearman correlation coefficients, and multiple linear regression were used. In general, tissues that contained high parasite burdens also had histopathological changes, especially from kra monkeys (p-value = 0.017). Interestingly, parasite burden was only weakly correlated with the tissue scores from the acute infections in either species (Spearman's $\rho \sim 0.4$). Neither parasitemia at necropsy, nor cumulative parasitemia contributed to histological damage, the latter of which is corroborated by a lack of increase in the histology score between acutely and chronically infected animals (Fig. 3.8). Both tissue and parasite burden significantly affected the histological scores. Tissue was the most important explanatory variable

in the multiple linear regression model. Its role may be explained by inflammatory processes specific to the tissues evaluated or their sensitivity to specific inflammatory insults.

Several tissues contained high parasite burden, but no pathology. Among them, are the eye and adrenal gland. The eye is an important site for parasite sequestration in falciparum malaria; specific fundoscopic changes signal the development of cerebral malaria, and these have been used as an important screening tool [203–206]. A field trial in knowlesi malaria found no specific fundoscopic changes in the eyes of *P. knowlesi*-infected patients, and likewise, found no association with severe disease [203]. Reflecting these results in both rhesus and kra monkeys, no histopathological changes were noted (no fundoscopic exam was performed pre- or post-mortem). Paradoxically, the eyes contained a high density of parasites. The lack of histological evidence for damage despite a high parasite burden may be due to the immune privileged status of the eye. It is possible that *P. knowlesi* does not elicit an inflammatory response that overcomes immune privilege in this tissue. The adrenal gland has been shown to modulate the inflammatory response and respond to hypoglycemia in malaria using mouse models [207]. It is was an important site for parasite accumulation, but showed no histopathological changes. Parasite accumulation in the adrenal glands has been documented with *P. vivax* infection of *Saimiri boliviensis* monkeys and in *P. falciparum* cases [63,85]. In rare cases, adrenal hemorrhage has been observed in humans with fatal *P. falciparum* infection, and in rhesus monkeys with *P. knowlesi* and hyperparasitemia [25,177].

The presence of parasites in the brain is important in the development of severe falciparum, but seemingly absent in this *P. knowlesi*-infected cohort. This corresponds with an absence of clinical signs consistent with cerebral malaria in the monkey cohorts, including seizure, obtundity, and coma, and the lack of histopathological changes in the eye [208]. Substantial parasite

accumulation in the brain of macaques has been observed in other studies, but not without hyperparasitemia (> 20% of total RBCs infected) [27]. Additionally, no instances of cerebral malaria as defined by WHO, have been reported in the *P. knowlesi* clinical literature, with the possible exception of a single fatal case, with hyperparasitemia, where the individual upon autopsy demonstrated significant evidence for parasite accumulation in the brain [56].

Perhaps one of the most surprising observations was clear microscopic evidence for sequestration, and presumptive cytoadhesion, with the magnitude of the phenotype associated with host species (p-value 0.029 by Fisher Exact Test) and therefore disease resilience. A clear preference for the margins of venules over the lumen was observed in the mucosal and submucosal vessels of the stomach, duodenum, jejunum, and colon that was frankly obvious in rhesus monkeys at relatively low parasitemias (1-3%).

SICA proteins were immediately hypothesized as a prime candidate to mediate an adherent interaction on the parasite side, due to their external localization and similarity in structure to *Plasmodium falciparum* erythrocyte membrane protein 1 (PfEMP1) [81]. Both of these proteins are encoded by repertoires of multi-domain, diverse gene families (*SICAvar* for SICA proteins, and *var* genes for PfEMP1) [209]. They are both large (roughly 200 kD for SICA proteins, and 300 kD for PfEMP1), and expressed at the surface of iRBCs [209]. SICA proteins were first identified as mediating agglutination of iRBCs when mixed with immune serum [179]. Later, they were discovered to mediate antigenic variation of *Plasmodium*-infected iRBCs, be regulated by the spleen, and be associated with virulence, however their biological function remains unknown [72,76,76]. To if SICA proteins mediate binding, monkeys were infected with a phenotypic negative strain derived from the *P. knowlesi* clone Pk (A+), i.e., SICA[+]. This clone was developed by passage through a splenectomized monkey, which was found to down-regulate SICA

protein expression (as assessed by decreased agglutination) [76,163]. When injected into a spleen-intact monkey, the animal either succumbed (if the parasite was able to express SICA proteins again, and the monkey was not treated for its rising parasitemia), or the animal was able to rapidly control and clear infection without the need for treatment (if the parasite could not express SICA proteins) [76]. Therefore, the parasite strain must be maintained in splenectomized individuals to avoid SICA protein expression.

When splenectomized rhesus monkeys were infected with SICA[-] parasites, the frank margination phenotype observed in spleen-intact monkeys infected with SICA [+] parasites was not observed. Upon quantification, SICA[+]-parasitized rhesus monkeys had more margination in the stomach, duodenum, jejunum, and colon than did either SICA [+] parasitized kra monkeys, or SICA[-] parasitized splenectomized rhesus monkeys, though the differences were only statistically significant between intact rhesus and kra monkeys for the stomach and colon tissues.

PfEMP1 is concentrated on the surface of *P. falciparum*-infected RBCs in knobs: small electron-dense structures that stud the cell membrane, which have been demonstrated to be essential to mediating efficient binding [57,210,211]. *P. knowlesi*-infected red blood cells do not have knobs on their surface [64]. However, electron microscopy of the gut tissues clearly shows direct contact between SICA[+] parasitized RBCs and the endothelium through what appears to be amoeboid-like projections of the iRBC that protrude to make contact with the endothelium. Such morphology has also been demonstrated in the brain of rhesus monkeys with hyperparasitemia [27]. No interactions between the endothelium and SICA[-] parasitized RBCs was observed.

The clear margination phenotype observed on light microscopy, coupled with its association with SICA protein expression, direct contact with the endothelium, and a lower-than-

expected number of circulating mature stages lead to the conclusion that *P. knowlesi* cytoadheres and sequesters, albeit not to the same degree as does *P. falciparum*. That *P. knowlesi* was found to accumulate and show apparent adhesion in the gastrointestinal tract, a system involved in patients with severe *P. knowlesi*, provided a tantalizing clue to understanding determinants of disease severity in human *P. knowlesi* infection. Of the rhesus monkeys infected, only one exhibited vomiting, and none had diarrhea; epigastric pain and nausea, are of course, impossible to assess. The lack of frank clinical signs may be related to the fact that the monkeys are prey animals, and do not exhibit overt signs of illness until they are very sick. Upon necropsy, one animal had notable congestion of the serosa of the large and small intestine, with loose intestinal contents. Histopathologically, rhesus monkeys had significant gastritis, with endothelial activation as evidenced by ICAM1 and MAdCAM1 expression and endothelial cell morphology. Kra monkeys suffered only mild gastritis. Interestingly, the duodenum, jejunum, and colon did not exhibit inflammatory changes; they did however, express MAdCAM1 above baseline levels (when compared to control animals), and levels were higher in intact rhesus monkeys than in kra monkeys. Therefore, it is possible that duodenitis, jejunumitis, and colonitis would have followed, had the monkeys been sacrificed later. The possibility that sequestration in the gut is not directly related to disease severity, in terms of gastrointestinal manifestation cannot be ruled out, as a clear association between clinical signs, gross pathology, and histopathology was not clear-cut. On the other hand, by providing a parasite reservoir, sequestration may augment replication, thereby increasing the risk for severe disease, with symptoms such as nausea, vomiting, and epigastric pain secondary to systemic inflammation.

Several hypotheses were proposed to explain the disparity in sequestration phenotype between rhesus and kra monkeys infected with SICA [+] parasites: that the natural host

downregulates SICA protein expression; that after passage through the mosquito, the SICA protein profile was different and resulted in different tissue tropism (as PfEMP1 switching can be associated with changes in binding characteristics) [212]; or that the natural hosts control inflammation, thereby reducing exposure of endothelial proteins for binding to parasite sequestration-mediating proteins.

The first two hypotheses can be addressed using RNAseq data providing information on the repertoire of *SICAvars* that were being expressed at peak parasitemia. While it is worth noting that RNA transcript data may not always represent a one-to-one correlation with protein expression, when it comes to SICA proteins, the transcript that is most abundant tends to be the one that is expressed on the cell surface [164]. RNAseq revealed that parasites from both kra and rhesus monkeys express *SICAvar genes* – therefore the natural host does not simply attenuate binding through complete *SICAvar* downregulation. Likewise, no clear expression clustering pattern was observed between those hosts that had sequestered iRBCs and those that did not. The lack of a one-to-one relationship between tissue tropism or phenotype and *SICAvar* gene is not altogether surprising, as a given genome may have as many as different *SICAvar* genes in its repertoire, and the genes are modular [67,68,209]. Modular binding domains present in PfEMP1 direct binding specificity, rather than the overall gene itself [78,80]. The remaining hypothesis: inflammatory modulation is supported by the temperature and inflammatory mediator data presented in Chapter 3, in addition to IHC performed here.

In addition to being a marker for inflammation, MAdCAM1 emerged as a candidate for mediating binding due to its restriction to the venules of the mucosa and submucosa of the gastrointestinal tract [196]. MAdCAM1 has two binding domains: one that interacts with the integrin, $\alpha 4\beta 7$, present on T lymphocytes that home specifically to the gut [188]. The other is a

lectin binding domain that mediates rolling adhesion [213]. Despite its attractiveness, no differential expression was quantified, and no binding to either purified protein or cell lines was observed.

Correlation of the expression of protein with the margination phenotype is not sufficient to prove binding. Therefore, a battery of *in vitro* binding studies were performed. First, two important *P. falciparum* binding partners, CD36 and ICAM1 were tested using transfected CHO cells. Modest binding to CD36 that was prevented by treatment of iRBCs with trypsin, was observed, however it was much less than that of the positive control, *P. falciparum* FVO, and it is unknown if it is biologically relevant. No binding was observed to ICAM1, which is in line with a lack of correlation of ICAM1 expression *in vivo* to the margination phenotype.

This study is not without its flaws. First, the standardized weights necessary to calculate whole-organ parasite numbers for all of the tissues that were collected are not available, in part due to the difficulty of dissecting out some of the tissues (e.g., the skin, thymus in adult animals, the omentum, the lymph nodes, etc). Second, the global knock-outs of the large and diverse *SICAvar* gene family has not been technically feasible. If this were possible, such knock outs could directly link SICA protein expression and sequeastration and allow infection in intact animals. Last, the proteins used in the binding studies were human proteins, which have the benefit of direct field applicability, but also the pitfall that should binding not be observed, the result may be attributed to differences between human and monkey in these protein structures and sequences, even if subtle.

In conclusion, we present the first study to directly compare the parasite tissue burden and relationship between parasite factors and histopathological consequences between the experimental host, *M. mulatta* and the natural host, *M. fascicularis* in *P. knowlesi* infection.

Parasites preferentially accumulate in some tissues over others in both hosts, however it is only in rhesus monkeys that a clear margination phenotype is observed. Though evidence of sequestration of iRBCs in the tissues has been presented for *P. knowlesi* in the past, most of these studies have occurred in the context of very high parasitemias, which can make specific scoring of the hallmarks of sequestration, including clear association with the endothelium over the lumen in vessels, and packing or plugging of capillaries with parasites, difficult. We provide evidence that sequestration occurs at lower parasitemias (1-3%) than previously observed, which are more reflective of those experienced by patients. While the relationship between parasite tissue burden, sequestration, and histopathology was not straightforward, sequestration may provide a mechanism for parasite replication and persistence, and in doing so, cause systemic severe disease.

Chapter 5: Discussion

Disease severity itself, and the factors that determine which disease outcome trajectories result from infection are topics of intense research. Malaria is no exception. While *Plasmodium* species have infected humans for millennia, there is still much to be learned in how host-parasite interactions drive pathophysiology and disease outcome. *Plasmodium knowlesi*, a relatively newly emergent zoonosis represents an opportunity to explore host-parasite interactions in way other model organisms do not: first, the zoonotic nature of the infection makes it directly relevant to human health, especially in Southeast Asia where it has become the most common cause of malaria in Malaysia [128]. Second, the natural parasite reservoirs are kra monkeys (*Macaca fascicularis*) and pig-tailed macaques (*M. nemestrina*), which are also established as important model organisms for biomedical research. Therefore, studying disease trajectories has the potential to not only elucidate how a natural host deals with infection, but also how this may have consequences for disease spread to humans. Lastly, the experimental host, the rhesus monkey (*M. mulatta*) exhibits nearly universal lethal outcomes when infected with *P. knowlesi*, allowing the ability to compare the differences between host and parasite factors that result in parasite control (in *M. fascicularis* or *M. nemestrina*), or overwhelming parasitemia and death (*M. mulatta*).

The research presented in this dissertation was designed to begin to answer the most basic and broad question of what determines host resiliency and susceptibility to the development of severe disease, with the ultimate goal of application of this knowledge to devise treatments to prevent severe malaria cases in humans. As in many instances in science, the results seemed to uncover more questions than answers. In Chapter 3, the clinical course of acute and chronic infections was mapped in *M. fascicularis* and *M. mulatta*. Perhaps the most surprising result from the clinical data was that *M. fascicularis* develops severe anemia, and therefore severe malaria, but

is able to recover without the need for antimalarial treatment. Additionally, when chronic infection was induced in rhesus macaques using subcurative treatment, the animals did not develop severe anemia, despite having higher parasitemia peaks and cumulative parasitemias, suggesting that the anemia suffered in kra monkeys is primarily due to bystander killing of healthy RBCs. The benefits/mechanistic function of moderate and controlled anemia in relation to warding off lethal outcome and the development of chronic infection is a topic that should be explored in the future. Another interesting finding was that timing of the host response seems to be key for controlling parasitemia. *Macaca fascicularis* responded an entire day sooner to patent infection with a temperature response (elevation from baseline) than did rhesus macaques, suggesting that the overwhelming parasitemias that rhesus macaques experience in infection are in part due to a failure of early control. If parasitemia is controlled by subcurative treatment, rhesus macaques eventually mount bone marrow and splenic responses that begin to resemble those of kra monkeys, and that coincide with parasite kinetics that are characteristic of chronicity, however they do not do so until approximately one month after being infected. That rhesus macaques are able to 'catch up' to kra monkeys in terms of marrow and splenic responses, and develop chronic infection when parasitemia is prevented from overwhelming them in acute infection can also be interpreted as evidence that a temporal response is key to controlling *P. knowlesi* infection.

The host must not only wage an early response, but a controlled one. Sequestration has been associated with severe disease in *P. falciparum* infections, and although it does not occur to the same extent in *P. knowlesi* and *P. vivax* infections, accumulation in the tissues is associated with pathological consequences in *P. vivax* (Chapter 2), and to a lesser extent, *P. knowlesi* (Chapter 4) [85,214]. A role for parasite accumulation in pathophysiology, whether by cytoadhesion, rheologic, or other factors may be direct: the presence of parasites in the tissue may cause failure

of nutrient and oxygen delivery (especially in cases in which microvessels are tightly packed with infected RBCs, as in the case in the gastrointestinal tissues of the cohorts infected with *P. knowlesi*), or indirect: the inflammation concomitant with parasite accumulation may cause tissue damage. Parasite accumulation in some tissues may also cause systemic consequences, including possible bacterial translocation from the intestines resulting in sepsis, as has been suggested in *P. falciparum*. Additionally, sequestration may also augment replication, having consequences on circulating parasitemia. A role for sequestration as a mechanism for increasing replication has yet to be verified.

Using the data presented in this dissertation as a foundation, future work can focus on factors (including genetic ones) such as immune response timing and magnitude to more finely probe what constitutes an appropriate, productive, well-targeted immune response, and what consequences this response has in acute and chronic infection. It is possible that a trade-off exists, for instance, between parasite control acutely, and the development of anemia chronically. Additionally, a role for sequestration beyond avoidance of the spleen should be explored, especially in the realm of replication augmentation, and in determining the threshold of the population of sequestered parasites at which biological consequences occur. Less destructive methods of data collection should also be employed, including endoscopy and colonoscopy with biopsy collection to measure sequestration in the gut tissue in the same individuals longitudinally, arterial blood gas collection and other measures of lung function to explore a role for respiratory complications (also a major presenting problem in *P. knowlesi* patients), and ultrasound to track splenic and other organ changes longitudinally [55].

Chapter 6: Appendix

6.1 APPENDIX TO CHAPTER 2: *Plasmodium vivax* parasite load is associated with histopathology in *Saimiri boliviensis* with findings comparable to *P. vivax* pathogenesis in humans

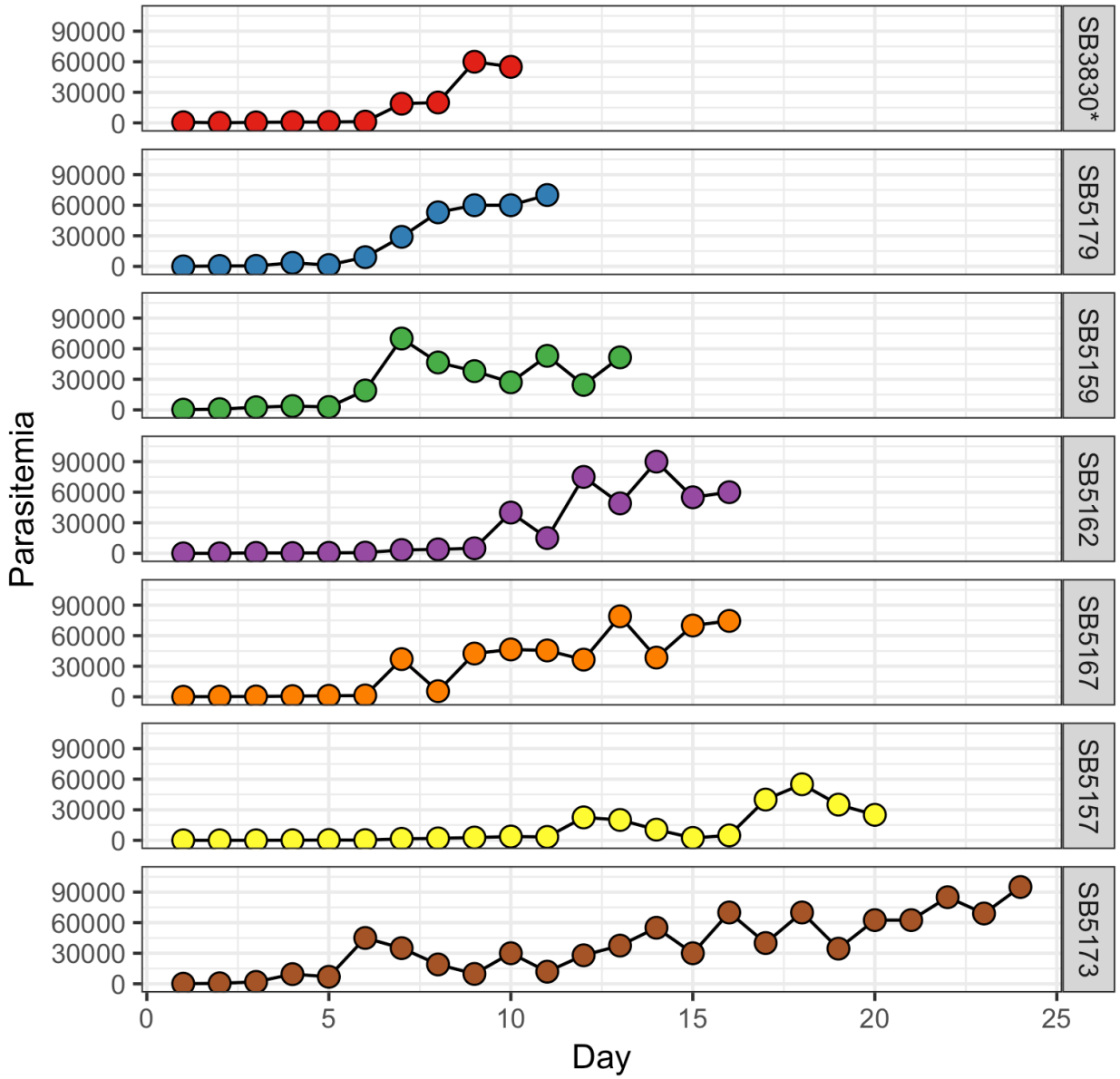

Figure 6.1: Parasitemia kinetics from seven *S. boliviensis* monkeys infected sequentially with *P. vivax* iRBCs. One monkey (SB3830*) was spleen-intact. Parasitemias were recorded daily as parasites/μL, and the animals were sacrificed once they sustained parasitemias of at least 1% (approximately 50,000 parasites/μL). Monkeys were serially inoculated. Thawed cryopreserved iRBCs were initially inoculated into donor monkey, SB 5145 (not included in this cohort),_and on day 12, 1 ml of infected blood was transferred into SB 5162 and SB 5159. On day 10 of their infection, infected blood was transferred to SB 5167 from SB 5162, and to SB 5157 from SB 5159. On day 11 of the SB5157 infection, blood was transferred from this animal to SB 5157 and SB 5173. Finally, SB 3830 was inoculated with infected blood transferred from SB 5173 on day 7 of its infection.

Table 6.1: Infection Parameter Summary

Parameter	Mean (Range)
Age of monkey (years)	**5** (4-11)
Maximum parasitemia (parasites/μl)	**70,572** (55,000-90,000)
Duration of infection (days)	**15.71** (10-24)
Days with parasitemia > 50,000 parasites/μl (days)	**3.57** (1-8)
Proportion of days of infection with parasitemia > 50,000 parasites/μl	**0.231** (0.05-0.364)
Parasitemia at necropsy (parasites/ul)	**61,572** (25,000-90,000)

Table 6.1: Review of experimental demographics and parasite kinetics. Maximum parasitemia refers to the total parasitemia above 50,000 parasites/μl infected RBCs out of total RBCs. Proportion of infection with parasitemia 50,000 parasites/μl is defined as the total number of parasitemic days exceeding 50,000 parasites/μl divided by the total number of days infected. Average parasitemias were rounded up to the first whole number.

Table 6.2: Summary of Histopathology by Tissue for Each Monkey

Histopathology	SB 5173	SB 5159	SB 5157	SB 5162	SB 5167	SB 5179	SB 3830*
Bone Marrow							
Hypercellularity	X	X	X	X	X	X	X
Lungs							
Pulmonary edema	X	X	X	X	X	X	X
Alveolar wall thickening	X	X	X	X	X	X	X
Type II hyperplasia	X	X	X	X	X	X	X
Fibrosis	O	O	O	X	O	O	X
Alveolar and alveolar wall infiltration	X	O	X	X	X	X	X
Hemorrhage	O	X	O	X	X	X	O
Liver							
Vacuolar degeneration	X	X	X	X	X	X	X
Periportal infiltrate	X	X	X	X	X	X	X
Sinusoidal infiltrate	X	X	X	X	X	X	X
Kupffer cell hyperplasia	X	X	X	X	X	X	X
Fibrosis	O	X	O	O	X	O	O
Kidney							
Nephritis	X	X	X	X	X	X	X
Tubular degeneration	X	X	X	X	X	O	X
Glomerular hypercellularity	X	X	X	X	X	X	X
Hemorrhage	O	O	X	O	O	O	O

Table 6.2: Summary of histopathological findings. The presence (X) or absence (O) of major histopathological findings in the relevant organ systems by monkey are shown.

Table 6.3: Tukey HSD Post-Hoc Pairwise Comparison of Histopathology Scores

Organ 1 (I)	Organ 2 (J)	Mean Difference (I-J)	Adjusted p-value	Significance	LB	UB
Brain	Colon	2.667	0.0524	NS	-0.187	5.352
	Kidney	7.000	0.0000	****	4.420	9.580
	Liver	6.143	0.0000	****	3.563	8.723
	Lung	7.286	0.0000	****	4.706	9.866
	Stomach	2.333	0.1192	NS	-0.352	5.019
Colon	Kidney	4.333	0.0033	**	1.648	7.019
	Liver	3.476	0.0052	**	0.791	6.162
	Lung	4.619	0.0001	***	1.933	7.304
	Stomach	-0.333	0.9991	NS	-3.120	2.453
Kidney	Liver	-0.857	0.9138	NS	-3.437	1.722
	Lung	-0.286	0.0001	***	-2.294	2.866
	Stomach	-4.667	0.7627	NS	-7.352	-1.981
Lung	Liver	1.143	0.0018	**	-1.437	3.723
Stomach	Liver	-3.810	0.0018	**	-6.495	-1.124
	Lung	-4.952	0.0000	****	-7.638	-2.267

Table 6.3: Pairwise histology score comparison. The Tukey HSD post-hoc pairwise comparison results for organ scores are summarized. Mean difference is significant at $\alpha = 0.05$; **< 0.005; *** < 0.0005; **** < 0.00005; NS = not significant. LB = Lower Bound, UB = Upper Bound in the 95% Confidence Interval.

Table 6.4: Tukey HSD Post-Hoc Pairwise Comparison of Parasite Organ Load

Organ 1 (I)	Organ 2 (J)	Mean Difference (I-J)	Adjusted p-value	Significance	LB	UB
Adrenal Gland	Bone Marrow	-4.229	1.0000	NS	-49.970	58.426
	Brain	33.249	0.3329	NS	-77.094	10.597
	GI	33.280	0.2469	NS	-76.833	8.274
	Heart	31.152	0.5112	NS	-77.211	14.907
	Kidney	27.845	0.6320	NS	-72.453	16.762
	Liver	-36.360	0.2530	NS	-9.985	81.705
	Lung	-16.996	0.9739	NS	-26.590	60.581
	Lymph Node	32.330	0.4395	NS	-78.003	13.342
	Reproductive Tract	34.400	0.3114	NS	-79.111	10.311
	Spleen	-170	0.0000	****	248.241	93.359
Bone Marrow	Brain	37.477	0.0550	NS	-75.330	0.376
	GI	38.508	0.0276	*	-74.857	-2.159
	Heart	35.381	0.1480	NS	-75.778	5.016
	Kidney	32.074	0.2114	NS	-70.807	6.660
	Liver	-32.131	0.2367	NS	-7.449	71.712
	Lung	-12.767	0.9906	NS	-24.785	50.319

	Lymph Node	36.559	0.1077	NS	-76.514	3.396
	Reproductive Tract	38.629	0.0528	NS	-77.481	0.223
	Spleen	-166.571	0.0000	****	92.358	240.785
Brain	GI	1.031	1.0000	NS	-18.533	16.471
	Heart	-2.096	1.0000	NS	-22.742	26.934
	Kidney	-5.403	0.9994	NS	-16.627	27.434
	Liver	-69.609	0.0000	****	46.121	93.096
	Lung	-50.244	0.0000	****	30.364	70.124
	Lymph Nodes	-0.918	1.0000	NS	-23.195	25.032
	Reproductive Tract	1.151	1.0000	NS	-23.389	21.087
	Spleen	-204.049	0.0000	****	137.022	271.076
GI	Heart	-3.127	1.0000	NS	-19.352	25.607
	Kidney	-6.434	0.9920	NS	-12.898	25.767
	Liver	-70.640	0.0000	****	49.662	91.617
	Lung	-51.276	0.0000	****	34.435	68.116
	Lymph Nodes	-1.949	1.0000	NS	-19.727	23.625
	Reproductive Tract	0.120	1.0000	NS	-19.689	19.448
	Spleen	-205.080	0.0000	****	138.890	271.269
Heart	Kidney	-3.307	1.0000	NS	-22.853	29.467
	Liver	-67.512	0.0000	****	40.114	94.911

	Lung	-48.148	0.0000	****	23.771	72.525
	Lymph Nodes	1.178	1.0000	NS	-29.115	26.759
	Reproductive Tract	3.248	1.0000	NS	-29.583	23.088
	Spleen	-201.952	0.0000	****	133.457	270.448
Kidney	Liver	-64.205	0.0000	****	39.324	89.086
	Lung	-44.841	0.0000	****	23.332	66.349
	Lymph Nodes	4.485	1.0000	NS	-29.958	20.987
	Reproductive Tract	6.555	0.9982	NS	-30.260	17.151
	Spleen	-198.645	0.0000	****	131.117	266.173
Liver	Lung	19.364	0.1912	NS	-42.363	3.634
	Lymph Nodes	68.690	0.0000	****	-95.433	-41.947
	Reproductive Tract	-70.760	0.0000	****	-95.825	-41.695
	Spleen	-134.440	0.0000	****	66.422	202.458
Lung	Lymph Nodes	49.326	0.0000	****	-72.964	-25.688
	Reproductive Tract	51.396	0.0000	****	-73.117	-29.674
	Spleen	-153.804	0.0000	****	86.947	220.662

Lymph Nodes	Reproductive Tract	2.070	1.0000	NS	-27.723	23.583
	Spleen	-203.130	0.0000	****	134.894	271.367
Spleen	Reproductive Tract	-205.200	0.0000	****	137.604	272.796

Table 6.4: Tukey HSD post-hoc pairwise comparison. Pairwise comparison of parasite counts is summarized. Mean difference is significant at $\alpha = 0.05$; **< 0.005; *** < 0.0005; **** < 0.00005; NS = not significant. LB = Lower Bound, UB = Upper Bound in the 95% Confidence Interval.

Table 6.5: Fisher Exact Test Contingency Table

	High Parasite Burden (%)	Low Parasite Burden (%)
High Score	12 (92%)	9 (33%)
Low Score	1 (8.3%)	18 (67%)

Appendix Table 6.5: Fisher exact test. The Fisher Exact Test Contingency table and results are summarized. $\alpha = 0.05$; $P = 0.0005712$; Odds ratio: 22.09.

Table 6.6: Linear Regression

	Model 1					Model 2				
	Estimate	Std. Error	t value	p-value	Significance	Estimate	Std. Error	t value	p-value	Significance
Intercept	3.676	0.549	6.699	0.0000	****	2.509	0.458	5.482	0.0000	****
Count	0.028	0.012	2.361	0.0235	*	-0.008	0.009	-0.858	0.3989	NS
Organ										
Brain						-2.495	0.754	-3.310	0.0022	**
Lung						5.193	0.891	5.828	0.0000	****
Liver						4.112	0.932	4.414	0.0001	****
Lung						4.546	0.756	6.015	0.0000	****
	N = 40; df = 38; Adjusted R^2 = 0.105; F-statistic = 5.545; p-value = 0.0235					N = 40; df = 34; Adjusted R^2 = 0.7505; F-statistic = 24.46; p-value = 0.0000				

Table 6.6: Multiple linear regression analysis. MLR was performed to test the relationship between score, count, and organ. For organ, GI tissue was selected as the reference tissue. Parameter is significant at $\alpha = 0.05$; **< 0.005; **** < 0.00005; NS= not significant.

Table 6.7: Spearman's Rank Coefficient Values

Variable 1	Variable 2	Spearman's ρ	Adjusted p-value	Significance
Histopathological Score	Parasite Burden	0.6034	0.0002	***
	Maximum Parasitemia	0.0768	1.0000	NS
	Days at Peak Parasitemia	-0.0037	1.0000	NS
	Proportion at Peak Parasitemia	0.0683	1.0000	NS
	Parasitemia at Necropsy	0.0163	1.0000	NS
	Duration of Infection	0.0508	1.0000	NS

Table 6.7: Spearman's Rank coefficient test. Parasite tissue burden (parasite counts) and other parameters were tested to determine their association with pathology score. Spearman's ρ is significantly not equal to 0 at $\alpha = 0.05$, ***<0.0005, NS = not significant. All tests are two-sided. p-values adjusted for multiple comparisons with Bonferroni Correction.

6.2 APPENDIX TO CHAPTER 3: Disease resilience and malaria: host resistance and disease severity in *Macaca mulatta* and *M. fascicularis* to *Plasmodium knowlesi* infection

Table 6.8 Cohort Summary (next page). Six monkey cohorts were involved in the macaque-*P. knowlesi* studies, five infected, and one control. They are described above by the chronological number in which they were sacrificed, the experiment code, the number of each species of animal were involved, the purpose, and if the cohort included telemetry. A brief summary is also provided.

Table 6.8: Cohort Summary

Cohort	Monkey Species (n)	Purpose	Monkey Codes	Description	Telemetry?
1 (E30)	*M. mulatta* (2)	Pilot	REd16, RKy15	Two *M. mulatta* monkeys were infected with cryopreserved *P. knowlesi* sporozoites, and time points were taken at pre-determined intervals through acute infection. One was euthanized at peak parasitemia and necropsied, the other subcuratively treated with artemisinin, and euthanized at the second peak and necropsied.	Yes
2 (E07)	*M. fascicularis* (7)	Acute and Chronic	11C131, 11C166, H12C8, H12C59, 12C44, 12C36, 12C53	Seven *M. fascicularis* monkeys were first inoculated with sporozoites from fresh prepared salivary gland dissections, but did not become infected. They were successfully infected with cryopreserved *P. knowlesi* sporozoites. Time	Yes

				points and necropsies were performed at pre-determined times throughout the infection.	
3 (E06)	*M. mulatta* (4)	Acute	RCl15, RIh16, RTe16, RUf16	Four *M. mulatta* monkeys were infected with cryopreserved *P. knowlesi* sporozoites. Time points were collected at pre-determined times throughout the infection. The animals were sacrificed the morning after the first peak of parasitemia.	Yes
4 (E33)	*M. mulatta* (2) *M. fascicularis* (4)	Post-Treatment	13C90, 14C15, 14C3, H13C110, RFz15, RNn9	To study the effects chloroquine administration have on host systems biology and pathology, six animals were infected with cryopreserved sporozoites and the rhesus monkeys were subcuratively treated with chloroquine at peak parasitemia to compare host response with untreated *M. fascicularis* monkeys. Time points were collected at regular, pre-determined	No

				intervals. Seven to ten days after inoculation, the cohort was necropsied.	
5 (E34)	*M. mulatta* (3) *M. fascicularis* (3)	Control	13C102,13C105, 13C129,RAa16, RBe16, RQs9	Three *M. mulatta* and three *M. fascularis* were sacrificed as normal controls for spleen and other solid organ weights, formalin-fixed, frozen, and RNAseq samples.	No
6 (E35)	*M. mulatta* (3) *M. fascicularis* (4)	Acute and Chronic	13_116, 13_136, RRz15, 13C33, 13C74, H13C101, H14C17	Three *M. mulatta* and four *M. fascicularis* macaques were infected with cryopreserved *P. knowlesi* sporozoites, and the infection was followed for 50 days. *Macaca mulatta* macaques were subcuratively treated with artemisinin when parasitemias reached above 1% to prevent rapid parasitemia rise and death, and to induce chronicity. *Macaca fascicularis* macaques were not treated. Time points at pre-determined intervals were taken throughout the experiment,	No

				along with daily parasitemia and CBC monitoring. At Days 48-50, the animals were necropsied.	
7 (Spx)	*M. mulatta* (2)	Acute	RBg14, RAd14	Two previously surgically splenectomized animals were infected with SICA[-] parasites to test if SICA protein expression is related to the margination phenotype	No

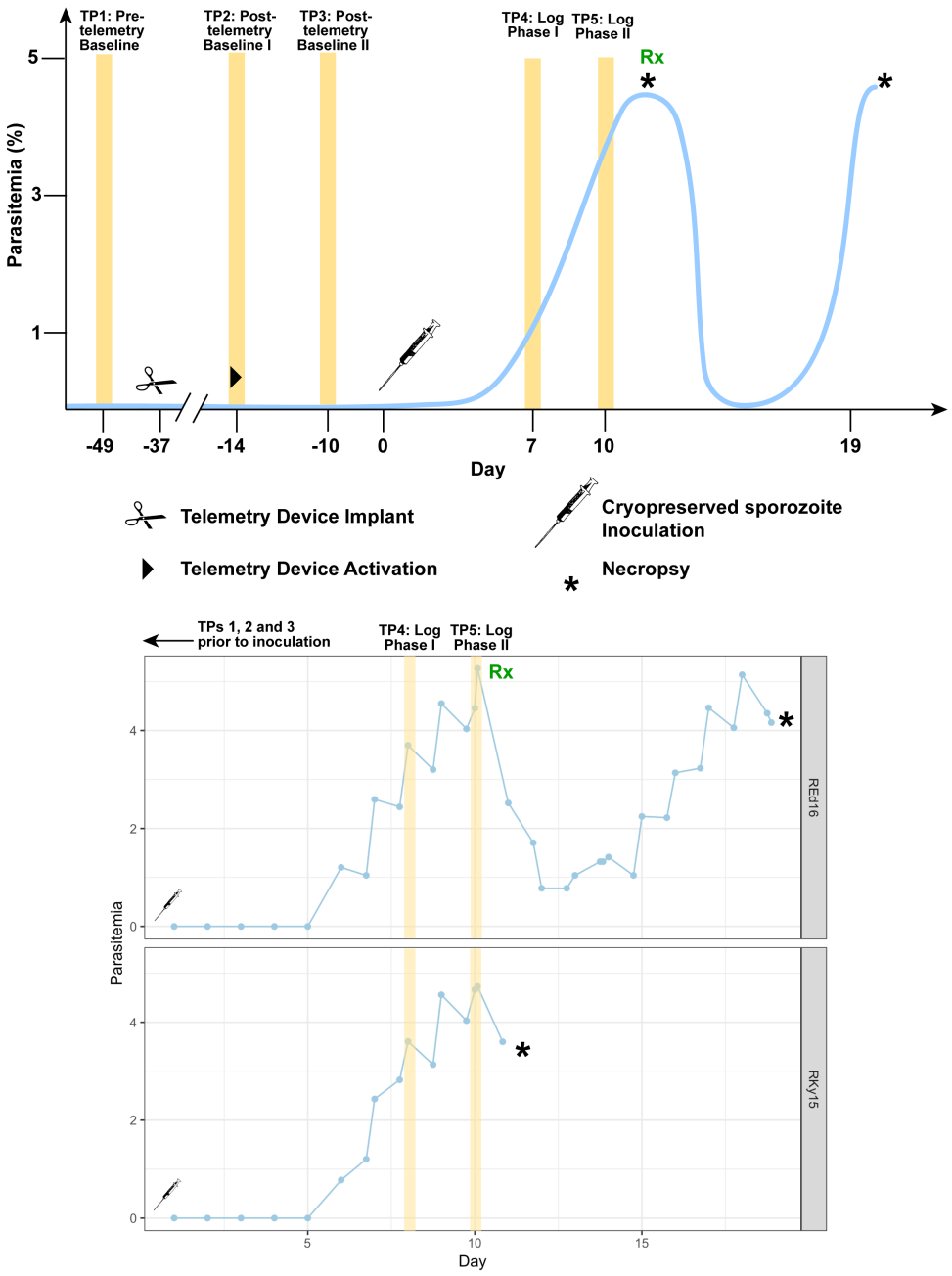

Figure 6.2 Experimental Design and Parasitemia for E30 (Pilot acute *P. knowlesi* infection in rhesus macaques). Top, schematic of predicted parasitemia kinetics with telemetry device planned timepoints, implant surgery and activation, and inoculation and necropsy indicated. Bottom, recorded parasitemias and indicated time points. Subcurative treatment with artemether indicated in green.

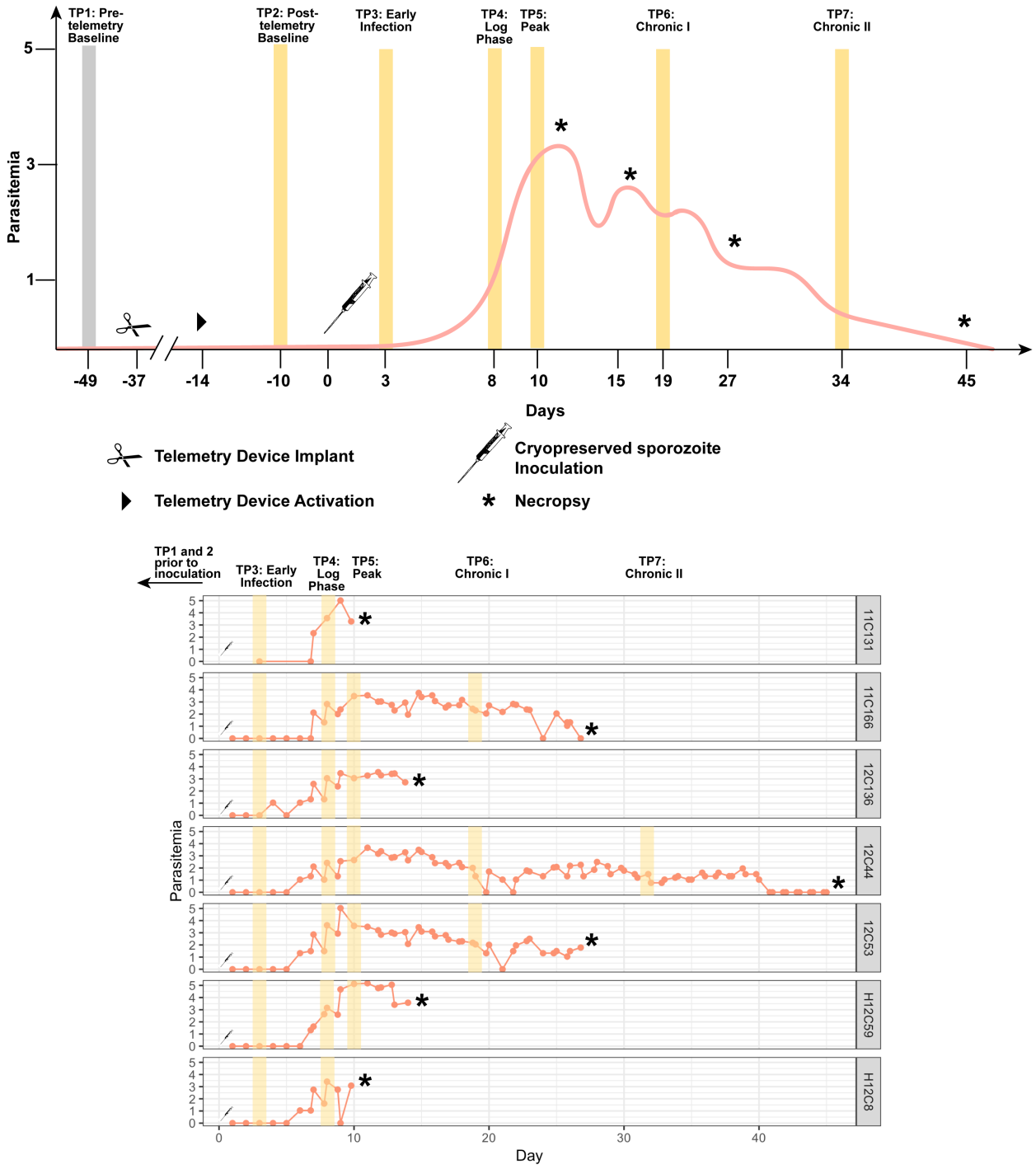

Figure 6.3 Experimental Design and Parasitemia for E07 (Longitudinal *P. knowlesi* infection in kra monkeys). Top, schematic of predicted parasitemia kinetics with telemetry device planned timepoints, implant surgery and activation, and inoculation and necropsy indicated. Bottom, recorded parasitemias and indicated time points.

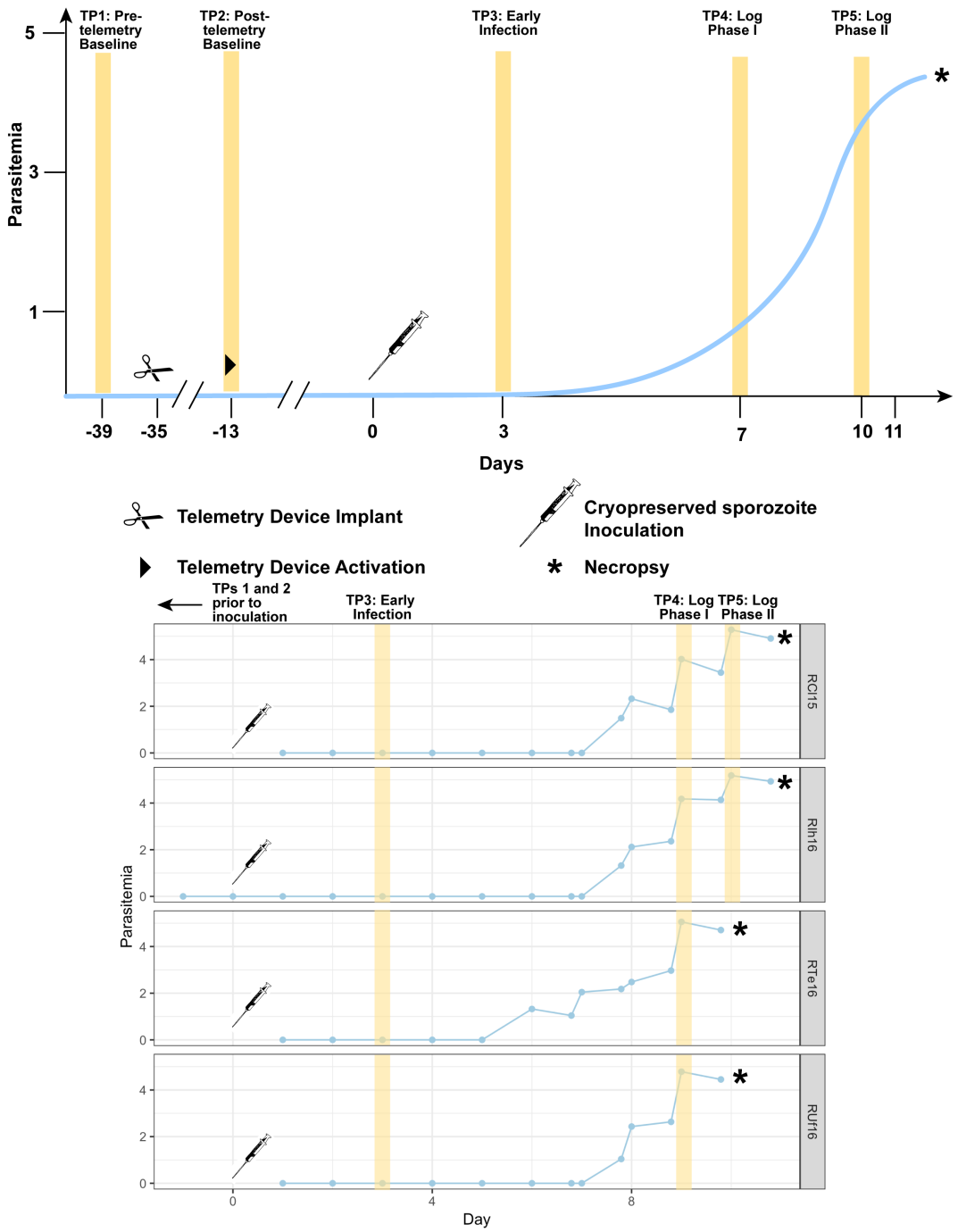

Figure 6.4 Experimental Design and Parasitemia for E06 (Acute *P. knowlesi* infection in rhesus macaques). Top, schematic of predicted parasitemia kinetics with telemetry device planned timepoints, implant surgery and activation, and inoculation and necropsy indicated. Bottom, recorded parasitemias and indicated time points.

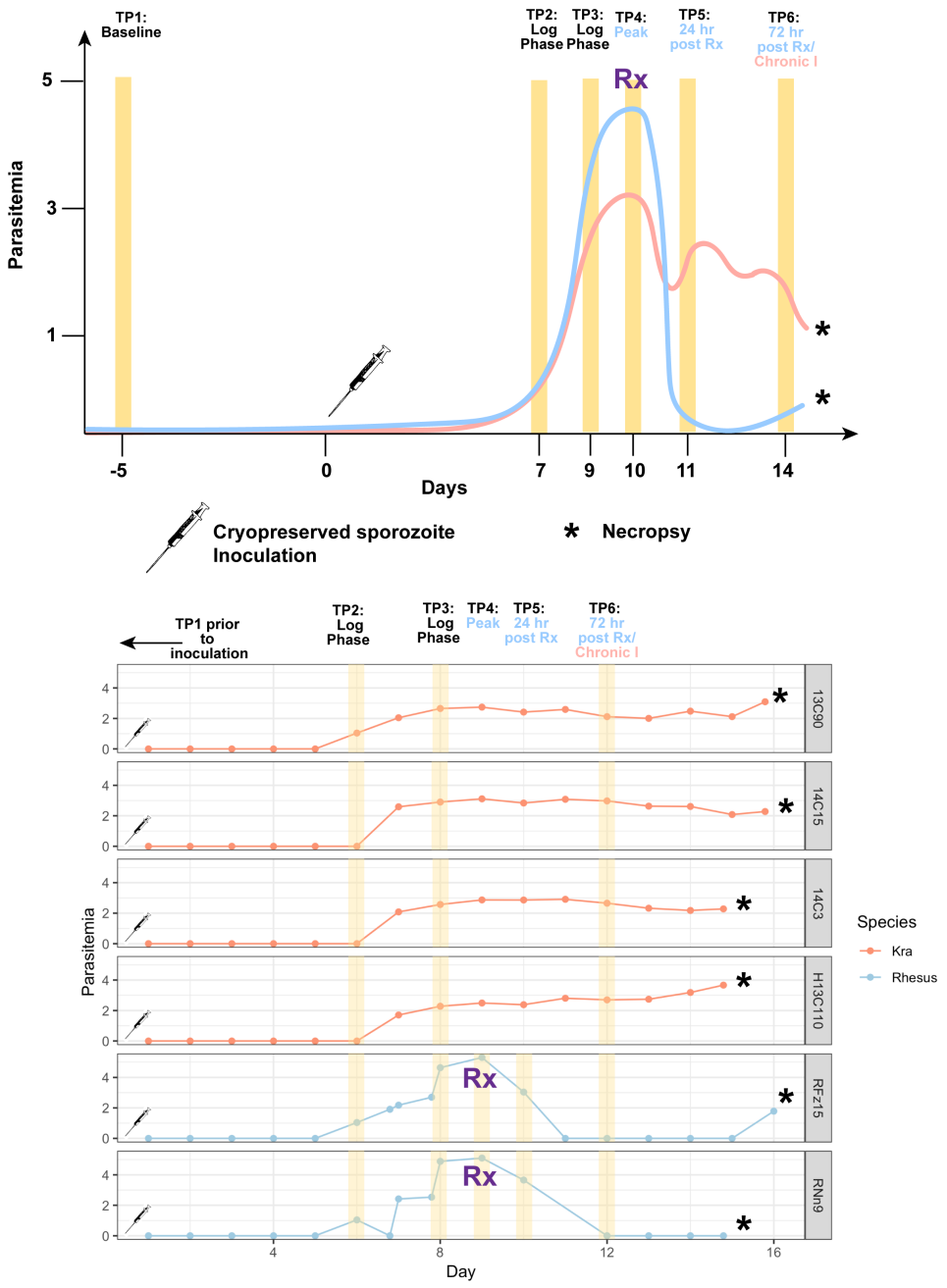

Figure 6.5 Experimental Design and Parasitemia for E33 (Chloroquine treatment in acute *P. knowlesi* infection in macaques). Top, schematic of predicted parasitemia kinetics with inoculation and necropsy indicated. Bottom, recorded parasitemias and indicated time points. Chloroquine treatment is indicated in purple.

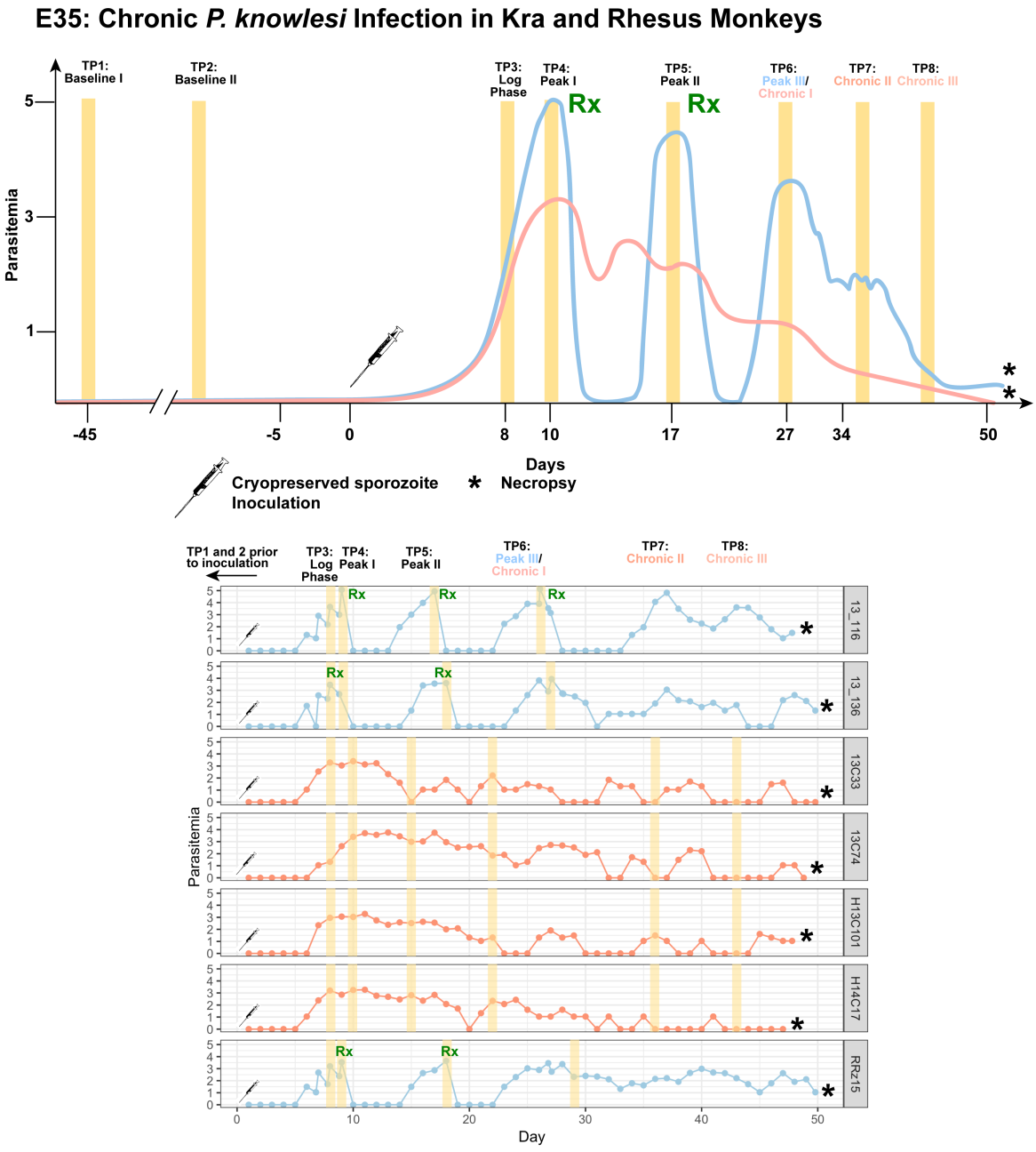

Figure 6.6 Experimental Design and Parasitemia for E35 (Chronic *P. knowlesi* infection in macaques). Top, schematic of predicted parasitemia kinetics with inoculation and necropsy indicated. Bottom, recorded parasitemias and indicated time points. Artemether treatment indicated in green.

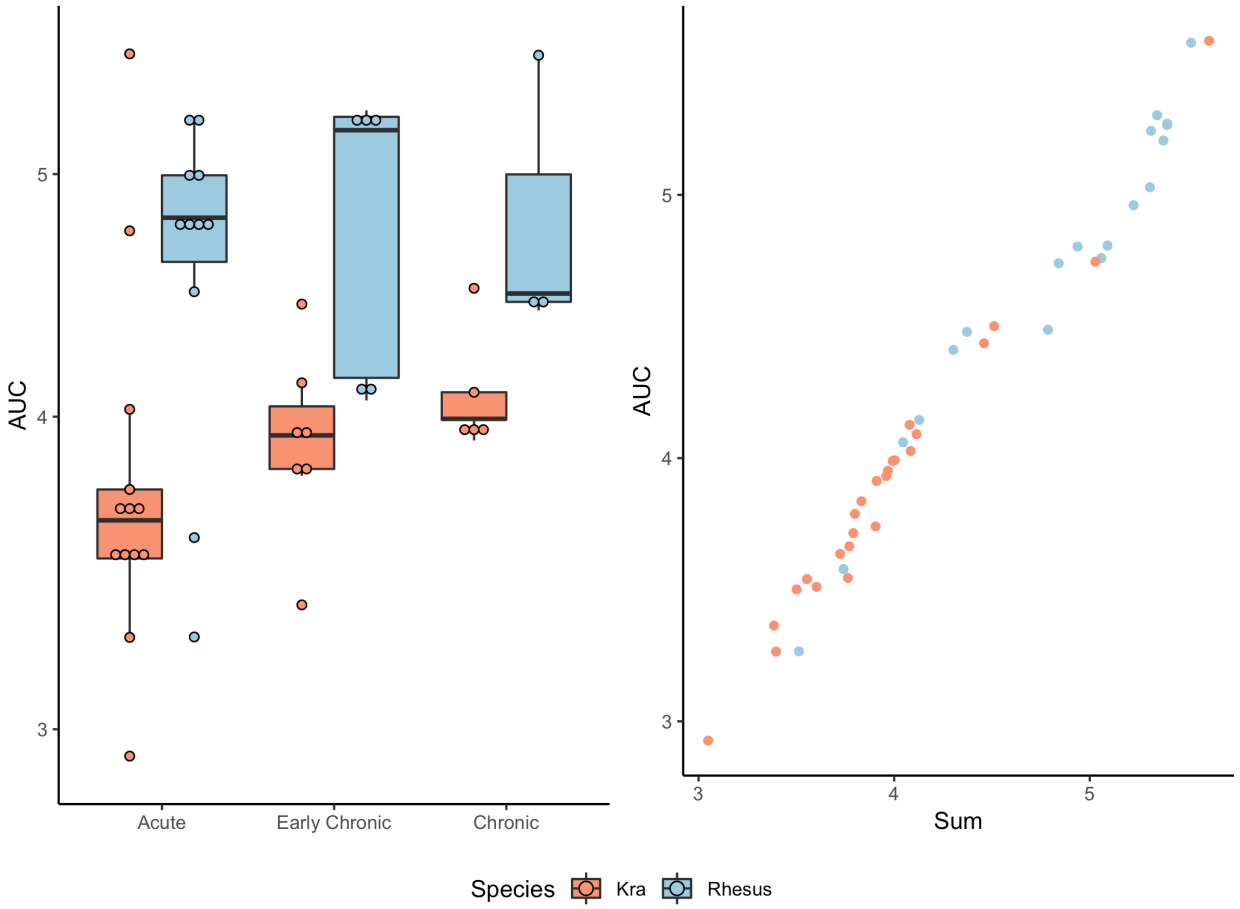

Figure 6.7 Area under the curve (AUC) as a measure of cumulative parasitemia in *P. knowlesi* infection of macaques. Left, AUC calculated for each species at three different stages of infection using the PKNCA package in R. Right, AUC vs. Sum was highly correlated (Pearson coefficient = 0.9881, p-value = p-value $< 2.2 \times 10^{-16}$; $r^2 = 0.9757$, slope = 0.9592, p-value $< 2.2 \times 10^{-16}$).

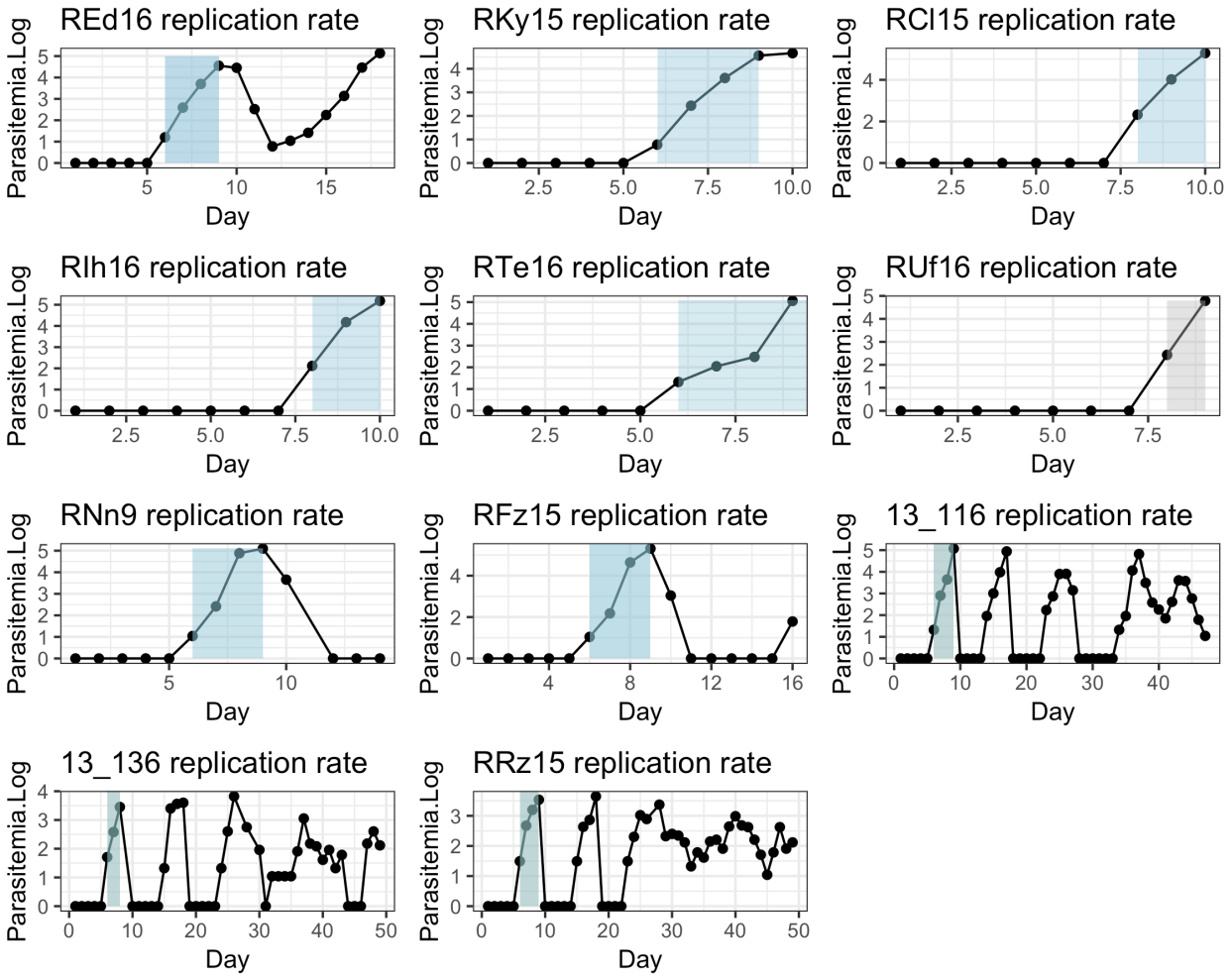

Figure 6.8 Replication rate of *P. knowlesi* infection in rhesus macaques. Parasite kinetics curves showing the intervals were considered for each monkey when calculating the replication rate highlighted in blue. The most linear portion of the curve between patency to peak or termination was chosen. Replication rates were included in the analysis if the number of points considered was greater than two (RUf16 was excluded, and is indicated in gray). Only afternoon timepoints were considered because the parasites were ring stage at this time and less likely to be sequestered, therefore giving the most accurate peripheral count.

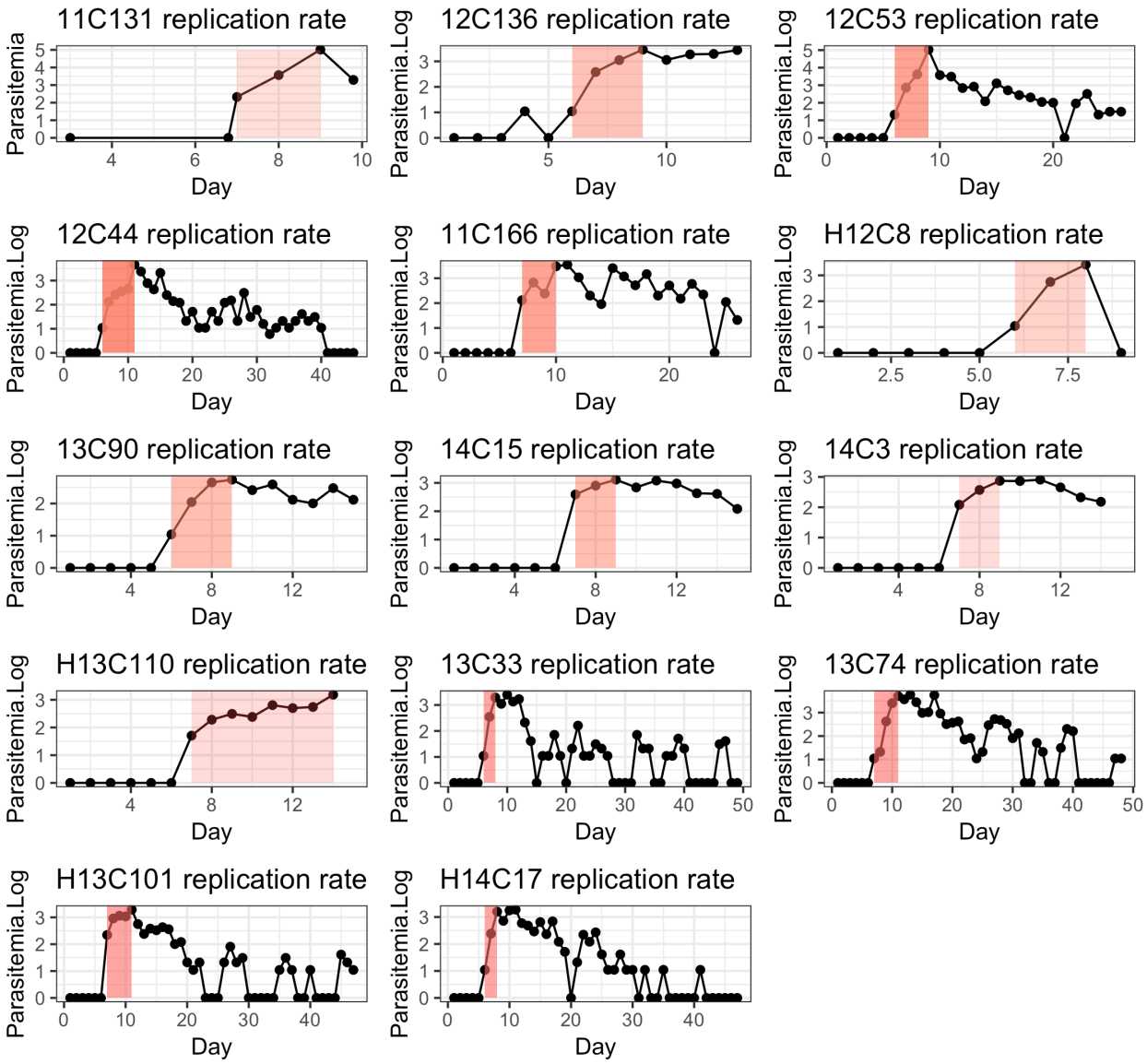

Figure 6.9 Replication rate of *P. knowlesi* infection in rhesus macaques. Parasite kinetics curves showing the intervals were considered for each monkey when calculating the replication rate highlighted in red. The most linear portion of the curve between patency to peak or termination was chosen. Replication rates were included in the analysis if the number of points considered was greater than two. Only afternoon timepoints were considered because the parasites were ring stage at this time and less likely to be sequestered, therefore giving the most accurate peripheral count.

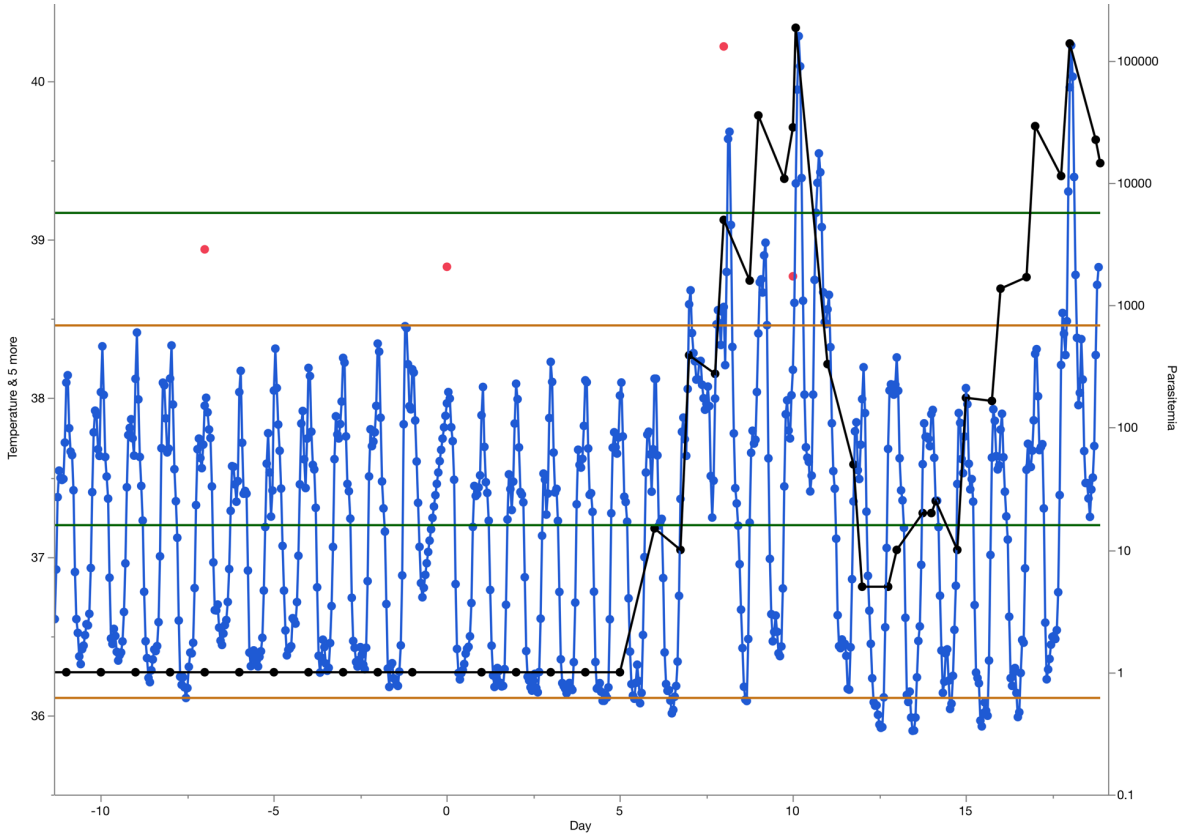

Figure 6.10 Telemetry and parasitemia for REd16. Down-sampled telemetric temperature data is represented by the blue trace, parasitemia by the black trace, and rectal temperatures by the red points. The amber lines represent the defined normal temperature of this individual based on the range of temperature minimums and maximums in the pre-infection period. The green lines represent the normal temperature range used by the Yerkes Primate Formulary. The pyrogenic threshold is defined as the parasitemia that occurs directly before the temperature increases above the individual animal's normal upper limit (amber line).

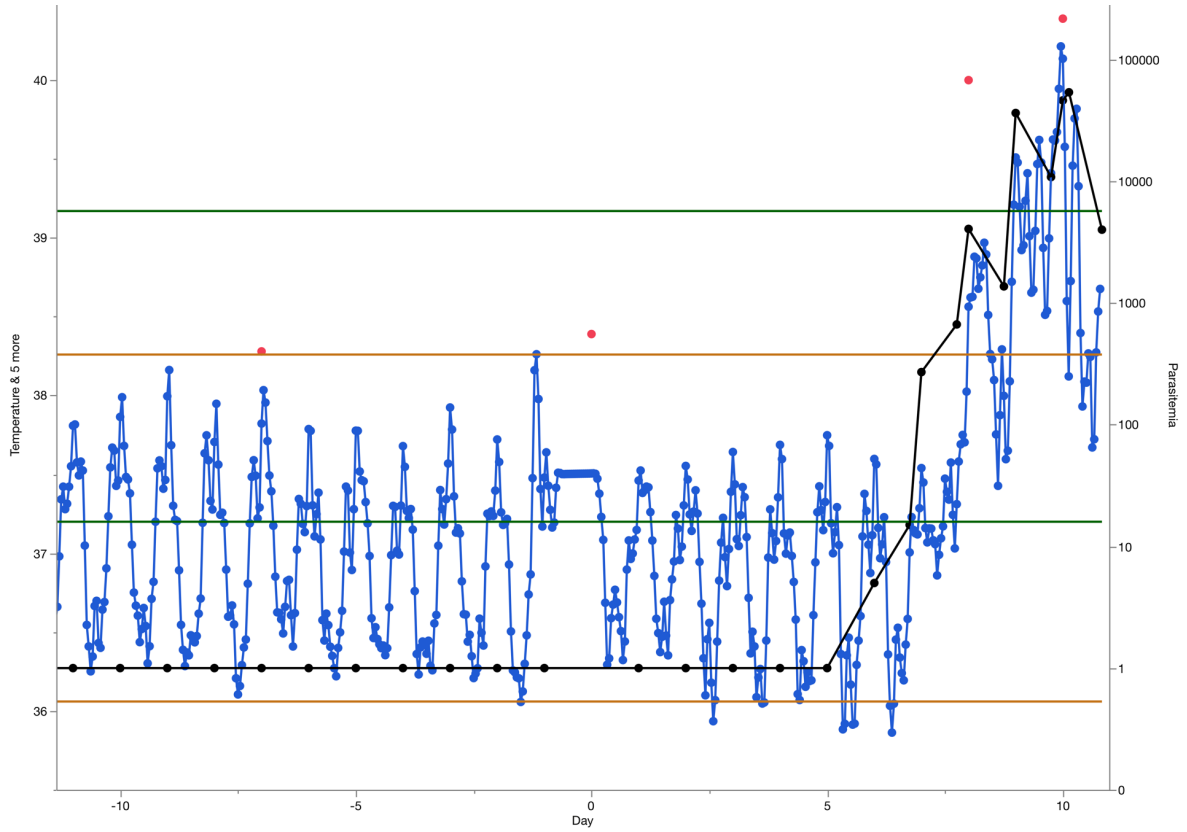

Figure 6.11 Telemetry and parasitemia for RKy15. Plot showing telemetric temperature readings and daily/semi-daily parasitemia readings for the calculation of pyrogenic threshold (see Fig. 6.10 for further details).

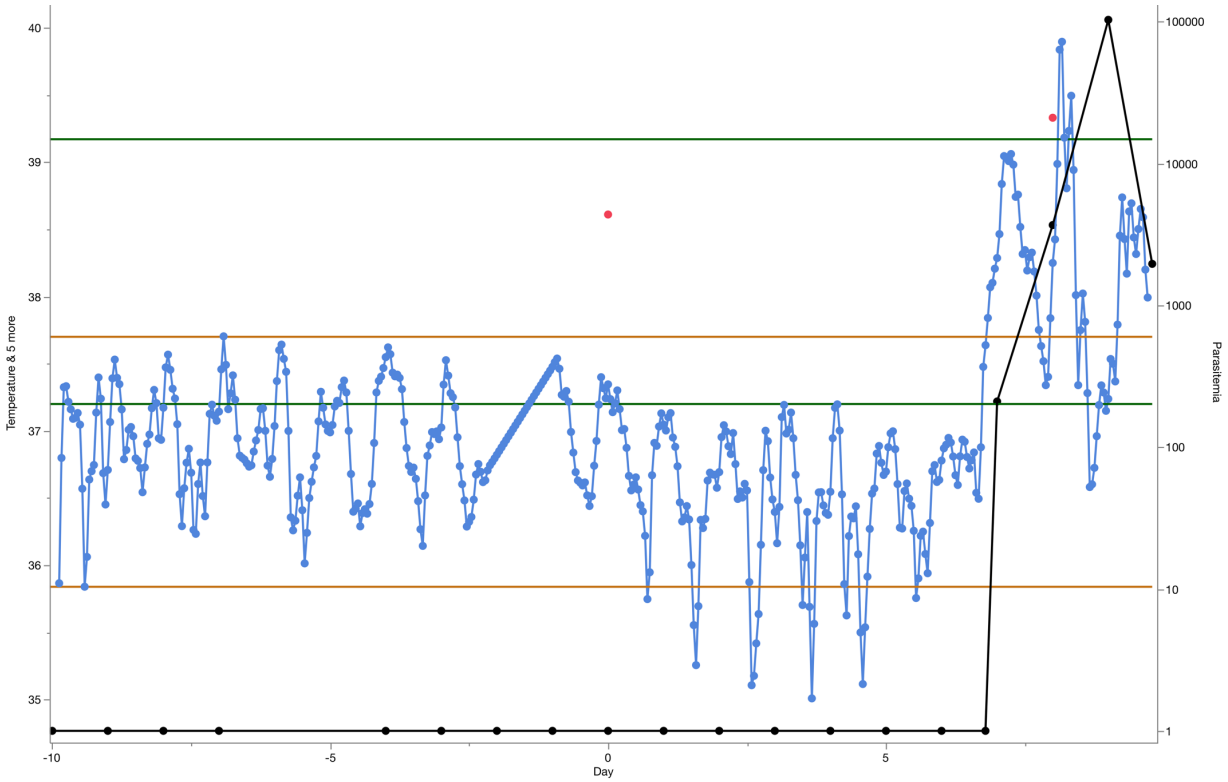

Figure 6.12 Telemetry and parasitemia for 11C131. Plot showing telemetric temperature readings and daily/semi-daily parasitemia readings for the calculation of pyrogenic threshold (see Fig. 6.10 for further details).

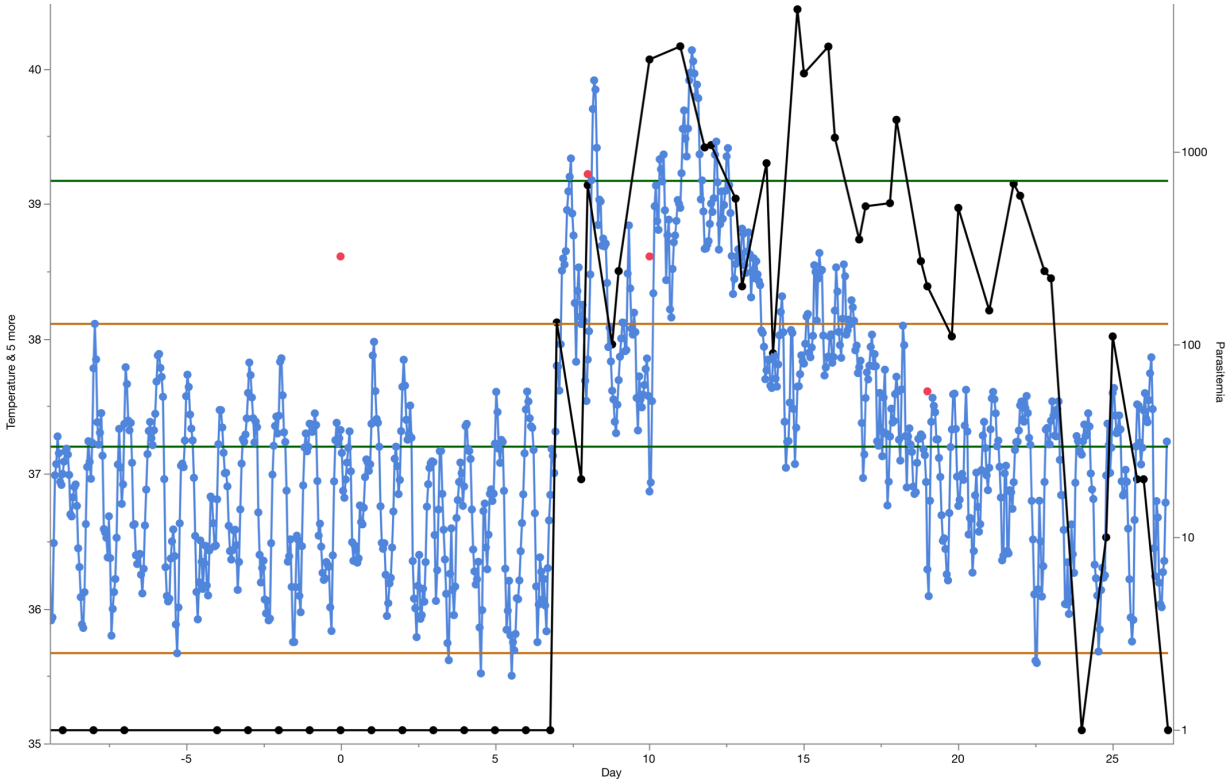

Figure 6.13 Telemetry and parasitemia for 11C166. Plot showing telemetric temperature readings and daily/semi-daily parasitemia readings for the calculation of pyrogenic threshold (see Fig. 6.10 for further details).

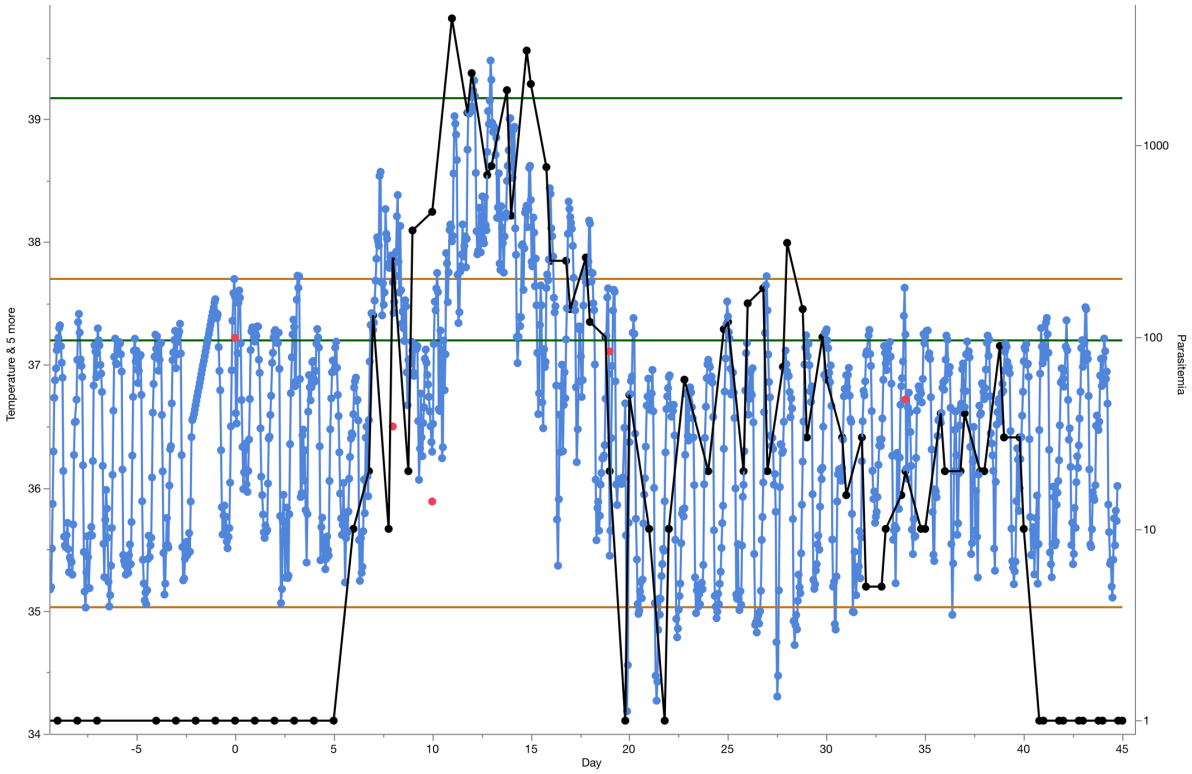

Figure 6.14 Telemetry and parasitemia for 12C44. Plot showing telemetric temperature readings and daily/semi-daily parasitemia readings for the calculation of pyrogenic threshold (see Fig. 6.10 for further details).

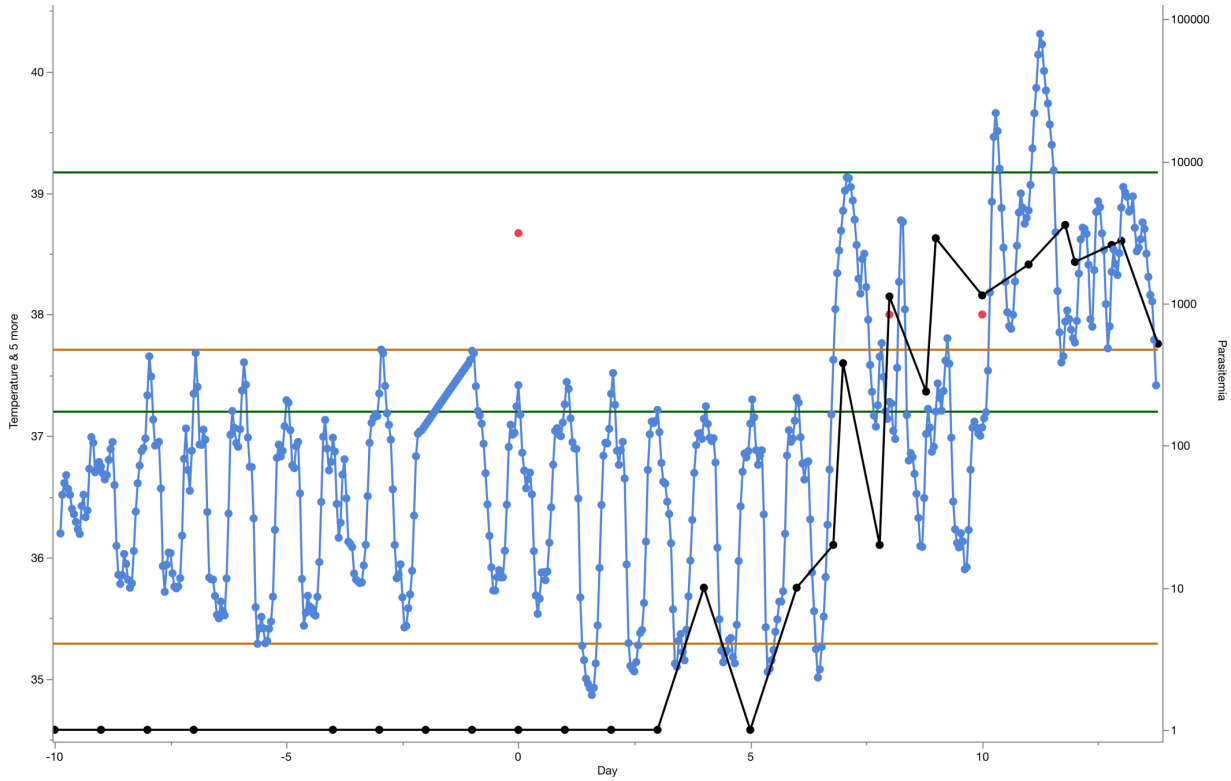

Figure 6.15 Telemetry and parasitemia for 12C136. Plot showing telemetric temperature readings and daily/semi-daily parasitemia readings for the calculation of pyrogenic threshold (see Fig. 6.10 for further details).

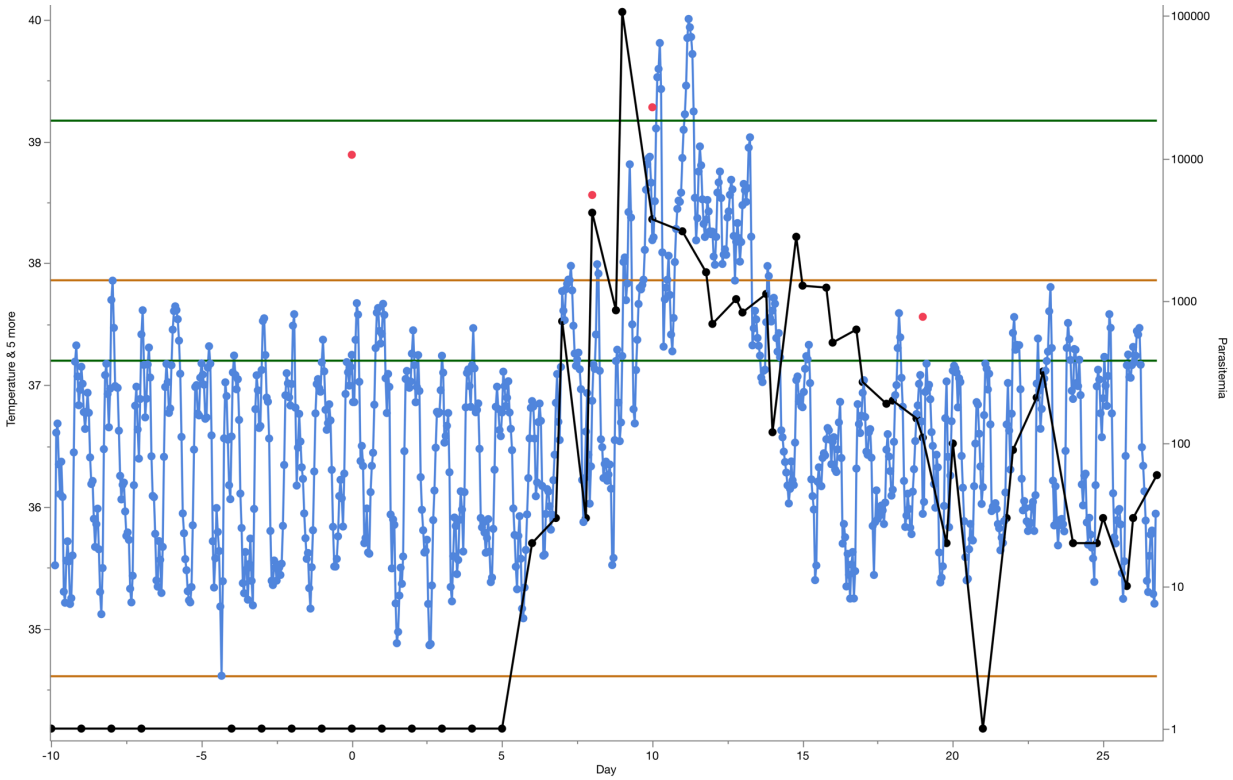

Figure 6.16 Telemetry and parasitemia for 12C53. Plot showing telemetric temperature readings and daily/semi-daily parasitemia readings for the calculation of pyrogenic threshold (see Fig. 6.10 for further details).

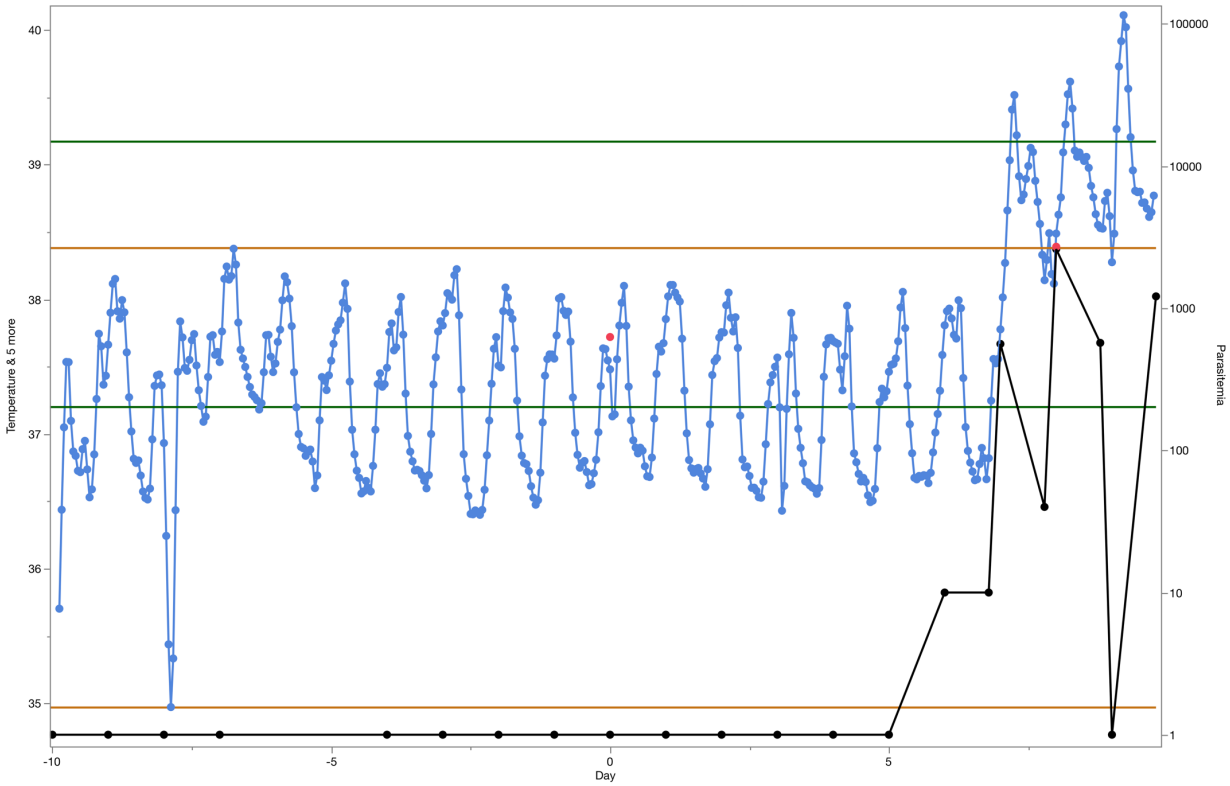

Figure 6.17 Telemetry and parasitemia for H12C8. Plot showing telemetric temperature readings and daily/semi-daily parasitemia readings for the calculation of pyrogenic threshold (see Fig. 6.10 for further details).

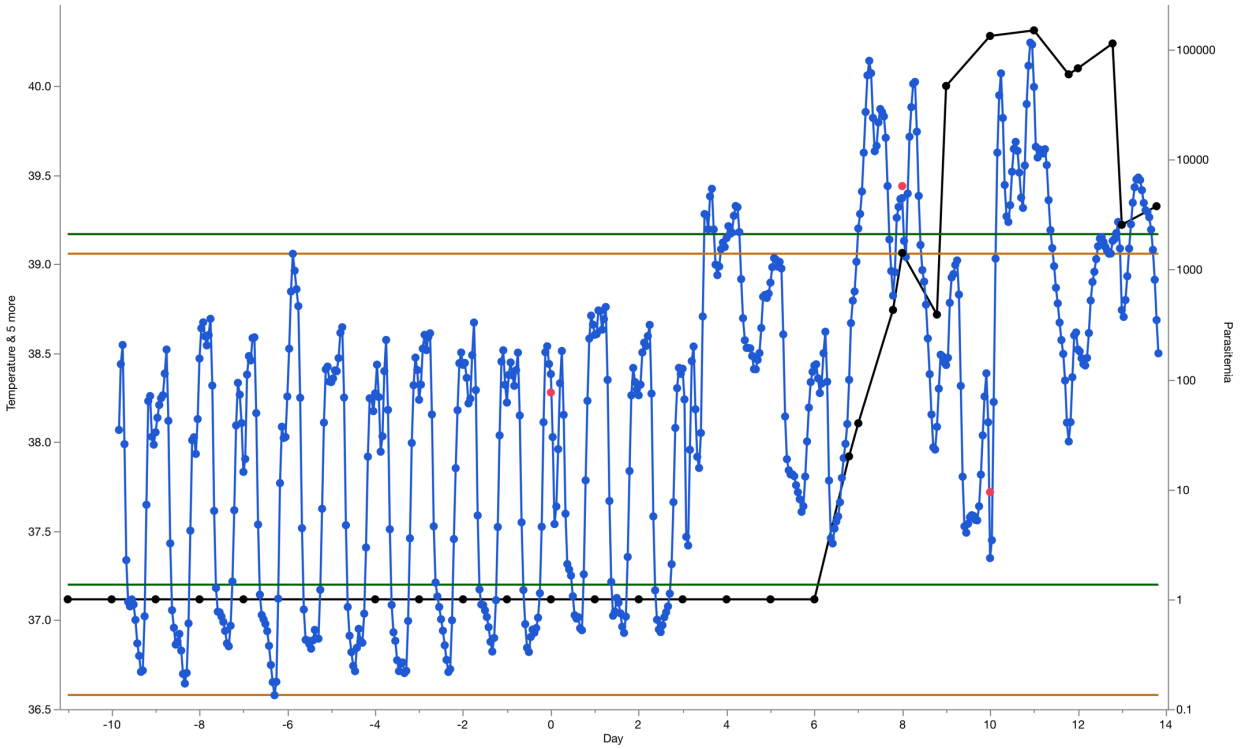

Figure 6.18 Telemetry and parasitemia for H12C59. Plot showing telemetric temperature readings and daily/semi-daily parasitemia readings for the calculation of pyrogenic threshold (see Fig. 6.10 for further details).

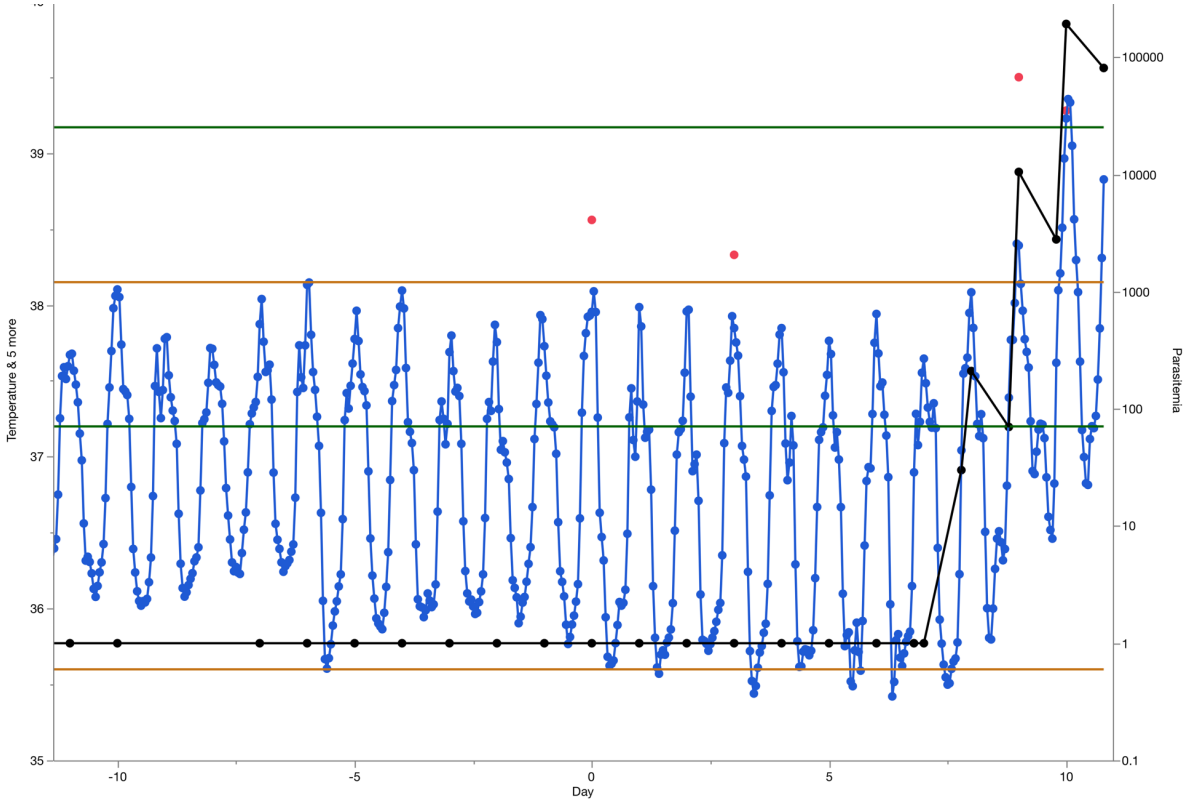

Figure 6.19 Telemetry and parasitemia for RCl15. Plot showing telemetric temperature readings and daily/semi-daily parasitemia readings for the calculation of pyrogenic threshold (see Fig. 6.10 for further details).

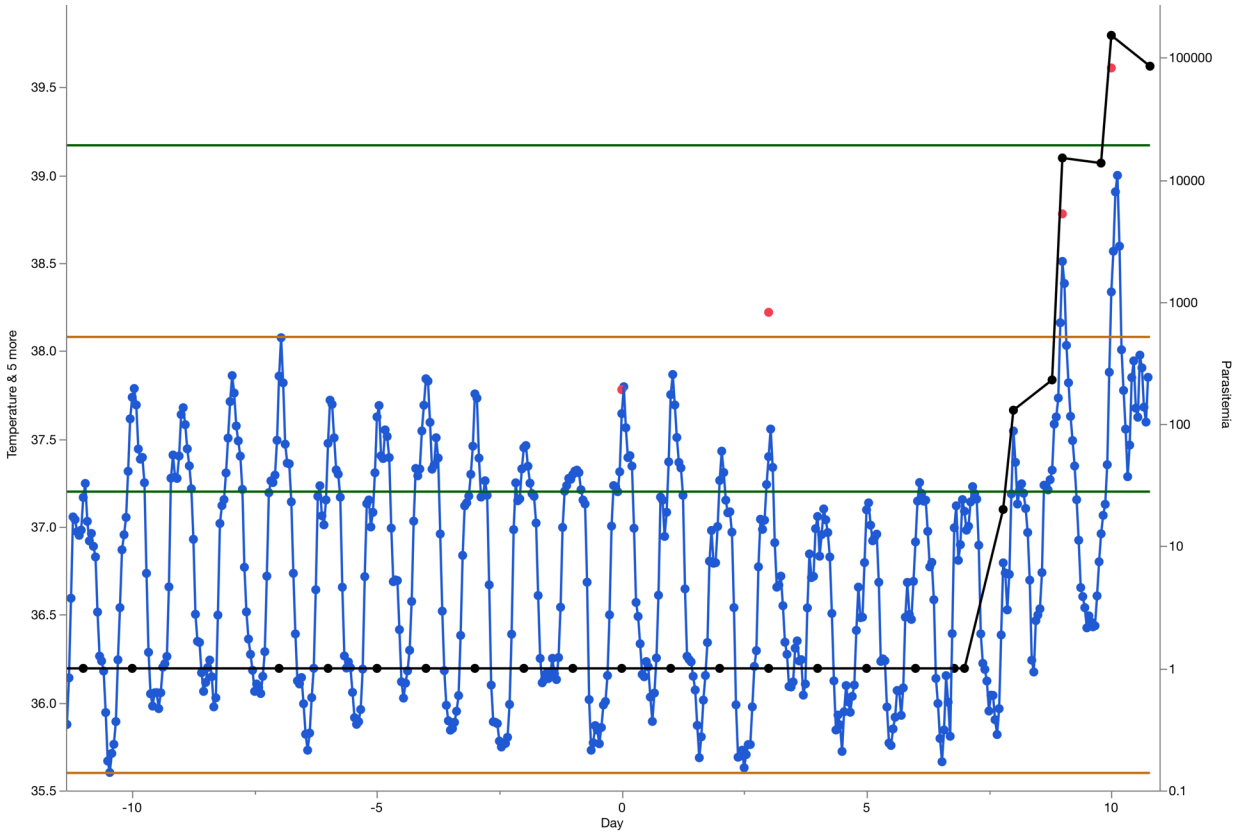

Figure 6.20 Telemetry and parasitemia for RIh16. Plot showing telemetric temperature readings and daily/semi-daily parasitemia readings for the calculation of pyrogenic threshold (see Fig. 6.10 for further details).

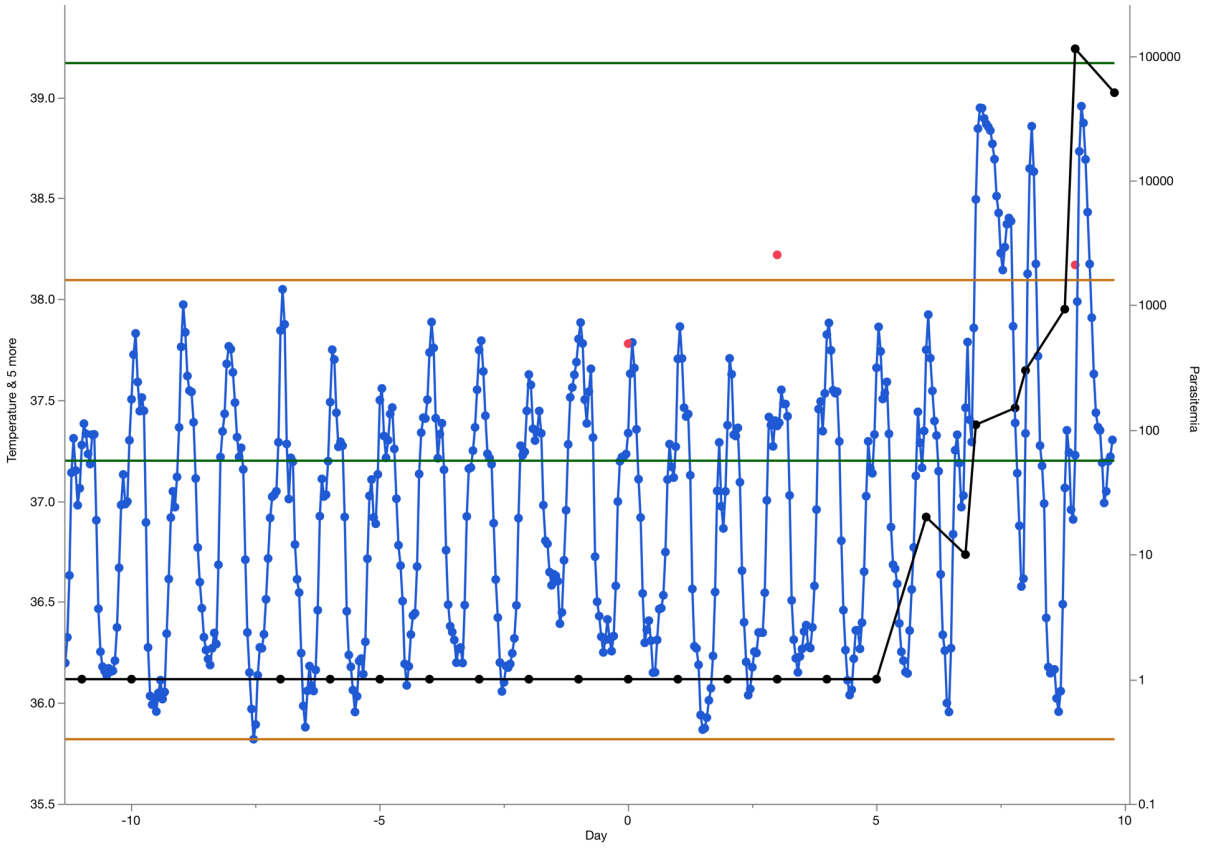

Figure 6.21 Telemetry and parasitemia for RTe16. Plot showing telemetric temperature readings and daily/semi-daily parasitemia readings for the calculation of pyrogenic threshold (see Fig. 6.10 for further details).

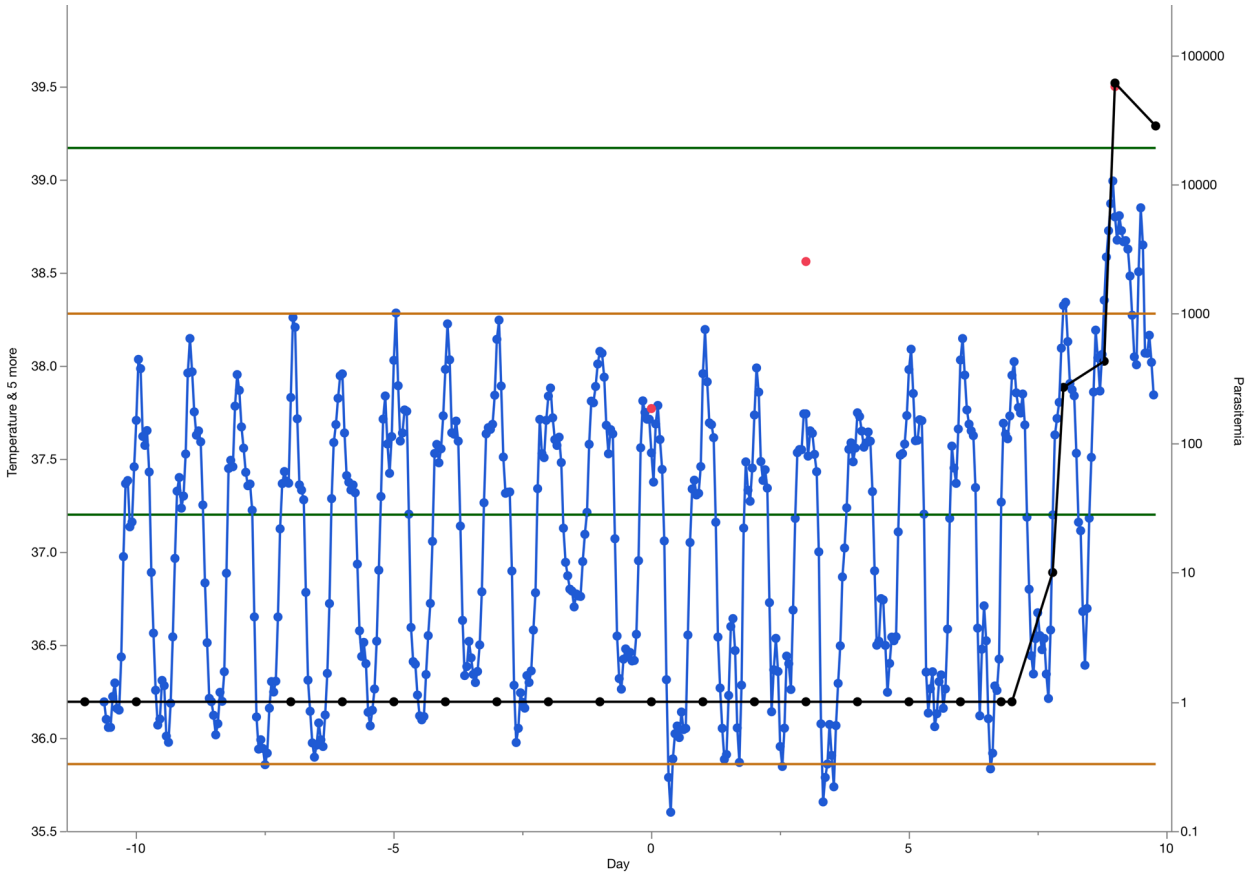

Figure 6.22 Telemetry and parasitemia for RUf16. Plot showing telemetric temperature readings and daily/semi-daily parasitemia readings for the calculation of pyrogenic threshold (see Fig. 6.10 for further details).

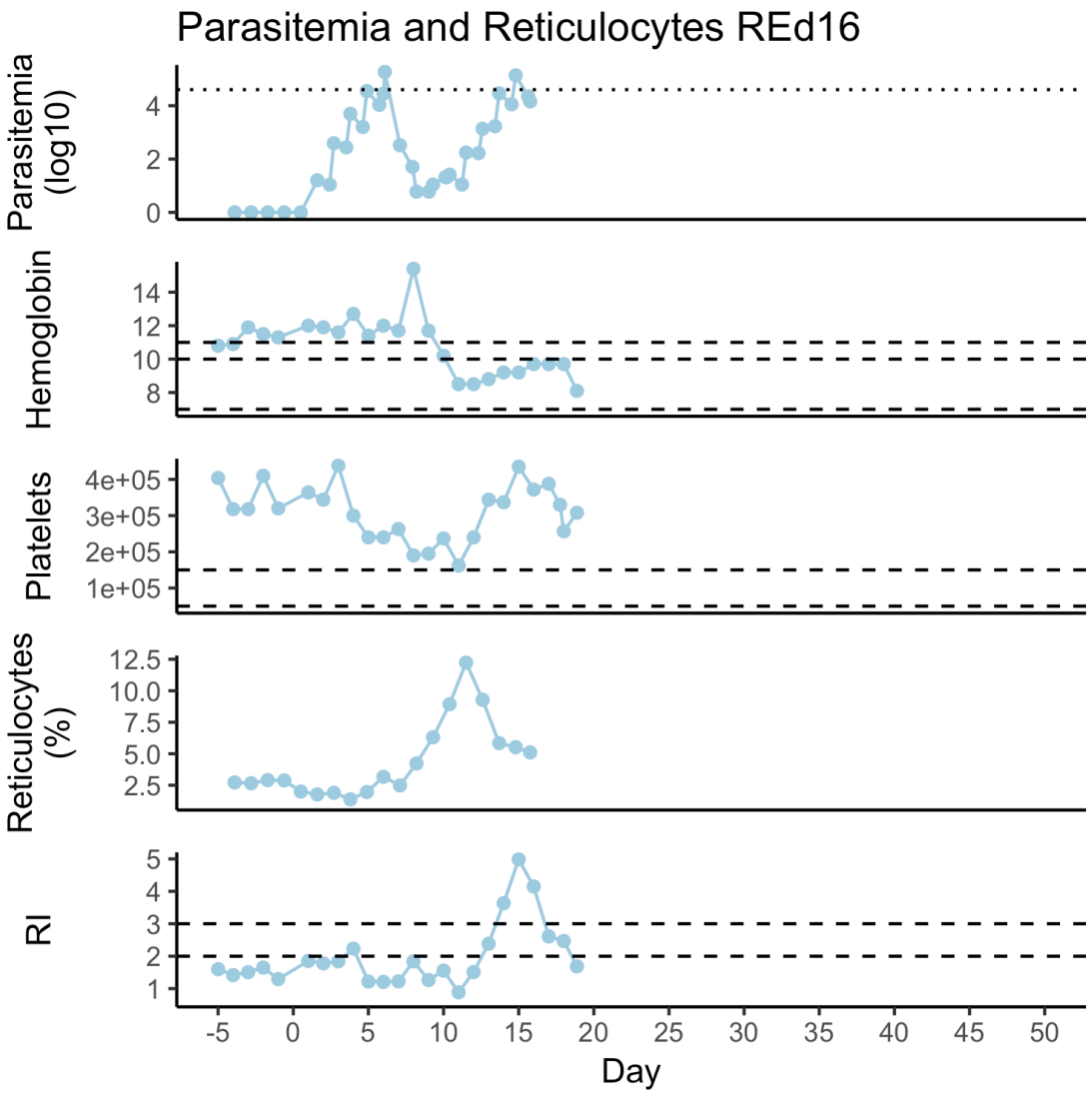

Figure 6.23 Parasitemia and select hematological parameters for REd16. Plot showing longitudinal parasitemia (first panel), hemoglobin (second panel), platelets (third panel), reticulocytes (fourth panel), and reticulocyte production index, or RI (fifth panel) plots. Lines denoting the equivalent of 1% parasitemia (50,000 parasites/μL), mild, moderate, and severe anemia (hemoglobin of 12, 10, and 8 g/dL, respectively), mild and moderate thrombocytopenia (150,000 and 50,000 platelets/ μL), and reticulocyte response (2, and 3 for sufficient response, and sufficient response with lysis, respectively) are given.

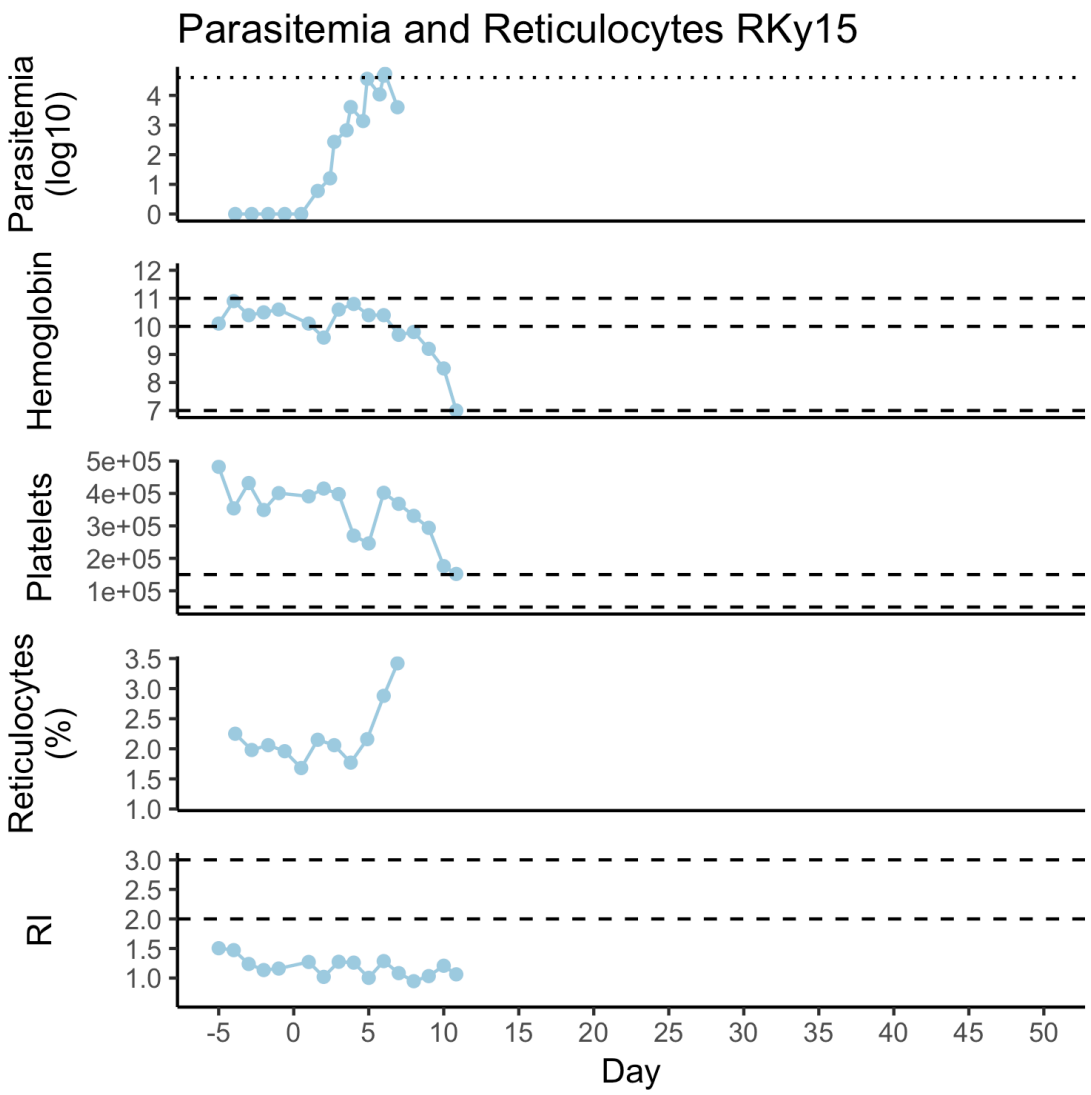

Figure 6.24 Parasitemia and select hematological parameters for RKy15. Plot showing longitudinal parasitemia (first panel), hemoglobin (second panel), platelets (third panel), reticulocytes (fourth panel), and reticulocyte production index, or RI (fifth panel) plots. Lines denoting the equivalent of 1% parasitemia (50,000 parasites/μL), mild, moderate, and severe anemia (hemoglobin of 12, 10, and 8 g/dL, respectively), mild and moderate thrombocytopenia (150,000 and 50,000 platelets/ μL), and reticulocyte response (2, and 3 for sufficient response, and sufficient response with lysis, respectively) are given.

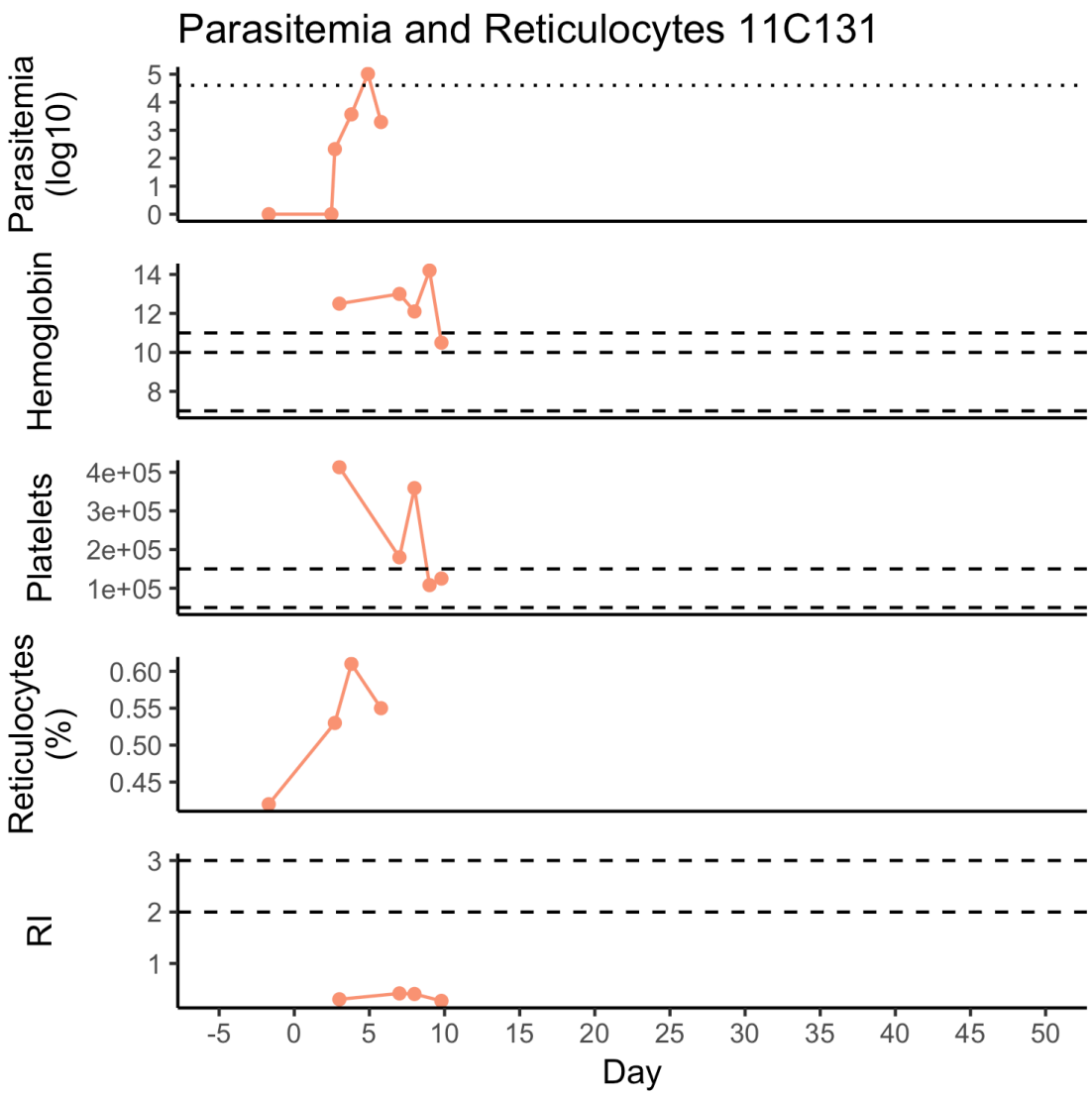

Figure 6.25 Parasitemia and select hematological parameters for 11C131 Plot showing longitudinal parasitemia (first panel), hemoglobin (second panel), platelets (third panel), reticulocytes (fourth panel), and reticulocyte production index, or RI (fifth panel) plots. Lines denoting the equivalent of 1% parasitemia (50,000 parasites/μL), mild, moderate, and severe anemia (hemoglobin of 12, 10, and 8 g/dL, respectively), mild and moderate thrombocytopenia (150,000 and 50,000 platelets/ μL), and reticulocyte response (2, and 3 for sufficient response, and sufficient response with lysis, respectively) are given.

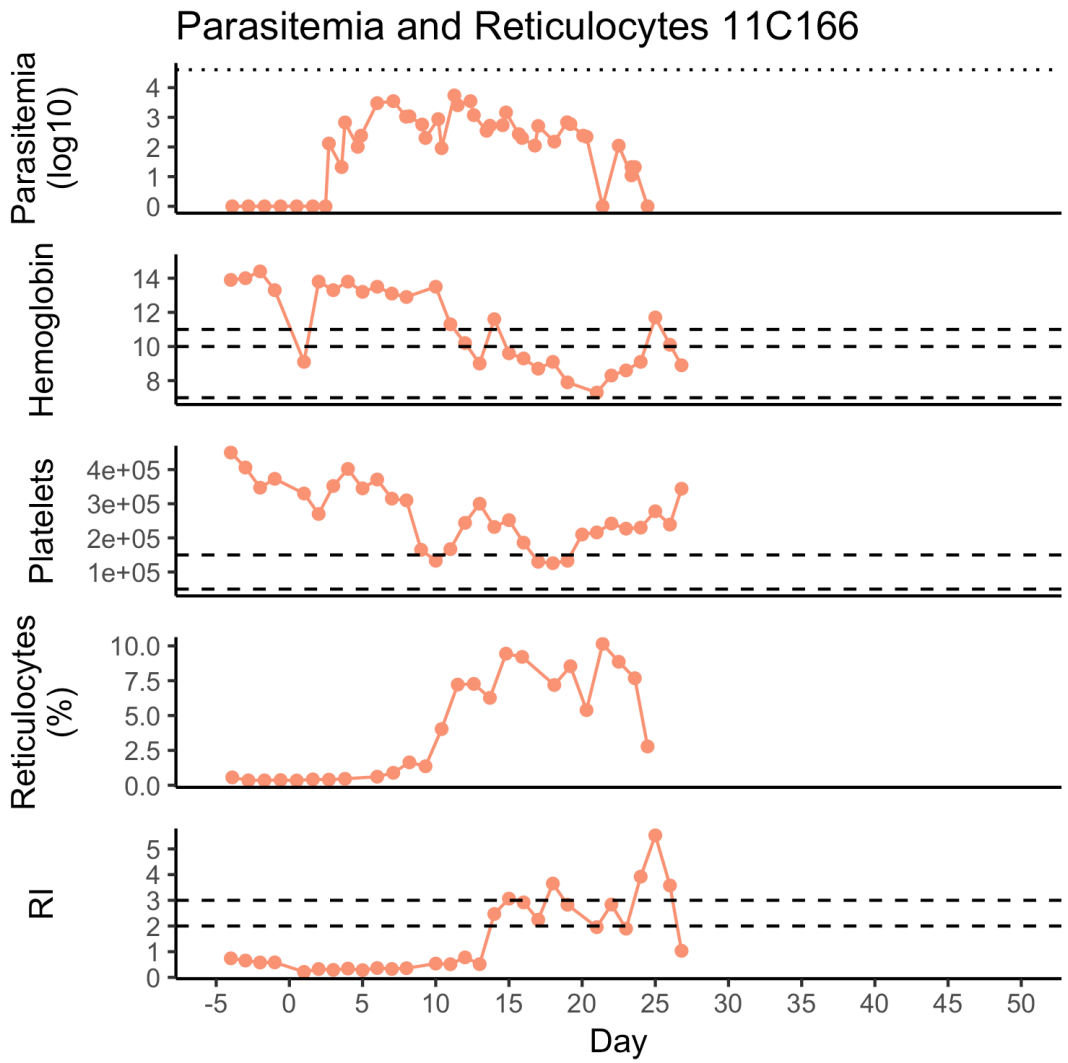

Figure 6.26 Parasitemia and select hematological parameters for 11C166 Plot showing longitudinal parasitemia (first panel), hemoglobin (second panel), platelets (third panel), reticulocytes (fourth panel), and reticulocyte production index, or RI (fifth panel) plots. Lines denoting the equivalent of 1% parasitemia (50,000 parasites/μL), mild, moderate, and severe anemia (hemoglobin of 12, 10, and 8 g/dL, respectively), mild and moderate thrombocytopenia (150,000 and 50,000 platelets/ μL), and reticulocyte response (2, and 3 for sufficient response, and sufficient response with lysis, respectively) are given.

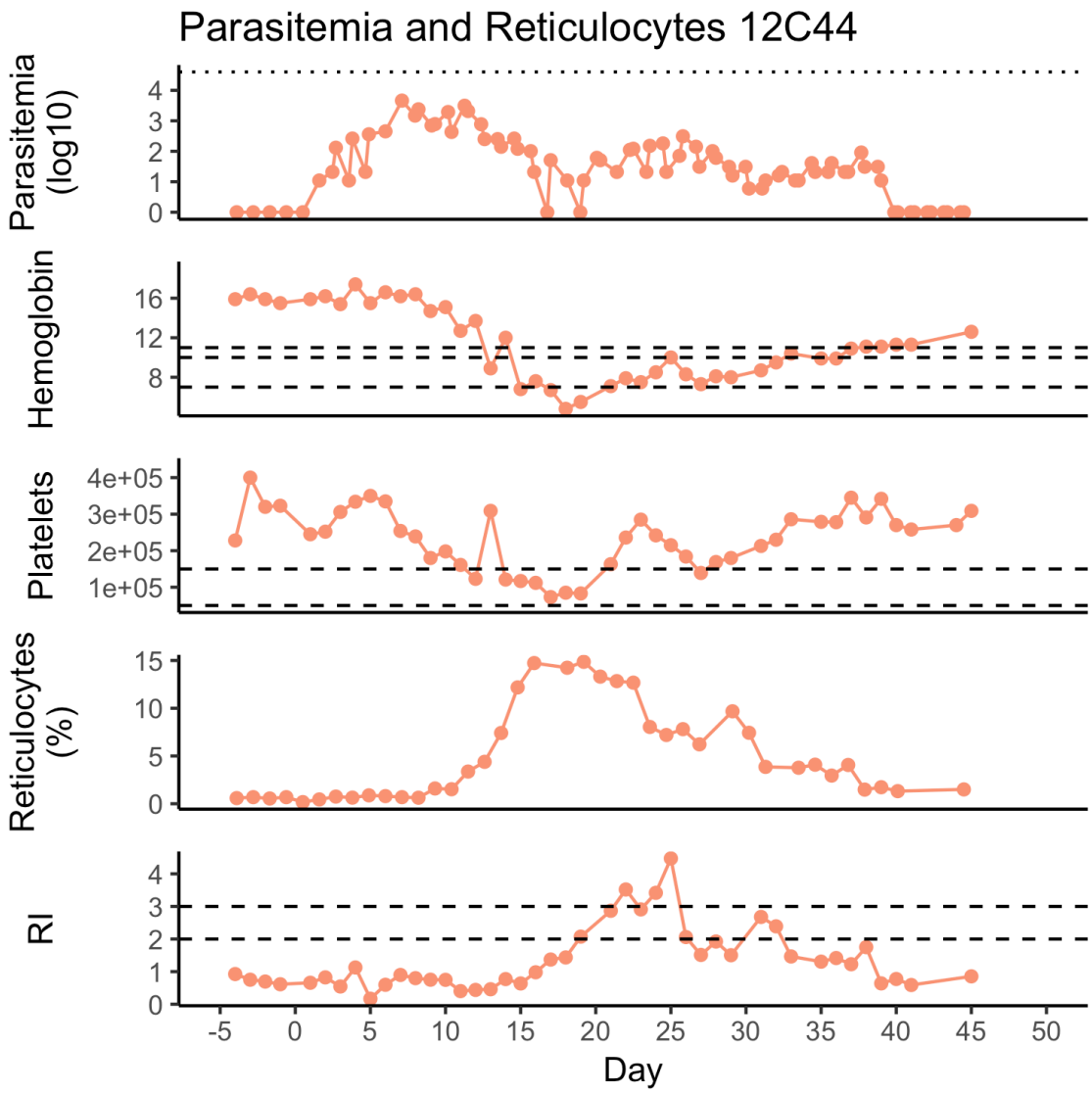

Figure 6.27 Parasitemia and select hematological parameters for 12C44. Plot showing longitudinal parasitemia (first panel), hemoglobin (second panel), platelets (third panel), reticulocytes (fourth panel), and reticulocyte production index, or RI (fifth panel) plots. Lines denoting the equivalent of 1% parasitemia (50,000 parasites/μL), mild, moderate, and severe anemia (hemoglobin of 12, 10, and 8 g/dL, respectively), mild and moderate thrombocytopenia (150,000 and 50,000 platelets/ μL), and reticulocyte response (2, and 3 for sufficient response, and sufficient response with lysis, respectively) are given.

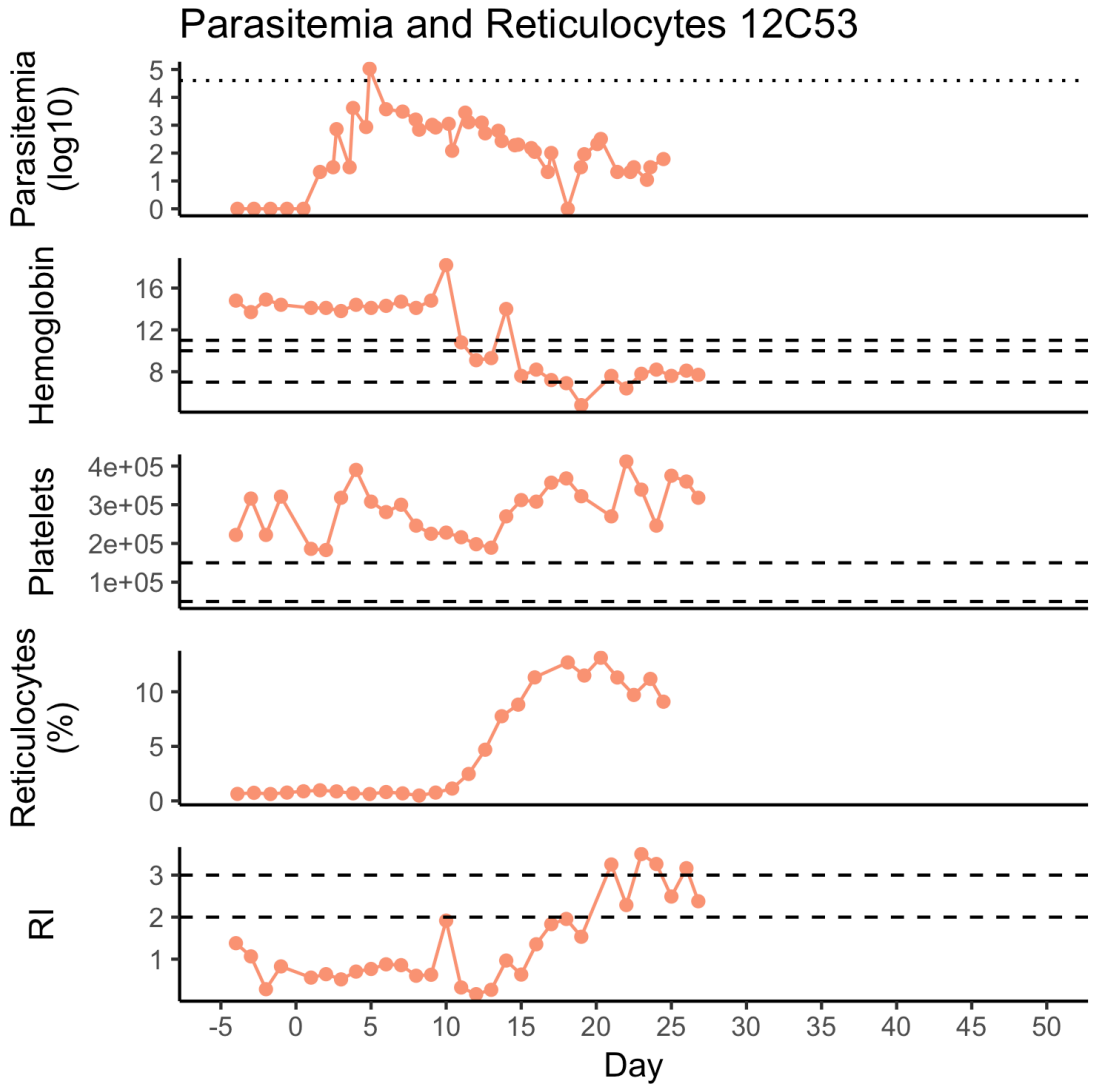

Figure 6.28 Parasitemia and select hematological parameters for 12C53. Plot showing longitudinal parasitemia (first panel), hemoglobin (second panel), platelets (third panel), reticulocytes (fourth panel), and reticulocyte production index, or RI (fifth panel) plots. Lines denoting the equivalent of 1% parasitemia (50,000 parasites/μL), mild, moderate, and severe anemia (hemoglobin of 12, 10, and 8 g/dL, respectively), mild and moderate thrombocytopenia (150,000 and 50,000 platelets/ μL), and reticulocyte response (2, and 3 for sufficient response, and sufficient response with lysis, respectively) are given.

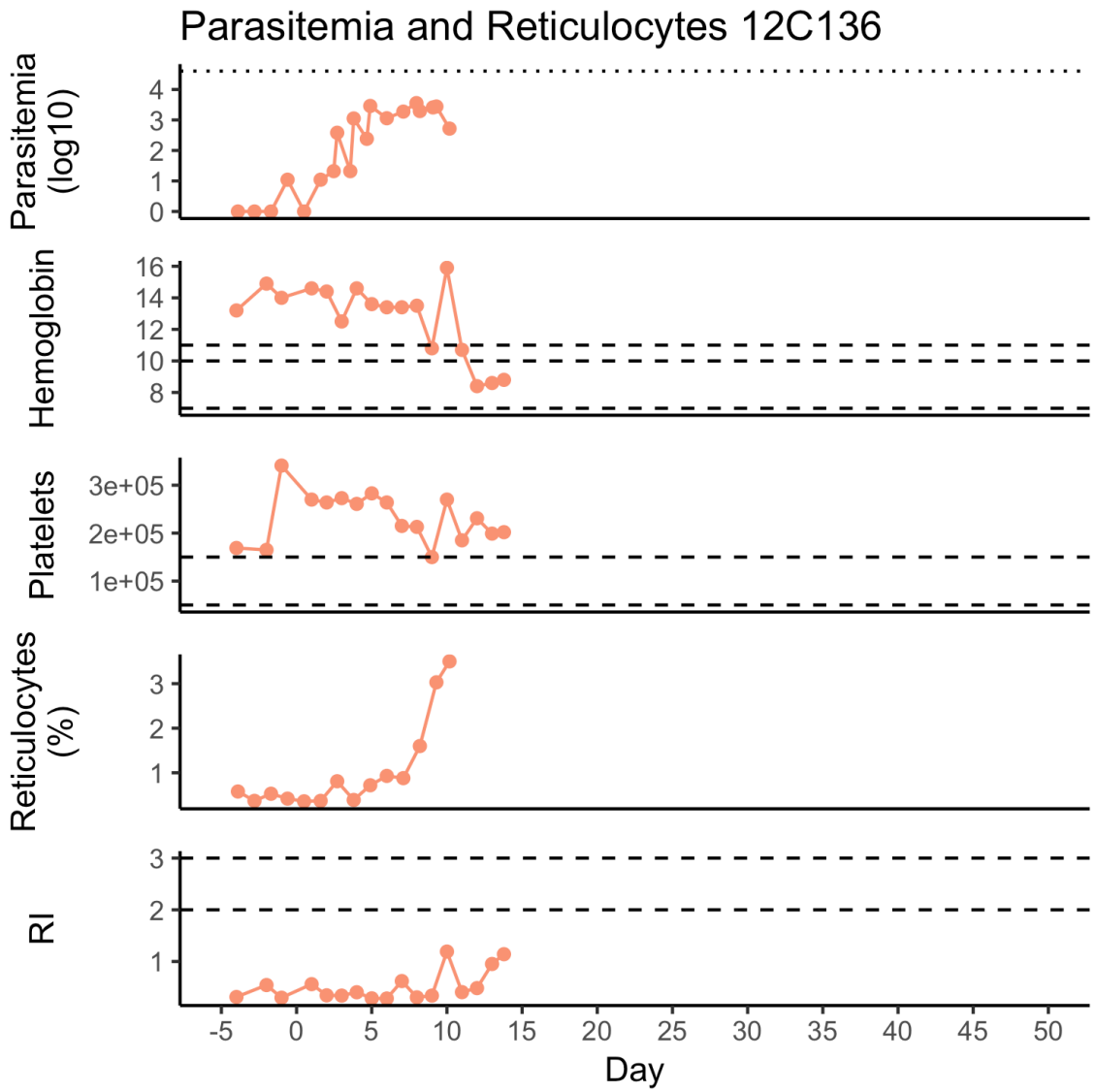

Figure 6.29 Parasitemia and select hematological parameters for 12C136. Plot showing longitudinal parasitemia (first panel), hemoglobin (second panel), platelets (third panel), reticulocytes (fourth panel), and reticulocyte production index, or RI (fifth panel) plots. Lines denoting the equivalent of 1% parasitemia (50,000 parasites/μL), mild, moderate, and severe anemia (hemoglobin of 12, 10, and 8 g/dL, respectively), mild and moderate thrombocytopenia (150,000 and 50,000 platelets/ μL), and reticulocyte response (2, and 3 for sufficient response, and sufficient response with lysis, respectively) are given.

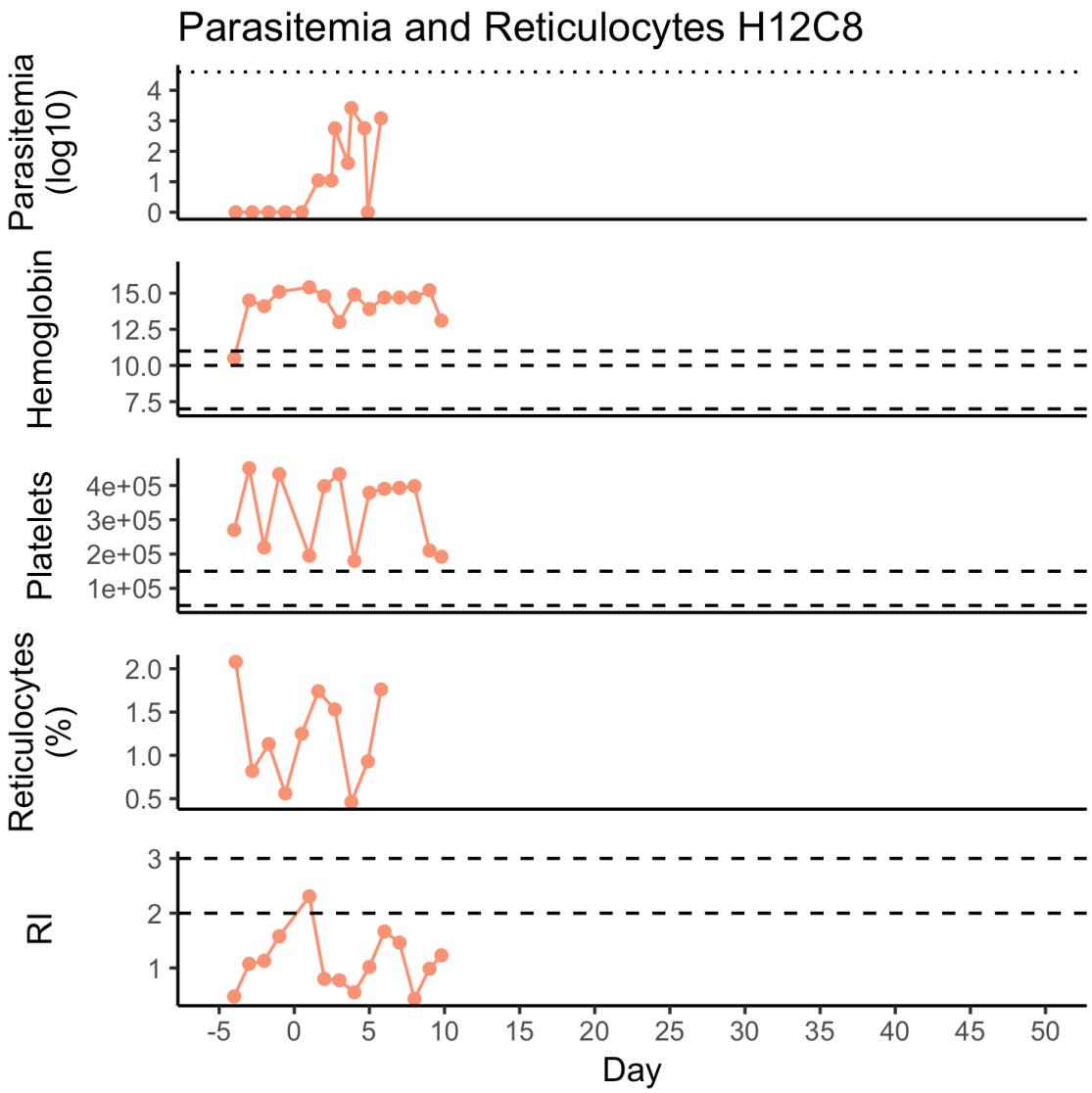

Figure 6.30 Parasitemia and select hematological parameters for H12C8. Plot showing longitudinal parasitemia (first panel), hemoglobin (second panel), platelets (third panel), reticulocytes (fourth panel), and reticulocyte production index, or RI (fifth panel) plots. Lines denoting the equivalent of 1% parasitemia (50,000 parasites/μL), mild, moderate, and severe anemia (hemoglobin of 12, 10, and 8 g/dL, respectively), mild and moderate thrombocytopenia (150,000 and 50,000 platelets/ μL), and reticulocyte response (2, and 3 for sufficient response, and sufficient response with lysis, respectively) are given.

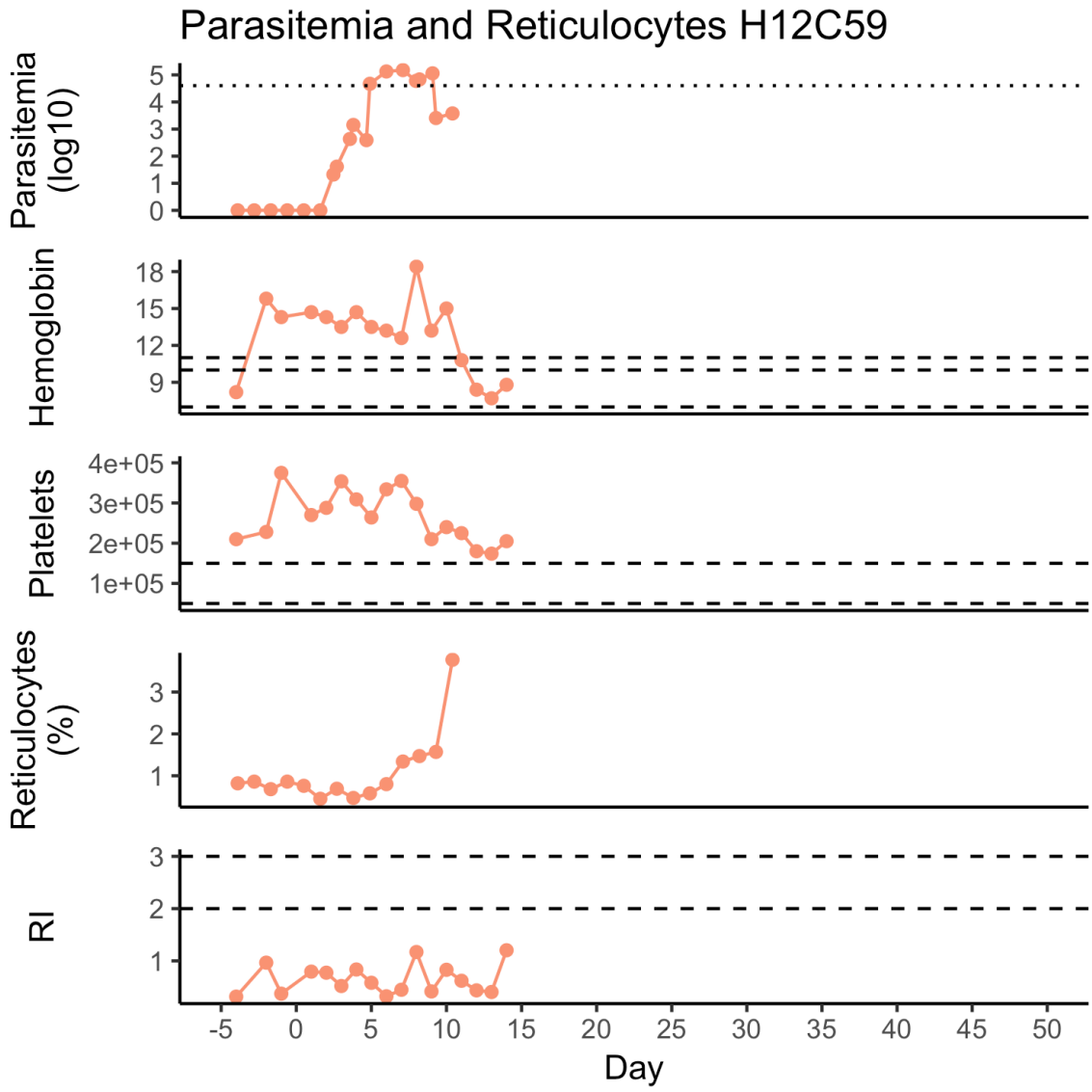

Figure 6.31 Parasitemia and select hematological parameters for H12C59. Plot showing longitudinal parasitemia (first panel), hemoglobin (second panel), platelets (third panel), reticulocytes (fourth panel), and reticulocyte production index, or RI (fifth panel) plots. Lines denoting the equivalent of 1% parasitemia (50,000 parasites/μL), mild, moderate, and severe anemia (hemoglobin of 12, 10, and 8 g/dL, respectively), mild and moderate thrombocytopenia (150,000 and 50,000 platelets/ μL), and reticulocyte response (2, and 3 for sufficient response, and sufficient response with lysis, respectively) are given.

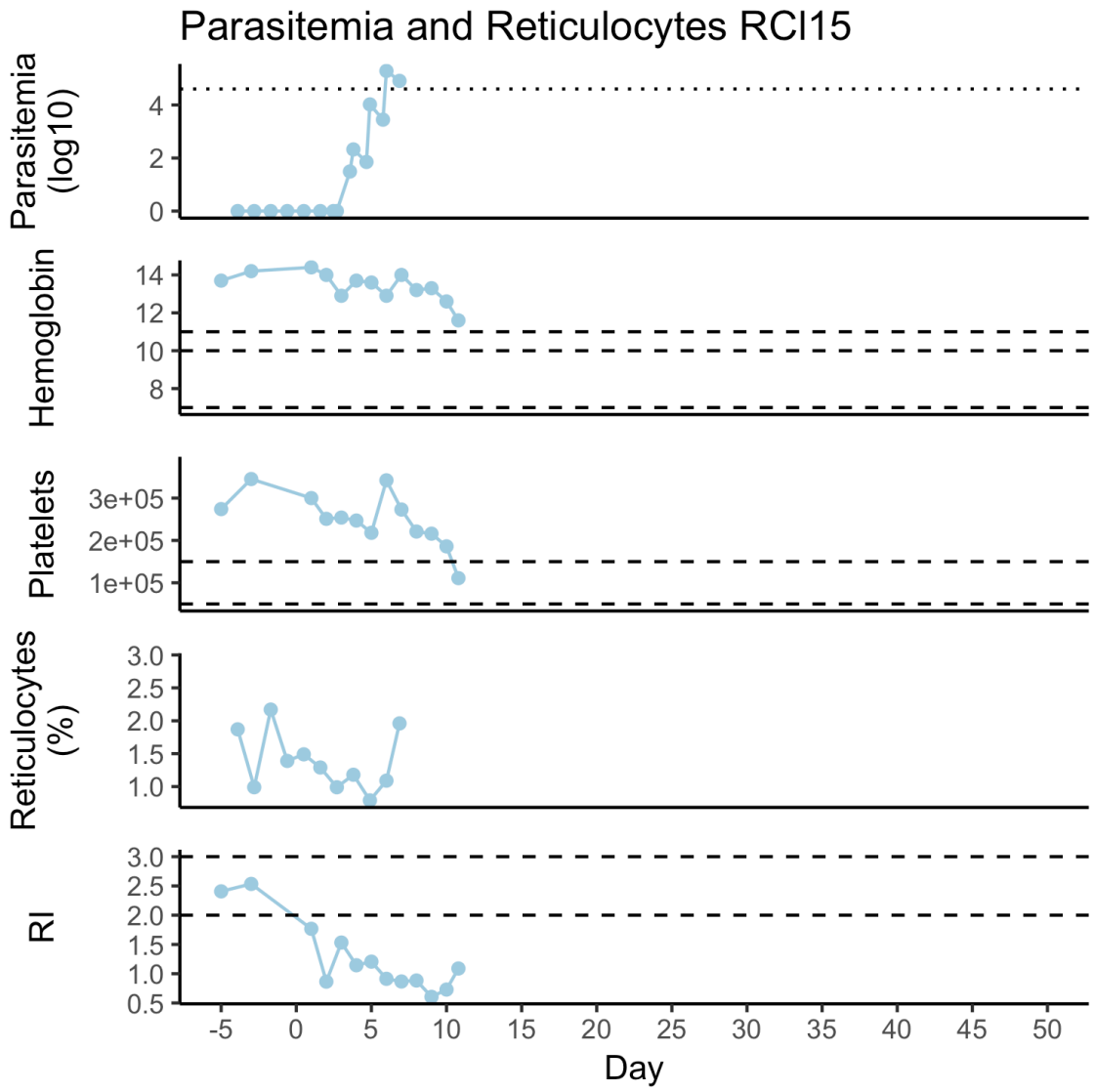

Figure 6.32 Parasitemia and select hematological parameters for RCI15. Plot showing longitudinal parasitemia (first panel), hemoglobin (second panel), platelets (third panel), reticulocytes (fourth panel), and reticulocyte production index, or RI (fifth panel) plots. Lines denoting the equivalent of 1% parasitemia (50,000 parasites/μL), mild, moderate, and severe anemia (hemoglobin of 12, 10, and 8 g/dL, respectively), mild and moderate thrombocytopenia (150,000 and 50,000 platelets/ μL), and reticulocyte response (2, and 3 for sufficient response, and sufficient response with lysis, respectively) are given.

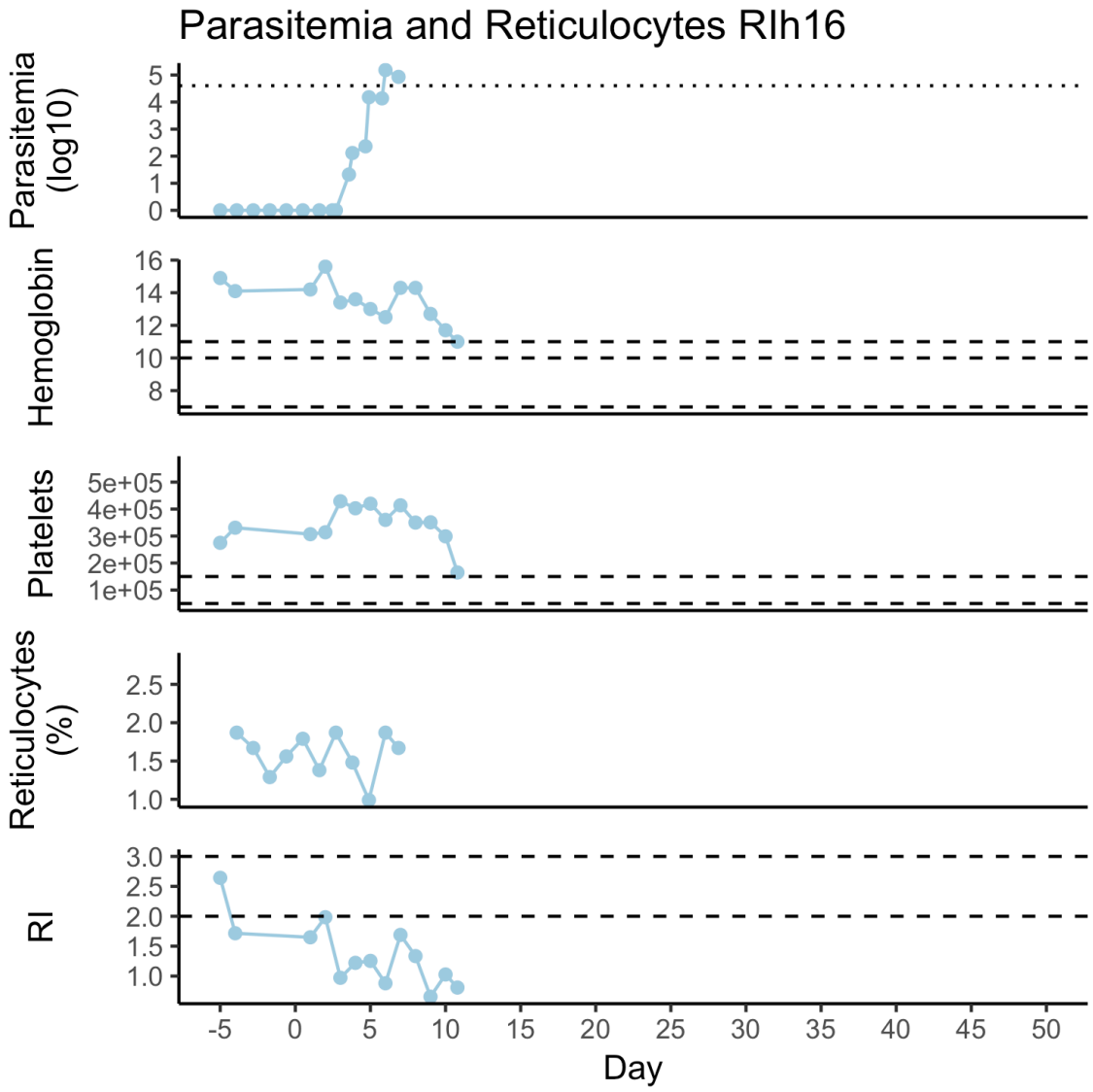

Figure 6.33 Parasitemia and select hematological parameters for RIh16. Plot showing longitudinal parasitemia (first panel), hemoglobin (second panel), platelets (third panel), reticulocytes (fourth panel), and reticulocyte production index, or RI (fifth panel) plots. Lines denoting the equivalent of 1% parasitemia (50,000 parasites/μL), mild, moderate, and severe anemia (hemoglobin of 12, 10, and 8 g/dL, respectively), mild and moderate thrombocytopenia (150,000 and 50,000 platelets/ μL), and reticulocyte response (2, and 3 for sufficient response, and sufficient response with lysis, respectively) are given.

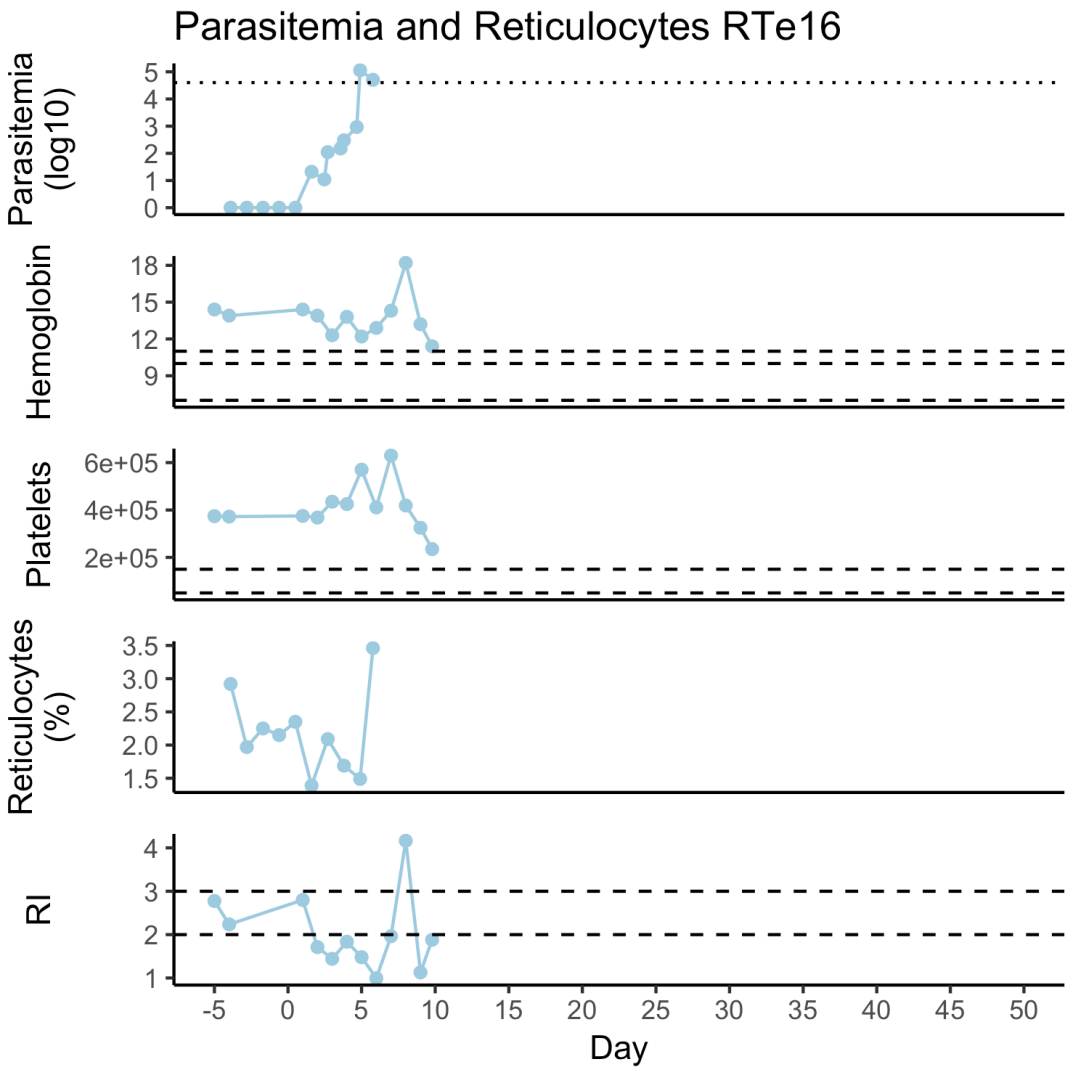

Figure 6.34 Parasitemia and select hematological parameters for RTe16. Plot showing longitudinal parasitemia (first panel), hemoglobin (second panel), platelets (third panel), reticulocytes (fourth panel), and reticulocyte production index, or RI (fifth panel) plots. Lines denoting the equivalent of 1% parasitemia (50,000 parasites/μL), mild, moderate, and severe anemia (hemoglobin of 12, 10, and 8 g/dL, respectively), mild and moderate thrombocytopenia (150,000 and 50,000 platelets/ μL), and reticulocyte response (2, and 3 for sufficient response, and sufficient response with lysis, respectively) are given.

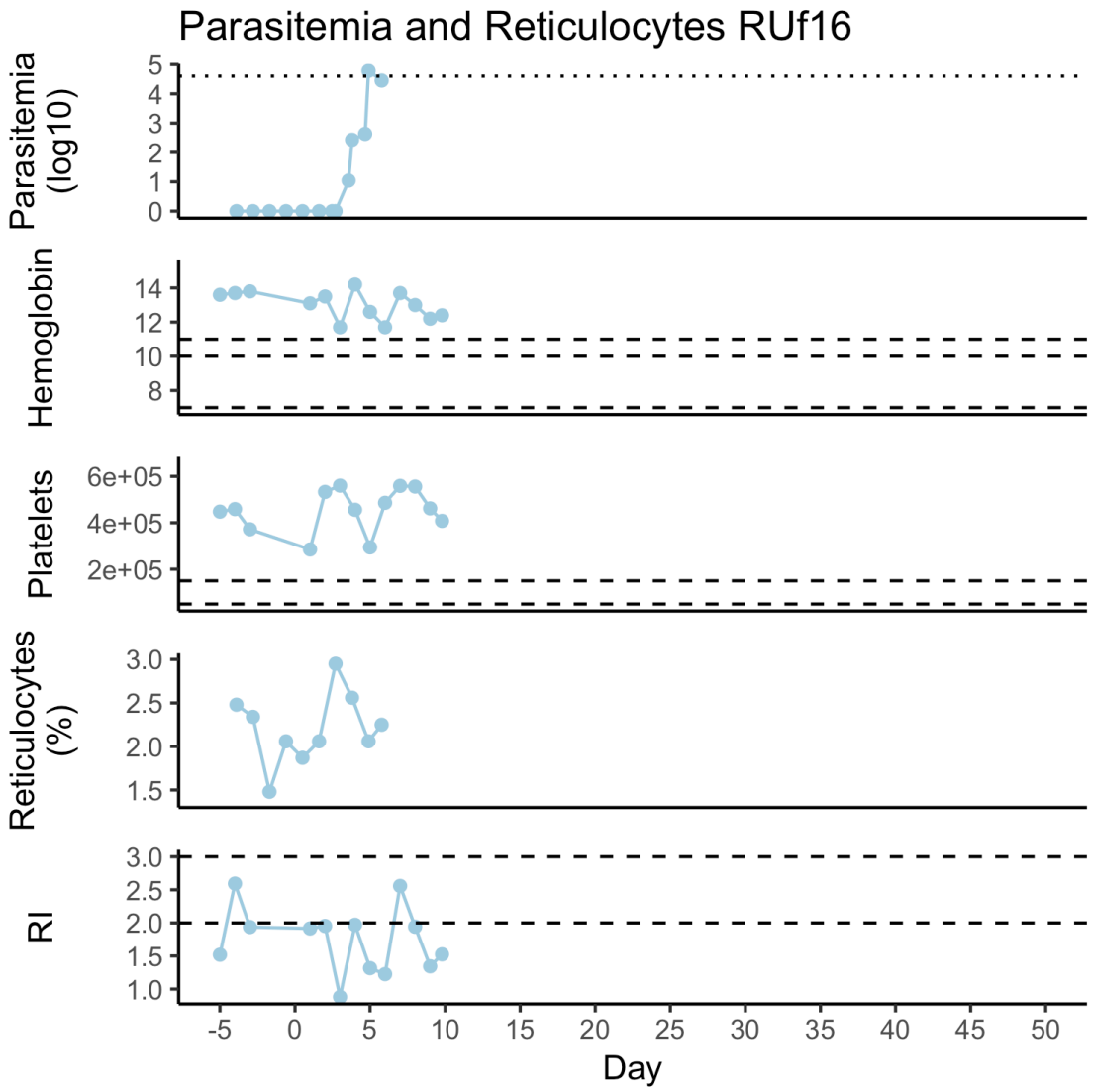

Figure 6.35 Parasitemia and select hematological parameters for RUf16. Plot showing longitudinal parasitemia (first panel), hemoglobin (second panel), platelets (third panel), reticulocytes (fourth panel), and reticulocyte production index, or RI (fifth panel) plots. Lines denoting the equivalent of 1% parasitemia (50,000 parasites/μL), mild, moderate, and severe anemia (hemoglobin of 12, 10, and 8 g/dL, respectively), mild and moderate thrombocytopenia (150,000 and 50,000 platelets/ μL), and reticulocyte response (2, and 3 for sufficient response, and sufficient response with lysis, respectively) are given.

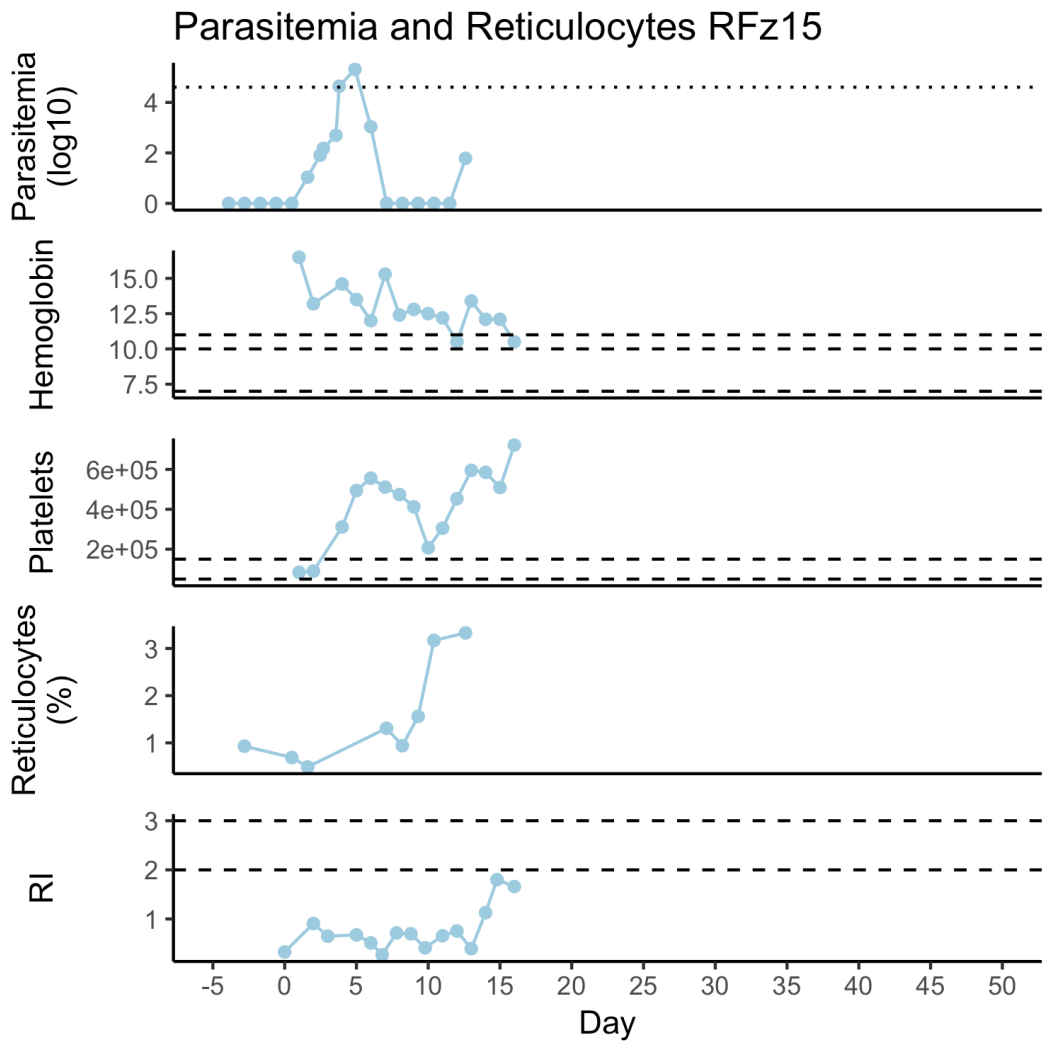

Figure 6.36 Parasitemia and select hematological parameters for RFz15. Plot showing longitudinal parasitemia (first panel), hemoglobin (second panel), platelets (third panel), reticulocytes (fourth panel), and reticulocyte production index, or RI (fifth panel) plots. Lines denoting the equivalent of 1% parasitemia (50,000 parasites/μL), mild, moderate, and severe anemia (hemoglobin of 12, 10, and 8 g/dL, respectively), mild and moderate thrombocytopenia (150,000 and 50,000 platelets/ μL), and reticulocyte response (2, and 3 for sufficient response, and sufficient response with lysis, respectively) are given.

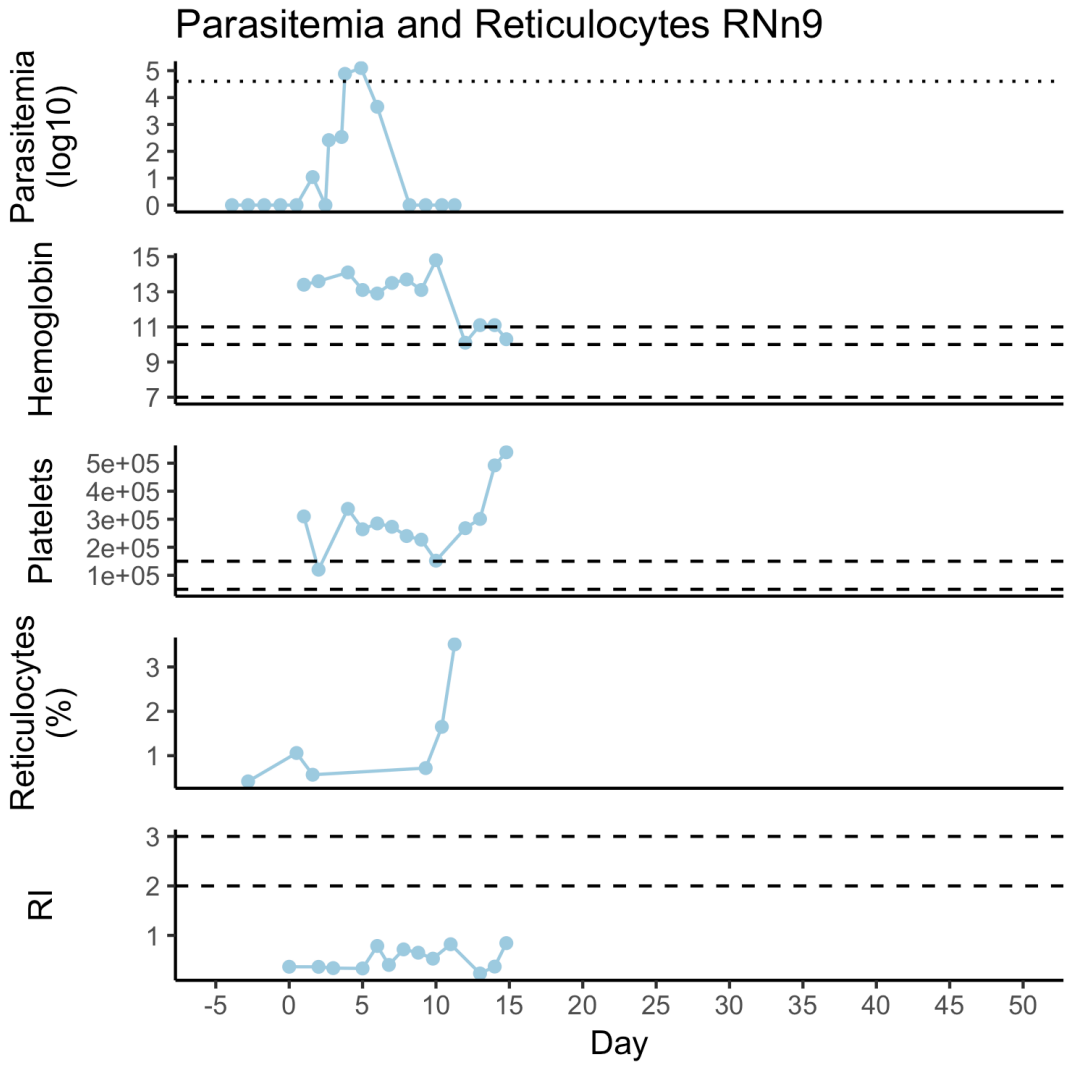

Figure 6.37 Parasitemia and select hematological parameters for RNn9. Plot showing longitudinal parasitemia (first panel), hemoglobin (second panel), platelets (third panel), reticulocytes (fourth panel), and reticulocyte production index, or RI (fifth panel) plots. Lines denoting the equivalent of 1% parasitemia (50,000 parasites/μL), mild, moderate, and severe anemia (hemoglobin of 12, 10, and 8 g/dL, respectively), mild and moderate thrombocytopenia (150,000 and 50,000 platelets/ μL), and reticulocyte response (2, and 3 for sufficient response, and sufficient response with lysis, respectively) are given.

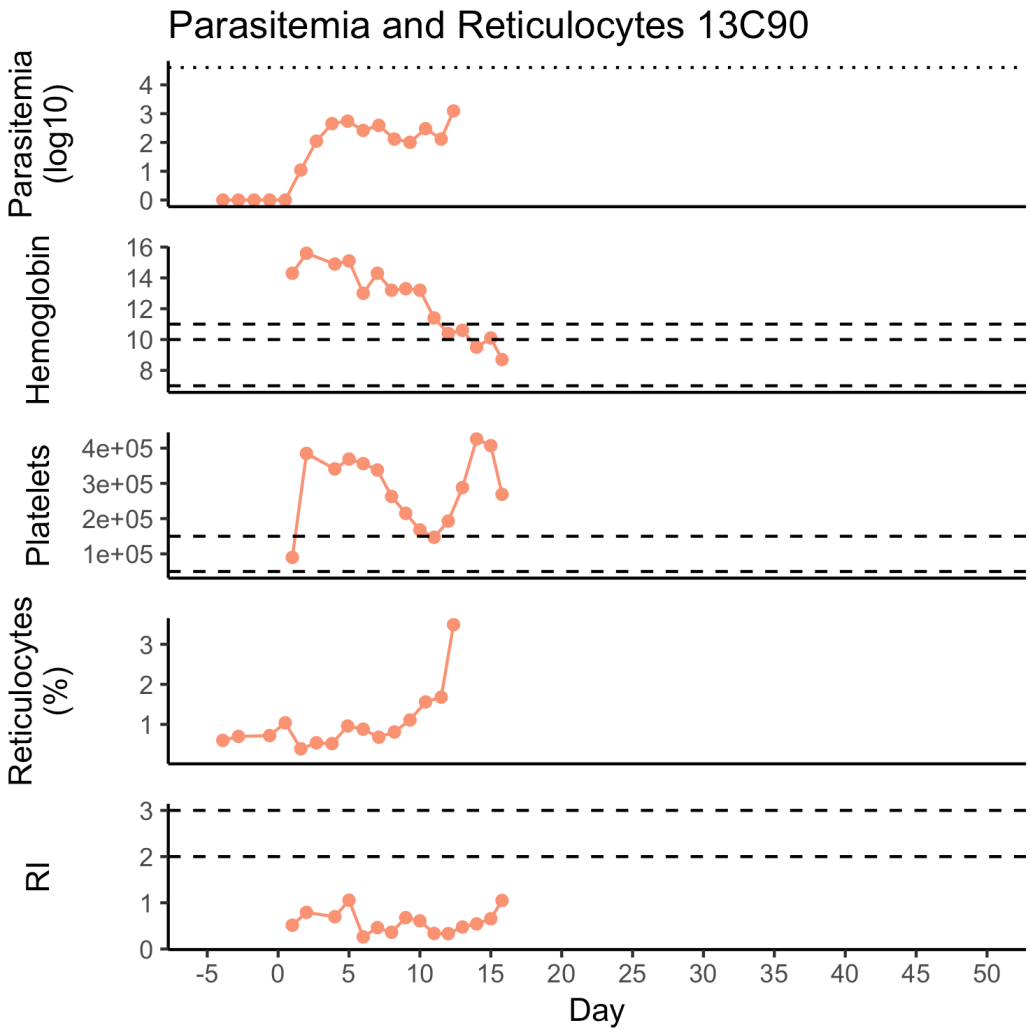

Figure 6.38 Parasitemia and select hematological parameters for 13C90. Plot showing longitudinal parasitemia (first panel), hemoglobin (second panel), platelets (third panel), reticulocytes (fourth panel), and reticulocyte production index, or RI (fifth panel) plots. Lines denoting the equivalent of 1% parasitemia (50,000 parasites/μL), mild, moderate, and severe anemia (hemoglobin of 12, 10, and 8 g/dL, respectively), mild and moderate thrombocytopenia (150,000 and 50,000 platelets/ μL), and reticulocyte response (2, and 3 for sufficient response, and sufficient response with lysis, respectively) are given.

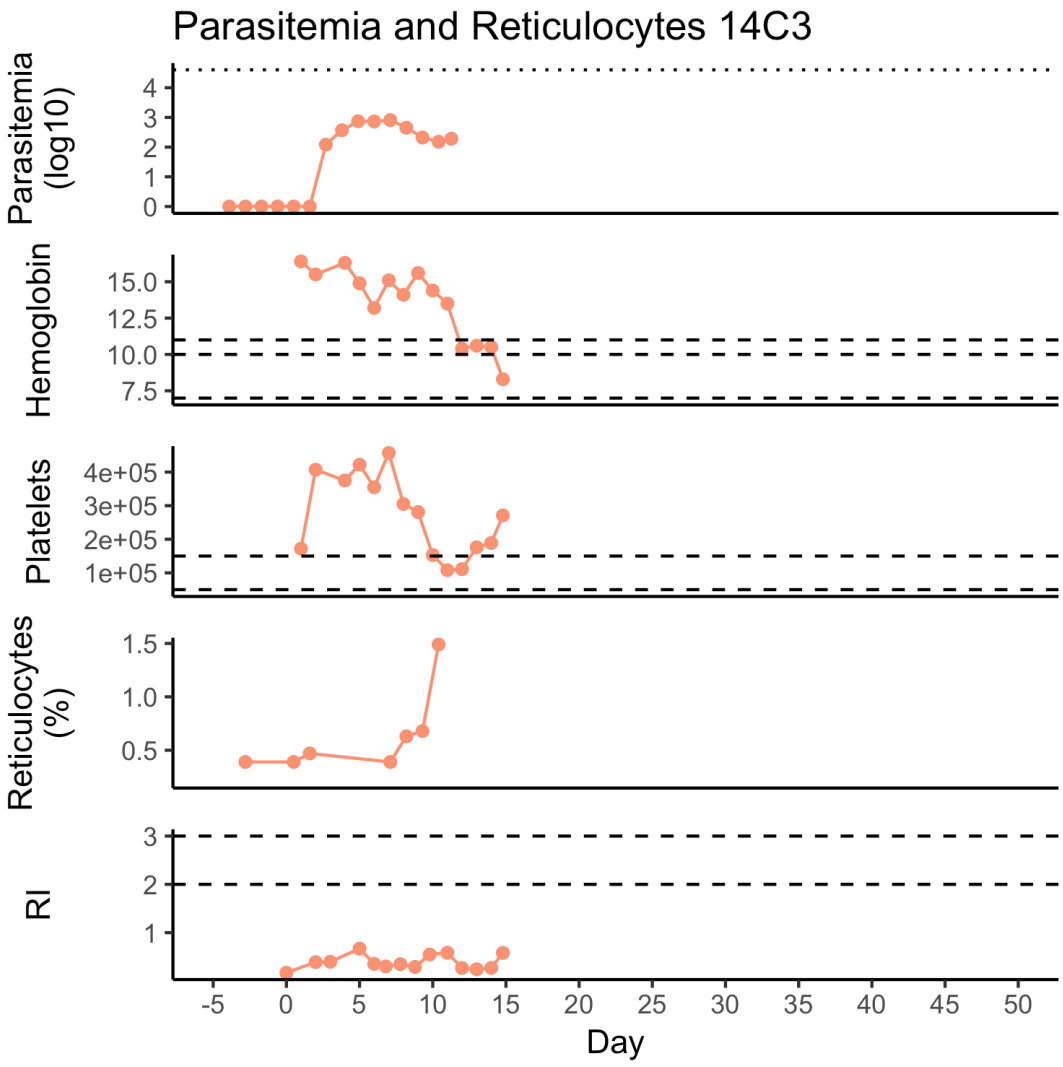

Figure 6.39 Parasitemia and select hematological parameters for 14C3. Plot showing longitudinal parasitemia (first panel), hemoglobin (second panel), platelets (third panel), reticulocytes (fourth panel), and reticulocyte production index, or RI (fifth panel) plots. Lines denoting the equivalent of 1% parasitemia (50,000 parasites/μL), mild, moderate, and severe anemia (hemoglobin of 12, 10, and 8 g/dL, respectively), mild and moderate thrombocytopenia (150,000 and 50,000 platelets/ μL), and reticulocyte response (2, and 3 for sufficient response, and sufficient response with lysis, respectively) are given.

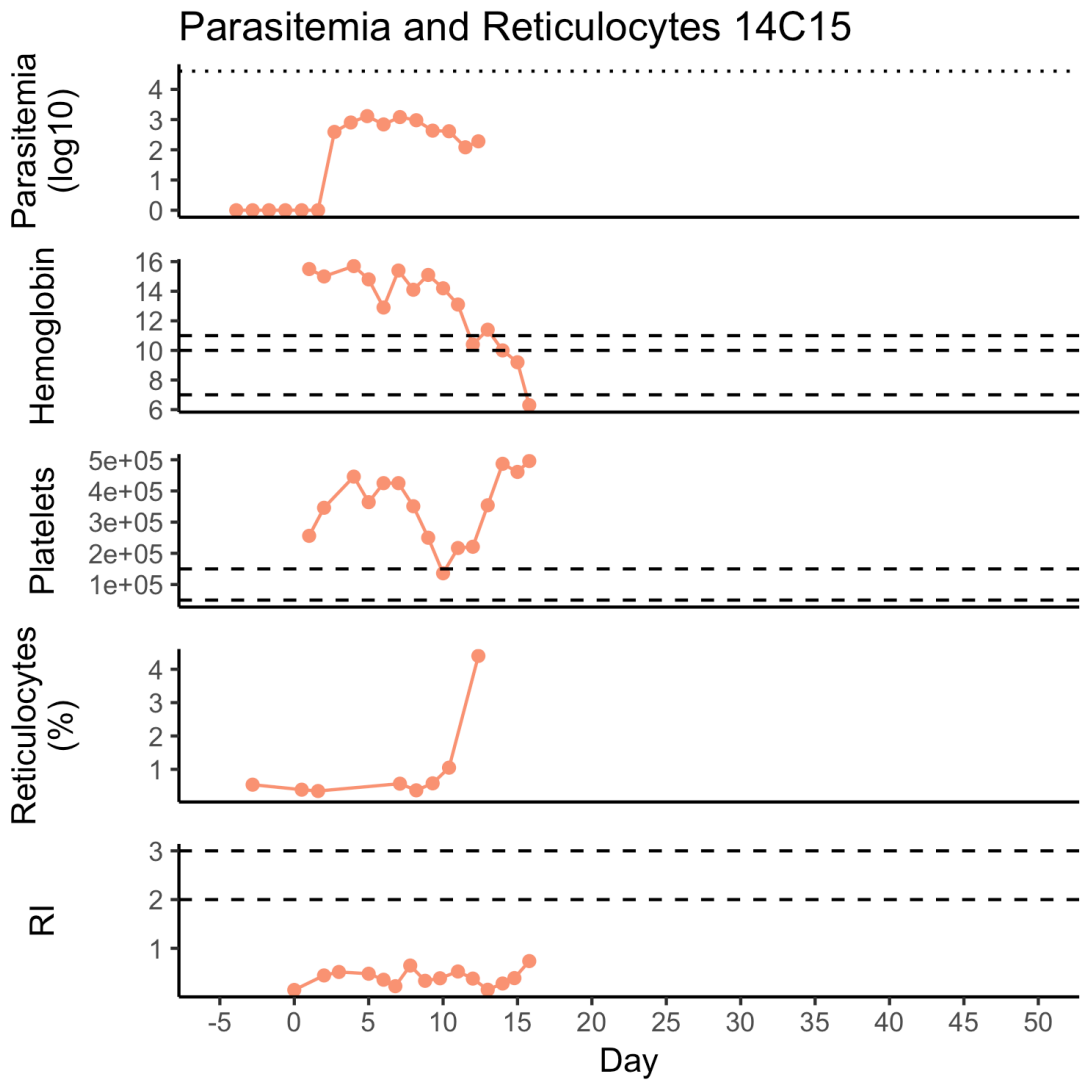

Figure 6.40 Parasitemia and select hematological parameters for 14C15. Plot showing longitudinal parasitemia (first panel), hemoglobin (second panel), platelets (third panel), reticulocytes (fourth panel), and reticulocyte production index, or RI (fifth panel) plots. Lines denoting the equivalent of 1% parasitemia (50,000 parasites/μL), mild, moderate, and severe anemia (hemoglobin of 12, 10, and 8 g/dL, respectively), mild and moderate thrombocytopenia (150,000 and 50,000 platelets/ μL), and reticulocyte response (2, and 3 for sufficient response, and sufficient response with lysis, respectively) are given.

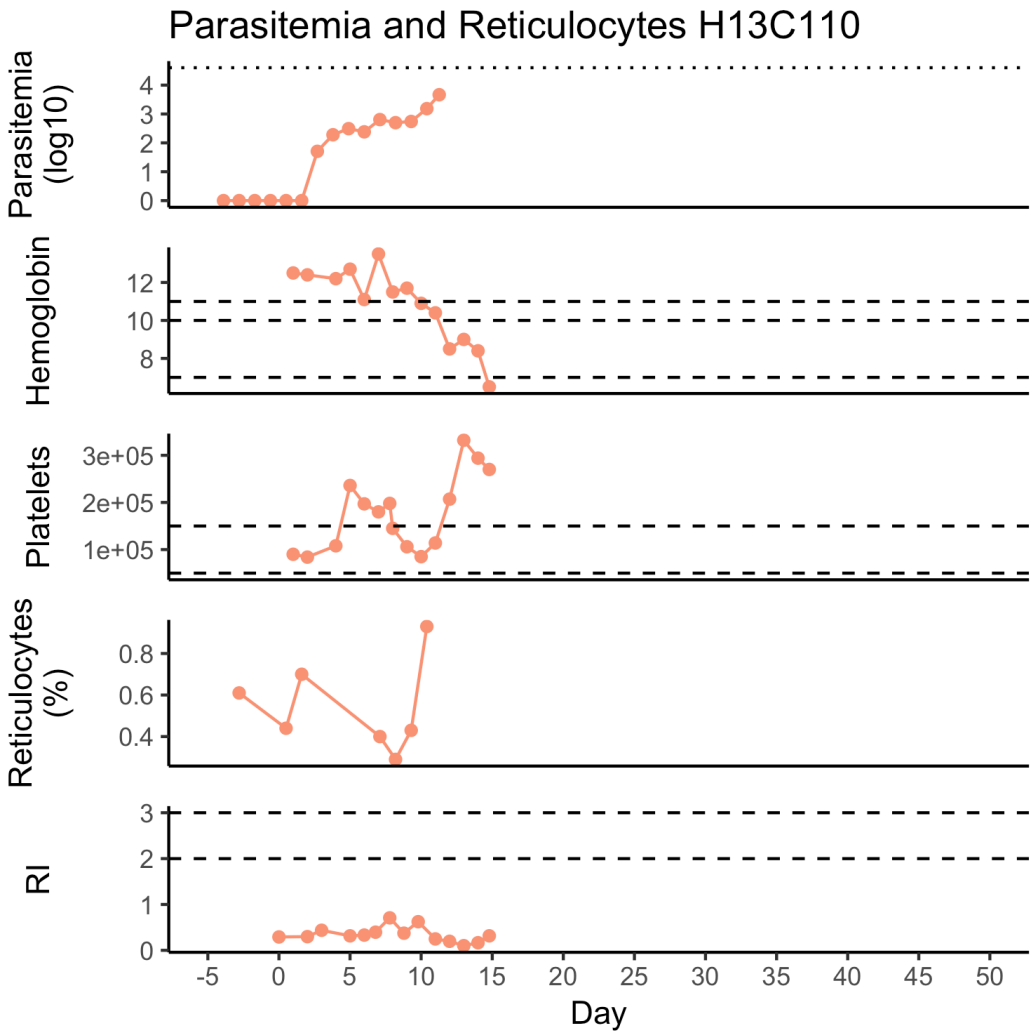

Figure 6.41 Parasitemia and select hematological parameters for H13C110. Plot showing longitudinal parasitemia (first panel), hemoglobin (second panel), platelets (third panel), reticulocytes (fourth panel), and reticulocyte production index, or RI (fifth panel) plots. Lines denoting the equivalent of 1% parasitemia (50,000 parasites/μL), mild, moderate, and severe anemia (hemoglobin of 12, 10, and 8 g/dL, respectively), mild and moderate thrombocytopenia (150,000 and 50,000 platelets/ μL), and reticulocyte response (2, and 3 for sufficient response, and sufficient response with lysis, respectively) are given.

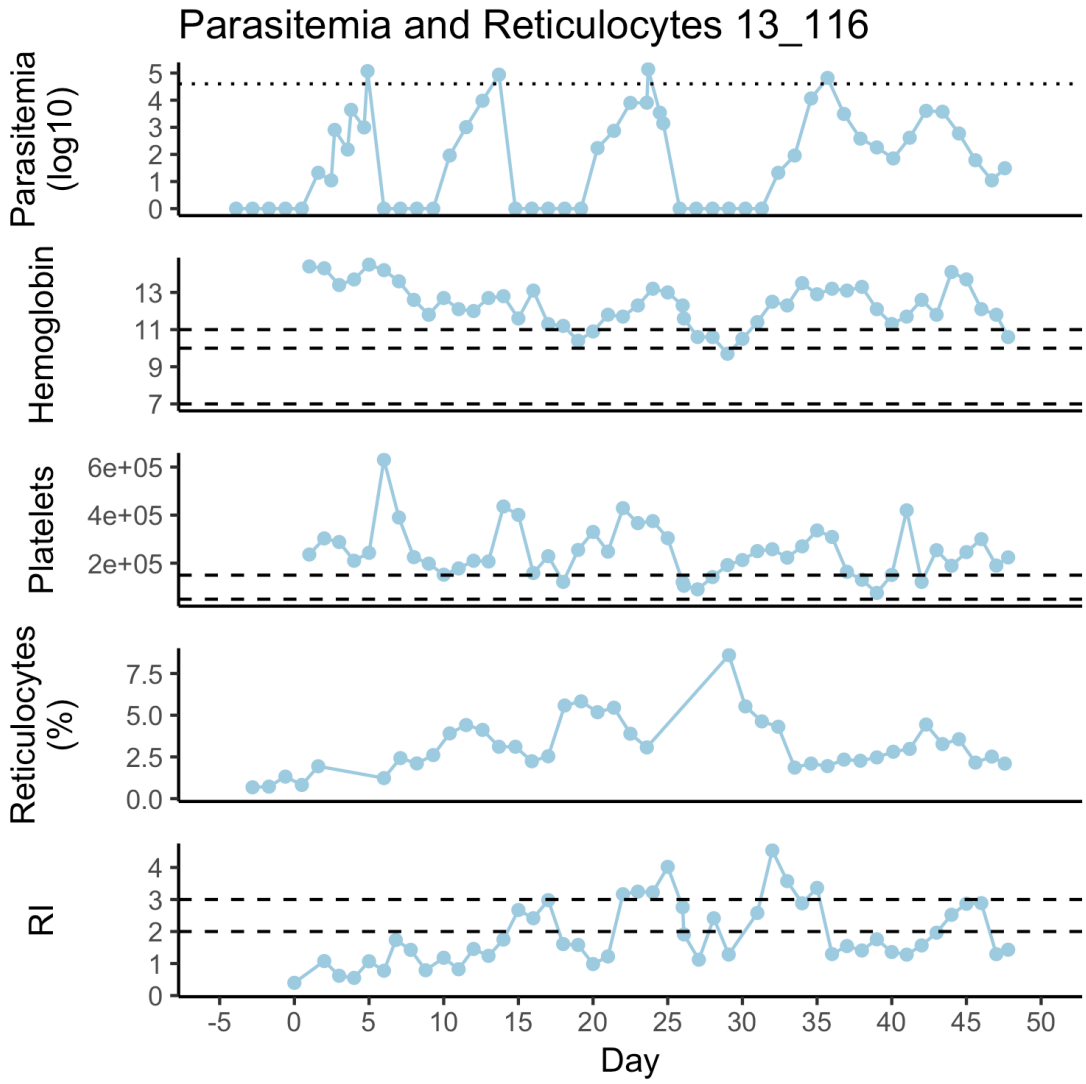

Figure 6.42 Parasitemia and select hematological parameters for 13_116. Plot showing longitudinal parasitemia (first panel), hemoglobin (second panel), platelets (third panel), reticulocytes (fourth panel), and reticulocyte production index, or RI (fifth panel) plots. Lines denoting the equivalent of 1% parasitemia (50,000 parasites/μL), mild, moderate, and severe anemia (hemoglobin of 12, 10, and 8 g/dL, respectively), mild and moderate thrombocytopenia (150,000 and 50,000 platelets/ μL), and reticulocyte response (2, and 3 for sufficient response, and sufficient response with lysis, respectively) are given.

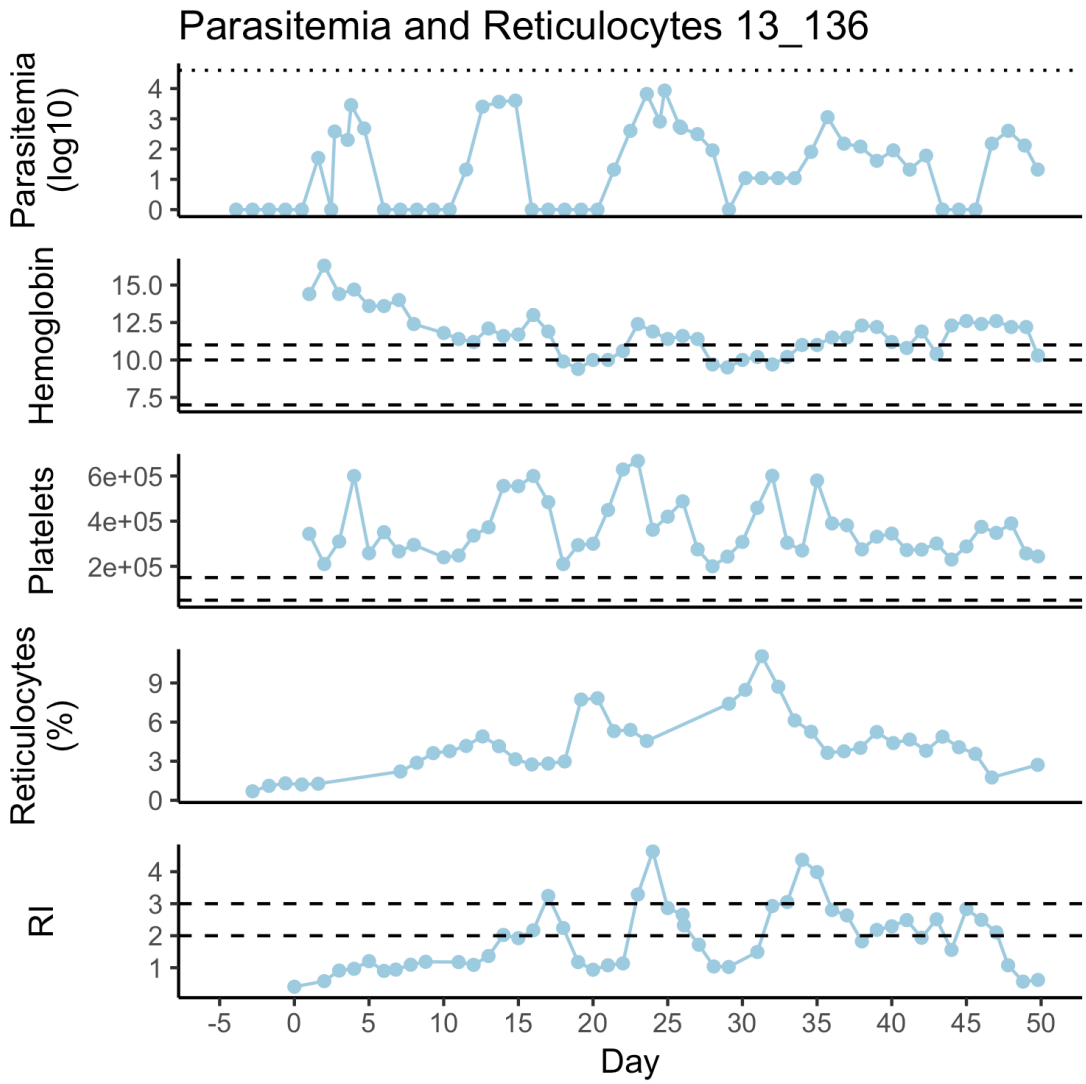

Figure 6.43 Parasitemia and select hematological parameters for 13_136. Plot showing longitudinal parasitemia (first panel), hemoglobin (second panel), platelets (third panel), reticulocytes (fourth panel), and reticulocyte production index, or RI (fifth panel) plots. Lines denoting the equivalent of 1% parasitemia (50,000 parasites/μL), mild, moderate, and severe anemia (hemoglobin of 12, 10, and 8 g/dL, respectively), mild and moderate thrombocytopenia (150,000 and 50,000 platelets/ μL), and reticulocyte response (2, and 3 for sufficient response, and sufficient response with lysis, respectively) are given.

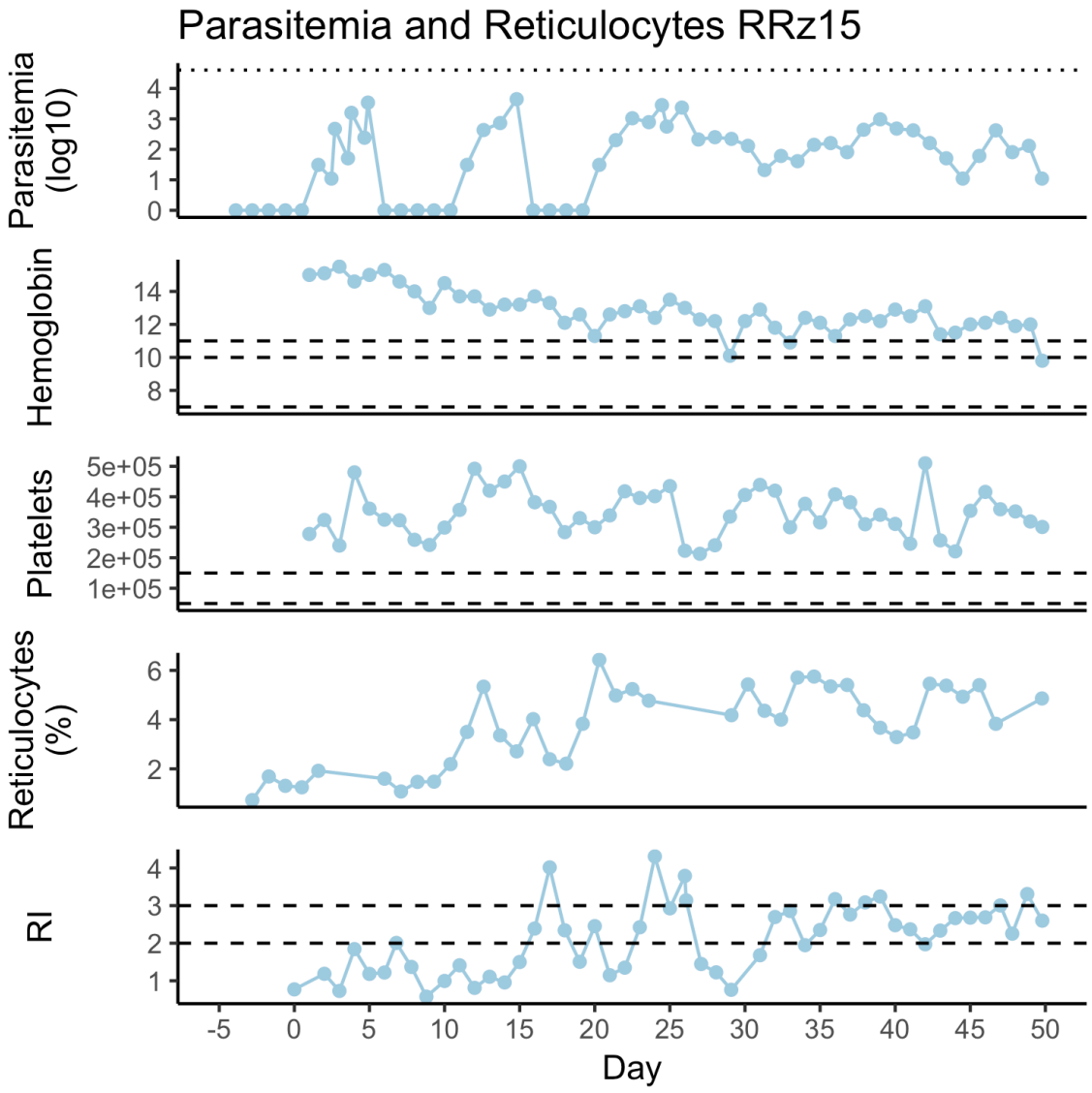

Figure 6.44 Parasitemia and select hematological parameters for RRz15. Plot showing longitudinal parasitemia (first panel), hemoglobin (second panel), platelets (third panel), reticulocytes (fourth panel), and reticulocyte production index, or RI (fifth panel) plots. Lines denoting the equivalent of 1% parasitemia (50,000 parasites/μL), mild, moderate, and severe anemia (hemoglobin of 12, 10, and 8 g/dL, respectively), mild and moderate thrombocytopenia (150,000 and 50,000 platelets/ μL), and reticulocyte response (2, and 3 for sufficient response, and sufficient response with lysis, respectively) are given.

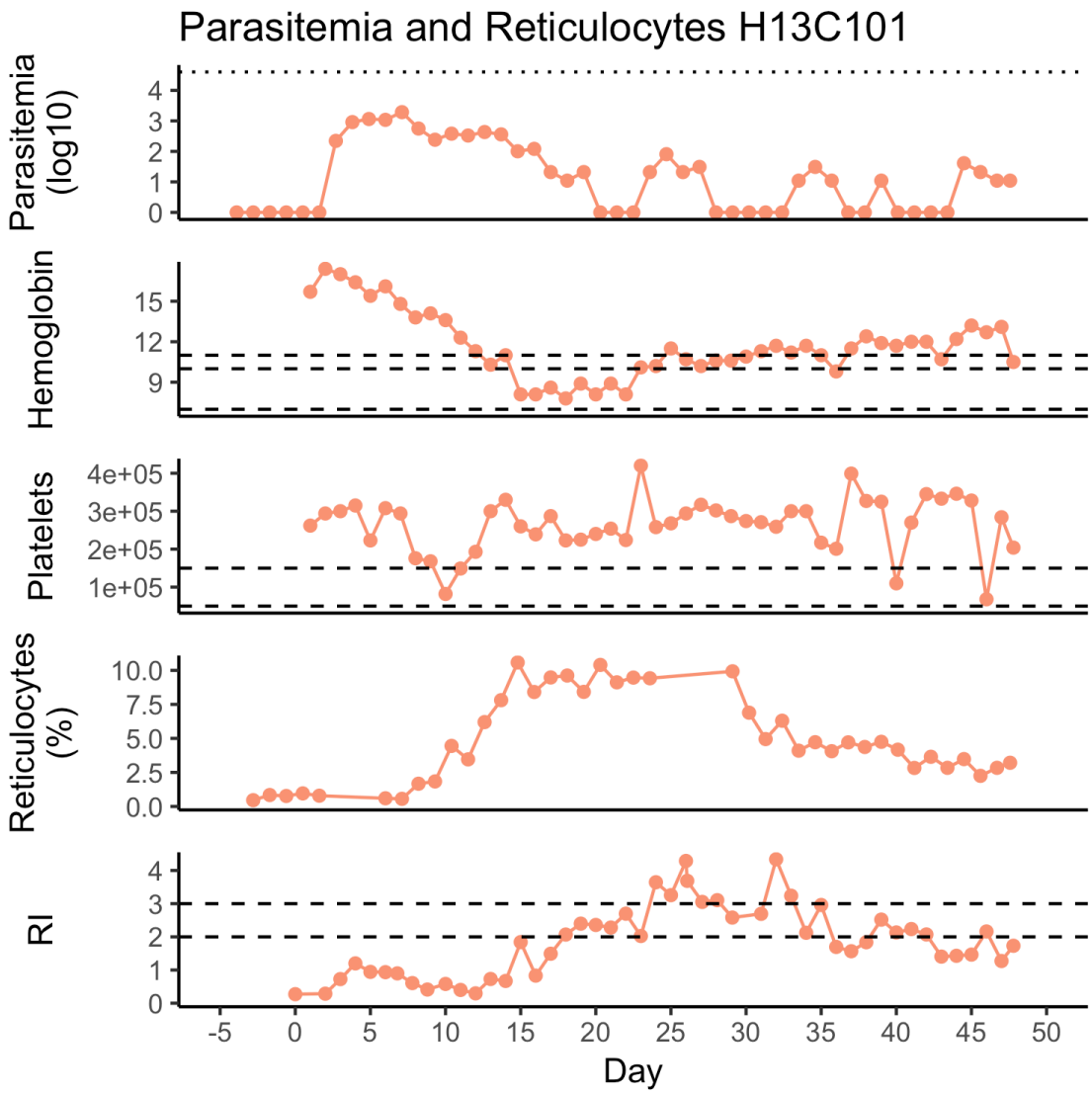

Figure 6.45 Parasitemia and select hematological parameters for H13C101. Plot showing longitudinal parasitemia (first panel), hemoglobin (second panel), platelets (third panel), reticulocytes (fourth panel), and reticulocyte production index, or RI (fifth panel) plots. Lines denoting the equivalent of 1% parasitemia (50,000 parasites/μL), mild, moderate, and severe anemia (hemoglobin of 12, 10, and 8 g/dL, respectively), mild and moderate thrombocytopenia (150,000 and 50,000 platelets/ μL), and reticulocyte response (2, and 3 for sufficient response, and sufficient response with lysis, respectively) are given.

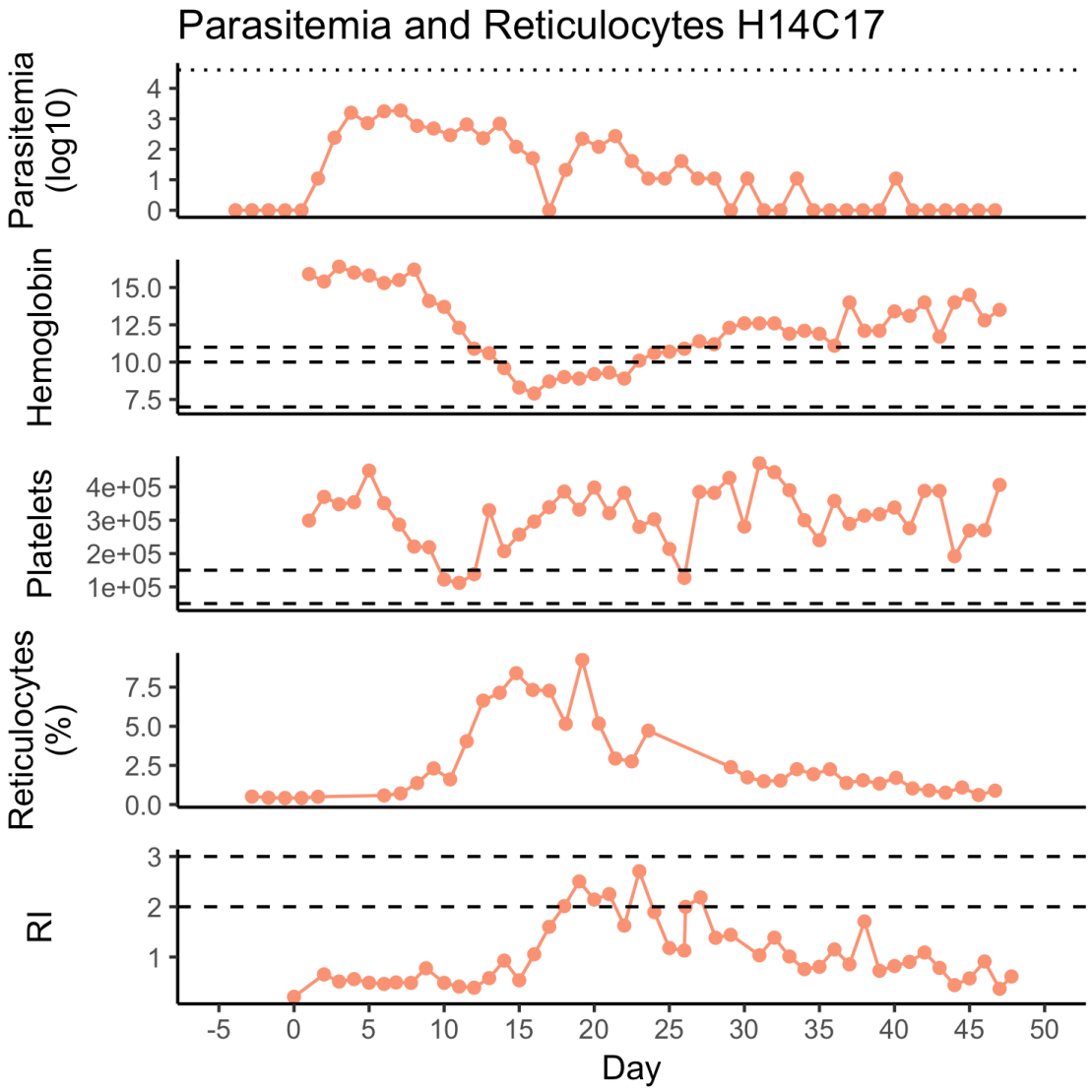

Figure 6.46 Parasitemia and select hematological parameters for H14C17. Plot showing longitudinal parasitemia (first panel), hemoglobin (second panel), platelets (third panel), reticulocytes (fourth panel), and reticulocyte production index, or RI (fifth panel) plots. Lines denoting the equivalent of 1% parasitemia (50,000 parasites/μL), mild, moderate, and severe anemia (hemoglobin of 12, 10, and 8 g/dL, respectively), mild and moderate thrombocytopenia (150,000 and 50,000 platelets/ μL), and reticulocyte response (2, and 3 for sufficient response, and sufficient response with lysis, respectively) are given.

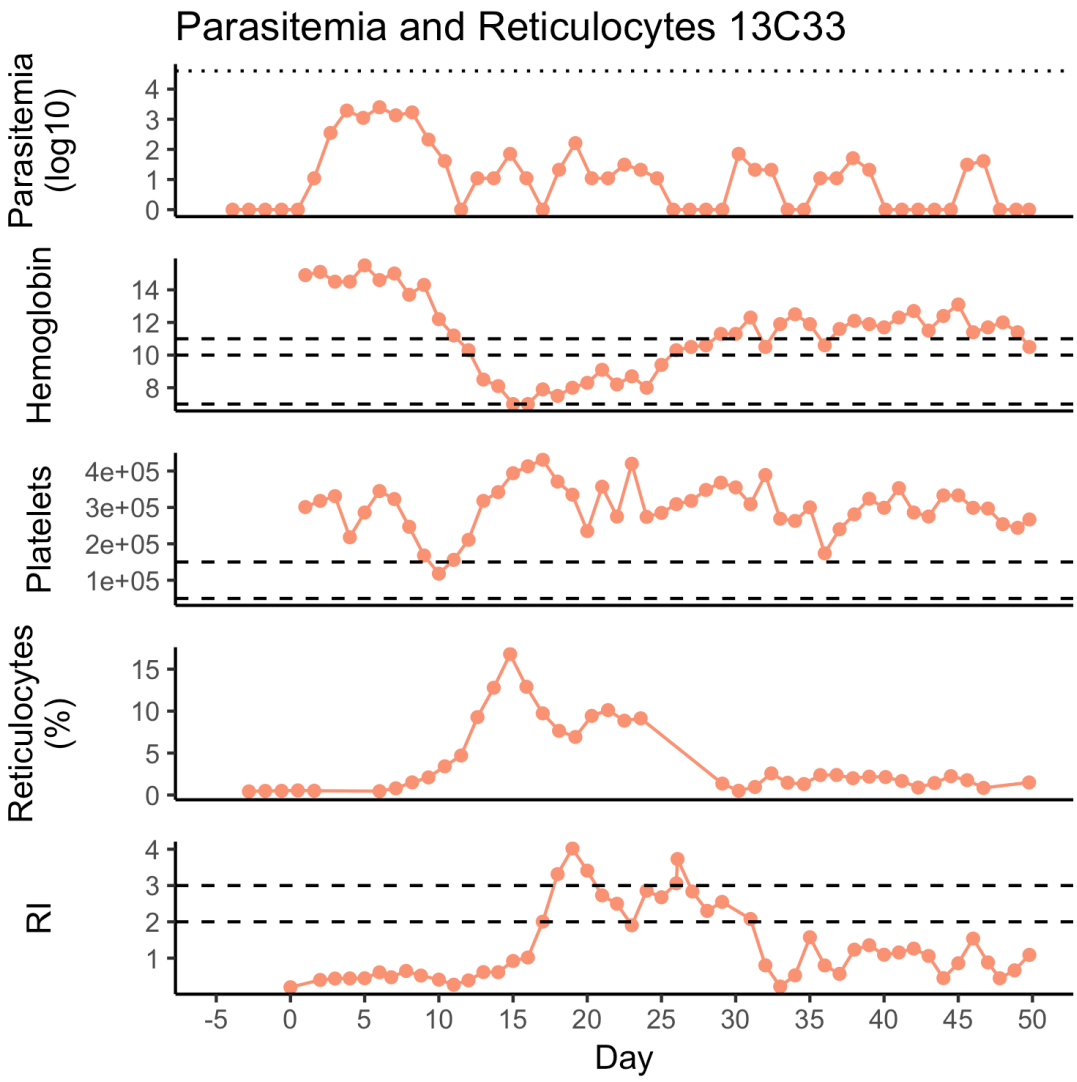

Figure 6.47 Parasitemia and select hematological parameters for 13C33. Plot showing longitudinal parasitemia (first panel), hemoglobin (second panel), platelets (third panel), reticulocytes (fourth panel), and reticulocyte production index, or RI (fifth panel) plots. Lines denoting the equivalent of 1% parasitemia (50,000 parasites/μL), mild, moderate, and severe anemia (hemoglobin of 12, 10, and 8 g/dL, respectively), mild and moderate thrombocytopenia (150,000 and 50,000 platelets/ μL), and reticulocyte response (2, and 3 for sufficient response, and sufficient response with lysis, respectively) are given.

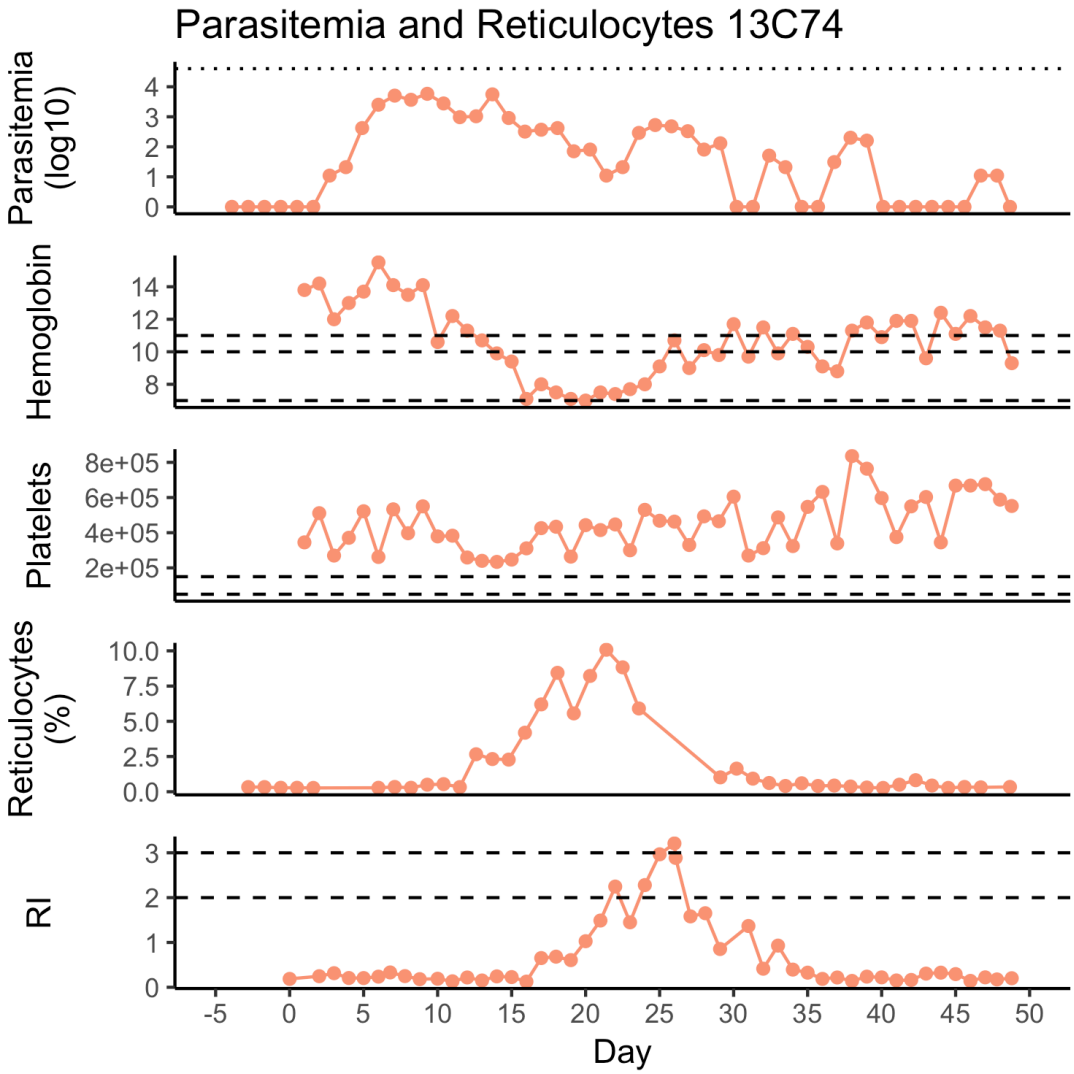

Figure 6.48 Parasitemia and select hematological parameters for 13C74. Plot showing longitudinal parasitemia (first panel), hemoglobin (second panel), platelets (third panel), reticulocytes (fourth panel), and reticulocyte production index, or RI (fifth panel) plots. Lines denoting the equivalent of 1% parasitemia (50,000 parasites/μL), mild, moderate, and severe anemia (hemoglobin of 12, 10, and 8 g/dL, respectively), mild and moderate thrombocytopenia (150,000 and 50,000 platelets/ μL), and reticulocyte response (2, and 3 for sufficient response, and sufficient response with lysis, respectively) are given.

Table 6.9 Summary of histopathology scores for *P. knowlesi*-infected macaques

	Rhesus Monkeys											Kra Monkeys														
Histopathology	RCl15	RIh16	RUf16	RTe16	RKy15	REd16	RNn9	RFz15	RRz15	13_116	13_136	11C131	11C166	12C44	12C53	12C136	H12C8	H12C59	13C90	13C33	14C3	14C15	H13C101	H13C110	H14C17	13C74
Colon																										
Inflammation	1	1	1	1	2	2	1	1	2	1	1	2	0	1	1	1	1	1	1	1	1	1	1	1	1	1
Edema	1	1	0	0	0	0	0	0	1	0	0	0	0	0	0	0	1	0	0	0	0	0	0	0	0	0
Duodenum																										
Inflammation	2	2	2	2	2	2	2	2	2	2	2	2	0	2	1	1	1	2	2	2	2	2	2	2	2	2
Jejunum																										
Inflammation	2	1	2	2	2	1	1	1	1	1	1	1	1	1	1	1	1	1	2	1	1	1	1	1	1	1
Stomach																										
Inflammation	3.5	3	3	3	3	4	2	1	0	2	3	2	2	2	2	0	1	0	1	3	2	0	4	2	0	0
Crypt Inflammation	0	0	0	1	3	0	0	0	0	0	0	0	0	0	0	0	0	0	0	0	0	0	0	0	0	0
Kidney																										
Inflammation	0	0	0	1	1	1	0	0	0	1	1	0	1	0	0	0	0	0	0	0	0	0	0	0	0	0

Hemorrhage	0	0	0	0	0	0	0	0	0	0	0	0	0	1	0	0	0	0	0	0	1	0	0	1	0	0
Tubular Degeneration	2	1	0	1	1	0	0	0	2	2	0	0	0	0	0	0	0	2	0	0	0	0	0	2	1	0
Glomerular Hypercellularity	2	1	1	1	2	2	1	1	2	1	1	1	1	1	1	1	1	1	1	1	1	1	1	1	1	1
Liver																											
Inflammation	2	2	2	2	3	3	2	2	2	2	3	2	2	2	2	2	2	2	2	2	2	2	1	2	2	1
Kupffer Cell Hyperplasia	3	2	2	2	3	3	2	2	3	3	3	2	2	2	2	3	3	2	2	2	2	2	1	2	2	2
Lung																											
Inflammation	0	0	0	0	0	0	0	0	0	0	0	0	0	0	0	0	0	0	0	0	0	0	0	0	1	2
Hemorrhage	0	0	0	3	2	0	0	0	2	1	2	0	0	0	0	0	0	0	1	2	0	0	1	0	0	1
Hyperplasia	1	2	1	0	1	1	1	1	1	1	1	1	0	1	1	0	2	1	1	1	1	1	1	1	1	2
Fibrosis	2	2	2	0	2	2	3	2	3	1	3	2	1	2	1	0	2	2	2	2	2	2	3	2	3	2
Ventricle																											
Inflammation	0	0	0	0	0	0	0	0	0	0	0	2	0	0	1	1	0	0	0	0	0	0	0	0	0	0	0
Edema	0	0	0	0	0	0	0	0	0	0	0	2	0	0	1	0	0	0	0	0	0	0	0	0	0	0	0
Hemorrhage	0	0	0	0	0	0	0	0	0	0	0	0	0	0	0	2	0	0	0	0	0	0	0	0	0	0	0

Table 6.9 Summary of histopathology scores for *P. knowlesi*-infected macaques. Semi-quantitative scores are presented in the above table as a heatmap to visually represent score severity, with 0 being no changes or damage, and 4 being diffuse changes. Organs were scored on several categories, including inflammation, edema, crypt inflammation (for the gastrointestinal organs), necrosis, hemorrhage, hyperplasia (including alveolar wall thickening/interstitial hyperplasia, in the case of the lung, Kupffer Cell hyperplasia in the liver, and glomerular hyperplasia in the case of the kidney), fibrosis, vasculitis, and tubular degeneration (in the case of the kidney). Categories with at least one monkey showing positive changes are represented in the table, all other categories were negative.

6.3 APPENDIX TO CHAPTER 4: Chapter 4: *Plasmodium knowlesi* sequestration is concomitant with the expression of MAdCAM1 on the endothelium in macaques

Expanded methods for purified protein binding assay

Materials:

- 60 mm polystyrene bacteriological Petri dish (Falcon, product number 351007) (one per test)
- Dubelcco's PBS (D-PBS), or D-PBS with Mg and Ca (D-PBS 2++).
- Trypsin-EDTA
- 1% w/v of bovine serum albumin
- Purified proteins in D-PBS at 100 μg/mL
    - ICAM1 (R&D systems)
    - CD36 (R&D systems)
    - MAdCAM1 (R&D systems)
    - MAdCAM1 full length (Origene)
    - NB: If protein is shipped in Tris with glycerol, or other buffer, it is imperative to perform a buffer exchange (such as cassette diffusion), or the protein will not properly adsorb to the plate
- Vented (for mammalian cells) and non-vented (for blood cultures) Falcon 25 cm^2 tissue culture treated flasks
- Blocking buffer
    - 1% BSA in D-PBS or D-PBS2++

- Binding buffer
    - For iRBCs: RPMI without bicarbonate, pH 6.8
        - NB: Bicarbonate interferes with binding, do not add
        - pH must be properly adjusted prior to assay
    - For HuT78 cells: D-PBS 2++, 1 mM MnCl2, 1% BSA
        - NB: Prepare a stock solution of 0.5 M MnCl2 and add to a final concentration of 1 mM to binding buffer to avoid precipitation before the assay
        - Mn, Mg, and Ca are essential for integrin-MAdCAM1 binding
    - Wash buffer
        - Incomplete RPMI or D-PBS2++
    - Buffers should be stored at 4 C, but allowed to equilibrate to at least room temperature prior to assay to avoid reversal of binding

Cells

- *Plasmodium falciparum* FVO strain (propagated in *Aotus* monkeys) – positive *Plasmodium* binding control
- HuT78 lymphoma cells – positive MAdCAM1 binding control
- Uninfected rhesus RBCs – negative binding control
- *Plasmodium knowlesi* SICA[+] strain – test
- *Plasmodium knowlesi* SICA [-] strain – test

NB: All parasites should be at two to four nucleated schizont stage

Protocol:

1. 24 hours prior to the assay, thaw parasitized RBCs (thaw *P. falciparum* first, earlier in the day to allow the parasites to be at similar stages at the time of the assay) according to standard protocol. Culture ex-vivo in fresh media without antibiotics to mature.

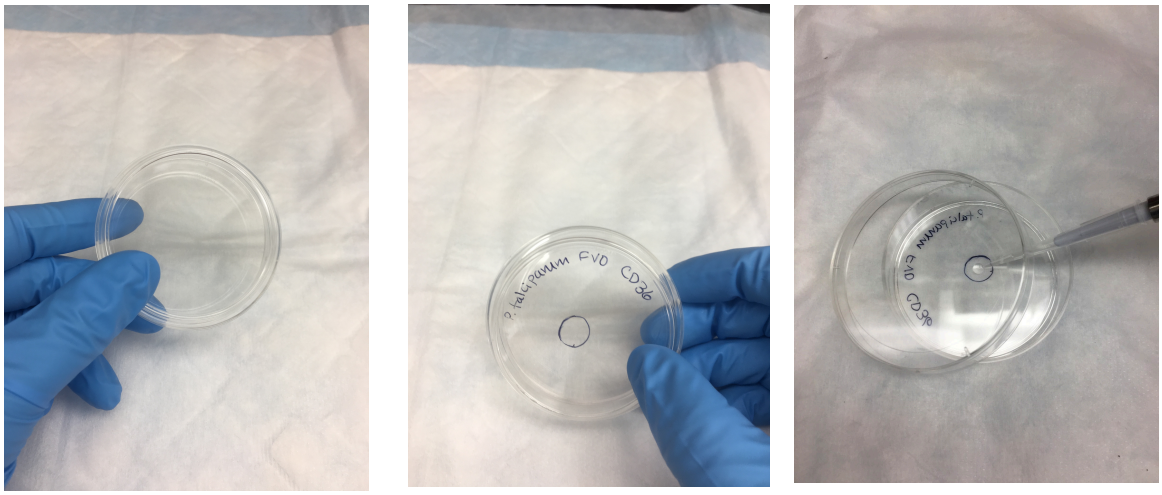

Figure 6.49 Plate set up for purified protein binding assay. Left, Example of plate to be used for assay. Middle, Label the bottom plate with test information and a circle to guide enumeration. Right, Pipette purified protein into the center of the circle.

2. Label one 60 mm polystyrene bacteriological Petri dish for each cell line and protein to be tested – each should have its own plate.
3. Draw a ~ 5 mm circle on the bottom center of the plate.
4. On the inside of the plate, pipette 20 µL of purified protein into the center of the circle (the circle serves as a guide for enumeration later).
5. Without disturbing the protein droplet, carefully place the plates in a humidified chamber and incubate at 4º C overnight *or* 37 º C for 4 hours.
6. Remove the excess protein by pipetting it off. Gently pipette 1.5 mL of blocking buffer onto the plate. Replace plates into the humidified chamber and block at 37 º C for 1 hour.
7. While the plates block, prepare the cells.

a. Untreated cells: Remove the parasites and HuT78 cells from the incubator and centrifuge at 800 xg for iRBCs and 150 xg for HuT78 cells for 3 minutes with no break. Wash twice with wash buffer. Resuspend in binding buffer at 1% hematocrit or 10^6 cells per mL.

b. For preparations treated with trypsin: wash once, add 2 mL of trypsin to the pellet and allow the cells to incubate for 2 minutes at 37 ºC or 4 minutes at room temperature. Centrifuge as above. Wash in complete mammalian cell culture media (with FBS) to deactivate trypsin. Wash again in wash buffer. Resuspend in binding buffer at 1% hematocrit or 10^6 cells per mL.

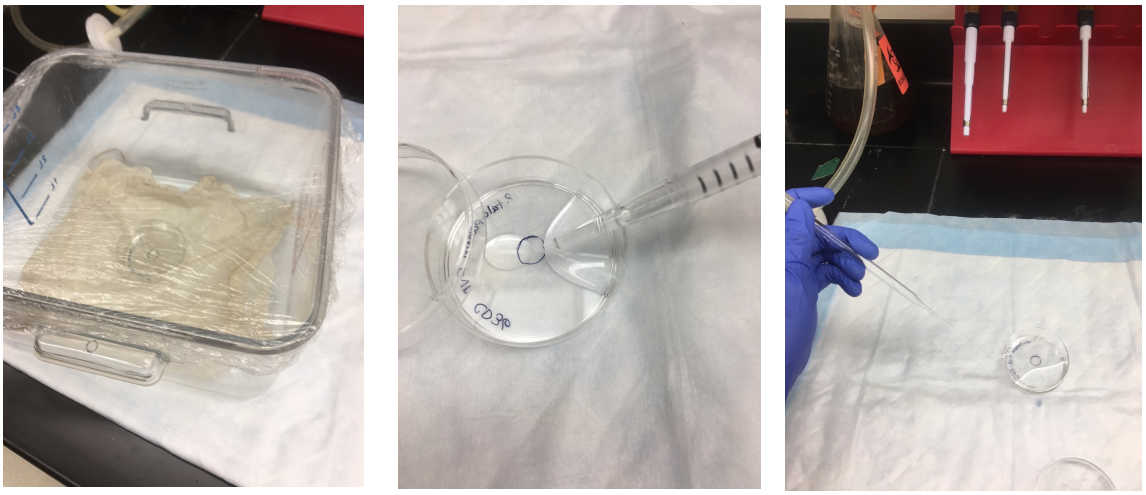

Figure 6.50: Humidified chamber, washing, and aspiration technique. Left, plates should be incubated at either 4 C overnight or 37 C for two to four hours in a humidified chamber, such as a plastic lab bin with damp paper towels in the bottom covered with a top lid or plastic wrap. Middle, pipette off the excess protein and flood plate with wash buffer, swirling and bathing plate three times with same buffer. Right, use aspiration to remove wash buffer.

8. Tip the plate to allow the buffer to pool at the bottom and aspirate the buffer off. Add 3 mL of wash buffer to each plate. Swirl then tip plate, pipette the wash buffer, and rewash the same plate three times. Tip plate and aspirate wash buffer.

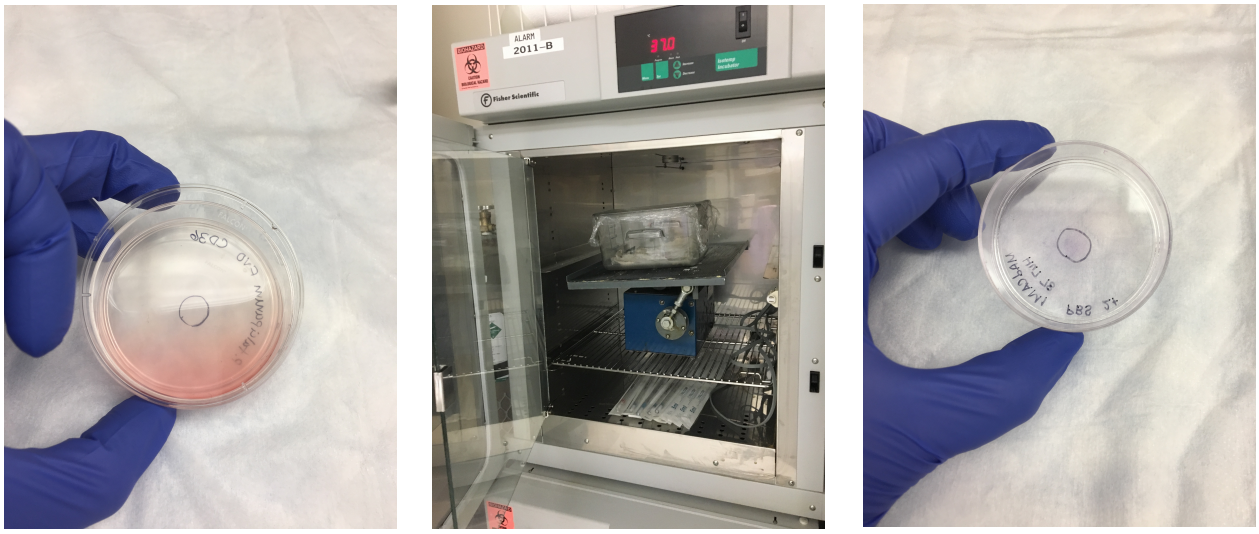

Figure 6.51: Binding and staining. Left, after washing and removing wash buffer, pipette cell suspension onto the plate (1% hematocrit or 10^5 cells per mL). Middle, place plates in the humidified chamber and place in the incubator on a rocker for 1 hour to allow to bind. Right, after washing, fix with glutaraldehyde and stain with Gurr, Bound cells well form a purple opacity grossly inside the reference circle. Quantify using 400x – 1000x.

9. Add 1.5 mL cell suspension mixture to each plate. Incubate at 37 ºC for 1 hour on a rocker in the humidified chamber.
10. Tip plate and aspirate cell suspension. Wash with 1.5 mL of wash buffer until cells no longer freely run from plate.
11. Fix with 0.5 % glutaraldehyde. Stain with 10% Gurr stain for 10 min. Enumerate by comparing cells bound in circle to those bound to blocked background.

Expanded methods for cell binding assay

Materials:

- 24 well plate (each well represents a test)
- 15mm diameter tissue-treated Thermanox coverslips (product number 174969)
- Sterile jewelers forceps (or needle-nose forceps that have been bent at the tip)
- Dubelcco's PBS (D-PBS), or D-PBS with Mg and Ca (D-PBS 2++).
- 1% w/v bovine serum albumin (BSA)
- Trypsin-EDTA
- Binding buffer
    - RPMI without bicarbonate, pH 6.8
        - NB: Bicarbonate interferes with binding, do not add
        - pH must be properly adjusted prior to assay
    - Wash buffer
        - Incomplete RPMI or D-PBS2++
    - Buffers should be stored at 4 C, but allowed to equilibrate to at least room temperature prior to assay to avoid reversal of binding
- Culture media for lawn cells
    - C32 Amelanotic Melanoma: Eagles Minimal Essential Medium (EMEM, ATCC) supplemented with 10% FBS
    - CHO lines: Kaighn's Modification of Ham's F-12 Medium (F-12K, ATCC), supplemented with FBS

    - HIMEC.1, HAMEC, HPLNEC: Optimem I with Glutamax (Gibco 51985) supplemented with 2% FBS, 0.4 gentamicin (stock of 10 mg/mL) and 0.2% amphotericin B (stock concentration 250 μg/mL).
    - Primary cells: specialized media from manufacturer.
- 0.1% Gelatin for primary cell adhesion
- Vented (for mammalian cells) and non-vented (for blood cultures) Falcon 25 cm^2 tissue culture treated flasks

Lawn Cells

- C32 Amelanotic melanoma cells
- Mock-transfected CHO
- ICAM1-transfected CHO
- CD36-transfected CHO
- HIMEC.1
- HAPEC.S1
- HPLNEC.B3
- HIMEC primary endothelial cells

Layer Cells for Testing

- *Plasmodium falciparum* FVO strain (propagated in *Aotus* monkeys) – positive *Plasmodium* binding control
- Uninfected rhesus RBCs – negative binding control
- *Plasmodium knowlesi* SICA[+] strain – test
- *Plasmodium knowlesi* SICA [-] strain – test

NB: All parasites should be at two to four nucleated schizont stage

Protocol

1. 24 hours prior to assay: thaw parasitized red blood cells, as in purified protein binding assay, using standard protocols. Seed 24-well plate:

Figure 6.52: Plate set up and lawn cell seeding. Top left, label the plate lid with the plate map. Top right, using jeweler's forceps (note hook at the end of the forceps), carefully place culture discs culture-treated-side-up in each well. Bottom left, pipette cell suspension into each well according to plate map. Bottom right, incubate in humidified incubator for mammalian cell culture overnight.

   a. Label the lid of the 24 well plate.
   b. Using sterile jeweler's forceps, carefully add one coverslip, treated side up, to each well that will contain cells.

c. Remove adherent cells from culture flasks using either a sterile scraper or trypsin. Add 1 mL 10^5 C32 amelanotic melanoma cells, or 10^4 CHO cells in fresh media. NB: the seeding concentration may vary depending on how well the cells are replicating. The goal is to aim for 30% confluency the next day.

d. Incubate at 37 ºC overnight

2. Check plates to ensure they are the proper confluency.
3. Prepare RBCs and iRBCs as described in purified binding protocol.
4. Aspirate media from each well. Wash twice with binding buffer and aspirate.
5. Add iRBC or RBC cell suspension to each well
6. Place on rocker at 37 ºC for 1 hour.
7. Prepare a reservoir of D-PBS and reserve D-PBS for washing and 0.5% glutaraldehyde for fixation.
8. Using jewelers forceps, hook the lip of the coverslip, and carefully remove it from the well, taking care to not drop it back into the well.

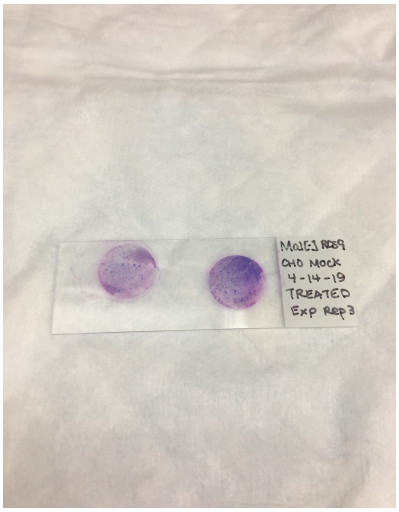

Figure 6.53: Stained slide. Lay discs flat onto glass microscopy slide, culture-side-up, allow to dry then visualize and quantify.

9. Dip coverslip in wash reservoir gently swirling to remove blood. Wash in this manner until all the blood runs off grossly.

   NB: Replace wash buffer when it's visibly soiled with blood.

10. Dip in glutaraldehyde to fix.
11. Lay on a glass slide cell-side-up. Allow to dry over night
12. Stain with 10% Gurr for 10 minutes, dry, and quantify.

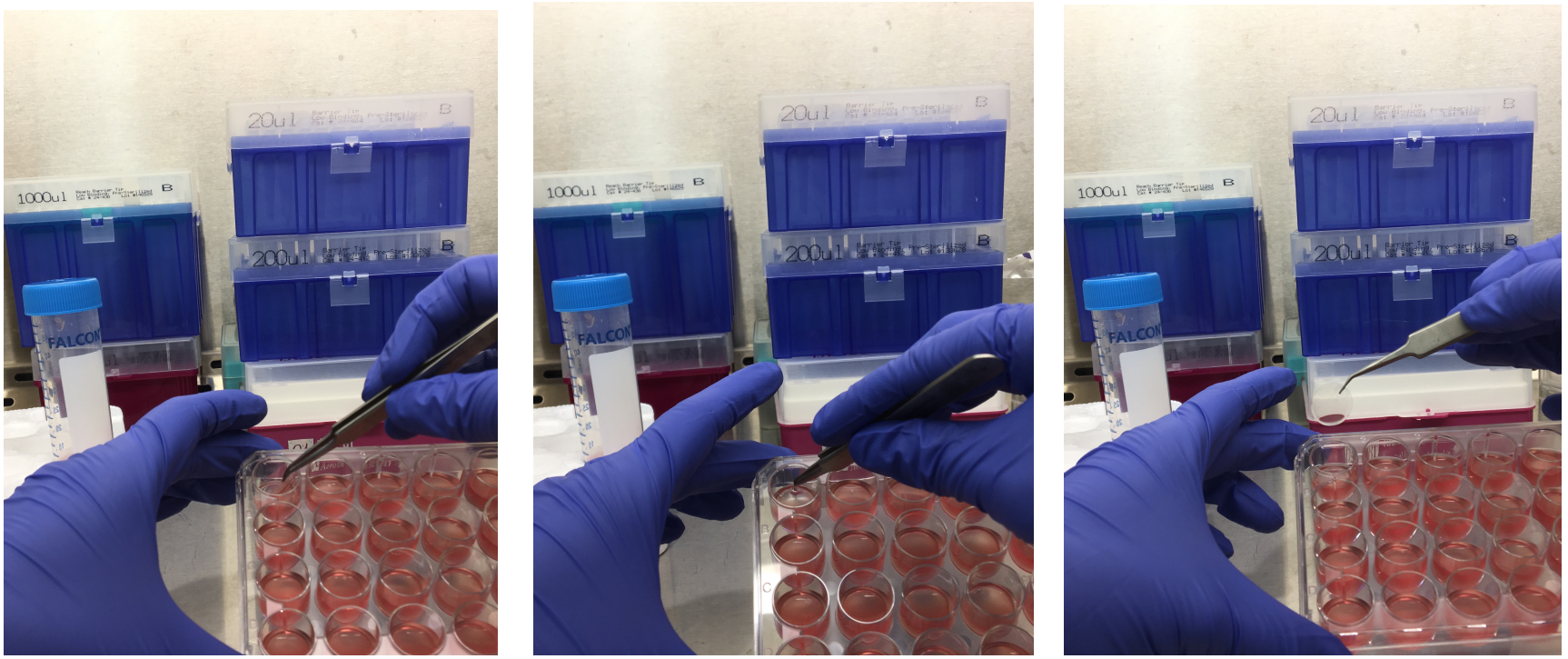

Figure 6.54: Technique for coverslip disc removal from well plate. Left, carefully tip well plate about 30 degrees and gently hook the lip of the coverslip. Avoid cross-contaminating the wells by tipping the plate too far and spilling the contents. Middle, with the end of the forceps hooked on the lip of the coverslip, gently push up so the coverslip stands vertically in the well. Take extreme care not to allow the coverslip to fall back down into the well, or the bound cells may be knocked off. Do not allow the coverslip to flip upside down. Right, with the coverslip vertical/perpendicular to the well, gently grab it by the margin and pull it out of the well to wash and fix. Place on a glass slide as in Fig. 6.53 after washing and fixation.

Table 6.10 Tissue parasite count means

	Rhesus						Kra					
	Acute			Chronic			Acute			Chronic		
Tissue	*Mean*	*SD*	*N*	*Mean*	*SD*	*N*	*Mean*	*SD*	*N*	*Mean*	*SD*	*N*
Adrenal Gland	105.000	112.820	6	0.667	0.577	3	16.500	4.509	4	4.143	8.783	7
Aorta	37.167	55.862	6	0.333	0.577	3	4.500	5.066	4	0.756	0.756	7
Bone Marrow	15.750	8.828	16	0.333	0.577	3	7.273	8.684	11	17.000	42.862	8
Cerebellum	20.333	12.291	6	0.000	0.000	3	10.250	8.617	4	0.750	1.165	8
Cerebrum	22.00	14.367	6	1.667	1.155	3	13.000	6.055	4	1.125	1.356	8
Colon	42.333	29.221	6	4.333	7.506	3	22.750	31.606	4	2.571	2.637	7
Duodenum	58.167	48.297	6	6.000	4.359	3	13.500	12.369	4	2.714	2.811	7
Eye	74.500	36.754	8	10.00	17.321	3	10.167	7.859	6	4.000	8.021	7
Jejunum	22.167	20.537	6	3.000	3.000	3	7.00	6.272	4	1.143	1.574	7
Kidney	93.167	62.477	6	1.000	0.000	4	14.000	8.831	4	2.000	1.633	7
Liver	47.167	26.317	6	6.286	11.176	7	10.250	3.594	4	6.286	11.176	7
Lung	86.333	42.683	6	3.000	2.944	4	15.000	9.345	4	9.143	17.218	7
Mesenteric LN	22.250	19.311	4	0.000	0.000	3	3.750	2.217	4	0.000	0.000	7

Midbrain	24.875	18.295	8	1.000	1.000	3	14.750	10.966	4	1.286	1.976	7
Omentum	12.000	8.877	6	0.333	0.577	3	2.250	1.893	4	0.429	0.787	7
Skeletal muscle	2.500	3.391	6	0.000	0.000	3	2.7500	2.217	4	0.000	0.000	7
Skin	12.333	19.232	6	0.000	0.000	3	1.250	1.258	4	0.2500	0.463	8
Spleen	171.167	141.173	6	0.333	0.577	3	20.500	9.399	4	4.167	4.665	6
Stomach	74.500	70.916	6	2.333	1.528	3	17.500	7.188	4	0.714	0.756	7
Testis	18.500	7.064	6	1.000	1.732	3	1.750	2.217	4	0.143	0.378	7
Thymus	14.333	12.580	6	0.000	0.000	3	1.750	1.258	4	0.250	0.463	8
Ventricle	49.000	26.974	6	1.667	2.887	3	19.000	13.166	4	0.500	0.535	8

Table 6.10 Tissue parasite count means. The means, standard deviations (SD), and sample size (number of sections, N), were calculated from the number of parasites enumerated in 10 consecutive high-power microscopy fields (oil immersion: 1000x) of each tissue collected at necropsy. Bone marrow collected from the costochondral junction and the femur were pooled in the Bone Marrow category. Animals from E33 were excluded because the entire suite of tissues was not collected.

Table 6.11 Relative tissue parasite counts

	Rhesus		Kra	
Tissue	**Acute**	**Chronic**	**Acute**	**Chronic**
Adrenal Gland	10.24	1.79	7.19	7.03
Aorta	3.62	0.89	1.96	0.49
Bone Marrow	1.54	0.89	3.17	28.86
Cerebellum	1.98	0.00	4.47	1.27
Cerebrum	2.15	4.46	5.67	1.91
Colon	4.13	11.61	9.92	4.37
Duodenum	5.67	16.07	5.88	4.60
Eye	7.26	26.79	4.43	6.79
Jejunum	2.16	8.04	3.05	1.94
Kidney	9.08	2.68	6.10	3.40
Liver	4.60	0.89	4.47	10.67
Lung	8.42	8.03	6.54	15.52
Mesenteric LN	2.17	0.00	1.63	0.00
Midbrain	2.43	2.68	6.43	2.18

Omentum	1.17	0.89	0.98	0.73
Skeletal muscle	0.24	0.00	1.20	0.00
Skin	1.20	0.00	0.54	0.42
Spleen	16.69	0.89	8.93	7.07
Stomach	7.26	6.25	7.63	1.21
Testis	1.80	2.68	0.76	0.23
Thymus	1.40	0.00	0.76	0.42
Ventricle	4.78	4.46	8.28	0.85

Table 6.11 Relative tissue parasite counts. Mean counts from each tissue for a given species were summed for chronic and acute stages of infection, and then each mean was divided by this sum to obtain a relative parasite burden to show the proportion each organ represents of the entire tissue compartment of the parasite burden. These numbers were then binned usng the mltools package and the bin_data command to produce the full body monkey heat maps. Bone marrow collected from the costochondral junction and the femur were pooled in the Bone Marrow category. Animals from E33 were excluded because the entire suite of tissues was not collected.

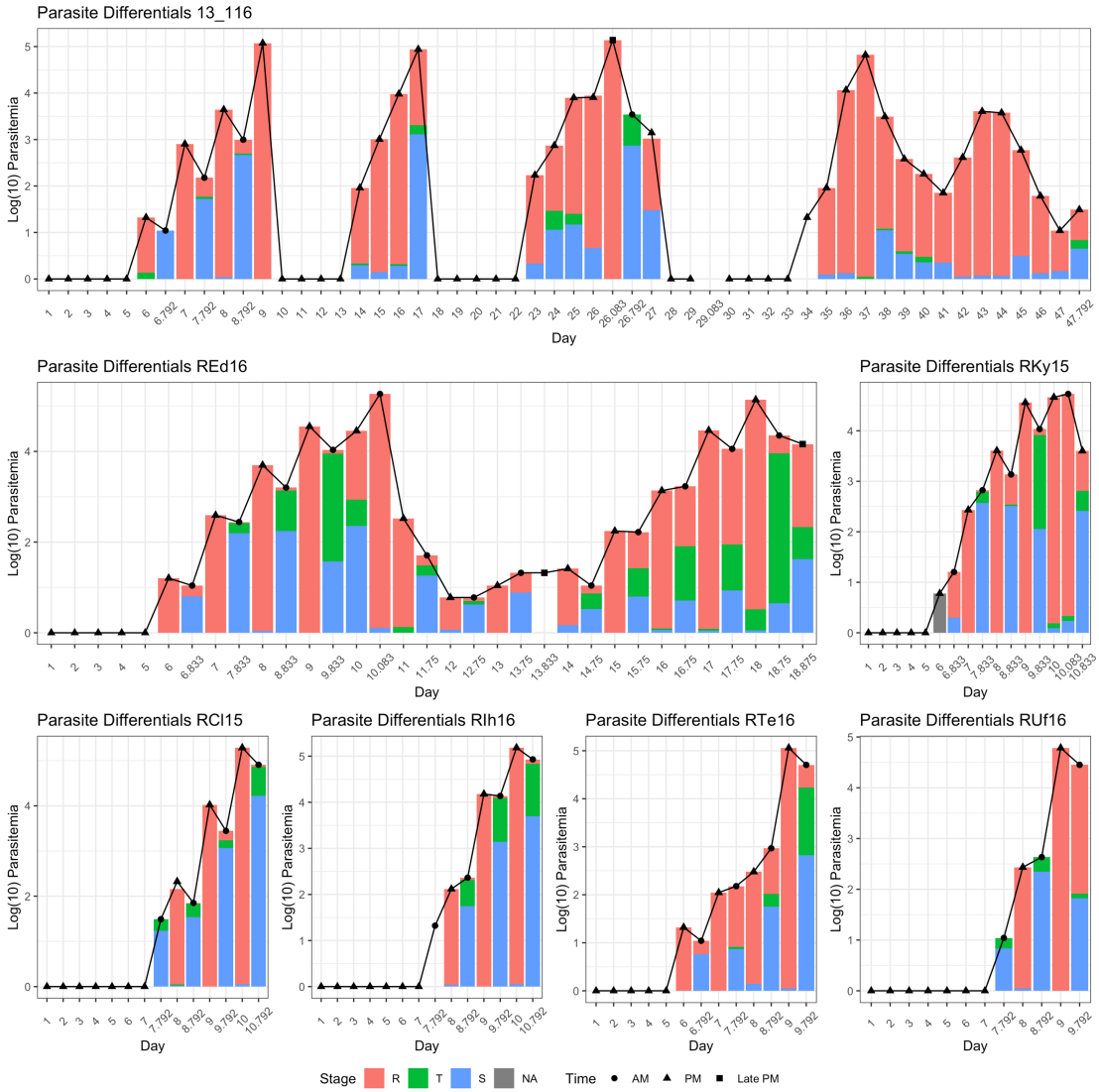

Figure 6.55: Sequestration and parasite kinetics. A subset of rhesus monkey slides were read and the stages were quantified. Many rhesus monkeys display a zig-zag pattern with parasitemia dipping in the morning, when there is an enrichment of mature stages. The one rhesus monkey, that did not show a clear margination phenotype (RIh16) does not have fewer than expected mature stages for many time points. Differentials and their proprotions are heavily dependant on the time the sample is taken.

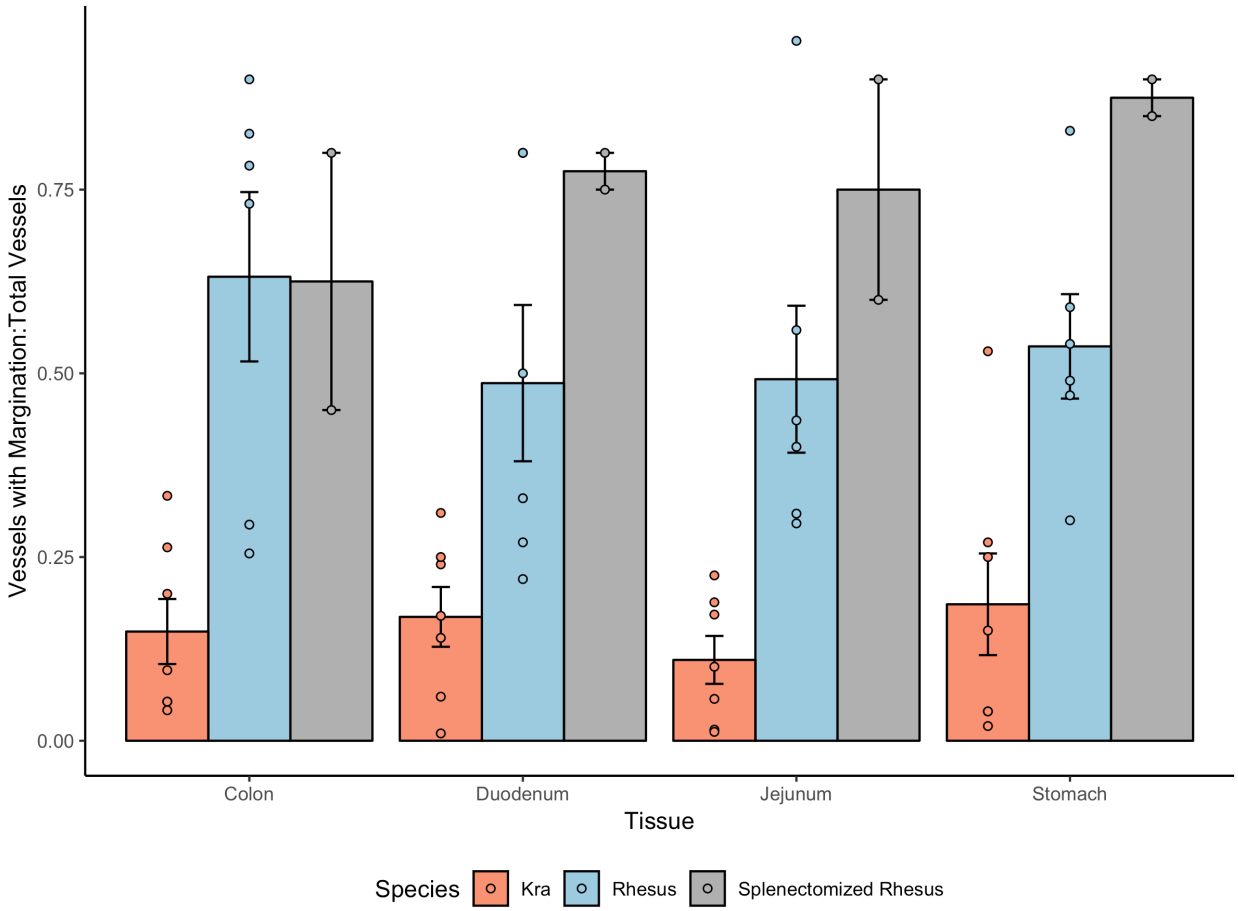

Figure 6.56 Fraction of vessels displaying margination. The proportion of vessels with at least one marginated parasite, over the total number of vessels counted for a given effort is represented in the above graph. Margination is defined conservatively as any parasite that appears to be close to the endothelial wall on light microscopy. This measure shows prevalence of marginated vessels but does not account for intensity of margination, nor does it control for parasitemia.

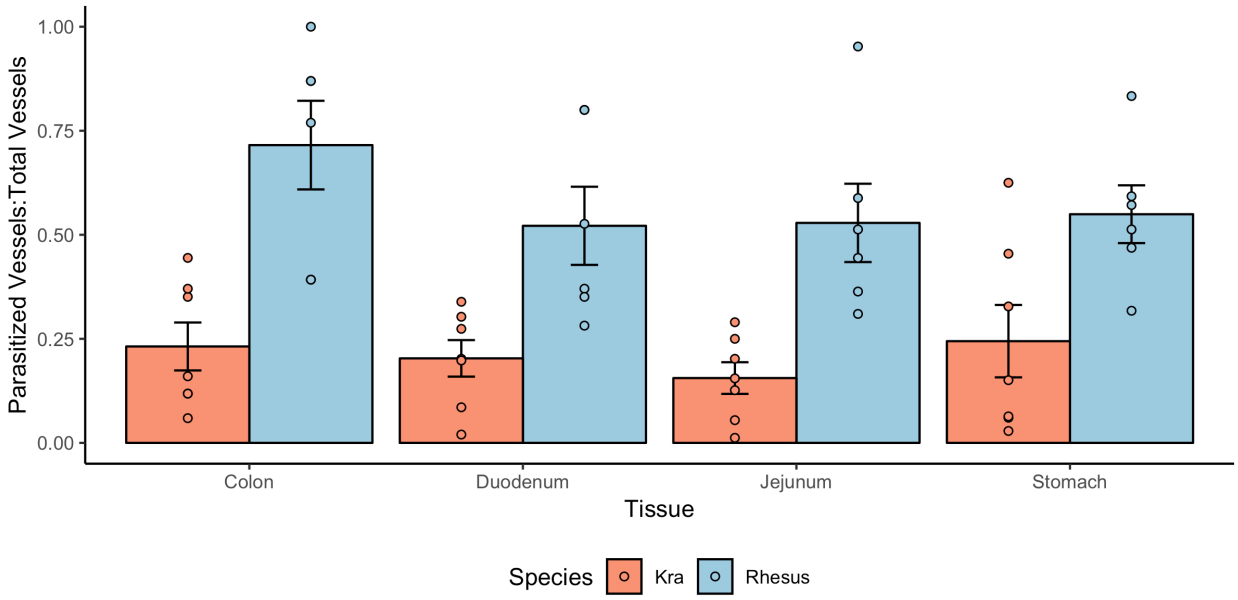

Figure 6.57 Fraction of parasitized vessels. The fraction of vessels with at least one parasite over the total number of vessels counted in a given effort is higher for rhesus monkeys than for kra monkeys, which is expected due to their comparatively larger parasitemias. All vessels counted in splenectomized rhesus monkeys were parasitized.

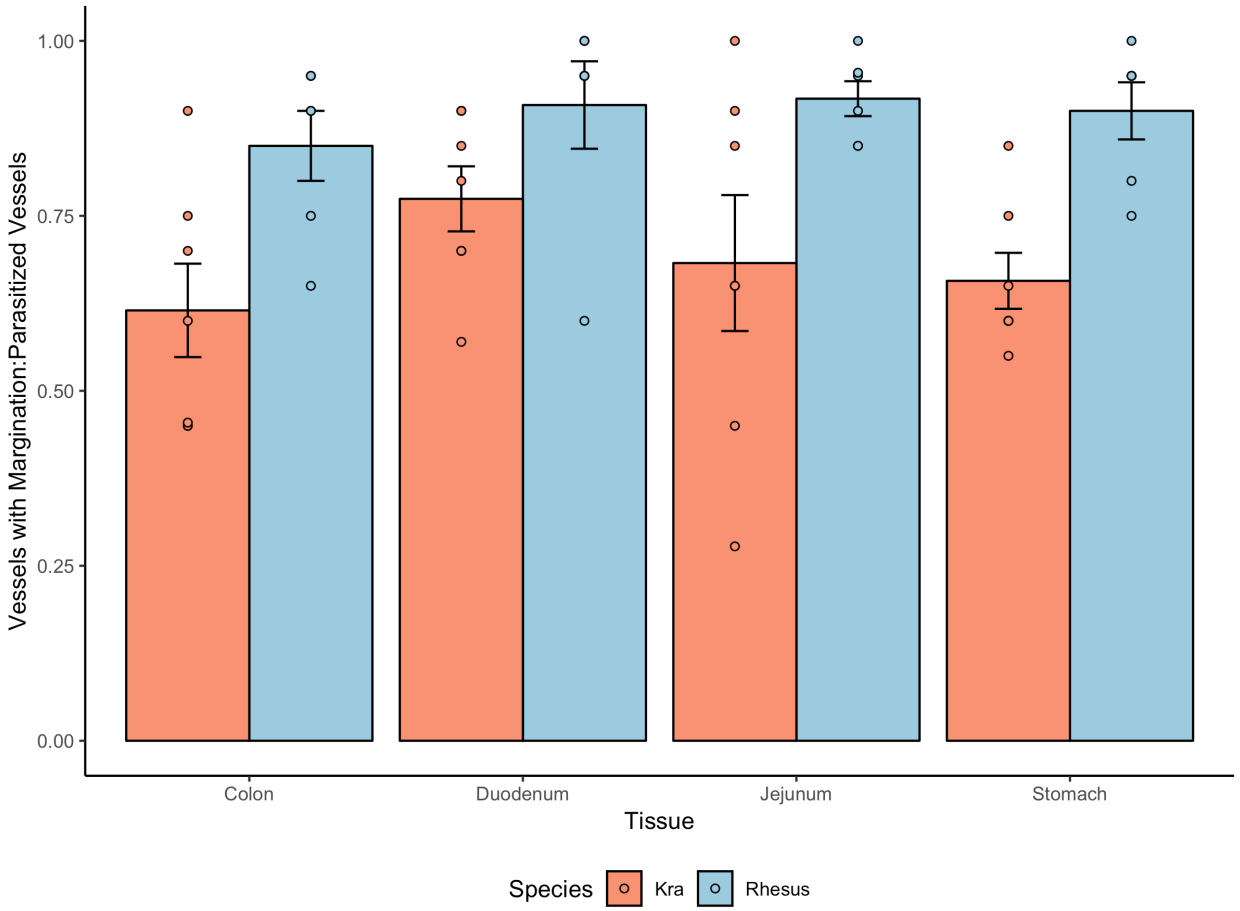

Figure 6.58 Fraction of vessels displaying margination normalized to parasitemia. To take the differences in prevalence of parasitized vessels (due to parasitemia), the number of vessels that had at least one marginated parasite was divided by the number of vessels with at least one parasite. Rhesus monkeys tended to have a higher number of vessels that were marginated when taking parasitemia into account.

Works Cited

1. Coatney GR. Chapter 4: Life Cycle and the Phenomenon of Relapse. *Primate Malarias*. US Department of Health, Education and Welfare; 1971. p. 29–40.
2. World Health Organization. World Malaria Report 2018. Geneva: World Health Organization; 2018.
3. Hume JCC, Lyons EJ, Day KP. Malaria in Antiquity: A Genetics Perspective. *World Archaeol.* **2003**; 35(2):180–192.
4. Gilles HM. Chapter 1: Historical Outline. *Essent Malariol.* 3rd ed. London: Arnold; 1993. p. 1–11.
5. Gilles HM. Chapter 2: The malaria parasites. *Essent Malariol.* 3rd ed. London: Arnold; 1993. p. 14–34.
6. Singh B, Kim Sung L, Matusop A, et al. A large focus of naturally acquired *Plasmodium knowlesi* infections in human beings. Lancet. **2004**; 363(9414):1017–24.
7. Cox-Singh J, Singh B. Knowlesi malaria: newly emergent and of public health importance? *Trends Parasitol.* **2008**; 24(9):406–10.
8. Cox-Singh J, Davis TME, Lee KS, et al. *Plasmodium knowlesi* malaria in humans is widely distributed and potentially life threatening. *Clin Infect Dis.* **2008**; 46(2):165–171.
9. Coatney GR; C WE; Contacos, PG. Chapter 26 *Plasmodium knowlesi. Primate Malarias.* Bethesda, MD: National Institute of Health; 1971. p. 317–334.

10. Garnham, P.C.C. Chapter 13: *Plasmodium knowlesi* and subspecies, *Plasmodium coatneyi* and P*lamsodium fragile*. *Malaria Parasites and Other Haemosporidia.* Oxford: Blackwell Scientific Publications; 1966. p. 323–356.
11. Taliaferro WH, Taliaferro LG. Asexual reproduction of *Plasmodium knowlesi* in rhesus monkeys. *J Infect Dis*. 85(2):107–125.
12. Warrell DA. Chapter 3: Clinical Features of Malaria. *Essent Malariol.* 3rd ed. London: Arnold; 1993. p. 35–49.
13. Nunn C L, Altizer S. Chapter 5: Host defenses: the immune system and behavioral counterstrategies. *Infectious Diseases of Primates: Behavioral Ecology and Evolution.* New York, NY: Oxford University Press; 2006. p. 134–175.
14. Ikadai H, Shaw Saliba K, Kanzok SM, et al. Transposon mutagenesis identifies genes essential for *Plasmodium falciparum* gametocytogenesis. *Proc Natl Acad Sci U S A.* **2013**; 110(18):E1676–E1684.
15. Divis PC, Singh B, Anderios F, et al. Admixture in Humans of Two Divergent *Plasmodium knowlesi* Populations Associated with Different Macaque Host Species. *PLoS Pathog.* **2015**; 11(5):e1004888.
16. Lee KS, Divis PC, Zakaria SK, et al. *Plasmodium knowlesi:* reservoir hosts and tracking the emergence in humans and macaques. *PLoS Pathog.* **2011**; 7(4):e1002015.
17. Siregar JE, Faust CL, Murdiyarso LS, et al. Non-invasive surveillance for *Plasmodium* in reservoir macaque species. *Malar J.* **2015**; 14(1):404.
18. Warren M, Cheong WH, Fredericks HK, Coatney GR. Cycles of jungle malaria in West Malaysia. *Am J Trop Med Hyg*. **1970**; 19(3):383–93.

19. Fooden J. Rhesus and Crab-Eating Macaques: Intergradation in Thailand. *Science.* **1964**; 143(3604):363–4.

20. Knowles R, Das Gupta B. A Study of Monkey-Malaria and its Experimental Transmission to Man. *Indian Med Gaz.* **1932**; 67:301–320.

21. W E Collins, J C Skinner, J R Broderson, et al. Susceptibility of Macaca fascicularis monkeys from Mauritius to different species of *Plasmodium. J Parasitol.* 78(3):505–511.

22. Butcher GA, Mitchell GH, Cohen S. *Plasmodium knowlesi* infections in a small number of non-immune natural hosts (*Macaca fascicularis*) and in rhesus monkeys (*M. mulatta*). *Trans R Soc Trop Med Hyg.* **2010**; 104(1):75–7.

23. Anderios F, Noorrain A, Vythilingam I. *In vivo* study of human *Plasmodium knowlesi* in *Macaca fascicularis. Exp Parasitol.* **2010**; 124(2):181–9.

24. Kakinuma C, Futamura Y, Kaga N, Shibutani Y. Plasma cytokine concentrations and splenic changes in cynomolgus monkeys (*Macaca fascicularis*) with malaria. *Lab Anim Sci.* **1999**; 49(1):101–104.

25. Spangler WL, Gribble D, Abildgaard C, Harrison J. *Plasmodium knowlesi* malaria in the Rhesus monkey. *Vet Pathol.* **1978**; 15(1):83–91.

26. Chen L, Li G, Lu Y, Luo Z. Histopathological changes of *Macaca mulatta* infected with *Plasmodium knowlesi. Chin Med J Engl.* **2001**; 114(10):1073–7.

27. Ibiwoye MO, Howard CV, Sibbons P, Hasan M, Velzen D van. Cerebral malaria in the rhesus monkey (*Macaca mulatta*): observations on host pathology. *J Comp Pathol.* **1993**; 108(3):303–310.

28. Knisely MH, Stratman-Thomas WK, Eliot TS, Bloch EH. *Knowlesi Malaria* In Monkeys Ii: A First Step In The Separation Of The Mechanical Pathologic Circulatory Factors Of One Sludge Disease From Possible Specific Toxic Factors Of That Disease. *Angiology.* **1964**; 15:411–416.

29. Wheatley BP. Malaria as a possible selective factor in the speciation of macaques. *J Mammal.* **1980**; 61(2):307–11.

30. Schmidt LH, Fradkin R, Harrison J, Rossan RN. Differences in the virulence of *Plasmodium knowlesi* for *Macaca irus* (*fascicularis*) of Philippine and Malayan origins. *Am J Trop Med Hyg.* **1977**; 26(4):612–22.

31. Rooyen CE van, Pile GR. Observations on Infection by *Plasmodium knowlesi* (Ape Malaria) in the Treatment of General Paralysis of the Insane. *Br Med J.* **1935**; 2(3901):662–6.

32. Daey Ouwens IM, Lens CE, Fiolet ATL, et al. Malaria Fever Therapy for General Paralysis of the Insane: A Historical Cohort Study. *Eur Neurol.* **2017**; 78(1–2):56–62.

33. Wagner-Jaureg. The Treatment Of General Paresis By Inoculation Of Malaria. *J Nerv Ment Dis.* **1922**; 55(5):369–389.

34. Albert MR. Fever therapy for general paresis. *Int J Dermatol.* **1999**; 38(8):633–637.

35. Chin W, Contacos PG, Coatney GR, Kimball HR. A Naturally Acquired Quotidian-Type Malaria in Man Transferable to Monkeys. *Science.* **1965**; 149(3686):865-.

36. Marchand RP, Culleton R, Maeno Y, Quang NT, Nakazawa S. Co-infections of *Plasmodium knowlesi*, *P. falciparum*, and *P. vivax* among Humans and *Anopheles dirus* Mosquitoes, Southern Vietnam. *Emerg Infect Dis.* **2011**; 17(7):1232–9.

37. Nakazawa S, Marchand RP, Quang NT, Culleton R, Manh ND, Maeno Y. *Anopheles dirus* co-infection with human and monkey malaria parasites in Vietnam. *Int J Parasitol.* **2009**; 39(14):1533–7.

38. Luchavez J, Espino F, Curameng P, et al. Human Infections with *Plasmodium knowlesi*, the Philippines. *Emerg Infect Dis.* **2008**; 14(5):811–3.

39. Khim N, Siv S, Kim S, et al. *Plasmodium knowlesi* infection in humans, Cambodia, 2007-2010. *Emerg Infect Dis.* **2011**; 17(10):1900–2.

40. Ng OT, Ooi EE, Lee CC, et al. Naturally acquired human *Plasmodium knowlesi* infection, Singapore. *Emerg Infect Dis.* **2008**; 14(5):814–6.

41. Berry A, Iriart X, Wilhelm N, et al. Imported *Plasmodium knowlesi* malaria in a French tourist returning from Thailand. *Am J Trop Med Hyg.* **2011**; 84(4):535–8.

42. Jongwutiwes S, Buppan P, Kosuvin R, et al. *Plasmodium knowlesi* Malaria in humans and macaques, Thailand. *Emerg Infect Dis.* **2011**; 17(10):1799–806.

43. Jongwutiwes S, Putaporntip C, Iwasaki T, Sata T, Kanbara H. Naturally acquired *Plasmodium knowlesi* malaria in human, Thailand. *Emerg Infect Dis.* **2004**; 10(12):2211–3.

44. Putaporntip C, Hongsrimuang T, Seethamchai S, et al. Differential prevalence of *Plasmodium* infections and cryptic *Plasmodium knowlesi* malaria in humans in Thailand. *J Infect Dis.* **2009**; 199(8):1143–50.

45. William T, Rahman HA, Jelip J, et al. Increasing incidence of *Plasmodium knowlesi* malaria following control of *P. falciparum* and *P. vivax* Malaria in Sabah, Malaysia. *PLoS Negl Trop Dis.* **2013**; 7(1):e2026.

46. Singh B, Daneshvar C. Human infections and detection of *Plasmodium knowlesi. Clin Microbiol Rev.* **2013**; 26(2):165–84.

47. William T, Jelip J, Menon J, et al. Changing epidemiology of malaria in Sabah, Malaysia: increasing incidence of *Plasmodium knowlesi. Malar J.* **2014**; 13:390.

48. Vythilingam I, Tan CH, Asmad M, Chan ST, Lee KS, Singh B. Natural transmission of *Plasmodium knowlesi* to humans by *Anopheles latens* in Sarawak, Malaysia. *Trans R Soc Trop Med Hyg.* **2006**; 100(11):1087–8.

49. Fornace KM, Abidin TR, Alexander N, et al. Association between Landscape Factors and Spatial Patterns of *Plasmodium knowlesi* Infections in Sabah, Malaysia. *Emerg Infect Dis.* **2016**; 22(2):201–9.

50. Wong ML, Chua TH, Leong CS, et al. Seasonal and Spatial Dynamics of the Primary Vector of *Plasmodium knowlesi* within a Major Transmission Focus in Sabah, Malaysia. *PLoS Negl Trop Dis.* **2015**; 9(10):e0004135.

51. Barber BE, William T, Dhararaj P, et al. Epidemiology of *Plasmodium knowlesi* malaria in north-east Sabah, Malaysia: family clusters and wide age distribution. *Malar J.* **2012**; 11:401.

52. Manin BO, Ferguson HM, Vythilingam I, et al. Investigating the Contribution of Peri-domestic Transmission to Risk of Zoonotic Malaria Infection in Humans. *PLoS Negl Trop Dis.* **2016**; 10(10):e0005064.

53. Imai N, White MT, Ghani AC, Drakeley CJ. Transmission and control of *Plasmodium knowlesi*: a mathematical modelling study. *PLoS Negl Trop Dis.* **2014**; 8(7):e2978.

54. Barber BE, William T, Grigg MJ, et al. A prospective comparative study of knowlesi, falciparum, and vivax malaria in Sabah, Malaysia: high proportion with severe disease from *Plasmodium knowlesi* and *Plasmodium vivax* but no mortality with early referral and artesunate therapy. *Clin Infect Dis.* **2013**; 56(3):383–97.

55. Daneshvar C, Davis TME, Cox-Singh J, et al. Clinical and Laboratory Features of Human *Plasmodium knowlesi* Infection. *Clin Infect Dis.* **2009**; 49(6):852–860.

56. Cox-Singh J, Hiu J, Lucas SB, et al. Severe malaria - a case of fatal *Plasmodium knowlesi* infection with post-mortem findings: a case report. *Malar J.* **2010**; 9:10.

57. Barnwell JW, Asch AS, Nachman RL, Yamaya M, Aikawa M, Ingravallo P. A human 88-kD membrane glycoprotein (CD36) functions in vitro as a receptor for a cytoadherence ligand on *Plasmodium falciparum*-infected erythrocytes. *J Clin Invest.* **1989**; 84(3):765–72.

58. Ockenhouse CF, Betageri R, Springer TA, Staunton DE. *Plasmodium falciparum*-infected erythrocytes bind ICAM-1 at a site distinct from LFA-1, Mac-1, and human rhinovirus. *Cell.* **1992**; 68(1):63–9.

59. Ockenhouse CF, Tegoshi T, Maeno Y, et al. Human vascular endothelial cell adhesion receptors for *Plasmodium falciparum*-infected erythrocytes: roles for endothelial leukocyte adhesion molecule 1 and vascular cell adhesion molecule 1. *J Exp Med.* **1992**; 176(4):1183–9.

60. Smith JD, Chitnis CE, Craig AG, et al. Switches in expression of *Plasmodium falciparum var* genes correlate with changes in antigenic and cytoadherent phenotypes of infected erythrocytes. *Cell.* **1995**; 82(1):101–10.

61. Miller LH. Distribution of Mature Trophozoites and Schizonts of *Plasmodium Falciparum* in the Organs of *Aotus Trivirgatus*, the Night Monkey*. *Am J Trop Med Hyg.* **1969**; 18(6):860–865.

62. Milner DA Jr, Whitten RO, Kamiza S, et al. The systemic pathology of cerebral malaria in African children. *Front Cell Infect Microbiol.* **2014**; 4:104.

63. Spitz S. The pathology of acute falciparum malaria. *Mil Surg.* **1946**; 99(5):555–72.

64. Miller LH, Fremount HN, Luse SA. Deep vascular schizogony of *Plasmodium knowlesi* in *Macaca mulatta.* Distribution in organs and ultrastructure of parasitized red cells. *Am J Trop Med Hyg.* **1971**; 20(6):816–24.

65. Knisely MH, Stratman-Thomas WK, Eliot TS, Bloch EH. I. Microscopic Pathological Circulatory Physiology of Rhesus Monkeys During Acute P*lasmodium knowlesi* Malaria. *J Natl Malar Soc.* **1945**; Dec(4):285–300.

66. Aley SB, Barnwell JW, Daniel W, Howard RJ. Identification of parasite proteins in a membrane preparation enriched for the surface membrane of erythrocytes infected with *Plasmodium knowlesi. Mol Biochem Parasitol.* **1984**; 12(1):69–84.

67. Chien JT, Pakala SB, Geraldo JA, et al. High-Quality Genome Assembly and Annotation for *Plasmodium coatneyi,* Generated Using Single-Molecule Real-Time PacBio Technology. *Genome Announc* [Internet]. **2016**; 4(5). Available from: https://www.ncbi.nlm.nih.gov/pubmed/27587810

68. Pain A, Bohme U, Berry AE, et al. The genome of the simian and human malaria parasite *Plasmodium knowlesi. Nature.* **2008**; 455(7214):799–803.

69. Corredor V, Meyer EV, Lapp S, et al. A *SICAvar* switching event in *Plasmodium knowlesi* is associated with the DNA rearrangement of conserved 3' non-coding sequences. *Mol Biochem Parasitol.* **2004**; 138(1):37–49.

70. Khedery B al-, Barnwell JW, Galinski MR. Antigenic variation in malaria: a 3' genomic alteration associated with the expression of a *P. knowlesi* variant antigen. *Mol Cell.* **1999**; 3(2):131–41.

71. Brown KN. Antibody induced variation in malaria parasites. *Nature.* **1973**; 242(5392):49–50.

72. Brown KN, Brown IN. Immunity to Malaria - Antigenic Variation in Chronic Infections of *Plasmodium Knowlesi. Nature.* **1965**; 208(5017):1286-.

73. Brown IN, Brown KN, Hills LA. Immunity to malaria: the antibody response to antigenic variation by *Plasmodium knowlesi. Immunology.* **1968**; 14(1):127–38.

74. Barnwell JW, Howard RJ, Miller LH. Influence of the spleen on the expression of surface antigens on parasitized erythrocytes. *Ciba Found Symp.* **1983**; 94:117–36.

75. Baruch DI, Pasloske BL, Singh HB, et al. Cloning the *P. falciparum* gene encoding PfEMP1, a malarial variant antigen and adherence receptor on the surface of parasitized human erythrocytes. *Cell.* **1995**; 82(1):77–87.

76. Barnwell J, Howard R, Coon H, Miller L. Splenic requirement for antigenic variation and expression of the variant antigen on the erythrocyte membrane in cloned *Plasmodium knowlesi* malaria. *Infect Immun.* **1983**; 40(3):985–994.

77. Brown K, Hills L. Antigenic variation and immunity to *Plasmodium knowlesi*: antibodies which induce antigenic variation and antibodies which destroy parasites. *Trans R Soc Trop Med Hyg.* **1974**; 68(2):139–142.

78. Hviid L, Jensen AT. Chapter Two-PfEMP1–A Parasite Protein Family of Key Importance in *Plasmodium falciparum* Malaria Immunity and Pathogenesis. *Adv Parasitol.* **2015**; 88:51–84.

79. Gardner MJ, Hall N, Fung E, et al. Genome sequence of the human malaria parasite *Plasmodium falciparum. Nature.* **2002**; 419(6906):498–511.

80. Kraemer SM, Smith JD. A family affair: var genes, PfEMP1 binding, and malaria disease. *Curr Opin Microbiol.* **2006**; 9(4):374–80.

81. Korir CC, Galinski MR. Proteomic studies of *Plasmodium knowlesi* SICA variant antigens demonstrate their relationship with *P. falciparum* EMP1. *Infect Genet Evol.* **2006**; 6(1):75–9.

82. Lopes SC, Albrecht L, Carvalho BO, et al. Paucity of *Plasmodium vivax* mature schizonts in peripheral blood is associated with their increased cytoadhesive potential. *J Infect Dis.* **2014**; 209(9):1403–7.

83. De las Salas B, Segura C, Pabon A, Lopes SC, Costa FT, Blair S. Adherence to human lung microvascular endothelial cells (HMVEC-L) of *Plasmodium vivax* isolates from Colombia. *Malar J.* **2013**; 12:347.

84. Carvalho BO, Lopes SC, Nogueira PA, et al. On the cytoadhesion of *Plasmodium vivax*-infected erythrocytes. *J Infect Dis.* **2010**; 202(4):638–47.

85. Peterson MS, Joyner CJ, Cordy RJ, et al. *Plasmodium vivax* Parasite Load Is Associated With Histopathology in *Saimiri boliviensis* With Findings Comparable to P vivax Pathogenesis in Humans. *Open Forum Infect Dis.* **2019**; 6(3):ofz021.

86. Romero A, Matos C, Gonzalez M, Nunez N, Bermudez L, Casto G de. [Changes in gastric muscosa in acute malaria]. *GEN Rev Soc Venez Gastroenterol*. 47(3):123–128.

87. Church JA, Nyamako L, Olupot-Olupot P, Maitland K, Urban BC. Increased adhesion of *Plasmodium falciparum* infected erythrocytes to ICAM-1 in children with acute intestinal injury. *Malar J.* **2016**; 15:54.

88. Butcher GA, Mitchell GH, Cohen S. Letter: Mechanism of host specificity in malarial infection. *Nature.* **1973**; 244(5410):40–1.

89. Lim C, Hansen E, DeSimone TM, et al. Expansion of host cellular niche can drive adaptation of a zoonotic malaria parasite to humans. *Nat Commun*. **2013**; 4:1638.

90. Dankwa S, Lim C, Bei AK, et al. Ancient human sialic acid variant restricts an emerging zoonotic malaria parasite. *Nat Commun.* **2016**; 7:11187.

91. Coatney GR; C WE; Contacos, PG. *Plasmodium knowlesi. Primate Malarias.* Bethesda, MD: US Department of Health, Education and Welfare; 1971. p. 317–333.

92. Barber BE, Grigg MJ, William T, et al. Effects of Aging on Parasite Biomass, Inflammation, Endothelial Activation, Microvascular Dysfunction and Disease Severity in *Plasmodium knowlesi* and *Plasmodium falciparum* Malaria. *J Infect Dis.* **2017**; 215(12):1908–1917.

93. WHO. Control and Elimination of *Plasmodium vivax* Malaria: A Technical Brief. Geneva: World Health Organization; 2015.

94. Lacerda MV, Fragoso SC, Alecrim MG, et al. Postmortem characterization of patients with clinical diagnosis of *Plasmodium vivax* malaria: to what extent does this parasite kill? *Clin Infect Dis.* **2012**; 55(8):e67-74.

95. Wassmer SC, Taylor TE, Rathod PK, et al. Investigating the Pathogenesis of Severe Malaria: A Multidisciplinary and Cross-Geographical Approach. *Am J Trop Med Hyg.* **2015**; 93(3 Suppl):42–56.

96. Costa FT, Lopes SC, Albrecht L, et al. On the pathogenesis of *Plasmodium vivax* malaria: perspectives from the Brazilian field. *Int J Parasitol.* **2012**; 42(12):1099–105.

97. Barber BE, William T, Grigg MJ, et al. Parasite biomass-related inflammation, endothelial activation, microvascular dysfunction and disease severity in vivax malaria. *PLoS Pathog.* **2015**; 11(1):e1004558.

98. Anstey NM, Handojo T, Pain MC, et al. Lung injury in vivax malaria: pathophysiological evidence for pulmonary vascular sequestration and posttreatment alveolar-capillary inflammation. *J Infect Dis.* **2007**; 195(4):589–96.

99. Obaldia N 3rd, Meibalan E, Sa JM, et al. Bone Marrow Is a Major Parasite Reservoir in *Plasmodium vivax* Infection. *MBio* [Internet]. **2018**; 9(3). Available from: https://www.ncbi.nlm.nih.gov/pubmed/29739900

100. Fremount HN, Rossan RN. Anatomical distribution of developing trophozoites and schizonts of *Plasmodium vivax* in *Aotus lemurinus lemurinus* and *Saimiri sciureus. J Parasitol.* **1990**; 76(3):428–30.

101. Yadava A, Hall CE, Sullivan JS, et al. Protective efficacy of a *Plasmodium vivax* circumsporozoite protein-based vaccine in *Aotus nancymaae* is associated with antibodies to the repeat region. *PLoS Negl Trop Dis.* **2014**; 8(10):e3268.

102. Valecha N, Pinto RG, Turner GD, et al. Histopathology of fatal respiratory distress caused by *Plasmodium vivax* malaria. *Am J Trop Med Hyg.* **2009**; 81(5):758–62.

103. Anderson DC, Lapp SA, Barnwell JW, Galinski MR. A large scale *Plasmodium vivax- Saimiri boliviensis* trophozoite-schizont transition proteome. *PLoS One.* **2017**; 12(8):e0182561.

104. Anderson DC, Lapp SA, Akinyi S, et al. *Plasmodium vivax* trophozoite-stage proteomes. *J Proteomics.* **2015**; 115:157–76.

105. Earle WC, Perez M. Enumeration of parasites in the blood of malarial patients. *J Lab Clin Med.* **1932**; 17(11):1124–1130.

106. Sheehan DC, Hrapchak BB. *Theory and Practice of Histotechnology.* 2nd ed. St Louis, MO: CV Mosby; 1980.

107. Hanscheid T. Diagnosis of malaria: a review of alternatives to conventional microscopy. *Clin Lab Haematol.* **1999**; 21(4):235–45.

108. Lawrence C, Olson JA. Birefringent Hemozoin Identifies Malaria. *Am J Clin Pathol.* **1985**; 86(3):360–363.

109. Piper R, Lebras J, Wentworth L, et al. Immunocapture diagnostic assays for malaria using *Plasmodium* lactate dehydrogenase (pLDH). *Am J Trop Med Hyg.* **1999**; 60(1):109–18.

110. Nguansangiam S, Day NP, Hien TT, et al. A quantitative ultrastructural study of renal pathology in fatal *Plasmodium falciparum* malaria. *Trop Med Int Health.* **2007**; 12(9):1037–50.

111. Joyner CJ, Consortium TM, Wood JS, Moreno A, Garcia A, Galinski MR. Case Report: Severe and Complicated Cynomolgi Malaria in a Rhesus Macaque Resulted in Similar Histopathological Changes as Those Seen in Human Malaria. *Am J Trop Med Hyg.* **2017**; 97(2):548–555.

112. Sarkar S, Saha K, Das CS. Three cases of ARDS: An emerging complication of *Plasmodium vivax* malaria. *Lung India.* **2010**; 27(3):154–7.

113. Londhe C, Ganeriwal A, deSouza R. Study of clinical profile of acute respiratory distress syndrome and acute lung injury in *Plasmodium vivax* malaria. *J Vector Borne Dis*. **2014**; 51(4):339–42.

114. Alexandre MA, Ferreira CO, Siqueira AM, et al. Severe *Plasmodium vivax* malaria, Brazilian Amazon. *Emerg Infect Dis.* **2010**; 16(10):1611–4.

115. Val F, Avalos S, Gomes AA, et al. Are respiratory complications of *Plasmodium vivax* malaria an underestimated problem? *Malar J.* **2017**; 16(1):495.

116. Viriyavejakul P, Khachonsaksumet V, Punsawad C. Liver changes in severe *Plasmodium falciparum* malaria: histopathology, apoptosis and nuclear factor kappa B expression. *Malar J.* **2014**; 13:106.

117. Joice R, Nilsson SK, Montgomery J, et al. *Plasmodium falciparum* transmission stages accumulate in the human bone marrow. *Sci Transl Med.* **2014**; 6(244):244re5.

118. Shio MT, Kassa FA, Bellemare MJ, Olivier M. Innate inflammatory response to the malarial pigment hemozoin. *Microbes Infect.* **2010**; 12(12–13):889–99.

119. Elias RM, Correa-Costa M, Barreto CR, et al. Oxidative stress and modification of renal vascular permeability are associated with acute kidney injury during *P. berghei* ANKA infection. *PLoS One.* **2012**; 7(8):e44004.

120. Lee MSJ, Maruyama K, Fujita Y, et al. *Plasmodium* products persist in the bone marrow and promote chronic bone loss. *Sci Immunol* [Internet]. **2017**; 2(12). Available from: https://www.ncbi.nlm.nih.gov/pubmed/28783657

121. Lamikanra AA, Theron M, Kooij TW, Roberts DJ. Hemozoin (malarial pigment) directly promotes apoptosis of erythroid precursors. *PLoS One.* **2009**; 4(12):e8446.

122. Castro-Gomes T, Mourao LC, Melo GC, Monteiro WM, Lacerda MV, Braga EM. Potential immune mechanisms associated with anemia in *Plasmodium vivax* malaria: a puzzling question. *Infect Immun*. **2014**; 82(10):3990–4000.

123. Fonseca LL, Alezi HS, Moreno A, Barnwell JW, Galinski MR, Voit EO. Quantifying the removal of red blood cells in *Macaca mulatta* during a *Plasmodium coatneyi* infection. *Malar J.* **2016**; 15(1):410.

124. Barber BE, Grigg MJ, Piera KA, et al. Intravascular haemolysis in severe *Plasmodium knowlesi* malaria: association with endothelial activation, microvascular dysfunction, and acute kidney injury. *Emerg Microbes Infect.* **2018**; 7(1):106.

125. Tagariello G, Sartori R, Inojosa WO, et al. Dramatic post-splenectomy onset of malaria caused by latent *Plasmodium vivax* in a female immigrant with severe immunological anaemia. *Blood Transfus.* **2014**; 12(3):428–30.

126. Zhang HW, Li SJ, Hu T, et al. Prolonged parasite clearance in a Chinese splenectomized patient with falciparum malaria imported from Nigeria. *Infect Poverty.* **2017**; 6(1):44.

127. Del Portillo HA, Ferrer M, Brugat T, Martin-Jaular L, Langhorne J, Lacerda MV. The role of the spleen in malaria. *Cell Microbiol.* **2012**; 14(3):343–55.

128. Yusof R, Lau YL, Mahmud R, et al. High proportion of knowlesi malaria in recent malaria cases in Malaysia. *Malar J.* **2014**; 13:168.

129. Figtree M, Lee R, Bain L, et al. *Plasmodium knowlesi* in human, Indonesian Borneo. *Emerg Infect Dis.* **2010**; 16(4):672–4.

130. Vythilingam I, Noorazian YM, Huat TC, et al. *Plasmodium knowlesi* in humans, macaques and mosquitoes in peninsular Malaysia. *Parasit Vectors.* **2008**; 1(1):26.

131. Fornace KM, Nuin NA, Betson M, et al. Asymptomatic and Submicroscopic Carriage of *Plasmodium knowlesi* Malaria in Household and Community Members of Clinical Cases in Sabah, Malaysia. *J Infect Dis.* **2016**; 213(5):784–7.

132. Knisely MH, Stratman-Thomas WK, Eliot TS, Bloch EH. Knowlesi malaria in monkeys; microscopic pathological circulatory physiology of rhesus monkeys during acute *Plasmodium knowlesi* malaria. *J. Natl Malar Soc.* **1945;** 4:285-300.

133. World Health Organization. Severe malaria. *Trop Med Int Health.* **2014**; 19 Suppl 1:7–131.

134. Butcher GA. Models for malaria: Nature knows best. *Parasitol Today* Pers Ed. **1996**; 12(10):378–382.

135. Greenwood BM, Bradley AK, Greenwood AM, et al. Mortality and morbidity from malaria among children in a rural area of The Gambia, West Africa. *Trans R Soc Trop Med Hyg.* **1987**; 81(3):478–486.

136. White NJ, Pukrittayakamee S, Hien TT, Faiz MA, Mokuolu OA, Dondorp AM. Malaria. *Lancet.* **2014**; 383(9918):723–35.

137. McGuinness D, Koram K, Bennett S, Wagner G, Nkrumah F, Riley E. Clinical case definitions for malaria: clinical malaria associated with very low parasite densities in African infants. *Trans R Soc Trop Med Hyg.* **1998**; 92(5):527–531.

138. Gatton ML, Cheng Q. Evaluation of the pyrogenic threshold for *Plasmodium falciparum* malaria in naive individuals. *Am J Trop Med Hyg.* **2002**; 66(5):467–73.

139. Dicko A, Mantel C, Kouriba B, et al. Season, fever prevalence and pyrogenic threshold for malaria disease definition in an endemic area of Mali. *Trop Med Int Health.* **2005**; 10(6):550–6.

140. Gazzinelli RT, Kalantari P, Fitzgerald KA, Golenbock DT. Innate sensing of malaria parasites. *Nat Rev Immunol.* **2014**; 14(11):744–757.

141. King T, Lamb T. Interferon-γ: The Jekyll and Hyde of Malaria. *PLOS Pathog.* **2015**; 11(10):e1005118.

142. Gonçalves RM, Lima NF, Ferreira MU. Parasite virulence, co-infections and cytokine balance in malaria. *Pathog Glob Health.* **2014**; 108(4):173–178.

143. Miller LH, Baruch DI, Marsh K, Doumbo OK. The pathogenic basis of malaria. *Nature.* **2002**; 415(6872):673–9.

144. Hugosson E, Montgomery SM, Premji Z, Troye-Blomberg M, Björkman A. Higher IL-10 levels are associated with less effective clearance of *Plasmodium falciparum* parasites. *Parasite Immunol.* **2004**; 26(3):111–117.

145. D'Ombrain MC, Robinson LJ, Stanisic DI, et al. Association of early interferon-gamma production with immunity to clinical malaria: a longitudinal study among Papua New Guinean children. *Clin Infect Dis Off Publ Infect Dis Soc Am.* **2008**; 47(11):1380–1387.

146. Robinson LJ, D'Ombrain MC, Stanisic DI, et al. Cellular tumor necrosis factor, gamma interferon, and interleukin-6 responses as correlates of immunity and risk of clinical *Plasmodium falciparum* malaria in children from Papua New Guinea. *Infect Immun.* **2009**; 77(7):3033–3043.

147. Portugal S, Moebius J, Skinner J, et al. Exposure-dependent control of malaria-induced inflammation in children. *PLoS Pathog.* **2014**; 10(4):e1004079.

148. Cox-Singh J, Singh B, Daneshvar C, Planche T, Parker-Williams J, Krishna S. Anti-inflammatory cytokines predominate in acute human *Plasmodium knowlesi* infections. *PloS One.* **2011**; 6(6):e20541.

149. Candia J, Cheung F, Kotliarov Y, et al. Assessment of Variability in the SOMAscan Assay. *Sci Rep.* **2017**; 7(1):14248.

150. Menendez C, Fleming AF, Alonso PL. Malaria-related Anaemia. *Parasitol Today.* **2000**; 16(11):469–476.

151. Joyner C, Moreno A, Meyer EV, et al. *Plasmodium cynomolgi* infections in rhesus macaques display clinical and parasitological features pertinent to modelling vivax malaria pathology and relapse infections. *Malar J.* **2016**; 15(1):451.

152. Ramírez JF, Porras B, Borrero E, Martínez SP. Factors associated with the severity and complication of patients with malaria hospitalized between 2009 and 2013 in three municipalities of Colombia, case control study. *Malar J.* **2016**; 15(1):514.

153. Willmann M, Ahmed A, Siner A, et al. Laboratory markers of disease severity in *Plasmodium knowlesi* infection: a case control study. *Malar J.* **2012**; 11:363.

154. Adamson J W, Longo D L. Anemia and Polycythemia. *Harrisons Principles of Internal Medicine.* 18th ed. McGraw Hill; 2012. p. 448–457.

155. Awandare GA, Kempaiah P, Ochiel DO, Piazza P, Keller CC, Perkins DJ. Mechanisms of erythropoiesis inhibition by malarial pigment and malaria-induced proinflammatory mediators in an in vitro model. *Am J Hematol.* **2011**; 86(2):155–162.

156. Casals-Pascual C, Kai O, Cheung JOP, et al. Suppression of erythropoiesis in malarial anemia is associated with hemozoin in vitro and in vivo. *Blood.* **2006**; 108(8):2569–2577.

157. Prouty HW. Correcting the Reticulocyte Count. *Lab Med.* **1979**; 10(3):161–163.

158. Barber BE, Grigg MJ, William T, Yeo TW, Anstey NM. Intravascular haemolysis with haemoglobinuria in a splenectomized patient with severe *Plasmodium knowlesi* malaria. *Malar J.* **2016**; 15:462.

159. Boo YL, Lim HT, Chin PW, Lim SY, Hoo FK. A case of severe *Plasmodium knowlesi* in a splenectomized patient. *Parasitol Int.* **2016**; 65(1):55–57.

160. Mahmoudvand H, Farivar L, Sharifi I, et al. Fatal Case of *Plasmodium vivax* Malaria in a Splenectomized Patient. *Iran J Parasitol.* **2012**; 7(3):99–102.

161. Kho S, Andries B, Poespoprodjo JR, et al. High Risk of *Plasmodium vivax* Malaria Following Splenectomy in Papua, Indonesia. *Clin Infect Dis Off Publ Infect Dis Soc Am*. **2019**; 68(1):51–60.

162. Galinski MR, Barnwell JW. Chapter 5 - Nonhuman Primate Models for Human Malaria Research A2 - Abee, Christian R. In: Mansfield K, Tardif S, Morris T, editors. *Nonhuman Primates in Biomedical Research*. 2nd Ed. Boston: Academic Press; 2012. p. 299–323.

Available from:

http://www.sciencedirect.com/science/article/pii/B9780123813664000055

163. Barnwell JW, Howard RJ, Miller LH. Altered expression of *Plasmodium knowlesi* variant antigen on the erythrocyte membrane in splenectomized rhesus monkeys. *J Immunol.* **1982**; 128(1):224–6.

164. Lapp SA, Korir-Morrison C, Jiang J, Bai Y, Corredor V, Galinski MR. Spleen-dependent regulation of antigenic variation in malaria parasites: *Plasmodium knowlesi SICAvar* expression profiles in splenic and asplenic hosts. *PLoS One.* **2013**; 8(10):e78014.

165. Siqueira AM, Lacerda MV, Magalhães BML, et al. Characterization of *Plasmodium vivax*-associated admissions to reference hospitals in Brazil and India. *BMC Med*. **2015**; 13(1):57.

166. Nayak KC, Kumar S, Gupta BK, et al. Clinical and histopathological profile of acute renal failure caused by falciparum and vivax monoinfection: an observational study from Bikaner, northwest zone of Rajasthan, India. *J Vector Borne Dis*. **2014**; 51(1):40–6.

167. Silva GB da, Pinto JR, Barros EJG, Farias GMN, Daher EDF. Kidney involvement in malaria: an update. *Rev Inst Med Trop São Paulo* [Internet]. **2017** [cited 2019 Jun 17]; 59. Available from: https://www.ncbi.nlm.nih.gov/pmc/articles/PMC5626226/

168. Anand AC, Puri P. Jaundice in malaria. *J Gastroenterol Hepatol.* **2005**; 20(9):1322–1332.

169. Briand V, Cottrell G, Massougbodji A, Cot M. Intermittent preventive treatment for the prevention of malaria during pregnancy in high transmission areas. *Malar J.* **2007**; 6:160.

170. Oppenheimer SJ, Gibson FD, Macfarlane SB, et al. Iron supplementation increases prevalence and effects of malaria: report on clinical studies in Papua New Guinea. *Trans R Soc Trop Med Hyg.* **1986**; 80(4):603–612.

171. Adam I. Anemia, Iron Supplementation and Susceptibility to *Plasmodium falciparum* Malaria. *EBioMedicine.* **2016**; 14:13–14.

172. Goheen MM, Wegmüller R, Bah A, et al. Anemia Offers Stronger Protection Than Sickle Cell Trait Against the Erythrocytic Stage of Falciparum Malaria and This Protection Is Reversed by Iron Supplementation. *EBioMedicine.* **2016**; 14:123–130.

173. Goheen MM, Bah A, Wegmüller R, et al. Host iron status and erythropoietic response to iron supplementation determines susceptibility to the RBC stage of falciparum malaria during pregnancy. *Sci Rep.* **2017**; 7(1):17674.

174. Lin J, Denker B M. Chapter 44 Azotemia and Urinary Abnormalities. *Harrison's Principles of Internal Medicine.* 18th ed. McGraw Hill; 2012. p. 334–340.

175. Galinski MR, Lapp SA, Peterson MS, et al. *Plasmodium knowlesi*: a superb in vivo nonhuman primate model of antigenic variation in malaria. *Parasitology.* **2018**; 145(1):85–100.

176. Berendt AR, Simmons DL, Tansey J, Newbold CI, Marsh K. Intercellular adhesion molecule-1 is an endothelial cell adhesion receptor for *Plasmodium falciparum. Nature*. **1989**; 341(6237):57–59.

177. Golden A, Overman RR. Experimental cortical necrosis of adrenal gland in the monkey in diphtheria and in malaria; with observations on a fatal human infection with *Plasmodium falciparum. Am J Clin Pathol.* **1949**; 19(10):899–906.

178. Howard RJ, Barnwell JW, Kao V. Antigenic Variation in *Plasmodium-Knowlesi* Malaria - Identification of the Variant Antigen on Infected Erythrocytes. *Proc Natl Acad Sci U S Am-Biol Sci.* **1983**; 80(13):4129–4133.

179. Eaton MD. The Agglutination Of *Plasmodium Knowlesi* By Immune Serum. *J Exp Med.* **1938**; 67(6):857–70.

180. Olupot-Olupot P, Urban BC, Jemutai J, et al. Endotoxaemia is common in children with *Plasmodium falciparum* malaria. *BMC Infect Dis.* **2013**; 13:117.

181. Milner DA, Valim C, Carr RA, et al. A histological method for quantifying *Plasmodium falciparum* in the brain in fatal paediatric cerebral malaria. *Malar J.* **2013**; 12(1):191.

182. Erle DJ, Briskin MJ, Butcher EC, Garcia-Pardo A, Lazarovits AI, Tidswell M. Expression and function of the MAdCAM-1 receptor, integrin alpha 4 beta 7, on human leukocytes. *J Immunol.* **1994**; 153(2):517–528.

183. Barnwell JW, Ockenhouse CF, Knowles DM 2nd. Monoclonal antibody OKM5 inhibits the in vitro binding of *Plasmodium falciparum*-infected erythrocytes to monocytes, endothelial, and C32 melanoma cells. *J Immunol.* **1985**; 135(5):3494–7.

184. Hasler T, Albrecht GR, Van Schravendijk MR, et al. An improved microassay for *Plasmodium falciparum* cytoadherence using stable transformants of Chinese hamster ovary cells expressing CD36 or intercellular adhesion molecule-1. *Am J Trop Med Hyg.* **1993**; 48(3):332–347.

185. Kieda C, Paprocka M, Krawczenko A, et al. New human microvascular endothelial cell lines with specific adhesion molecules phenotypes. *Endothel J Endothel Cell Res*. **2002**; 9(4):247–261.

186. Fatih FA, Siner A, Ahmed A, et al. Cytoadherence and virulence - the case of *Plasmodium knowlesi* malaria. *Malar J.* **2012**; 11:33.

187. Rowe JA, Claessens A, Corrigan RA, Arman M. Adhesion of *Plasmodium falciparum*-infected erythrocytes to human cells: molecular mechanisms and therapeutic implications. *Expert Rev Mol Med.* **2009**; 11:e16.

188. Berlin C, Berg EL, Briskin MJ, et al. Alpha 4 beta 7 integrin mediates lymphocyte binding to the mucosal vascular addressin MAdCAM-1. *Cell.* **1993**; 74(1):185–195.

189. Montgomery J, Mphande FA, Berriman M, et al. Differential *var* gene expression in the organs of patients dying of falciparum malaria. *Mol Microbiol.* **2007**; 65(4):959–67.

190. Seydel KB, Milner, Jr. DA, Kamiza SB, Molyneux ME, Taylor TE. The Distribution and Intensity of Parasite Sequestration in Comatose Malawian Children. *J Infect Dis*. **2006**; 194(2):208–205.

191. Miller LH, Usami S, Chien S. Alteration in the rheologic properties of *Plasmodium knowlesi*--infected red cells. A possible mechanism for capillary obstruction. *J Clin Invest.* **1971**; 50(7):1451–1455.

192. Cooke BM, Stuart J, Nash GB. The cellular and molecular rheology of malaria. *Biorheology.* **2014**; 51(2–3):99–119.

193. Shelby JP, White J, Ganesan K, Rathod PK, Chiu DT. A microfluidic model for single-cell capillary obstruction by *Plasmodium falciparum*-infected erythrocytes. *Proc Natl Acad Sci U S A.* **2003**; 100(25):14618–14622.

194. Masciantonio MG, Lee CKS, Arpino V, Mehta S, Gill SE. Chapter Three - The Balance Between Metalloproteinases and TIMPs: Critical Regulator of Microvascular Endothelial Cell Function in Health and Disease. *Prog Mol Biol Transl Sci.* **2017;** 147: 101–131.

195. Turner GDH, Morrison H, Jones M, et al. An Immunohistochemical Study of the Pathology of Fatal Malaria. *Am J Pathol.* **1994**; 145(5):1057–1069.

196. Briskin M, Winsor-Hines D, Shyjan A, et al. Human mucosal addressin cell adhesion molecule-1 is preferentially expressed in intestinal tract and associated lymphoid tissue. *Am J Pathol.* **1997**; 151(1):97–110.

197. Butcher EC, Scollay RG, Weissman IL. Organ specificity of lymphocyte migration: mediation by highly selective lymphocyte interaction with organ-specific determinants on high endothelial venules. *Eur J Immunol.* **1980**; 10(7):556–561.

198. McGregor IA, Wilson ME, Billewicz WZ. Malaria infection of the placenta in The Gambia, West Africa; its incidence and relationship to stillbirth, birthweight and placental weight. *Trans R Soc Trop Med Hyg.* **1983**; 77(2):232–44.

199. Amulic B, Salanti A, Lavstsen T, Nielsen MA, Deitsch KW. An upstream open reading frame controls translation of *var2csa*, a gene implicated in placental malaria. *PLoS Pathog*. **2009**; 5(1):e1000256.

200. Dockrell HM, Souza JB de, Playfair JH. The role of the liver in immunity to blood-stage murine malaria. *Immunology.* **1980**; 41(2):421–430.

201. Wunderlich F, Al-Quraishy S, Dkhil MA. Liver-inherent immune system: its role in blood-stage malaria. *Front Microbiol* [Internet]. **2014** [cited 2019 Aug 6]; 5. Available from: https://www.ncbi.nlm.nih.gov/pmc/articles/PMC4219477/

202. Handayani S, Chiu DT, Tjitra E, et al. High Deformability of *Plasmodium vivax*–Infected Red Blood Cells under Microfluidic Conditions. *J Infect Dis.* **2009**; 199(3):445–450.

203. Govindasamy G, Barber BE, Ghani SA, et al. Retinal Changes in Uncomplicated and Severe *Plasmodium knowlesi* Malaria. *J Infect Dis.* **2016**; 213(9):1476–1482.

204. Beare N, Taylor T, Harding S, Lewallen S, Molyneux M. Malarial Retinopathy: A Newly Established Diagnostic Sign In Severe Malaria. *Am J Trop Med Hyg.* **2006**; 75(5):790–797.

205. Lewallen S, Harding SP, Ajewole J, et al. A review of the spectrum of clinical ocular fundus findings in *P. falciparum* malaria in African children with a proposed classification and grading system. *Trans R Soc Trop Med Hyg.* **1999**; 93(6):619–622.

206. Hidayat AA, Nalbandian RM, Sammons DW, Fleischman JA, Johnson TE. The diagnostic histopathologic features of ocular malaria. *Ophthalmology.* **1993**; 100(8):1183–1186.

207. Vandermosten L, Pham T-T, Knoops S, et al. Adrenal hormones mediate disease tolerance in malaria. *Nat Commun* [Internet]. **2018** [cited 2019 Aug 7]; 9. Available from: https://www.ncbi.nlm.nih.gov/pmc/articles/PMC6207723/

208. Hora R, Kapoor P, Thind KK, Mishra PC. Cerebral malaria - clinical manifestations and pathogenesis. *Metab Brain Dis* [Internet]. **2016**; . Available from: http://www.ncbi.nlm.nih.gov/pubmed/26746434

209. Galinski MR, Corredor V. Variant antigen expression in malaria infections: posttranscriptional gene silencing, virulence and severe pathology. *Mol Biochem Parasitol.* **2004**; 134(1):17–25.

210. Aikawa M, Rabbege JR, Udeinya I, Miller LH. Electron microscopy of knobs in *Plasmodium falciparum*-infected erythrocytes. *J Parasitol.* **1983**; 69(2):435–7.

211. Leech JH, Barnwell JW, Aikawa M, Miller LH, Howard RJ. *Plasmodium falciparum* malaria: association of knobs on the surface of infected erythrocytes with a histidine-rich protein and the erythrocyte skeleton. *J Cell Biol*. **1984**; 98(4):1256–64.

212. Bachmann A, Petter M, Krumkamp R, et al. Mosquito Passage Dramatically Changes *var* Gene Expression in Controlled Human *Plasmodium falciparum* Infections. *PLoS Pathog.* **2016**; 12(4):e1005538.

213. Berg EL, McEvoy LM, Berlin C, Bargatze RF, Butcher EC. L-selectin-mediated lymphocyte rolling on MAdCAM-1. *Nature.* **1993**; 366(6456):695–698.

214. Sherman IW, Eda S, Winograd E. Cytoadherence and sequestration in *Plasmodium falciparum:* defining the ties that bind. *Microbes Infect.* **2003**; 5(10):897–909.